

Torques in total hip replacements

Ama Amponsah Frimpong

Submitted in accordance with the requirements for the degree of
Doctor of Philosophy

School of Mechanical Engineering

November 2021



UNIVERSITY OF LEEDS

The candidate confirms that the work submitted is her own and that appropriate credit has been given where reference has been made to the work of others.

This copy has been supplied on the understanding that it is copyright material and that no quotation from the thesis may be published without proper acknowledgment.

The right of Ama Amponsah Frimpong to be identified as Author of this work has been asserted by her in accordance with the Copyright, Designs and Patents Act 1988.

© 2021 The University of Leeds and Ama Amponsah Frimpong

To Annalie...

You're my biggest motivation.

Acknowledgements

This Industrial CASE PhD was kindly funded by the EPSRC, the University of Leeds and DePuy Synthes as part of the Centre for Doctoral Training in Medical and Biological Engineering.

Staying the course on this journey has been by far the most challenging thing I've ever had to do, and it would not have been possible without the help, support and guidance of my supervisors Prof. Sophie Williams and Prof. Ruth Wilcox. To past and present iMBE staff, Dr Claire Brockett, Prof Joanne Tipper, Prof John Fisher, Dr Mazen Al-Hajjar, Philippa Withers (DePuy Synthes), Phil and the rest of the technical team, who helped me through this project, thank you.

My family have been my backbone and have propped me up numerous times when I could not go on by myself. To my husband, dearest Marv, thank you for all the times you didn't know what the right thing to say was... but tried anyway. I know the last few years have been a challenge and I appreciate your patience and love (and all the cake). To my not so little bundle of joy, Annalie, you don't know it yet, but you are my biggest motivation. I will do anything for you.

To all my family, my parents - Alex and Hannah, Raymond and Mina, I cannot thank you enough for your encouragement and prayer support, and everything in between.

Ruth and Philippa, thank you for those evenings you let me disrupt your life to ask questions and bounce ideas off you. To everyone else who continue to support me in one way or the other, thank you. Wendy, koda Y'AWIE! And Kiya, you no longer have to check how long I've gone without sleep!

Thank you, God, because it is You that gave me the inner strength I needed to push.

Abstract

Elevated frictional torques at the articulating interface of total hip replacements (THRs), if transferred, have the potential to affect component fixation and/or induce micro motion linked to fretting and corrosion at modular junctions. Pre-clinical testing of friction behaviour in THRs has predominantly been assessed under simplified test conditions using uniaxial simulators. These methodologies and simulators are not sufficient if assessment of friction under more clinically relevant conditions, such as multi-axis motion and consideration of surgical implant positioning, are to be investigated.

To identify a suitable measuring system and develop methodologies for assessing the frictional torques in THRs, studies were conducted whereby comparisons between a newly developed electromechanical multi-axis single station hip simulator (SSHS) and an existing uniaxial hip simulator as well as a custom-built friction measuring subsystem were made. Additionally, analyses of free-body diagrams in static equilibria and functional verification testing of the SSHS was completed. The assessments conducted showed that the SSHS could detect THR frictional torques without the use of the custom-built friction subsystem; and that the sub system did not provide the additional information expected.

Methodologies for assessing THR frictional torques were developed on the SSHS and used to assess the effects of translational positioning (i.e. testing when there was offset between the head and cup centres of rotation) on THR frictional torques. Increasing the applied medial-lateral (ML) translation, as might occur in a patient when there is a lateral misalignment between the centres of the femoral head and acetabular cup, under 1kN constant load and biaxial motion increased the measured frictional torques at the bearing interface of 36mm metal-on-polymer bearings, to over 15Nm. Elevated frictional torques, if transferred to the fixation interface of the acetabular cup, may induce shear stresses that could result in cup displacement.

To determine whether the measured elevated frictional torques observed during simulator testing could cause potential displacement in an implanted press-fit acetabular cup, a load-to-failure test that applied a simultaneous 300N or 3kN femoral head load was developed. Results indicated that the elevated frictional torques measured under ML translation on the SSHS were not likely to cause cup displacement in 10 and 20pcf Sawbone blocks when either axial load was applied.

This thesis reports on developed new methodologies for assessing THR frictional torques under variations in surgical positioning and for assessing torques required to cause cup loosening under axial loading in load-to-failure tests. It was demonstrated for the first time using a multi-axis hip simulator that surgical implant malpositioning can result in elevated frictional torques at the bearing interface of THRs. However, the impact of these elevated frictional torques on cup fixation requires further work to examine surgical implant malpositioning in THRs under more representative loading and motion conditions.

Table of Contents

CHAPTER ONE

Literature Review

1.1.	Introduction	1
1.2.	Total Hip Replacements	2
1.2.1.	Motions and Loads	3
1.2.2.	Reasons for Total Hip Replacements	5
1.2.3.	Total Hip Replacement Complications and Failure	5
1.3.	Tribology of Total Hip Replacements	6
1.3.1.	Friction in Total Hip Replacements	6
1.3.2.	Lubrication in Total Hip Replacements	9
1.4.	Factors that Influence the Tribology of Total Hip Replacements	11
1.4.1.	Motion and Loading	11
1.4.2.	Surface Sphericity and Roughness	12
1.4.3.	Contact Mechanics	13
1.4.4.	Variations in Surgical positioning of Total Hip Replacements	16
1.5.	Pre-Clinical Testing of Total Hip Replacements	19
1.5.1.	Early assessments of total hip replacements	20
1.5.2.	Hip Joint Simulators	20
1.5.3.	Acetabular Cup Stability: Load-to-failure testing	25
1.6.	Summary of Literature Review and Project Rationale	27
1.7.	Project Aims & Objectives	28
1.7.1.	Objectives	29

CHAPTER TWO

Assessment of frictional torques in total hip replacements using a pendulum friction hip simulator

2.1	Introduction	30
2.2	Materials	32
2.2.1	Lubrication	33
2.3	Pre-testing protocols	34
2.3.1	Bearing Diameter and Clearance	35
2.3.2	Surface Profile and Analysis	35
2.3.3	Component set up	37
2.4	Pendulum Friction Hip Simulator	38
2.4.1	Calibration	39
2.5	Input Parameters	39

2.5.1	Axial loading.....	40
2.5.2	Motion	40
2.5.3	Summary of input parameters used	42
2.5.4	Data Output.....	42
2.6	Results	44
2.6.1	Assessing the effects of increasing load on the frictional torque of THR 46	
2.6.2	Assessing the effects of increasing range of applied motion on the frictional torque of THR	48
2.6.3	Assessing the effects of materials combination on the frictional torque of THR	50
2.7	Discussion	52
2.8	Conclusion	54
CHAPTER THREE		
Comparison of two multi-axis systems for the measurement of frictional torques in total hip replacements		
3.1	Introduction	55
3.2	The two multi-axis friction measuring systems.....	58
3.2.1	Single Station Hip Simulator (SSHS)	58
3.2.2	Modified SSHS with a custom-built friction measuring subsystem ..	60
3.2.3	Comparison of capabilities of both systems.....	62
3.3	Calibration Methods.....	63
3.3.1	SSHS calibration	63
3.3.2	Modified SSHS with friction measuring subsystem calibration	65
3.4	Data Collection	65
3.4.1	Single Station Hip Simulator.....	66
3.4.2	Modified SSHS with friction measuring subsystem	66
3.5	Frictional torque analysis	67
3.5.1	THR frictional torque determined using the six-axis load cell measurement on the SSHS.....	67
3.5.2	THR frictional torque determined using the two uniaxial load cell measurements of the subsystem.....	78
3.6	Discussion	82
3.6.1	Calibration	83
3.6.2	Frictional torque measurement	84
3.7	Conclusion	86

CHAPTER FOUR

Assessment of a multi-axis hip simulator for the measurement of frictional torques in total hip replacements

4.1	Introduction	87
4.2	Multi-Axis Single Station Hip Simulator (SSHS)	88
4.3	Materials	88
	Component Preparation and Pre-Test Procedures.....	89
	Component set up.....	89
4.4	Testing and Data Collection.....	91
4.3.1	Data processing.....	91
4.3.2	4.5 Assessments of SSHS for measuring THR frictional torque.....	92
4.4.1	Assessing the friction measuring capacity of the SSHS in the AA direction.....	92
4.5.1	Assessing the effects of anterior-posterior and medial-lateral translation restriction on the measured frictional torques.....	95
4.5.2	Comparison of outputs between pendulum friction hip simulator and	
4.5.3	SSHS 103	
4.5.4	Assessing the effects of applied motions on the measured torques by the SSHS.....	111
4.6	Conclusion	114

CHAPTER FIVE

Assessing the effects of variations in translational positioning on the frictional torques in total hip replacements

5.1	Introduction.....	115
5.2	Materials.....	118
	5.2.1 Component Preparation and Pre-Test Procedures.....	118
5.3	Multi-Axis Single Station Hip Simulator	119
5.4	Input parameters.....	119
	5.4.1 Axial Loading	119
	5.4.2 Motion	120
	5.4.3 Medial-lateral translation	121
	5.4.4 Summary of conducted tests	122
5.5	Data output	123
5.6	Data processing	124
5.7	Results.....	125
	5.7.1 Frictional torque of 36mm MOP THRs using a modified SSHS (baseline).....	125
	5.7.2 Assessing the relative effects of varying medial-lateral translation on the torques of THRs measured under constant axial load.....	128

5.7.3	Comparison of the relative effects of varying medial-lateral translation on the THR frictional torques measured under constant and dynamic loading	130
5.8	Discussion.....	133
5.8.1	Limitations and further study.....	136
5.9	Conclusion	138
CHAPTER SIX.....		140
Methodology to assess the torque required to displace uncemented acetabular cups in total hip replacements		140
6.1	Introduction.....	140
6.2	Study Objectives.....	143
6.3	Materials.....	144
6.3.1	Total hip replacement components.....	144
6.3.2	Synthetic bone	144
6.3.3	Acetabular shell insertion	146
6.3.4	Instron® universal testing machine.....	150
6.4	Assessing the torque required to displace uncemented acetabular cups (Lever-out method)	151
6.4.1	Method	151
6.4.2	Results and Discussion	153
6.5	Experimental Method Development for assessment of acetabular shell displacement under load.....	154
6.5.1	Design requirements for custom rig and accompanying fixtures.....	155
6.5.2	Design description of custom rig and accompanying fixtures	156
6.5.3	Rim-loading load-to-failure study with axial femoral head loading	159
6.5.4	Rim-loading load-to-failure study without axial femoral head loading..	161
6.6	Method	162
6.6.1	Data output, processing and statistics.....	162
6.7	Results.....	163
6.8	Discussion.....	165
6.8.1	Limitations and future recommendations for the study.....	168
CHAPTER SEVEN		169
Discussion and Conclusion.....		169
7.1	Introduction/ Clinical Need	169
7.2	Multi-axis measurement of frictional torque in total hip replacements	172
7.3	Assessment of the effects of medial-lateral translation on the frictional torques of total hip replacements	174
7.4	Assessment of the torques required to displace uncemented acetabular components in total hip replacements.....	177

7.5	Summary of Future Work	178
7.6	Clinical and Research Impact	179
7.7	Conclusion	180
	REFERENCES.....	182
	APPENDICES.....	194

List of Figures

Figure 1.1 – Total hip replacement showing positioning in the acetabulum and the femur (Image by Laboratoires Servier is licensed under CC BY-SA 3.0)	3
Figure 1.2 – Gait cycle showing a twin peak loading profile and angular motion in flexion-extension, abduction-adduction and internal-external rotation	4
Figure 1.3 - Concept of low friction arthroplasty as illustrated by Sir John Charnley. The large femoral head is shown to generate greater frictional forces than the smaller femoral head.	9
Figure 1.4 - Types of lubrication regimes illustrated using conventional THR components (metal femoral head against polyethylene cup liner) (a) boundary (b) mixed (c) fluid film lubrication, showing the interaction between surface asperities and the presence of a lubricant between the surfaces.	10
Figure 1.5 – Schematic of ball and head joint showing surface sphericity and surface roughness	13
Figure 1.6 - Schematic of femoral head articulating with an acetabular cup showing the femoral head radius (R_{head}), the acetabular cup radius (R_{cup}) and the radial clearance (C) (Sonntag et al., 2013)	14
Figure 1.7 - Concentric alignment of femoral head and acetabular cup	16
Figure 1.8 - Schematic of possible variation in rotational positioning of THR components using high cup inclination as an example (coronal plane)	17
Figure 1.9 - Schematic of possible variation in translational positioning of THR components	18
Figure 1.10 - Simple tribometers primarily for screening of tribological joint replacement parameters (a) Pin-on-disc and (b) Pin-on-plate.....	21
Figure 1.11 - Illustration of load-to-failure tests previously used in literature (a) push out test (b) edge loading tests (c) twist out or torque test (d) pull out test and (e) lever out test	27

Figure 2.1 – 36mm THR components (a) metal femoral head (b) UHMWPE cup liner (c) ceramic femoral head (d) ceramic cup liner showing the positioning of alignment marks to ensure repeatable positioning during testing (alignment marks are coloured in for visibility) 34

Figure 2.2 – Location of surface analysis traces taken on femoral head and acetabular cup components.....36

Figure 2.3 - Femoral head fixture for pendulum friction hip simulator, showing COR position37

Figure 2.4 – Acetabular assembly for pendulum friction hip simulator, showing COR position. UHMWPE cup liner used for illustration38

Figure 2.5 – Example graphical representation input profile for a forward test showing the relationship between the axial loads (constant and dynamic) and flexion-extension motion for testing on a pendulum friction hip simulator. Shaded region shows high velocity region where data is collected.41

Figure 2.6 – Sample frictional torque trace measured in cycle number 64 of a 36mm MOP bearing tested under 1kN constant load with $\pm 10^\circ$ FE motion. Graphs shows frictional torque in forward and reverse directions45

Figure 2.7 - Mean forward and reverse frictional torques measured in 36mm MOP bearings (n=6) and 36mm COC bearings (n=6) tested in 25% (v/v) bovine calf serum, under 1kN and 2kN constant loads with $\pm 25^\circ$ FE motion (mean $\pm 95\%$ confidence)45

Figure 2.10 - Mean frictional torque measured in (i) 36mm MOP and (ii) 36mm COC bearings tested in 25% (v/v) bovine calf serum under 1kN and 2kN constant load and $\pm 25^\circ$ FE motion using a pendulum friction simulator (mean $\pm 95\%$ confidence, n=6)47

Figure 2.11 - Mean frictional torque measured in (i) 36mm MOP and (ii) 36mm COC bearings tested under both 2kN constant load and 2kN peak load with 100N

swing phase load, and two ranges of motion ($\pm 10^\circ$ and $\pm 25^\circ$ FE) using a pendulum friction simulator (mean $\pm 95\%$ confidence, n=6)	49
Figure 2.12 - (i) Mean frictional torque and (ii) mean friction factor measured in 36mm MOP and 36mm COC bearings tested under 2kN peak load with 100N swing phase load and $\pm 25^\circ$ FE motion using a pendulum friction simulator (mean $\pm 95\%$ confidence, n=6)	51
Figure 3.1 – Schematic of the Single Station Hip Simulator (SSHS)	60
Figure 3.2 – CAD assembly of subsystem, showing positioning of the tension-compression load cells (AA direction only shown) and universal joint, including all supporting structures.	61
Figure 3.3 – Example screenshot of GUI screen generated during SSHS axial force calibration.....	64
Figure 3.4 – Free body diagram of an ideal setup of the THR and SSHS in the sagittal plane, showing forces and moments on the system. This FBD considers FE motion such that the femoral head contacts the acetabular cup at point A, producing a normal force F_{NFE} and tangential friction force F_{RFE}	69
Figure 3.5 - Free body diagram of an ideal setup of the THR and SSHS in the coronal plane, showing forces and moments on the system. This FBD considers AA motion such that the femoral head contacts the acetabular cup at point A, producing a normal force F_{NAA} and tangential friction force F_{RAA}	71
Figure 3.6 - Free body diagram of the representative THR and SSHS setup in the sagittal plane, showing forces and moments on the system. This FBD considers FE motion such that the femoral head contacts the acetabular cup at point A, producing a normal force F_{NFE} and tangential friction force F_{RFE} , and the presence of lateral force F_z	73
Figure 3.7 - Free body diagram of the representative THR and SSHS setup in the coronal plane, showing forces and moments on the system. This FBD considers AA motion such that the femoral head contacts the acetabular cup at point A,	

producing a normal force F_{NAA} and tangential friction force F_{RAA} , and the presence of lateral force F_x	75
Figure 3.9 - Free body diagram of the subsystem on the SSHS, illustrating the position of the universal joint (pivot B), and the position of one uni-axial load cell in relation to the bearing (sagittal plane)	80
Figure 3.10 - Free body diagram of the subsystem on the SSHS, illustrating the position of the universal joint (pivot B), and the position of one uni-axial load cell in relation to the bearing (coronal plane).....	82
Figure 4.1 - Femoral head fixture for SSHS, showing COR position.....	90
Figure 4.2 - Acetabular cup fixture for SSHS, showing COR position. Acetabular shell cemented with dental grade poly-methyl methacrylate bone cement.....	90
Figure 4.3 – Front view of mounted components in the SSHS during the measurements in the AA axis assessment, illustrating the two orientations used. Orientation 1: FE direction of components coincided with FE direction of SSHS. Orientation 2: FE direction of components coincided with AA direction of SSHS.	93
Figure 4.4 – Position of AP translation linear bearing and positioning of shoulder screw to lock AP translation on the SSHS	96
Figure 4.5 - Position of ML actuator and positioning of shoulder screw to lock ML translation on the SSHS.....	97
Figure 4.6 – Mean torques in the FE, AA and IE directions of a 36mm COP bearing measured using a SSHS whilst applying four different combinations of AP and ML translation. Graphs illustrate mean \pm 95% confidence limits (n=3)	100
Figure 4.7 - Free body diagram of the representative THR and SSHS setup in the sagittal plane, showing the linear roller bearing and the presence of lateral force (F_z) as a result of some friction in the bearing	102
Figure 4.8 - Free body diagram of the THR and SSHS setup in the sagittal plane, showing the removal of the lateral translation and the introduction of resistive force (F_{zP})	102

Figure 4.9 - Example graphical representation input profile for a forward test showing the relationship between the axial loads (constant and dynamic) and flexion-extension motion for the comparative study on the pendulum friction hip simulator and SSHS.....	106
Figure 4.10 - Mean frictional torque measured in 36mm MOP and 36mm COC bearings tested under 2kN peak load with 100N swing phase load and $\pm 25^\circ$ FE motion on the SSHS (mean $\pm 95\%$ confidence, n=6).....	109
Figure 4.11 - Mean frictional torque measured in 36mm MOP and 36mm COC bearings tested under 1kN and 2kN constant load and $\pm 25^\circ$ FE motion tested on the SSHS (mean $\pm 95\%$ confidence, n=6)	109
Figure 4.12 – Effects of different combinations of FE, AA and IE motion on the torques of 36mm THRs when tested on a multi-axis single station hip simulator under 3kN twin peak and 300N swing phase load. Graphs illustrate mean $\pm 95\%$ confidence limits	113
Figure 5.1 - Schematic of possible variation in rotational positioning of THR components	116
Figure 5.2 - Schematic of possible variation in translational positioning of THR components	117
Figure 5.3 – Sample input profile showing relationship between FE and AA, ranges of $\pm 10^\circ$ and $\pm 7^\circ$ respectively.....	121
Figure 5.4 - Sample input profile showing position of applied ML translation during the gait cycle, with a constant load of 500N and $\pm 10^\circ$ of FE motion	122
Figure 5.5 - Mean frictional torques in FE and AA directions measured under 500N constant load and indicating FE, AA, or IE measurements (shaded regions) detected in directions not coincident with the direction of applied motion, n= 3 (Mean $\pm 95\%$ confidence level)	127
Figure 5.6 - Mean frictional torques in FE and AA directions measured under 1kN constant load and indicating FE, AA, or IE measurements (shared regions)	

detected in directions not coincident with the direction of applied motion, n= 3 (Mean \pm 95% confidence level)	127
Figure 5.7 – Mean ML forces in response to varying levels of ML translation under 500N and 1kN constant load for 36mm MOP bearings, n= 3 (Mean \pm 95% confidence level)	128
Figure 5.8 – Mean FE torque difference in response to increasing levels of medial lateral translation measured in 36mm MOP bearings (n=3) under 1kN constant load and FE or FEAA motion (Mean \pm 95% confidence level)	129
Figure 5.9 - Mean AA frictional torque difference in response to increasing levels of medial lateral translation measured in 36mm MOP bearings (n=3) under 1kN constant load and AA or FEAA motion (Mean \pm 95% confidence level).....	130
Figure 5.10 - Mean ML forces in response to increasing levels of ML translation under dynamic loading for 36mm MOP bearings, n= 3 (Mean \pm 95% confidence level).....	131
Figure 5.11 - Mean FE torque difference in response to increasing levels of medial lateral translation measured in 36mm MOP bearings (n=3) under dynamic loading and FE or FEAA motion (Mean \pm 95% confidence level)	132
Figure 5.12 - Mean AA torque difference in response to increasing levels of medial lateral translation measured in 36mm MOP bearings (n=3) under dynamic loading and AA or FEAA motion (Mean \pm 95% confidence level)	132
Figure 6.1 - Illustration of load-to-failure tests previously used in literature (a) push out test (b) edge loading tests (c) twist out or torque test (d) pull out test and (e) lever out test	141
Figure 6.2 – (a) Smooth 47mm diameter cavity in a Sawbone block obtained from CNC reaming (b) Reamed 55mm diameter cavity in a Sawbone block showing horizontal grooves created by clinical reamer	145
Figure 6.3 – Illustration of the custom rig in the acetabular shell insertion configuration	147

Figure 6.4 - Acetabular shell fully inserted into the saw bone block, showing coverage of Porocoat® coating only leaving the shell inner lip visible 148

Figure 6.5 - Porocoat® acetabular shell showing region of engagement following insertion to a depth of 30mm in a Sawbone block (10pcf) 149

Figure 6.6 - Lever out study set up on an Instron® 3366 universal testing machine 151

Figure 6.7 - Illustration showing the position of the applied load and the distance from the pivot..... 151

Figure 6.8 – Graph showing the mean torque required to displace uncemented acetabular shells in 10 and 20pcf Sawbone using the lever-out load to failure method (n=3, error bars represent 95% confidence) 153

Figure 6.9 – Schematic of the custom rig in the rim-loading with axial loading test configuration 155

Figure 6.10 – CAD illustration of clamping mechanism; showing tightening nuts and direction of static axial femoral head load 156

Figure 6.11 - Attachment mechanism for Instron® 3366 universal testing machine; also showing cross section of connector..... 157

Figure 6.12 – Schematic of load application fixtures 157

Figure 6.13 – Schematic of curved-end add-on for the modular loading fixture illustrating how contact with rim was maintained regardless of acetabular shell displacement (cross-sectional view) 158

Figure 6.14 – Load-to-failure study with axial femoral head loading set up on an Instron® 3366 universal testing machine 159

Figure 6.15 – Schematic of the custom rig in the rim-loading without axial loading test configuration..... 160

Figure 6.16 - Illustration showing the position of the applied edge load and the distance from the centre of rotation of the bearing..... 161

Figure 6.17 – Mean torques required to displace uncemented acetabular shells measured in a lever-out load-to-failure test, and rim-loading tests with and without

axial loading using 10 and 20pcf Sawbone density (n=3, error bars represent 95% confidence limits) 163

List of Tables

Table 1.1 - Typical lubrication regimes found in different total hip replacement bearings.....	11
Table 2.1 - Details of components used (ID: inner diameter, OD: outer diameter)	33
Table 2.2 - Average roughness (R_a) values \pm standard deviation (SD) pre-test for MOP and COC components (n=6)	37
Table 2.3 - Summary table of comparative study input parameters for MOP and COC components (n = 6) on both pendulum friction and single station hip simulators	42
Table 2.4 - Comparison of mean friction factors for serum-lubricated 36mm MOP & COC bearings under dynamic loading and a flexion-extension angle of $\pm 25^\circ$ measured in this study and published literature.....	54
Table 3.1 – Comparison of SSHS and modified SSHS capabilities.....	62
Table 4.1 - Summary of conducted tests for the assessment of directional sensitivity of torque measured (orientations described in Figure 4.3)	93
Table 4.2 - Summary of conducted tests for assessing the effects of AP and ML translation restriction on the output torque	98
Table 3.3 – Differences between the Pendulum Friction Hip Simulator and the Single Station Hip Simulator (<i>Italicised text indicate component that motion or displacement is applied to</i>)	105
Table 4.4 - Summary table of comparative study input parameters for six MOP and six COC components on both pendulum friction and single station hip simulators	106
Table 6.1 - Details of THR components tested in study (ID: inner diameter, OD: outer diameter).....	143

Table 6.2 - Mean height of Sawbone-acetabular shell engagement region for acetabular shells inserted at different depths 149

Table 6.3 – Sample sizes used for each study conducted in this chapter 160

List of Abbreviations

AA	-	Abduction-adduction
AF	-	Axial force
ANOVA	-	Analysis of variance
AP	-	Anterior-posterior
ASTM	-	American Society for Testing and Materials
CAD	-	Computer Aided Design
COC	-	Ceramic-on-ceramic
COP	-	Ceramic-on-polymer
COR	-	Centre of Rotation
FBD	-	Free body diagram
FE	-	Flexion-extension
IER	-	Internal External
ISO	-	International Organisation for Standardisation
kN	-	Kilo Newton
ML	-	Medial-lateral
MOM	-	Metal-on-metal
MOP	-	Metal-on-polymer
N	-	Newton
NJR	-	National Joint Registry
SSHS	-	Single station hip simulator
THR	-	Total hip replacement
UHMWPE	-	Ultra-high molecular weight polyethylene
v/v	-	Volume per volume

Glossary

- Acetabular cup - Also cup. Part of total hip replacement that is implanted into the acetabulum.
- Bearing - The two surfaces articulating within the total hip replacement (femoral head on acetabular cup)
- Biaxial - Having or relating to two axes
- Coronal plane - Vertical plane that divides the body into front and back sections
- Crosstalk - Phenomenon where signal transmitted in one channel of transmission creates an undesired or unwanted signal in adjacent channel(s)
- Electromechanical - Relating to a mechanical device that is electrically controlled
- Femoral head - Also head. Part of total hip replacement that is implanted into the femur.
- Friction - Temporary resistance offered to a body moving tangentially on the surface of another body with which it is in contact
- Frictional torque - Torque generated by the frictional force between surfaces in motion
- In vitro* - Outside the patients' body in a controlled environment
- In vivo* - Within the patients' body
- ISO 14242-1:2014 - Implants for surgery — Wear of total hip-joint prostheses — Part 1: Loading and displacement parameters for wear-testing machines and corresponding environmental conditions for test
- ISO 14242-2:2016 - Implants for surgery — Wear of total hip-joint prostheses — Part 2: Methods of measurement
- ISO 14242-3:2009 - Implants for surgery — Wear of total hip-joint prostheses — Part 3: Loading and displacement parameters for orbital bearing type wear testing machines and corresponding environmental conditions for test

ISO 14242-4:2018	- Implants for surgery — Wear of total hip-joint prostheses — Part 4: Testing hip prostheses under variations in component positioning which results in direct edge loading
Lateral	- Away from the middle of the body
Medial	- Towards the middle of the body
Modular	- Composed of more than one piece
Multiaxial	- Having or relating to more than two axes
Primary hip replacement	- First time a hip replacement is implanted into the hip of a patient
Prosthesis	- Implant used in the joint replacement procedure
Resultant torque	- Single torque obtained by combining torques in different directions via vector addition
Revision hip replacement	- Follow-on procedure conducted to add, remove or modify component(s) of a hip replacement
Sagittal plan	- Also longitudinal plane. Divides the body into left and right sections.
Transverse plane	- Plane that divides the body into superior and inferior sections.
Uncemented	- Also cementless. Prosthesis that is fixed into bone by a press-fit and relies on bone ingrowth and/or ongrowth.
Uniaxial	- Having or relating to one axis

CHAPTER ONE

Literature Review

1.1. Introduction

The implantation of total hip replacements (THRs) is a successful and reliable treatment for end-stage hip disease. In England, Wales and Northern Ireland, more than one million hip replacements were implanted between 2003 and 2020 (NJR, 2021). Historically, THRs have been implanted in elderly, less active patients. However, there is an increase in demand for younger and/or more active patients to have hip prostheses and this has resulted in the need for increased functionality and longevity of THRs, and subsequently, more research and testing into their performance and behaviour.

In vitro testing methods using hip joint simulators have been used to study and assess the performance of THRs, however reducing wear has often been a focus of these studies. The result has been an increased use of cross-linked ultra-high molecular weight polyethylene or use of ceramics in hard-on-hard couples. The use of these lower wearing materials in THR has led to an increase in the use of larger diameter bearings (i.e., >28mm). However, these larger bearings can be

associated with increased frictional torques due to the increased contact area and lever arm. Acetabular cup loosening may be caused by detrimental overloading resulting from high frictional torques being transferred from the bearing interface to the fixation. In addition, fretting and corrosion at the taper-neck junction resulting in adverse local tissue reaction observed in some of these lower wearing material couples (e.g., metal-on-metal) also point to the potential influence of transferred high friction from the bearing interface to the taper-neck junction.

Although technological advancements in the development of wear and friction hip joint simulators have resulted in increased functionality that has allowed for assessment of THRs under more clinically relevant conditions, the study of *in vitro* friction behaviour of THRs still lags behind that of wear. Very few studies into the friction and frictional torques of THRs have been conducted on multi-axis hip simulators with the ability to test under representative conditions. There is therefore a need to do so and to understand the influence of friction and frictional torques on the performance and longevity of THRs under clinically relevant conditions.

1.2. Total Hip Replacements

Total hip replacements (THRs) are implanted to replace the damaged hip joint, reducing pain, and restoring motion. Typical THRs consist of a metal stem inserted into the femur and a femoral head that articulates with an acetabular cup component inserted into the acetabulum of the pelvis (Figure 1.1) (Sonntag et al., 2013). The materials of the bearing head and cup and the method of fixation of the components vary. Bearing materials can be metal, ceramic or polymeric. The femoral head-on-acetabular cup combinations of bearing materials for THRs used clinically are predominantly metal-on-polymer (MOP), ceramic-on-polymer (COP), and ceramic-on-ceramic (COC). These bearings may be fixed with or without bone cement. The uncemented components typically have a porous external surface for osseointegration of bone (Bentley, 2009).

The three main types of metals used in total joint replacements include cobalt-based alloys, titanium-based alloys and stainless steels, with cobalt-chromium-molybdenum (Co-Cr-Mo) currently being the most commonly used for femoral heads due to its corrosion and wear resistance (Ratner et al., 2012). Polymeric acetabular cup liners are made from ultra-high molecular weight polyethylene (UHMWPE) or modified UHMWPE (Kurtz, 2004; Hanna *et al.*, 2016). The ceramics available on the market now include alumina or composites of alumina and zirconia that combine their desirable hardness, scratch resistance and toughness properties (Revell, 2008; Ratner et al., 2012). Overall, from 2003 to 2020, in England and Wales, cemented MOP bearings have been the most commonly used bearing combination. However, since 2006 the use of this combination is declining and the use of hybrid bearing combinations (cemented femoral stem, uncemented acetabular component) are significantly rising in primary hip replacement procedures (NJR, 2021).

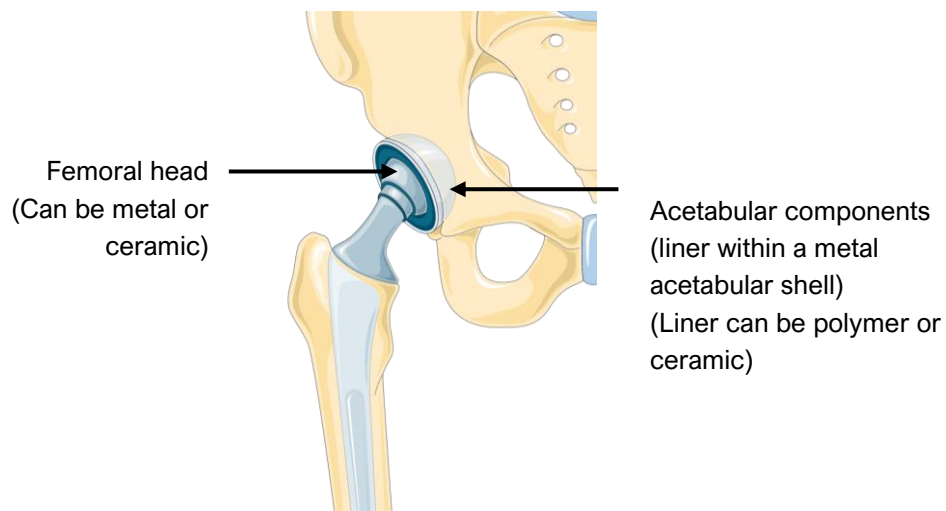


Figure 1.1 – Total hip replacement showing positioning in the acetabulum and the femur (Image by Laboratoires Servier is licensed under CC BY-SA 3.0)

1.2.1. Motions and Loads

The hip joint has motion in three degrees of freedom. These include flexion-extension, abduction-adduction, and internal-external rotation (Figure 1.2). The largest range of motion of the hip joint is flexion-extension, in the sagittal plane,

ranging from 20° in extension to 120° in flexion. Abduction-adduction occurs in the frontal plane and ranges from 45° in abduction and 30° in adduction. Internal-external rotation occurs in the transverse plane and ranges about 40° in both internal and external rotation (Berry and Lieberman, 2012).

The gait cycle is divided into two main phases. The stance phase spans 60% of the cycle and the swing phase the remaining 40% (Figure 1.2). The forces that act on the hip joint have been estimated to be up to four times body weight during normal gait (Paul, 1966; Bergmann et al., 2001). This force is at a maximum during heel strike and toe off, and at a minimum during swing phase (Paul, 1966). The loads applied across the natural hip joint have been estimated to range from about 150 to 3200 N (Palastanga *et al.*, 2011).

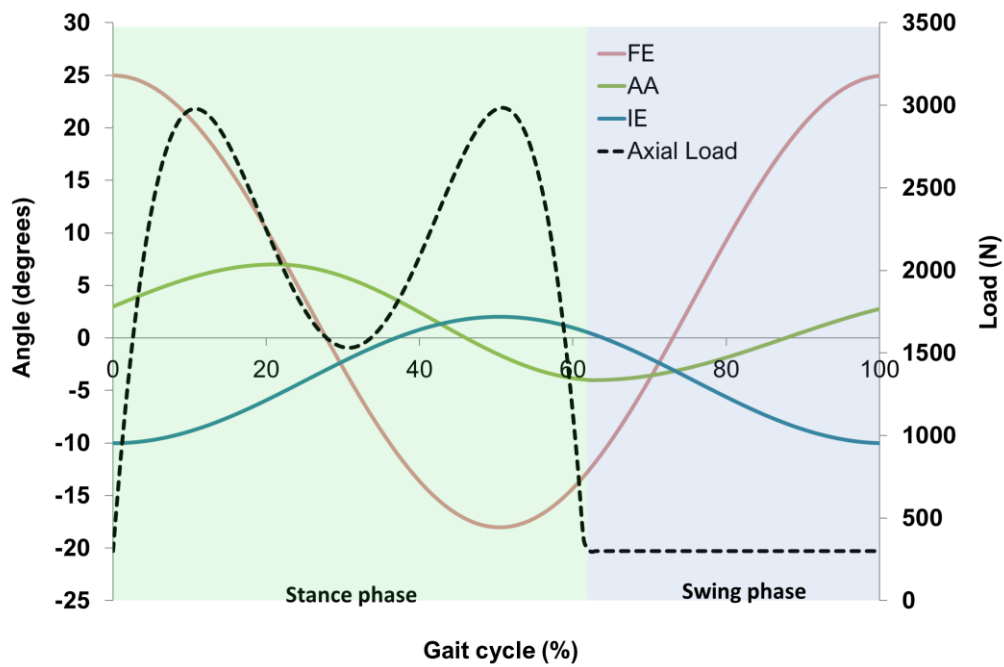


Figure 1.2 – Gait cycle showing a twin peak loading profile and angular motion in flexion-extension, abduction-adduction, and internal-external rotation

1.2.2. *Reasons for Total Hip Replacements*

Osteoarthritis is the most common type of arthritis, and accounts for 88.1% of the diagnosis for all primary hip replacement surgeries conducted between 2003 and 2020 (NJR, 2021). Osteoarthritis is degenerative, affecting the cartilage and the entire hip joint. Biological factors including the action of matrix metalloproteinases, cytokines, or growth factors, as well as mechanical factors may cause the onset of osteoarthritis. These lead to the breakdown of the articular hyaline cartilage, exposing the underlying bone. Osteoarthritis manifests in patients as pain resulting in limited function and range of motion (Rosen *et al.*, 1999).

1.2.3. *Total Hip Replacement Complications and Failure*

THR procedures are one of the most successful and relatively cost-effective surgical procedures at present. THR failure and subsequent revision surgeries are painful and undesirable for patients. Approximately 3% of all implanted primary hip replacements were however associated with a first revision between 2003 and 2020. The most commonly cited indications for revision procedures documented by the National Joint Registry are aseptic loosening, dislocation or subluxation, adverse soft tissue reaction to particulate debris, periprosthetic fracture, infection and pain. However, of these indications, malalignment, infection and some mechanically induced failure modes such as dislocation or subluxation and fracture are more prevalent less than 1 year after surgery (NJR, 2021).

Aseptic loosening generally occurs in the longer term and is reported to occur via two main mechanisms. Mechanical loosening as a result of excessive loading in the joint that compromises the fixation at the bone-implant interface or via biological loosening caused by osteolysis around the implant in response to debris in the joint space (Pacheco *et al.*, 1988; Hukkanen *et al.*, 1997; NJR, 2021).

1.3. Tribology of Total Hip Replacements

The failure modes of THRs are often influenced by complex and multifactorial parameters such as design, size, surrounding tissue characteristics, implant positioning, load and motion. Biotribological assessment (experimental and computational) is important in distinguishing the effects of the factors that influence THR performance and longevity.

1.3.1. Friction in Total Hip Replacements

1.3.1.1. General Principles of Friction

Friction is the “*temporary resistance offered to a body moving tangentially on the surface of another body with which it is in contact*” (Mohindroo, 1997). The direction of the tangential friction force acts opposite to the direction of motion (Bhushan, 2013).

The type of friction that exists between two contacting surfaces is determined by the nature of the contact, motion and presence of lubrication between them. Static friction is experienced when there is no motion between the two contacting surfaces, whereas dynamic (also kinetic) friction describes the force experienced by the surfaces if at least one surface begins to move (Bansal, 2005). Further to this, if there is no lubrication between the contacting surfaces, the friction present is called ‘dry (or solid) friction’, whereas fluid friction will refer to the friction present when there is a lubricant between the surfaces (Bhushan, 2013).

The basic principles of friction are (Tadmor and Gogos, 2013; Bhushan, 2013);

- i. The force of friction (F_R) is directly proportional to the normal load (W), where the proportionality constant is called the coefficient of friction (μ) given in equation 1.1;

$$F_R = \mu \cdot W \quad (1.1.)$$

- ii. The force of friction is independent of the apparent contact area between the contacting bodies.
- iii. The kinetic friction force, the friction force of a moving object, is independent of the sliding velocity once motion starts.

Frictional torque, coefficient of friction and friction factor

The frictional torque is the torque generated by the frictional force between surfaces in motion. Where the coefficient of friction (μ) is a dimensionless ratio between the force of friction (F_R) and the applied normal load (W) given in equation 1.2;

$$\mu = \frac{F_R}{W} \quad (1.2.)$$

This coefficient of friction between the interacting surfaces is highly dependent on the nature of these surfaces especially in the presence of biological lubricants (Jin et al., 2006). Friction factor (f) is a dimensionless term used particularly for artificial hip joints to differentiate itself from the coefficient of friction, by accounting for the femoral head radius (equation 1.3) (Dowson et al., 2000; Cornelius, 2009);

$$f = \frac{T}{Wr} \quad (1.3.)$$

Where f is the friction factor, T is the frictional torque, W is the normal load and r is the femoral head radius

1.3.1.2. Friction in total hip replacements

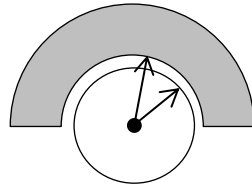
The mode of friction in both natural and artificial joints is dependent on the material properties of the bearing surface (Davim, 2013).

Sir John Charnley reported his concerns about friction and frictional torque induced component loosening in total hip replacements, and sought to curb this with his low-friction arthroplasty (LFA) design (Charnley et al., 1961; Hall and Unsworth, 1997). The engineering solution he employed to reduce the motion at the bone-implant interface included the smallest possible diameter of the femoral head component capable of withstanding anticipated *in-vivo* loads, articulating with a thick-walled acetabular cup component with the intention to reduce the moment of frictional force (Figure 1.3) (Charnley et al., 1961; Hall and Unsworth, 1997). This was expressed mathematically using equation 1.6 which gives the frictional force (F_R) at the bone-implant fixation interface from the force/moment equilibrium.

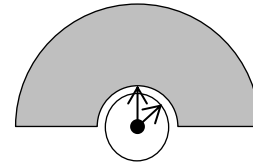
$$F_R = \frac{\mu W R_F}{R_C} \quad (1.4.)$$

Where W is the normal load, R_F is radius of the femoral head and R_C is the radius of the acetabular cup component

Using this equation for frictional force, it can be shown that a smaller femoral head radius articulating with an acetabular cup component produces a lower frictional force that was transferred to the fixation interface (Figure 1.3). This suggests that there would be a lower incidence of cup loosening caused by frictional forces in such smaller diameter bearings.



Large femoral head articulating with thin-walled acetabular cup



Small femoral head articulating with thick-walled acetabular cup

Figure 1.3 - Concept of low friction arthroplasty as illustrated by Sir John Charnley. The large femoral head is shown to generate greater frictional forces than the smaller femoral head.

The success of the LFA design was however never experimentally or otherwise demonstrated to be as a direct result of the reduced frictional torque (Hall and Unsworth, 1997). It was uncertain whether the LFA design's success stemmed from reduced wear properties or from reduced frictional torques. *In-vitro* hip joint simulator findings by Fisher and Dowson (1991) showed an insignificant frictional torque of approximately 1-2 Nm in MOP THR when compared to the reported 100 Nm threshold for static frictional torque required to unfix an acetabular component. This led to questions that wear characteristics were more important in THR longevity than was frictional torque (Hall and Unsworth, 1997).

Therefore it was concluded that friction and frictional torque did not significantly affect component loosening and subsequent failure (Dumbleton, 1981; Fisher and Dowson, 1991; Hall and Unsworth, 1997). With implant loosening still a major cause of revision surgeries, hypotheses around the potential effect high friction may have on implant loosening have re-arisen (Smith et al., 2012; Bishop et al., 2013b).

1.3.2. Lubrication in Total Hip Replacements

1.3.2.1. General Principles of Lubrication

Lubrication is the process by which a substance, the lubricant, is placed between two contacting surfaces in relative motion to reduce their interaction with each other and subsequently reduce the frictional force between them (Jones, 1971;

Hutchings, 1992). The lubricant achieves this by presenting itself as a material with lower shear strength than the materials of the articulating surfaces. Lubricants may be gases, liquids or solids, however in natural or implanted artificial joints, the lubricant present is synovial fluid or pseudo-synovial fluid.

There are three main types of lubrication: boundary lubrication, mixed lubrication and fluid film lubrication. By general definition, boundary lubrication refers to the condition where the surface asperities are primarily in contact due to incomplete coverage of the lubricant, whereas fluid film lubrication refers to when the contacting surfaces are completely separated by a fluid film. Mixed lubrication is however a mix of these two conditions where the surface asperities are part separated and part in contact (Figure 1.4) (Hutchings, 1992; Hori, 2006).

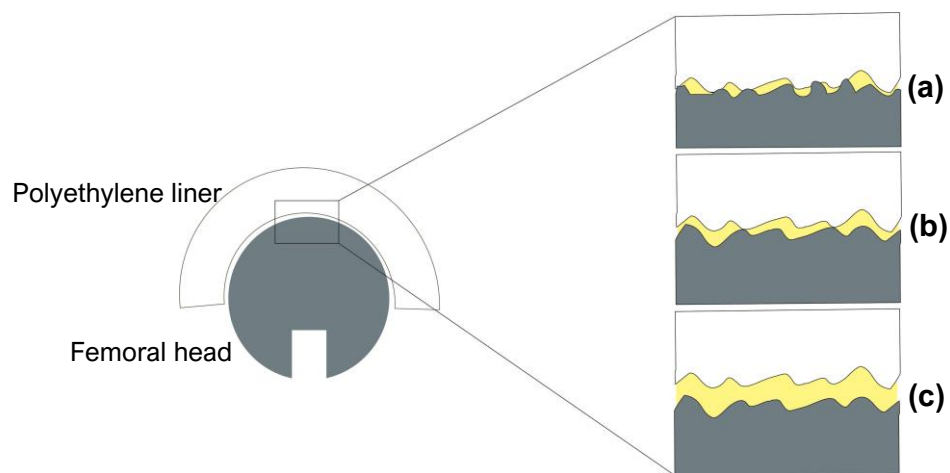


Figure 1.4 - Types of lubrication regimes illustrated using conventional MOP THR components; (a) boundary (b) mixed (c) fluid film lubrication, showing the interaction between surface asperities and the presence of a lubricant between the surfaces.

1.3.2.2. Lubrication in total hip replacements

Lubrication is important in reducing excessive friction and wear potentially leading to subsequent failure of bearings. This same principle applies in total hip replacements where excessive wear and wear debris formation is known to induce failure via osteolysis and aseptic loosening. The ideal lubrication regime for total hip replacements has been identified to be fluid film lubrication due to its

ability to separate the bearing surfaces (Jin et al., 2006). This separation by the fluid film is not synonymous however with a complete absence of wear as there are circumstances, such as during motion start or stop, when the fluid film can breakdown (Jin et al., 2006). Interestingly, wear can occur at the interface even when the bearing surfaces are not in contact due to erosion from the lubricating film or from fatigue resultant from contact pressures (Jin et al., 2006).

The lubrication regimes that typically exist in the different types of total hip replacements under ideal conditions are shown in Table 1.1;

Table 1.1 - Typical lubrication regimes found in different total hip replacement bearings

BEARINGS	LUBRICATION REGIME
Metal-on-UHMWPE	Mixed
Ceramic-on-Ceramic	Fluid film
Metal-on-Metal	Mixed

1.4. Factors that Influence the Tribology of Total Hip Replacements

1.4.1. Motion and Loading

Total hip replacements *in-vivo* through their lifetime will experience a varied range of loading conditions such as walking, sitting, standing, stair climbing and lying. A study by Morlock et al., (2001) on 42 patients with total hip replacements showed that the hierarchy of common everyday activity was (1) sitting, (2) standing, (3) walking, (4) lying and (5) stair climbing. The peak loads associated with sitting and standing, approximately 1.55 and 1.73 times body weight respectively is comparatively lower than is observed in walking (Bergmann et al., 2001). However, walking is considered to be the single most important physical activity that affects total hip replacements (Seedhom and Wallbridge, 1985). The average

number of walking cycles per year is estimated at approximately 1 million cycles, although more recent studies have shown that there are approximately 10 million cycles per 3.9 years for active patients (Schmalzried et al., 1998; Bergmann et al., 2010). This equates to more than 2.5million cycles per year for active patients. Activities such as stair climbing may increase the peak load to about five times body weight whereas isolated critical incidents like stumbling may induce peak loads as high as thirteen times body weight (Bergmann et al., 2010).

There is a change in patient demographic leaning towards an overweight, young and/or active population. This change in demographic may mean that the current *in-vitro* standards based on the research of Paul, (1966) governing the ranges of axial loading used in *in-vitro* simulator tests may no longer be representative. This is because these are based on a patient with an average weight of 70kg (Ambrosio, 2009). *In-vitro* hip simulator tests have shown that altering the loading on the hip joint during the swing phase affects the wear and the friction of total hip replacements. Studies using a pendulum friction simulator have shown that increased swing phase load increases the friction factor of a range of different total hip replacements (Brockett et al., 2007).

1.4.2. Surface Sphericity and Roughness

The texture of articulating surfaces affects how these interact with each other, subsequently affecting the friction and wear. Surface texture refers to the waviness (sphericity) and roughness of the articulating surface (Figure 1.5). Differences in sphericity occur due to the vibrations that occur during the manufacturing process and vary from product to product (Revell, 2008).

Spherical conformity of the bearing can be used to determine the clearance in all positions around the bearing surface. Surface roughness (Ra) refers to fine irregularities on the bearing surface (Figure 1.5) and usually results from

machining and polishing processes in manufacturing. Surface roughness and the representative film thickness of the bearing (h_{min}) can be used to theoretically predict the lubrication regime (Jin et al., 2006).

In general, for THRs, ceramic bearing surfaces have the lowest surface roughness (0.005-0.01 μm), followed by metal surfaces (0.01-0.025 μm), with polyethylene being the highest (0.1-2.5 μm).

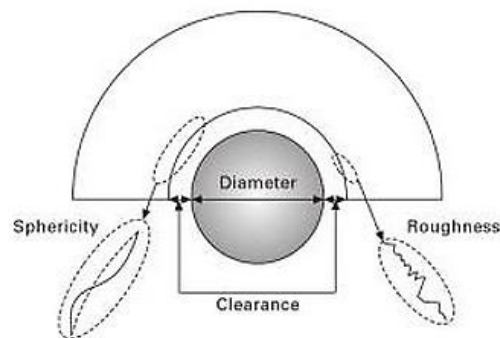


Figure 1.5 – Schematic of hip joint showing surface sphericity and surface roughness

1.4.3. Contact Mechanics

Contact mechanics can be defined as the study of the behaviour, particularly the load transfer, that occurs when two bodies come into contact (Totten, 2006). The contact area and contact stress distribution obtained can be used to understand or predict the possible failure mechanisms of a bearing, in this case total hip replacement. The contact stress is inversely proportional to the contact area at the interface and is a function of the bearing material's properties (Callaghan et al., 2007).

The contact mechanics of total hip replacement bearings is affected by a range of implant factors such as the diameter of the femoral head, the clearance between the head and the cup and the cup coverage (Berry and Lieberman, 2012). The radial clearance is expressed as the difference between the cup radius (R_{cup}) and the head radius (R_{head}) (Figure 1.6) (Sonntag et al., 2013).

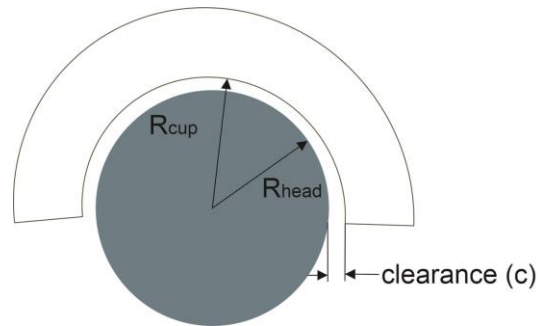


Figure 1.6 - Schematic of femoral head articulating with an acetabular cup showing the femoral head radius (R_{head}), the acetabular cup radius (R_{cup}) and the radial clearance (C)

1.4.3.1. Clearance

High conformity polar contact is synonymous with optimal clearance at the contact, and is dependent on the bearing material (Miller et al., 2012). Optimal clearance refers to a small enough clearance to increase conformity of the surfaces without areas of increased stress from eccentric contact. In contrast, for the given bearing, very large clearances result in a reduced contact area and therefore localised high contact pressures (Revell, 2008).

Attaining optimal clearance is very important in the tribology of THR bearings (Rieker et al., 2005). However, very small clearances may lead to equatorial contact, edge contact and loading of the cup, as well as lubricant starvation thereby leading to high friction and wear. While there is dependency between the measured friction and wear rates, theoretical and experimental studies often struggle to find a consensus regarding this. For example, in MOP bearings, an increase in clearance and contact stress resulted in reduced bearing friction using

32mm to 36mm diameter bearings (Wang et al., 2001). Due to the potential dependency on adhesive wear mechanisms, this was attributed to the separation of surface asperities at the bearing interface thereby reducing wear and friction. In contrast however, some computational studies predicted that increasing radial clearance and contact stress in MOP bearings resulted in increased wear and friction (Jin et al., 1994).

1.4.3.2. Femoral head diameter

Debate about the implications of varying the femoral head diameter in a bearing on the range of motion, and the stability provided from the large jumping distance to dislocation has been around for a while. Although Charnley's choice of a small diameter head for the low friction arthroplasty was widely accepted in the 1960s, use of large diameter femoral heads especially in MOM and resurfacing implants grew in the mid-2000s in the UK due to theoretically demonstrated benefits of larger range of motion.

MOP bearings in contrast to COC bearings are theoretically believed to be prone to more wear debris generation when the femoral head diameter is increased as the contact area and sliding distance increases (Livermore et al., 1990; Affatato, 2012). Increased contact area in MOP bearings result in increased interfacing with surface asperities which result in disruption of the lubricant and thereby increases wear.

Theoretical calculations have shown that increasing the bearing diameter increases the frictional torque, and has been hypothesised as contributing to the wear and corrosion at taper junctions or acetabular cup loosening (Bishop *et al.*, 2013).

1.4.4. Variations in Surgical positioning of Total Hip Replacements

The ability to accurately incorporate essential biomechanical factors in design and surgery may lead to optimum positioning and alignment such that femoral head and acetabular cup centres are concentric throughout the gait cycle (Figure 1.7). In this configuration, the contact area between the femoral head and the acetabular cup – the contact patch – remains within the articulating surface and does not come into contact with the rim. *In-vitro* simulator studies have shown that in this configuration, referred to as ‘standard conditions’, wear of COC and MOP bearings are generally low approximately less than 0.05mm³/million cycles and less than 13mm³/million cycles respectively (Al-Hajjar et al., 2010; Ali et al., 2016). Fisher (2011) reported that around 85% of patients present these low wear conditions in clinical practice.



Figure 1.7 - Concentric alignment of femoral head and acetabular cup

Deviations from these standard conditions have been attributed elevated wear rates. The elevated wear rates reported as a result of these deviations may be due to rim contact with the contact patch which specifically leads to stripe wear on the femoral component and rim wear on the cup of COC bearings (Nevelos et al., 2000; Fisher, 2011). Non-optimum surgical positioning of the femoral head and acetabular cup components leads to this deviation from standard conditions and results in subsequent elevated wear. Due to the three rotational and three translational degrees of freedom of both head and cup components, malalignment can occur in different ways (Fisher, 2011). These are divided into assessments of

rotational and translational positioning to reflect the axes in which the malalignment occurs.

Non-optimum rotational positioning commonly refers to the excessive inclination or version of the acetabular cup component such that the femoral head intersects the rim of the cup (Figure 1.8). Rotation of the acetabular cup observed along the frontal or coronal plane is described as cup inclination whereas the rotation in the transverse plane is described as cup version.

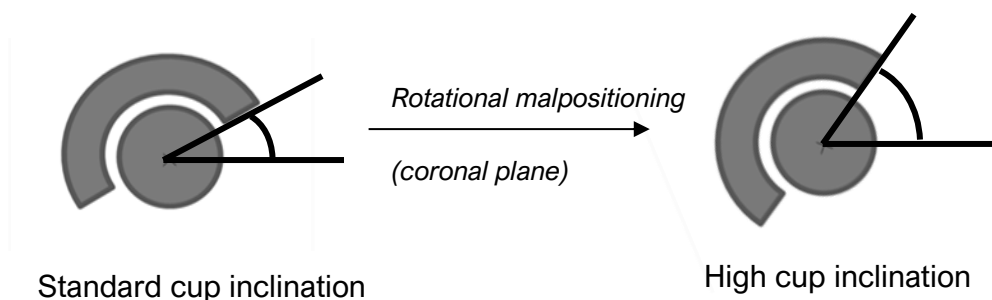


Figure 1.8 - Schematic of possible variation in rotational positioning of THR components using high cup inclination as an example (coronal plane)

Non-optimum translational positioning is described as a failure to restore femoral head or acetabular cup centres following a medial-lateral or superior-inferior translation thereby resulting in head-rim contact (Figure 1.9). This could be due to poor initial surgical placement, acetabular cup or femoral head translation, offset deficiencies, stem subsidence or head-neck impingement (Fisher, 2011). This non-optimum translational position, also known as separation or lateralisation, has also been associated with patient activity, prosthesis design and bearing materials used. It occurs during the swing phase of the gait cycle when the applied load on the hip joint is minimal leading to a lateral movement of the femoral head followed by an upward displacement of the head back into the acetabular cup upon loading during the stance phase. Due to the preceding lateral displacement, this causes an edge loading effect upon relocation of the head (Hua et al., 2014).

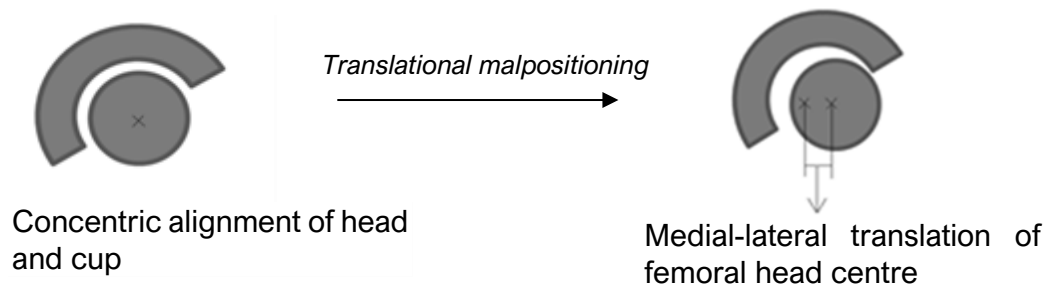


Figure 1.9 - Schematic of possible variation in translational positioning of THR components

Edge loading subsequently may lead to abnormal wear rates, damage and/or cracking of acetabular cup rims in MOP bearings. It has however been observed that translational malpositioning has a more dominant effect on the wear rate in *in-vitro* studies (Williams et al., 2013; Ali et al., 2016; Ali et al., 2017). For both MOP and COC bearings, the wear rate marginally increased with cup inclination angle (45° to 65°) from 0.99 to 2.65mm³/million cycles and from 13 to 15mm³/million cycles respectively. The wear rates however increased to 4.44mm³/million cycles and 20mm³/million cycles following increased translation (Al-Hajjar et al., 2013; Ali et al., 2016).

The effects of these translational and rotational malpositioning on other tribological factors (friction and lubrication) have not been as extensively investigated. Currently, two studies in the literature have investigated the individual effects of edge loading or steep cup inclination on the friction of total hip replacements, both on uniaxial hip simulators (Sariali *et al.*, 2010; Bishop *et al.*, 2013b). Sariali *et al.*, 2010 applied edge loading along and across the rim of ceramic liners inclined at 75° using a ceramic femoral head in an inverted setup. Although the study had limitations such as the inverted setup and changing head-cup contact by cutting the acetabular liner to prevent impingement, the study found that head-rim contact as a result of a high cup abduction angle of 75° resulted in an increased friction coefficient from 0.02 to 0.085. Similarly, Bishop *et al.*, (2013) found an increase in friction factors as a result of increasing the cup

inclination angles to 60° for COC bearings from 0.06 to 0.11. Assessing the effects of translational positioning have also been considered in a limited number of studies. A simplified computational model of femoral head contact on the acetabular cup rim was used to predict the offset loads and subsequently the torques generated that could be detrimental to the fixation interface (Liu et al., 2013). The torque was found to significantly increase with increased translation in COC, and MOP bearings. To date, Al-Hajjar et al., (2015) is the only experimental study to investigate the effects of translation on the measured torques. Using a uni-axial simulator, and applying motion in one axis only, the study found an increase in torques in response to increasing translation. Further study is needed to study the effects of translation on the measured torques in THRs using advanced simulation capabilities available in multi-axis simulators. Section 1.5 discusses pre-clinical testing of THRs including the use of hip simulation and why uni-axial simulators such as that used by Al-Hajjar et al., (2015) were limited in their assessment.

1.5. Pre-Clinical Testing of Total Hip Replacements

Pre-clinical testing is an integral part of the total hip replacement life cycle. It is a regulatory requirement and is essential for device manufacturers to be able to evaluate their devices for performance, possible modes of failure and safety (Trommer and Maru, 2017). The biomechanics and tribology of total hip replacements are critical factors that can influence the longevity of implants. Multiple factors such as geometry, materials combinations, loading and motion may influence the behaviour and performance of THRs and have been investigated in pre-clinical studies reported in literature. This section discusses the assessment of total hip replacement through pre-clinical hip simulation testing and load-to-failure testing.

1.5.1. Early assessments of total hip replacements

Initial tribological assessments were carried out using simple and relatively inexpensive tribometers such as the pin-on-disc and pin-on-plate systems, which assessed variables by simple sliding tests between a pin and a continually rotating or reciprocating rotating disc (Figure 1.10) (Besong et al., 2001). These tests were usually unidirectional and improved to include multidirectional motion analysis to allow ensure better comparison with *in-vivo* conditions (Saikko, 1998; Besong et al., 2001). Although primarily used in wear testing, the friction properties of some bearing materials such as stainless steel and zirconia-toughened alumina ceramic nanocomposite were tested using these (Henry and Takadoun, 2009; Ma and Rainforth, 2012). These tribometers, although useful in the evaluation of tribology of THRs, were not able to assess representative geometries of bearings, only partially simulated the motions present in the hip joint and were only useful as screening strategies (Dowson et al., 2003; Jin et al., 2006).

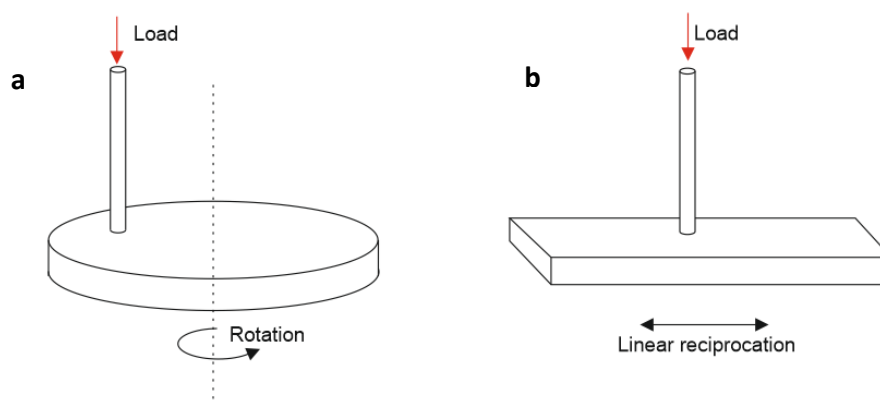


Figure 1.10 - Simple tribometers primarily for screening of tribological joint replacement parameters (a) Pin-on-disc and (b) Pin-on-plate

1.5.2. Hip Joint Simulators

Hip joint simulators are designed be able to convey loading and motion patterns that simulate *in-vivo* biomechanical conditions to artificial hip joints (Mejia and

Brierley, 1994; Galanis and Manolakos, 2011; Davim, 2013). Hip simulators currently available vary in level of complexity and functionality across institutions. Although there may be variation in the applied degrees of freedom, kinematics and applied forces, there are standardised protocols issued by the International Organisation for Standardisation that give guidelines for the *in-vitro* simulation of THRs primarily for wear testing such as ISO 14242-1, -2, -3 and -4.

The use of simulators have and still remain instrumental in both research and pre-clinical testing and the outputs of these result in the reduction of patient risk and improved implant designs (Galanis and Manolakos, 2011). There are several types of hip joint simulators, ranging from uniaxial, biaxial to multi-axial motion simulators (Revell, 2008).

1.5.2.1. Uni-axial hip joint simulators

The most common method of *in-vitro* friction measurements for hip replacements to date remains the uni-axial (also known as pendulum-type) friction hip simulators (Dowson et al., 2003). These designs originated from the original pendulum comparator device built by Sir John Charnley to assess friction of the McKee Farrar MOM hip prostheses (McMinn, 2009). Frictional torque data was directly obtained from these pendulum friction simulators by means of transducers positioned in line with the axis of motion (Brockett et al., 2007). These simulators relied on a fixed frame lower stage supported on hydrostatic bearings which meant that all recorded frictional torque emanated from the friction generated in the hip implant (Dowson et al., 2003; Brockett et al., 2007). These floating pressurised hydrostatic bearings for the lower friction stage ensured that the system had friction much lower (approximately two orders of magnitude less) than the friction in the hip replacement such that it was considered negligible (Brockett et al., 2007).

These pendulum friction simulators evolved from the application of constant loads to dynamic loading regimes, although there was the need to simplify the applied loads and motions due to limitations of the devices (Saikko, 1996; Dowson et al., 2003). The most common of these was the application of a vertical load on a hip implant undergoing flexion - extension motion using the pendulum simulator, with the frictional torque measurement acquired at the peak of the loading regime . These simulators operate on the principle that the abduction - adduction and internal - external rotation motions of level walking is relatively smaller than the flexion - extension motion and pose a negligible effect on measured frictional torque .

The two main pendulum-type simulators used in recent years for friction testing have been the Durham Hip Function simulator and the ProSim Pendulum Friction Hip Simulator (Scholes and Unsworth, 2000; Scholes *et al.*, 2000a; Scholes *et al.*, 2000b; Williams et al., 2006; Brockett et al., 2007; Sariali et al., 2010). These studies have investigated the effects lubricants and their constituent proteins, bearing diameter and clearance, bearing materials, standard as well as adverse loading conditions on the bearing friction. Even with some of these studies replicating *in-vivo* phenomena such as steep cup inclination and edge loading, the simplicity of pendulum-type simulators result in limited clinical relevance of obtained data.

1.5.2.2. Biaxial rocking motion hip simulator

Friction measurements in the context of wear simulation has not been commonplace. Uni-axial hip simulators were not used for wear studies and therefore study of friction was predominantly isolated from the wear behaviour of the bearing. It is however important to understand this co-dependency between wear and friction. To date, a standardised friction measuring accessory or mechanism does not exist. In an attempt to allow friction assessment under more representative conditions and alongside wear testing, some friction testing was

conducted by Bowsher and Shelton (2001), Liao et al., (2003), Saikko (2009) and Longaray et al., (2013), using a biaxial rocking motion (BRM) hip simulator. The design and kinematics of the BRM simulator was such that the lower component makes a two-axis sinusoidal rocking motion, usually $\pm 23^\circ$, which is equivalent to flexion - extension and abduction - adduction with a 90° phase difference and incorporated a vertical load. The lower component can either be the acetabular cup or the femoral component (Berry and Lieberman, 2012). For the measurement of friction, a torque cell with three degrees of freedom was mounted on the vertical axis or about the leaning axis for internal - external rotation (Saikko, 2009).

While a step forward in being able to test under representative conditions, the use of this type of simulator still did not allow the testing of friction under all possible motion and loading in a gait cycle.

1.5.2.3. Multi-axis hip joint simulators

Multi-axis hip simulators, generally have motion and load functionalities in three orthogonal axes. This means these simulators are capable of motions such as flexion - extension, abduction - adduction, internal - external rotation as well as the application of dynamic axial loads (Haider et al., 2016; Sonntag et al., 2017). In addition, some of these multi-axis simulators may also be able to apply and/or measure medial/lateral and anterior/posterior displacements and forces that can enable the assessment of variations in implant position.

Sub-optimal in-vivo implant position can contribute to the clinical failures THRs. The complexity of the mechanical load environment that this can result in is challenging to simulate and cannot be simulated by uni-axial hip simulators with limited functionality. Freely programmable multi-axial simulators, however, allow for effective testing of these clinically relevant parameters and scenarios, independently or together, to understand their effects on THRs.

Multi-axial simulator development and use has primarily been with respect to wear testing. More recently, the study of bearing friction is beginning to be studied alongside wear in these multi-axis hip simulators. It has likely been recognised with increasing demands on total hip replacements in terms of patient expectations, there is a need to accurately characterise the tribology of these devices making simplified testing systems and methodologies no longer enough (Weisenburger et al., 2011).

Vesa Saikko in 1996 developed a third-generation hip simulator capable of assessing both wear and friction of total hip replacements (Saikko, 1996). Unfortunately, the friction measurements in this study were obtained from the flexion - extension axis and can therefore not be considered as a representation of the frictional torque behaviour under full physiological loading.

Few research groups have attempted to measure force and moment data for all three rotational axes found in the human gait cycle for the purposes of understanding friction behaviour of total hip replacements (Wiesenberger *et al.*, 2013; Haider *et al.*, 2016; Sonntag *et al.*, 2017). The studies by Wiesenberger *et al.* (2013) and Haider *et al.* (2016) both assessed the effects of artificially abrading the articulating surfaces vs no artificial abrasion on the friction measured in a range of MOP bearings during an extended wear test. This was conducted as a verification assessment of their friction measuring capability, and the system predictably found that abrasion at the bearing interface increased the measured friction. Sonntag *et al.*, (2017) investigated the effects of increasing the femoral head diameter of COP bearings on the friction and recorded higher friction in 40mm than in 28mm bearing sizes. These tests indicate advances in friction testing where more representative loading and motion conditions need to be explored, to further develop our understanding of friction behaviour in THRs.

Increased clinical use of modular THR designs with taper interfaces in a range of material combinations have also seen an increase in taper-related fretting and

corrosion in retrievals (Gilbert et al., 1993; Goldberg et al., 2002; Ratner et al., 2012; Bishop et al., 2013; Morlock et al., 2017). Taper connections are most efficient when loads are transferred along the taper axis. In-vivo however, this is not the case, as the taper axis may not be aligned with the joint load and leads to non-symmetrical compressive radial stress distributions (Morlock et al., 2017). Materials properties, patient body weight and varied patient activities have all been found to increase the joint moment and subsequently these non-symmetric stresses that lead to micro-motions or loss of contact at the taper junction.

To date however, there has yet to be further study of THR friction under non-optimum or adverse surgical implant positioning conditions in a multi-axis hip simulator system. Studies have so far only tested under 'standard conditions' where the femoral head and acetabular cup components remain in a concentric configuration throughout testing. Although this is the optimum configuration for total hip replacement bearings, as discussed in Section 1.4.4, this is not always true *in-vivo* and has the potential to aggravate and elevate friction at the bearing interface and subsequently propagate to the fixation interface.

1.5.3. Acetabular Cup Stability: Load-to-failure testing

As mentioned in Section 1.2.3, aseptic loosening is the most common indication for revision hip surgery and can occur as early as less than a year after a primary hip replacement has been implanted (NJR, 2021). Clinically, the rates of aseptic loosening incidence are fairly similar in uncemented MOP THRs and all cemented THRs. However, approximately 60% of all primary hip replacements have an uncemented acetabular cup and there is a need to understand the effects of elevated forces and friction on the stability of the fixation interface (NJR, 2021).

Load-to-failure studies are a type of pre-clinical test employed to determine the stability of the fixation interface of implanted acetabular cups. While migration and micro-motion studies are employed to determine longer term and potentially

fatigue-related failure modes, static load to failure tests assess acetabular cups under extreme conditions to determine and investigate their design limits (Crosnier et al., 2014).

Primary stability of acetabular components is defined as the initial stable bone-prosthesis interface that is created during surgical implantation, and may be achieved via line-to-line or press-fit fixation (Callaghan et al., 2007). Particularly for uncemented prostheses, primary stability is crucial to minimise the occurrence of micro-motion and migration, and allow osseointegration of bone into the component (Cameron et al., 1973; Soballe et al., 1992).

The types of static load to failure tests that exist to assess extreme or worst-case scenarios regarding the stability of implanted prostheses are lever-out tests (Adler et al., 1992; Macdonald et al., 1999), pull-out tests (Macdonald et al., 1999), push-out (Crosnier et al., 2014), twist out or torque tests (Kody et al., 1990; Clarke et al., 1991; Curtis et al., 1992) and edge (or rim) loading tests (Saleh et al., 2008; Huber and Noble, 2014) (Figure 1.11).

Using these simplified tests, the influence of implant design features such as fins, coatings, screw fixation, acetabular cup shape, type and direction of applied load and motion on the fixation interface can be assessed. Using a rim loading test with a displacement sensor to detect gross acetabular cup movement, Saleh et al., (2008) determined that an elliptical shell with no screw holes and with small sintered beads on its fixation surface achieved good primary stability by measuring the torque required to displace the cup. Huber and Noble, (2014) also using a rim loading study with a displacement sensor found that acetabular cup designs tested with fins on the fixation surface exhibited good primary stability by measuring the load required to displace the cup.

To date, only one reported study has incorporated the use of a femoral head loading synonymous with the weight of the patient during cup stability assessment (Crosnier et al., 2014). Using displacement sensors, this study investigated the

micromotion resulting from cyclical loading of the acetabular cup component with the femoral head for 1000 cycles. The study found that press-fit acetabular components achieved less stability when implanted into lower density sawbone and that micromotion did occur but was dominant in one direction only.

In addition to measuring the micromotion present, it would be useful to measure under similar conditions, the torque that may be result in displacement of the acetabular cup and subsequently cause fixation loosening.

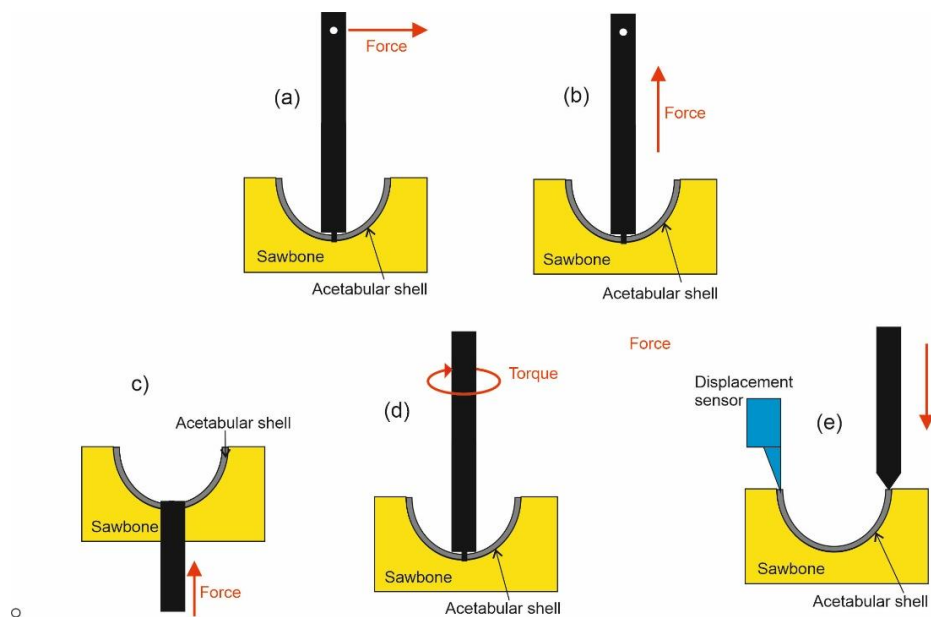


Figure 1.11 - Illustration of load-to-failure tests previously used in literature (a) push out test (b) edge loading tests (c) twist out or torque test (d) pull out test and (e) lever out test

1.6. Summary of Literature Review and Project Rationale

Although total hip replacement surgery is a very successful intervention, revision surgeries still occur with the most common cited reason being due to component loosening (NJR, 2021). Due to the influence of wear debris on the biological cascade leading to osteolysis and subsequent loosening, the focus of pre-clinical testing remained on wear hip simulation for many years. Incidence of cup loosening and retrieval analysis of taper corrosion of modular implants have

brought up questions about the possible involvement of high friction in total hip replacements, and their potential detrimental effects on the longevity of implants.

Current experimental studies that exist on friction of total hip replacements have been conducted on uniaxial hip simulators that convey simplified loading profiles of the gait cycle along the flexion-extension axis only. Although these non-physiological testing methodologies have provided a basis for assessing torque and friction of total hip replacements, they do not fully consider the conditions that may generate increased torques. In addition to the limited functionalities of current uniaxial simulators, the differences in methodologies across institutions have shown that there is a need for the development of a standardised *in-vitro* friction test protocol that can provide consensus understanding of the friction behaviour of total hip replacements. This would facilitate more standardised research to inform the next generation of implant designs and surgical tools.

Factors such as loading and range of motion, as well as variations in bearing design and size have been shown to affect friction of total hip replacements theoretically and experimentally. The roles of these factors in total hip replacement failures may however be compounded by clinical factors such as variations in implant positioning. Pre-clinical testing validated against initial retrievals analysis of COC bearings also highlighted the limitation of pre-clinical testing conducted under assumed standard optimum conditions. There is a gap in the literature regarding the assessment of total hip replacement friction under more physiological loading and motion, and under non-optimum conditions such as variations in implant positioning. In addition, there is a lack of standardised methodology governing the *in-vitro* assessment of total hip replacement friction resulting in varied methodologies with different limitations.

1.7. Project Aims & Objectives

A new multi-axis single station hip simulator with the capacity to test total hip replacements under more representative loading and motion conditions was used in this research. The aim of this project was to develop a pre-clinical testing method using this multi-axis hip simulator to assess the frictional torques present at the bearing interface of total hip replacements under both standard and non-optimum implant positions, with a particular focus on variations in translational implant position.

Elevated frictional torques, if transferred to the backside of the acetabular cup, could result in acetabular cup displacement. As such, this project also developed an *in-vitro* load-to-failure study for investigating the torques required to cause acetabular cup displacement at the fixation interface.

1.7.1. Objectives

The aims of this research project were addressed by the following objectives:

- i. Assess total hip replacement frictional torques using a pendulum friction hip simulator for comparison with the new multi-axis hip simulator, to verify the simulator's functional capacity.
- ii. Assess the frictional torque measurements of the six-axis load cell on the multi-axis single station hip simulator and compare it with the frictional torque measurement functionality of a custom-built friction measuring system.
- iii. Verify the overall functionality of the new multi-axis hip simulator for the measurement of frictional torques in total hip replacements through a series of preliminary tests.
- iv. Assess the effects of medial-lateral translation on the frictional torques of total hip replacements using the multi-axis hip simulator.
- v. Assess the torques required to displace well-seated uncemented acetabular cups, to understand the potential impact of elevated frictional torques on the fixation of acetabular cups.

CHAPTER TWO

Assessment of frictional torques in total hip replacements using a pendulum friction hip simulator

2.1 Introduction

Pendulum friction hip simulators have been previously used and validated for assessing the effects of different materials combinations (Auger *et al.*, 1993; Scholes and Unsworth, 2000; Brockett *et al.*, 2007), loading conditions (Williams *et al.*, 2006; Yan *et al.*, 2009), lubrication (Scholes and Unsworth, 2000, 2006) and implant positioning (Sariali *et al.*, 2010) on the friction and frictional torques of total hip replacements (THR).

Studies using pendulum friction hip simulators only apply simplified loading profiles and motion in the flexion-extension direction. These are not representative of the complex loading and motion observed during the human gait cycle. More recent studies have begun to investigate the frictional torque of THRs under more clinically representative loading conditions by applying twin peak loads and introducing abduction-adduction (Bowsher and Shelton, 2001; Saikko, 2009) as

well as internal-external rotation (Weisenburger, Garvin and Haider, 2013; Haider, Weisenburger and Garvin, 2016).

There is evidence that non-optimum component positioning significantly increases wear *in-vitro* and in explants, but as yet the frictional response under these conditions has not been investigated (Nevelos *et al.*, 1999, 2001; Al-Hajjar *et al.*, 2013). This is important because elevated frictional response generates larger shear stresses which may facilitate mechanical loosening which could subsequently further elevate the wear, and progressively lead to failure (Bishop, Waldow and Morlock, 2008; Bergmann *et al.*, 2012; Damm *et al.*, 2013).

This chapter describes a control study undertaken to generate data on an existing and previously validated pendulum friction hip simulator, conducting tests that can be verified against theoretical predictions or published studies to ensure the dataset was reliable. The data generated was used as a comparison in the first stage of validating a new multi-axis hip simulator for THR frictional torque testing. A comparative study with the results from this chapter was then undertaken on the multi-axis hip simulator (Chapter 3). The research objectives for the study discussed in this chapter were:

- a) To examine the effects of increasing applied load on THR frictional torques

Theoretically, friction is proportional to the applied load. It was therefore expected that the pendulum friction hip simulator would be able to measure the difference in frictional torques when the applied load is increased. Under a constant applied load, the accuracy of the piezoelectric transducer measurement could be verified by assessing the symmetry of frictional torque traces collected in the forward and reverse directions of motion.

- b) To examine the effects of increasing range of flexion-extension on THR frictional torques

A decreased range of motion may affect the lubrication, and elevate the measured friction but this was not the case in a previous study by Sonntag *et al.*, (2017) using a free pendulum simulator. In this study, it was found that varying range of motion did not change the measured frictional torque. Nevertheless, it was important to understand the effects varying range of motion in this simulator for future studies.

- c) To examine the effects of different bearing materials on THR frictional torques

Experimental studies by Scholes *et al.*, 2000 and Brockett *et al.*, 2007 have shown that under serum-lubricated conditions, 28mm metal-on-polymer bearings have higher friction when compared to 28mm ceramic-on-ceramic bearings. This may have been due to the relatively smoother bearing surface coupled with a reduced clearance in the ceramic-on-ceramic bearings, and subsequently what lubrication regime was present. In this study, frictional torques in 36mm metal-on-polymer and ceramic-on-ceramic bearings were investigated to determine the ability of simulator to differentiate between differing bearing materials.

2.2 Materials

Total hip replacement components 36mm in diameter were supplied by DePuy Synthes (Leeds, UK) for use in the studies conducted as part of this chapter. These components included Articul/eze® metal and BioloX® Delta ceramic femoral head components, as well as Marathon™ and BioloX® Delta ceramic acetabular liners and Porocoat® acetabular shells from the PINNACLE® cup system. Further details including constituent materials and product reference

numbers are provided in Table 2.1. A sample size of six was used for the tests conducted and discussed in this chapter.

Table 2.1 - Details of components used (ID: inner diameter, OD: outer diameter)

Commercial name	Material specification	Product reference
Femoral components, 36mm OD		
Articul/eze® metal	Cobalt-Chromium-Molybdenum (CoCrMo)	1365-52-000
BioloX® Delta ceramic	Zirconia-toughened, platelet-reinforced alumina (ZTPA) (CeramTec, 2012)	1365-36-320
Acetabular components (liners & acetabular shell), 36mm ID & 56mm OD		
BioloX® Delta ceramax ceramic liner	Zirconia-toughened, platelet-reinforced alumina (ZTPA)	1218-81-756
Marathon™ polyethylene acetabular liner	Ultra-high molecular weight cross-linked polyethylene (UHMWPE)	1219-36-056
Porocoat® acetabular shell	Titanium with a sintered titanium bead surface	1217-01-056

A combination of CoCrMo femoral heads articulating with UHMWPE acetabular liners were referred to as metal-on-polymer bearings (MOP) and ZTPA femoral heads with ZPTA liners, ceramic-on-ceramic (COC) bearings. Acetabular liners are inserted into acetabular shells of corresponding sizes for fixation into pelvic bone *in-vivo*. This combination of acetabular liners and shells was referred to as the acetabular assembly.

2.2.1 Lubrication

New-born bovine calf serum (Harlan Sera-Labs, Loughborough - UK) diluted to 25% (v/v) with the use of 0.03% (v/v) sodium azide solution was used as lubricant substitute for human synovial for simulator testing. A 0.03% sodium azide solution was made from 0.1% sodium azide and deionised water, and was used to minimise

bacterial degradation of the serum. The approximate protein concentration of 25% bovine calf serum was 15.46 g/L in accordance with ISO 14242-1:2012. The primary protein content in new-born bovine calf serum was albumin.

2.3 Pre-testing protocols

This section discusses the procedures that were undertaken to prepare the test components prior to testing. Alignment marks were placed onto non-articulating surfaces of femoral heads and acetabular liners to ensure repeatable orientation during testing (Figure 2.1). All components were washed prior testing to remove contaminants using detergent solution, rinsed in Distel High Level Laboratory Disinfectant (Tristel Solutions Ltd, UK) and wiped with 70% (v/v) isopropanol. After testing, components were washed with detergent, rinsed with Distel and then rinsed further with deionised water. They were then immersed in isopropanol in an ultrasonic bath for ten minutes.

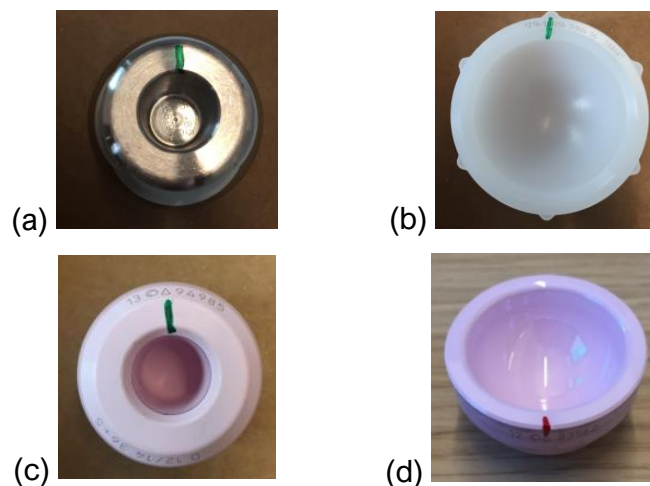


Figure 2.1 – 36mm THR components (a) metal femoral head (b) UHMWPE cup liner (c) ceramic femoral head (d) ceramic cup liner showing the positioning of alignment marks to ensure repeatable positioning during testing (alignment marks are coloured in for visibility)

2.3.1 Bearing Diameter and Clearance

Geometric measurements were made using a Kemco Legex 322 coordinate measuring machine (CMM) (Keeling Metrology, UK) to ascertain the precise diameter of the femoral head components and the inner diameter of the acetabular liner bearing surface. The machine has a resolution of $\pm 3\mu\text{m}$ and an accuracy of $1\mu\text{m}$. A 2mm diameter probe on the CMM was used to demarcate 25 points on the bearing surface, from which the diameter of the bearing was determined. The deviation of the bearing surface form from a perfect sphere was also computed.

The diametral clearance of the bearing pairs were calculated using equation 2.1:

$$\text{Diametral clearance} = ID_{\text{liner}} - D_{\text{head}} \quad (2.1)$$

Where ID_{liner} is the inner diameter of the acetabular liner and D_{head} is the diameter of the femoral head component

2.3.2 Surface Profile and Analysis

Surface roughness of the bearing articulating surfaces was assessed using a two-dimensional (2D) contact profilometry which maps out the irregularities on the surface. The arithmetic mean deviation, also known as the average roughness or centre line average (R_a), is the average from the centre line of the sampling length (equation 2.2). R_a values are high when the surface is rough, represented by a large number of peaks and valleys across the sampling area.

$$Ra = \frac{1}{l} \int_0^l |z(x)| dx \quad (2.2)$$

Where Ra is the average roughness, l is the length of the trace and z is the height of the surface irregularity.

R_a is widely used in orthopaedic research, but it does not indicate peaks and valleys. The skewness (R_{sk}) measured the symmetry of the profile about the mean line and therefore allowed differentiation between asymmetrical profiles that may have the same R_a . The maximum peak height (R_p) and the minimum valley height (R_v) were also investigated together with R_a and R_{sk} to provide a more accurate description of the bearing surface.

Roughness parameters R_a , R_{sk} , R_p and R_v were assessed before and after each study in accordance with ISO 4288:1998 using a Form Talysurf (Taylor Hobson, UK). Three 17mm traces were taken per sample (Figure 2.2). Due to the hemispherical nature of THR component surfaces, the traces taken were arcs. A Gaussian filter was used to suppress the waviness and form of the components, allowing only roughness to be assessed. A Gaussian cut-off of 0.08mm with a bandwidth of 100:1 was used for metal and ceramic components, and 0.25mm with a bandwidth of 100:1 for polymeric components. The components were orientated during testing such that:

All 'P1' traces were along the flexion-extension path

All 'P2' traces were perpendicular to the flexion-extension path

All 'P3' traces were in the areas of the bearing that was not in contact during testing.

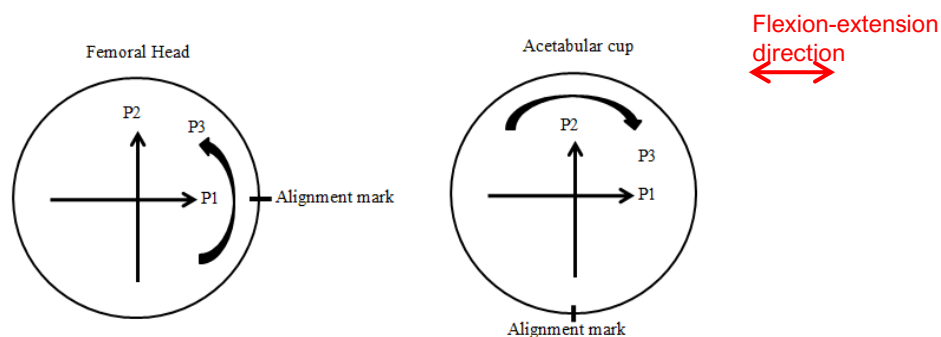


Figure 2.2 – Location of surface analysis traces taken on femoral head and acetabular cup components

R_a values measured prior to the start of testing for MOP and COC samples are provided in Table 2.2.

Table 2.2 - Average roughness (R_a) values \pm standard deviation (SD) pre-test for MOP and COC components (n=6)

Components	Femoral head, R_a ($\mu\text{m}\pm\text{SD}$)	Acetabular liner, R_a ($\mu\text{m}\pm\text{SD}$)
36mm MOP	0.004 ± 0.001	0.703 ± 0.264
36mm COC	0.005 ± 0.001	0.009 ± 0.002

2.3.3 Component set up

The centre of rotation (COR) of the femoral head and acetabular assembly were aligned with the COR of the motion arm to minimise experimental errors. This ensured that the frictional torque was a direct result of the friction in the bearing measured by the piezoelectric transducer and not from offset loads.

Using a height gauge and custom-made fixtures, the COR of the femoral head was fixed at a set distance of 72.83mm from the base of the fixture, corresponding with the COR position of the motion arm (Figure 2.3).

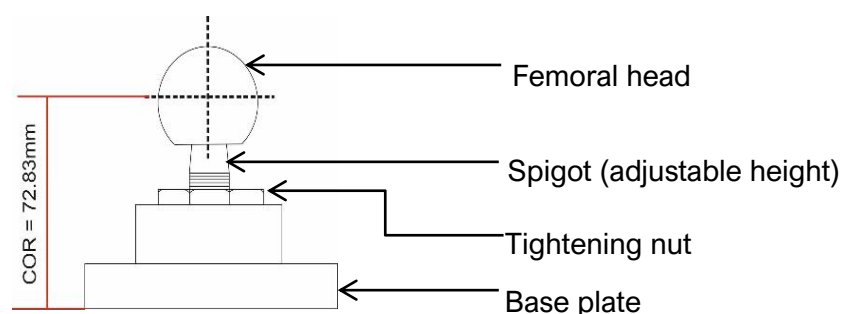


Figure 2.3 - Femoral head fixture for pendulum friction hip simulator, showing COR position

Using a locking ring and an adjustment screw positioned in the base of a custom fixture for the acetabular component, the COR of the acetabular assembly was fixed at a set distance of 63.24mm, corresponding with the COR position of the motion arm (Figure 2.4).

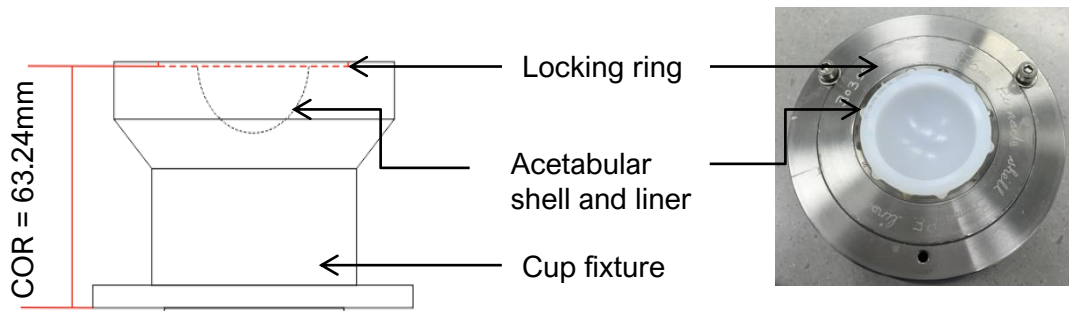


Figure 2.4 – Acetabular assembly for pendulum friction hip simulator, showing COR position. UHMWPE cup liner used for illustration

2.4 Pendulum Friction Hip Simulator

A single station servo-hydraulic machine (ProSim, Manchester - UK) with a maximum capacity of applied axial loading of 3kN and simple harmonic motion of up to $\pm 25^\circ$ was used. It was controlled by a personal computer via an on-board microprocessor and consisted of a motion frame arm positioned above a carriage. Constant or dynamic axial loads were applied directly to the bearing through the femoral head component mounted to the superior motion arm.

A piezoelectric crystal transducer was positioned in front of the friction measuring carriage. The acetabular assembly was positioned in a carriage externally supported by pressurised hydrostatic bearings that ensure component self-centring during testing. Any rotation to the carriage that generated a detectable signal by the transducer was attributed to the friction in the bearing system and was computed. All tested THR components were mounted in an inverted position relative to *in-vivo* conditions.

2.4.1 Calibration

The axial load applied by the pendulum friction hip simulator was calibrated using the automatic calibration function provided via the accompanying ProSim simulator software.

The load calibration procedure included the progressive opening of the air pressure valve, which caused the application of a range of axial loads through the simulator load cell. An externally calibrated load cell (Omegadyne, Connecticut-USA) was placed centrally between the load cell and the loading frame such that it coincided with the principal action of the applied axial load. The outputs of the external load cell were entered into the simulator software for the calculation of the calibration constants. The calculated calibration constants were re-entered into the ProSim simulator software to correct the demand load applied by the simulator, ensuring the accurate application of specified loads.

Frictional torque calibration was also conducted using the ProSim simulator software automatic calibration function. Calibrated weights were positioned at a known distance on a loading arm from the centre of the load cell, and the output torque entered to calculate the calibration constant. The calibrated weights were positioned in the forward test (front) and reverse test (rear) directions. The calculated calibration constants for each direction was compared to ensure similarities in magnitude and re- entered into the ProSim simulator software.

2.5 Input Parameters

After calibration, the femoral head and acetabular components were assembled and mounted into the machine. Accurate alignment of mounted components was ensured by passing an alignment rod through the COR of the motion arm.

Approximately 1mL of 25% newborn bovine calf serum was placed within the acetabular liner and the femoral head manually lowered into contact. Tests were conducted at room temperature. Lubricant was removed after testing, and

components cleaned. The input parameters were specified for the study using the graphical user interface on the pendulum friction hip simulator and are discussed in this section.

2.5.1 Axial loading

2.5.1.1 Dynamic loading

A simple sinusoidal wave was used to apply a dynamic peak load of 2kN, forming 60% of the loading cycle, and a swing phase load (SPL) of 100N over the remaining cycle. This was based on the simplified gait cycle defined by Paul (1966). In a normal gait cycle, the hip joint is under loading approximately 60% of the time, with the other 40% spent in the swing phase. A single peak dynamic load profile replicated this in a simplified manner by eliminating the trough seen in a 'twin peak' load profile. The trough in the twin peak loading denotes the double stance phase where both joints share the body weight.

2.5.1.2 Constant loading

Constant loads of 1kN and 2kN were also applied to THR components in this study. The application of constant and dynamic loads was facilitated by the hydraulic pressure applied through the loading frame. The accuracy of the piezoelectric transducer measurement was assessed by investigating the magnitude and symmetry of the output frictional torque under constant load.

2.5.2 Motion

Flexion-extension (FE) angles of $\pm 10^\circ$ and $\pm 25^\circ$ were applied to mounted components through the motion arm at a rate of 1Hz, representing the average walking speed. FE motion of $\pm 25^\circ$ was a similar range to the FE motion seen in the human gait cycle, and as defined by ISO14242-1:2012 for *in-vitro* simulator testing, whereas $\pm 10^\circ$ was used to represent conditions with limited FE motion.

All dynamic tests were conducted with motion in forward and reverse to reduce possible errors from offset loads generated as a result of the position of the motion arm with respect to the piezoelectric transducer during peak loading. The forward direction of the test refers to data collection when the motion arm was moving towards the transducer and the reverse, when the motion arm was moving away from the transducer. This was done by inverting the polarity of the applied motion in the forward direction for the reverse direction (Figure 2.5).

An example input profile showing the relationship between constant or dynamic loads, and motion in forward and reverse is shown in Figure 2.5.

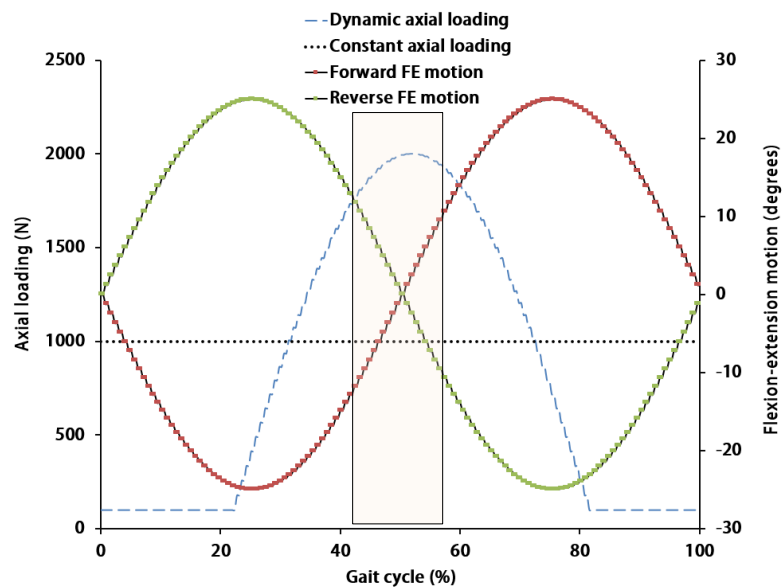


Figure 2.5 – Example graphical representation input profile for a forward test showing the relationship between the axial loads (constant and dynamic) and flexion-extension motion for testing on a pendulum friction hip simulator. Shaded region shows high velocity region where data is collected.

2.5.3 Summary of input parameters used

Using the ProSim simulator software, the input parameters shown in Table 2.3 were specified to replicate different loading conditions for THR components.

Table 2.3 - Summary table of comparative study input parameters for MOP and COC components (n = 6) on both pendulum friction and single station hip simulators

Load			Flexion-extension angle	
1kN constant	2kN constant	2kN peak, 100N swing phase load	±10°	±25°
✓				✓
	✓		✓	
	✓			✓
		✓	✓	
		✓		✓

2.5.4 Data Output

Using the ProSim simulator software, a test program was written to ensure the required load, FE motion and frequency variables were applied. The applied loads were ramped up during the first 10 cycles from 0N to the maximum specified load. All tests were conducted in forward and reverse direction (Figure 2.5), and the mean frictional torque calculated. Tests were run for 125 cycles, with data logged at 255 points per cycle. Data was recorded over five cycles at 30 cycle intervals (ie. 30-34...120-124).

The mean frictional torque was the absolute mean value calculated from the frictional torque logged at peak loading, and high velocity region of the FE motion and recorded for the forward and reverse directions (Figure 2.5) (Equation 2.3).

$$\text{Mean frictional torque (T)} = \frac{T_f - T_r}{2} \quad (2.3)$$

Where T_f is frictional torque in the forward direction and T_r is frictional torque in the reverse direction. T_f and T_r are both measured in Nm.

The friction factor was also calculated for the dynamic tests conducted, to allow comparison with existing literature (Equation 2.4).

$$\text{Friction factor (f)} = \frac{T}{R \times W} \quad (2.4)$$

Where R is the bearing radius (measured in m) and w is the peak applied load (measured in N)

Frictional torque data from forward and reverse directions should have similar magnitude but opposite polarity. These were analysed individually for all dynamic tests to ensure any inconsistencies were not masked by the mean frictional torque calculations. Mean frictional torque for the five data points in the high velocity region of the applied motion was calculated for each recorded cycle. A mean for all recorded cycles per test was then calculated and repeated for all six samples.

2.5.4.1 Statistical analysis

Statistical testing to determine the effects of the different test objectives on the mean frictional torques was conducted. With the data meeting the assumptions of normality and equal variance, a one-way ANOVA with a post-hoc analysis Tukey range test was conducted at significance level of 0.05 to assess the following hypotheses:

Objective 1: To examine the effects of increasing applied load on THR frictional torques

H_0 = No difference between the mean frictional torques measured under 1kN and 2kN constant loads and $\pm 25^\circ$ FE motion.

Objective 2: To examine the effects of increasing range of flexion-extension on THR frictional torques

H_0 = No difference between the mean frictional torques measured under $\pm 10^\circ$ and $\pm 25^\circ$ FE motion under both 2kN constant and dynamic load

Objective 3: To examine the effects of different bearing materials on THR frictional torques

H_0 = No difference between the mean frictional torques measured in MOP and COC bearings when tested under dynamic loading and $\pm 25^\circ$ FE motion.

2.6 Results

A torque-time plot is shown in Figure 2.6 showing measured frictional torques in forward and reverse.

Figure 2.10 shows the magnitude of measured frictional torques in both forward and reverse under 1kN and 2kN constant loads for 36mm MOP and COC bearings (n=6 for each group). Under these test conditions, the statistical analysis conducted failed to reject the null hypothesis that there was no difference between the frictional torques measured in forward and reverse directions.

In subsequent results, the mean frictional torque is presented, calculated using data collected in both forward and reverse.

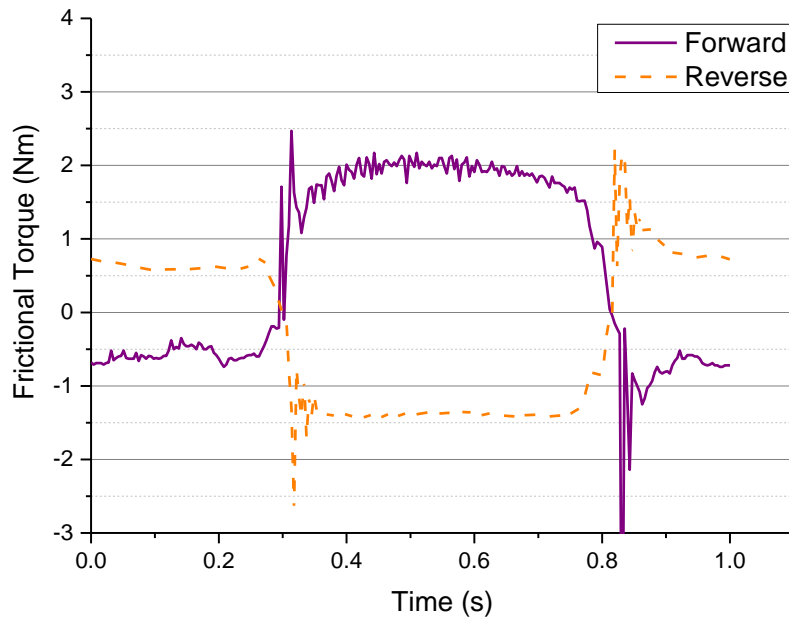


Figure 2.6 – Sample frictional torque trace measured in cycle number 64 of a 36mm MOP bearing tested under 1kN constant load with $\pm 10^\circ$ FE motion. Graphs shows frictional torque in forward and reverse directions

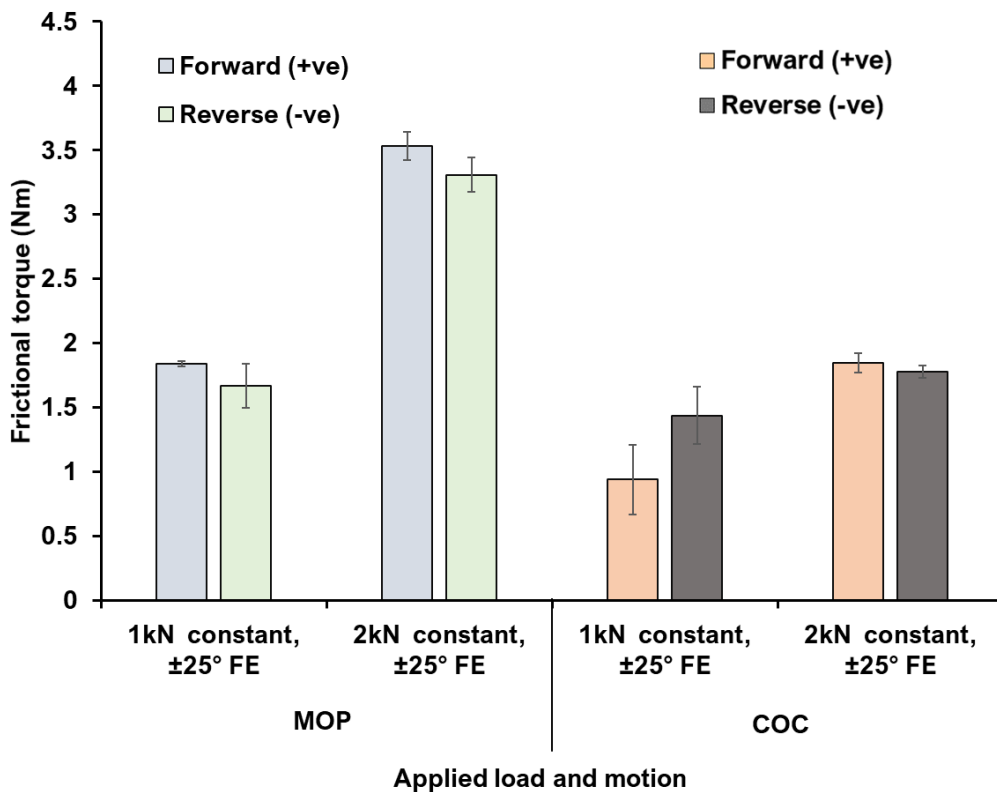


Figure 2.7 - Mean forward and reverse frictional torques measured in 36mm MOP bearings (n=6) and 36mm COC bearings (n=6) tested in 25% (v/v) bovine calf serum, under 1kN and 2kN constant loads with $\pm 25^\circ$ FE motion (mean $\pm 95\%$ confidence)

2.6.1 Assessing the effects of increasing load on the frictional torque of THRs

The mean frictional torque measured increased from 1.75 ± 0.12 Nm to 3.42 ± 0.06 Nm in 36mm MOP bearings, and 1.19 ± 0.07 Nm to 1.81 ± 0.08 Nm in 36mm COC bearings when the applied load increased from 1kN to 2kN (Figure 2.10).

The statistical analysis conducted rejected the null hypothesis which assumed that there was no significant difference between the frictional torques measured under 1kN and 2kN constant load for both MOP and COC bearings.

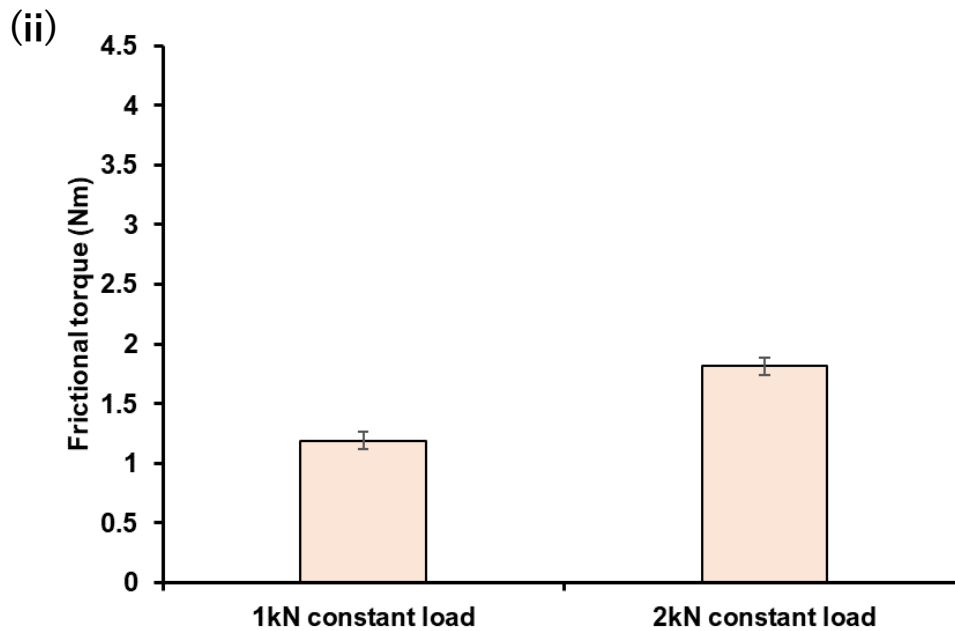
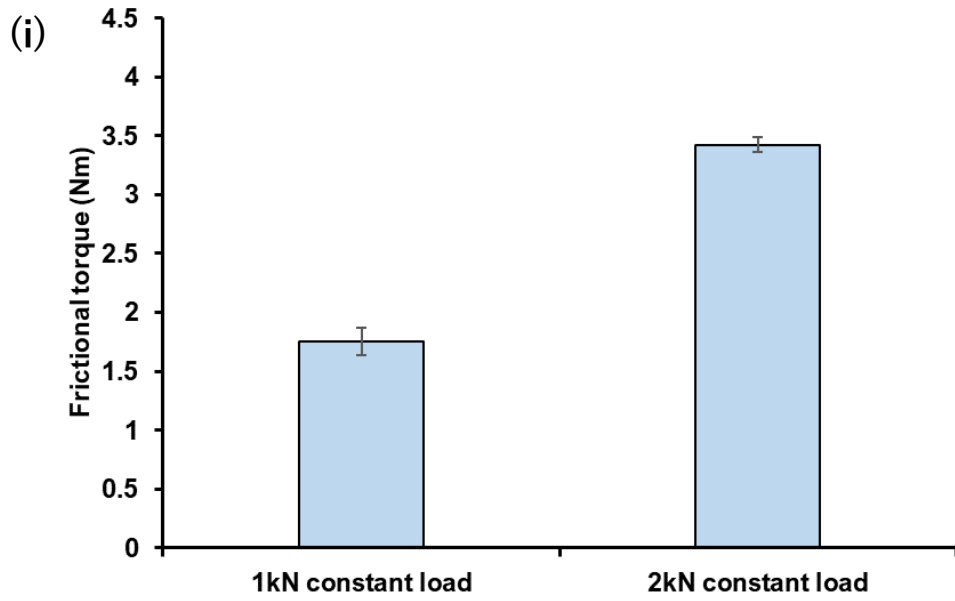


Figure 2.8 - Mean frictional torque measured in (i) 36mm MOP and (ii) 36mm COC bearings tested in 25% (v/v) bovine calf serum under 1kN and 2kN constant load and $\pm 25^\circ$ FE motion using a pendulum friction simulator (mean $\pm 95\%$ confidence, n=6)

2.6.2 Assessing the effects of increasing range of applied motion on the frictional torque of THRs

The mean frictional torques measured under 2kN constant load in the 36mm MOP bearings were 3.73 ± 0.24 Nm under $\pm 10^\circ$ FE motion, and 3.42 ± 0.06 Nm under $\pm 25^\circ$ FE motion. The mean frictional torques under 2kN constant load measured in the 36mm COC bearings were 1.98 ± 0.04 Nm under $\pm 10^\circ$ FE motion, and 1.81 ± 0.07 Nm under $\pm 25^\circ$ FE motion.

The mean frictional torques measured under dynamic loading in the 36mm MOP bearings were 1.49 ± 0.52 Nm under $\pm 10^\circ$ FE motion, and 1.74 ± 0.18 Nm under $\pm 25^\circ$ FE motion. The mean frictional torques measured under dynamic loading in the 36mm COC bearings were 1.12 ± 0.13 Nm under $\pm 10^\circ$ FE motion, and 1.17 ± 0.49 Nm under $\pm 25^\circ$ FE motion.

The statistical analysis conducted failed to reject the null hypothesis under all tested conditions, indicating that for the samples tested there was no significant difference when the applied FE motion was increased from $\pm 10^\circ$ to $\pm 25^\circ$ for both MOP and COC bearings.

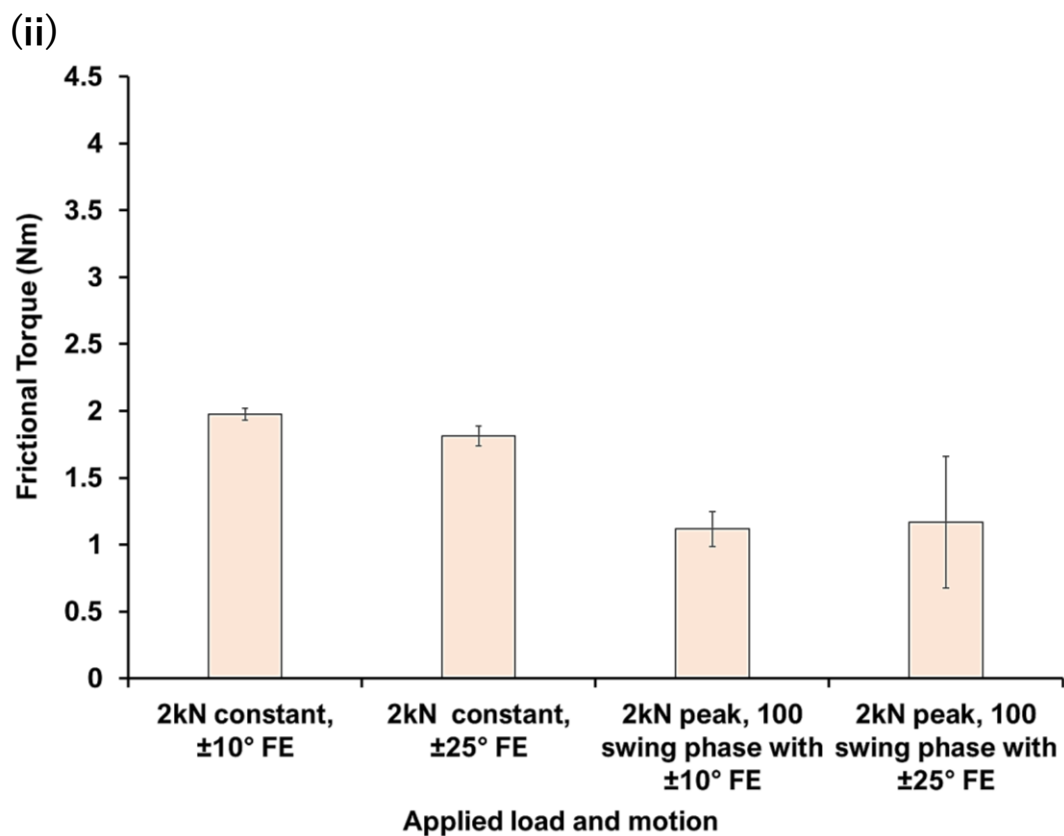
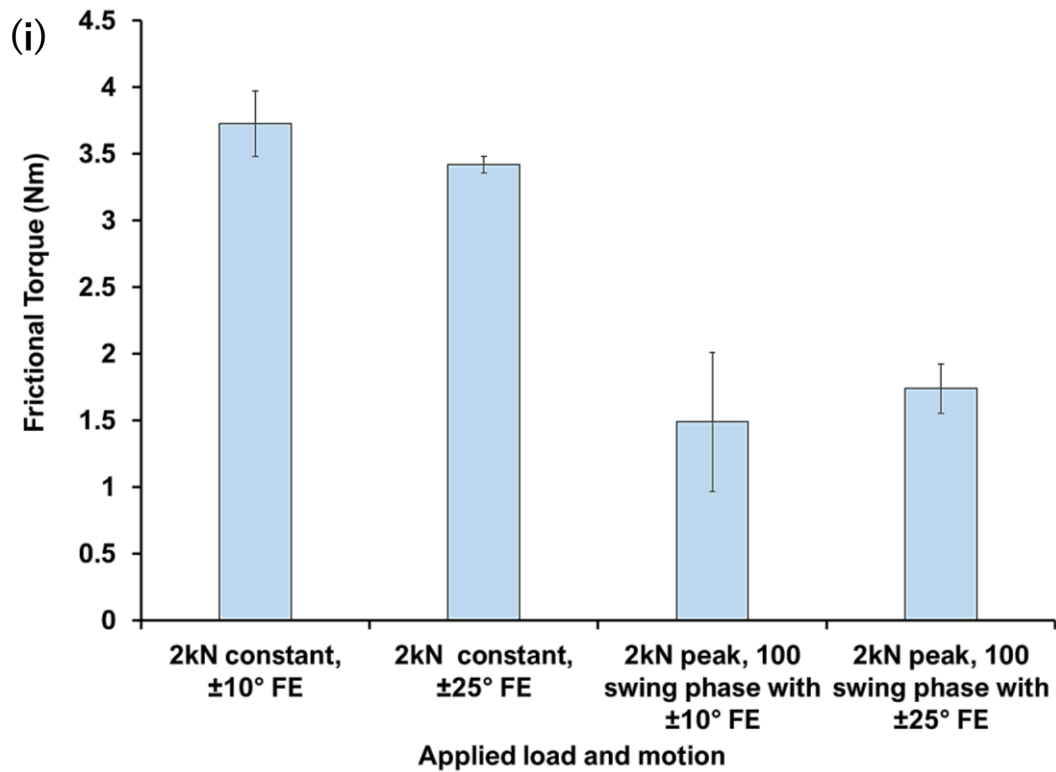


Figure 2.9 - Mean frictional torque measured in (i) 36mm MOP and (ii) 36mm COC bearings tested under both 2kN constant load and 2kN peak load with 100N swing phase load, and two ranges of motion ($\pm 10^\circ$ and $\pm 25^\circ$ FE) using a pendulum friction simulator (mean $\pm 95\%$ confidence, n=6)

2.6.3 Assessing the effects of materials combination on the frictional torque of THRs

The mean frictional torque measured under dynamic loading and $\pm 25^\circ\text{FE}$ motion was 1.74 ± 0.18 Nm in the 36mm MOP bearings and 1.17 ± 0.49 Nm in 36mm COC bearings.

Using equation 2.4, these measured frictional torques were used to derive the friction factor. The friction factor for the MOP bearings was 0.48 Nm and 0.03 Nm for the COC bearings.

The statistical analysis conducted rejected the null hypothesis, and indicated that there was a statistically significant difference between the frictional torques measured in MOP and COC bearings.

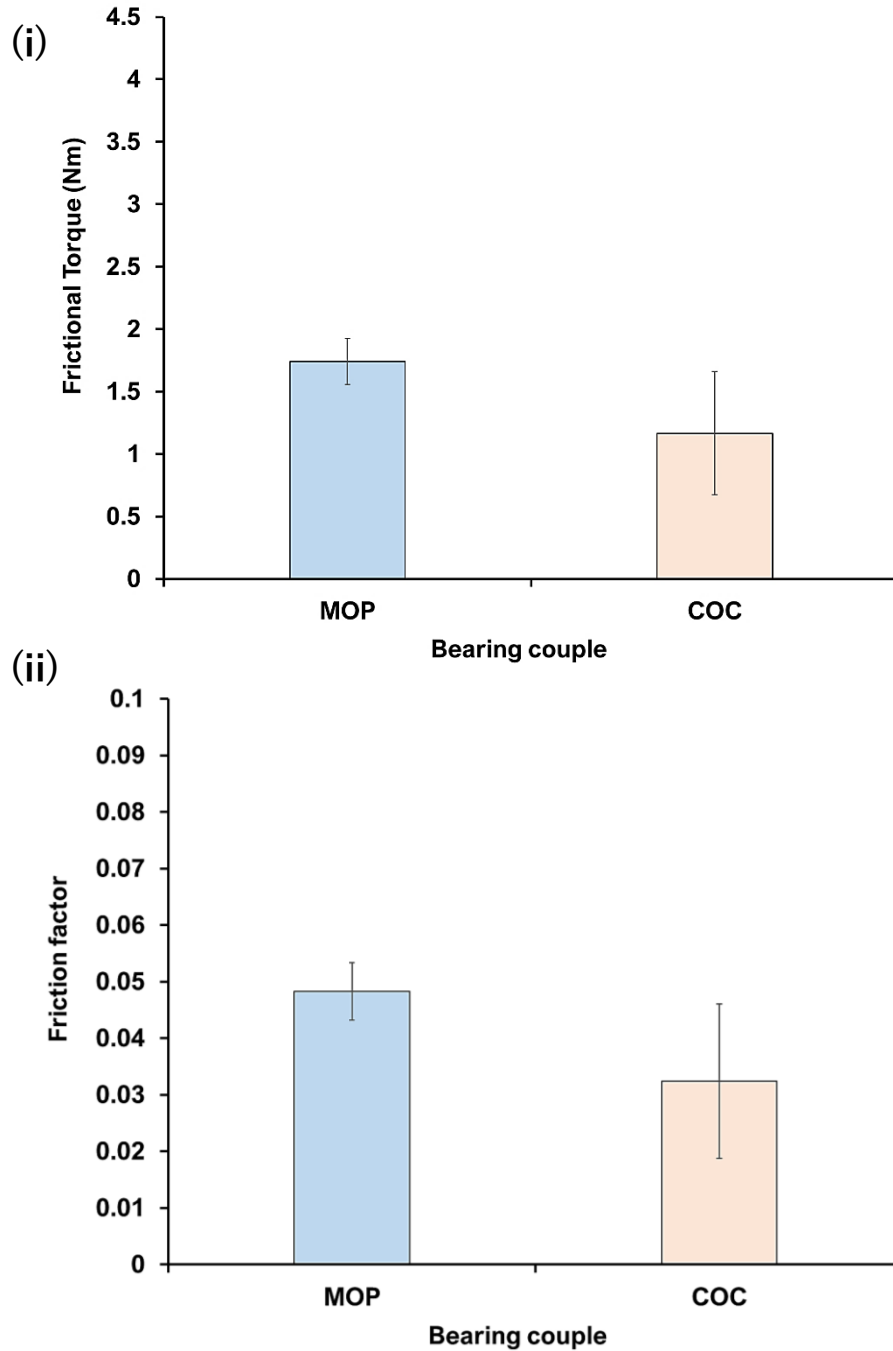


Figure 2.10 - (i) Mean frictional torque and (ii) mean friction factor measured in 36mm MOP and 36mm COC bearings tested under 2kN peak load with 100N swing phase load and $\pm 25^\circ$ FE motion using a pendulum friction simulator (mean $\pm 95\%$ confidence, n=6)

2.7 Discussion

This study assessed the frictional response of 36mm MOP and COC bearings under different loading and two ranges of FE motion using a pendulum friction hip simulator to obtain comparative data for subsequent testing on a multi-axis single station hip simulator. In addition to presenting frictional torque data, results from the dynamic loading conditions were reported as friction factors to aid comparison with published literature.

There was an interest in investigating the frictional response of 36mm diameter THRs as clinical reports had indicated increased failure rates for diameters of 36mm and above for hard-on-soft bearings, supporting theoretical suggestions of large diameters increasing frictional torque in bearings (Charnley, 1961; NJR, 2017). More recent studies have assessed frictional behaviour of 36mm THRs (Brockett *et al.*, 2013), although majority of previously conducted studies focussed on smaller diameters (22-32mm) (Unsworth, 1978; Gore, Higginson and Kornberg, 1981; Unsworth and Percy, 1988; Saikko, 1992; Scholes and Unsworth, 2000; Scholes *et al.*, 2000; Wimmer *et al.*, 2001; Brockett *et al.*, 2007).

In previous studies with differing bearing sizes, despite other factors such as type of lubricant and applied loads also differing, the friction factors calculated in this study were found to be of the similar order of magnitude. The results also indicated lower friction factors in COC bearings than MOP bearings, similar to that of published literature (Scholes and Unsworth, 2000; Brockett *et al.*, 2007). The friction factor of 0.032 (± 0.01) for 36mm COC bearings was similar to that found by Brockett *et al.* (2013), indicating similarities between the present study and the literature. The friction factor of 36mm MOP bearings was found to be 0.048 (± 0.005). It is important to note that the friction factors in this study and that of Brockett *et al.* (2013) for 36mm bearings are lower than those conducted for 28mm bearings in previous studies shown in Table 2.4 (Scholes and Unsworth, 2000; Brockett *et al.*, 2007), even though large diameters have been reported to

have higher frictional torques (Longaray *et al.*, 2013). Having tested under similar load, motion and frequency conditions, this difference could potentially be due to factors such as protein concentration and subtleties in the test set up due to differences in the test machines.

According to the equation of friction force, for a given friction coefficient the friction force is proportional to applied normal load (Johnson, 2011). This implied that for this study, as long as the bearing size remained the same, the frictional torque output will be proportional to the applied load. While this study did observe an increase when the applied load was doubled from 1kN to 2kN, the measured frictional torques for both 36mm MOP and COC bearings did not double.

A comparison of this study results with published literature with similar test conditions is shown in Table 2.4. Unless otherwise stated, the quoted friction factors in Table 2.4 are for 36mm nominal diameter bearings tested under a 2kN peak load, 100N swing phase load and $\pm 25^\circ$ FE motion with 25% bovine calf serum as a lubricant in a pendulum type friction hip simulator.

Studies conducted on a free pendulum simulator under static load, where damping resulted in an assessment/comparison of different swing velocities have shown that THR frictional torques remain constant even as range of the motion decreased over time (Sonntag *et al.*, 2017). While it was not expected that comparing the two FE angles would find significant differences in measured frictional torque, it was still important to assess these potential effects as future tests under adverse conditions may have needed to be conducted under limited motion conditions.

While there was some agreement in the present findings with published literature, the results are at risk of Type II errors due to low statistical power resulting from the small sample sizes used. Further testing will be required to gather more data

with an increased sample size, to increase the statistical power and reduce the chance of Type II errors.

Table 2.4 - Comparison of mean friction factors for serum-lubricated 36mm MOP & COC bearings under dynamic loading and a flexion-extension angle of $\pm 25^\circ$ measured in this study and published literature

Reference	Friction factor		Comments
	MOP	COC	
This study	0.048	0.032	-
Brockett <i>et al.</i>, 2013	-	0.03	-
Brockett <i>et al.</i>, 2007	0.062	0.041	28mm diameter
Scholes and Unsworth, 2000	0.06	0.04	28mm diameter

2.8 Conclusion

This study reported comparable results to existing studies and was deemed sufficient for use as a comparative data set for subsequent testing on the multi-axis hip simulator. The tests conducted in this chapter will be repeated for the comparative testing on the multi-axis hip simulator, and will assess the new simulator's ability to:

- i.* Assess symmetry of frictional torque data under constant loading of THRs
- ii.* Assess effects of increasing constant load on the frictional torques of THRs
- iii.* Assess the effects of increasing range of applied motion on the frictional torques of THRs
- iv.* Assess effects of materials combination on the frictional torques of THRs

CHAPTER THREE

Comparison of two multi-axis systems for the measurement of frictional torques in total hip replacements

3.1 Introduction

High friction at the articulating interfaces of THRs has been hypothesised to be involved in a range of failure modes. Besides potentially accelerating wear, high friction may also contribute to the mechanical loosening of components by directly introducing shear stresses at the bone–implant interface or indirectly by accelerating corrosion mechanisms at the femoral head-neck junction (Bergmann *et al.*, 2012; Bishop *et al.*, 2013; Damm *et al.*, 2013). The assessment of friction at the articulating interfaces of THRs has evolved from the use of free pendulum systems, simplified tribometers (McKellop *et al.*, 1981; Dowson *et al.*, 1985; Saikko, 1993) to uni-axial (pendulum-type) friction hip simulators (Scholes, Unsworth and Goldsmith, 2000; Williams *et al.*, 2006; Brockett *et al.*, 2007; McMinn, 2009) to the

use of biaxial rocking motion simulators (Bowsher and Shelton, 2001; Liao *et al.*, 2003; Saikko, 2009). The disadvantage of these previously used devices includes an inability to replicate bearing geometries, as was seen in tribometers (in the case of simplified tribometers), or the lack of replication of physiological motion and loading in uni- and biaxial simulators.

While multi-station experimental simulator studies for assessing the wear of THRs have advanced to include clinically relevant loading and motion cycles replicating gait, few studies have been able to replicate these physiological load and motion conditions and simultaneously assess friction at the bearing interface.

Using a multi-axis simulator (12-station AMTI hip simulator), Haider *et al.* (2016) measured the friction at the articulating interface of bearings that had been artificially abraded and compared to the friction measured in bearings with unabraded articulating surfaces. The study predictably reported that the friction increased for all bearing types tested with increased levels of abrasion.

Sonntag *et al.*, (2017) also reported the use of a multi-axis simulator (single station Minibionix 852 hip simulator) for measuring frictional torques at the articulating interface in THRs by investigating the effects of increased femoral head diameter. Increases in femoral head diameter had previously been theoretically predicted to increase friction moments in THRs (Morlock *et al.*, 2011; Malik, 2015). In agreement with the theoretical predication, this study found that measured frictional torques increased when the femoral head diameter increased from 28mm to 40mm.

In this chapter, two electromechanical measuring systems were assessed for the purpose of detecting the frictional torque at the articulating interface of total hip replacements within a multi-axis single station hip simulator (SSHS). The two systems were (i) an embedded six-axis load cell in the SSHS (ii) a custom-built biaxial friction measuring subsystem.

The single station hip simulator (SSHS) was newly acquired by the Institute of Medical and Biological Engineering and had capacity to simulate more representative physiological load and motion, and measure frictional torques in the three orthogonal axes (compared to the pendulum friction simulator discussed in Chapter 2). The custom-built friction measuring subsystem was designed and developed by the author as a supplementary system on the SSHS for solely measuring frictional torques in the two horizontal axes, while utilising the load and motion capabilities on the SSHS. Further details of the subsystem design are provided in Appendix 8.1.

The overall aim of this chapter was therefore to analyse the functional capacities of the two multi-axis systems and to determine their capability for robustly measuring the frictional torques present at the bearing interface of total hip replacements.

3.2 The two multi-axis friction measuring systems

In this chapter, two multi-axis friction measuring systems were considered. These are described below:

3.2.1 Single Station Hip Simulator (SSHS)

The SSHS was an electromechanically operated anatomical wear and friction simulator for hip replacements (Figure 3.1) (ProSim, UK). The simulator was set up to mount THR components in a physiological orientation, with the acetabular cup assembly positioned superior to the femoral head component.

The simulator was equipped with five motor drives, which controlled axial loading, flexion-extension and abduction-adduction motion, internal-external rotation as well as medial-lateral (ML) load and displacement independently or simultaneously. Anterior-posterior displacement was passive.

A six-axis load cell was located above the acetabular cup component and was used to monitor the forces and moments in all three orthogonal axes. All axes of motion and displacement were driven by electromechanical actuators (Baldor, Arizona - USA). The ranges of load, motion and displacement available on the SSHS were as follows:

- **Axial loading**

The SSHS was capable of applying 0-5kN constant or dynamic vertical load (y-axis) through the acetabular cup to the femoral head via a cam (Figure 3.1). This had a 1% non-repeatable error of $\pm 50\text{N}$.

- **Flexion-extension (FE) motion and torque**

The SSHS had a range of $\pm 60^\circ$ FE motion, applied by moving the femoral head component. This movement was controlled by an electromechanical motor with a sensitivity of 0.03° . FE motion is illustrated as rotation about x-axis (Figure 3.1). The maximum allowable range of measured torque for this motion was $\pm 100\text{Nm}$, with a 1% non-repeatable error of $\pm 1\text{Nm}$.

- **Abduction-adduction (AA) motion and torque**

The SSHS had a range of $\pm 25^\circ$ AA motion, applied by moving the femoral head component. This movement was controlled by an electromechanical motor with a sensitivity of 0.03° . AA motion is illustrated as rotation about z-axis (Figure 3.1). The maximum allowable range of measured torque for this motion was $\pm 100\text{Nm}$, with a 1% non-repeatable error of $\pm 1\text{Nm}$.

- **Internal-external (IE) rotation and torque**

The SSHS had a range of $\pm 25^\circ$ IE rotation, applied by rotating the femoral head component on-axis (about the y-axis) (Figure 3.1). This movement was controlled by an electromechanical motor with a sensitivity of 0.03° . The maximum allowable range of measured torque for this motion was $\pm 50\text{Nm}$, with a 1% non-repeatable error of $\pm 0.5\text{Nm}$.

- **Medial-lateral (ML) force and displacement**

The ML axis was coincident with the z-axis (Figure 3.1 **Error! Reference source not found.**). The SSHS had a range of 0-2kN ML force and 5mm ML displacement, applied through the acetabular cup component. This was facilitated via an additional force and displacement sensor. ML force measurements had a 1% non-repeatable error of $\pm 20\text{N}$, and a sensitivity of 0.2mm for ML displacement.

- **Anterior-posterior (AP) force and displacement**

The AP axis was coincident with the x-axis (Figure 3.1). Displacement in the AP direction was passive and free-floating, with a maximum allowable displacement of $\pm 10\text{mm}$. The force generated in the AP direction was however measured by the six-axis load cell, with a 1% non-repeatable error of $\pm 20\text{N}$.

All load, motion and displacement/translation capacities of the SSHS, described in this section, were programmable using the custom ProSim HipSim software on the accompanying personal computer.

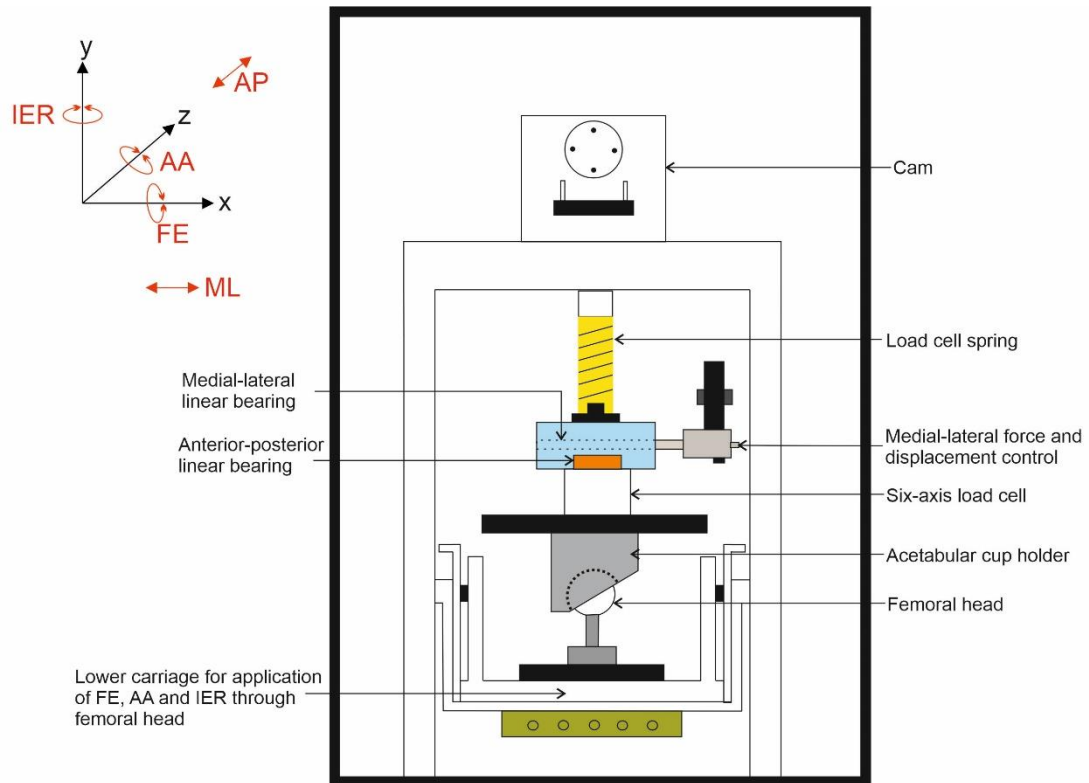


Figure 3.1 – Schematic of the Single Station Hip Simulator (SSHS)

3.2.2 Modified SSHS with a custom-built friction measuring subsystem

A custom-built biaxial friction measuring subsystem was developed and integrated into the SSHS, described in section 3.2.1, for detecting the frictional torques at the bearing interface of total hip replacements.

The measurement of THR friction by the subsystem was via two tension-compression load cells (load capacity 445N) vertically positioned at the level of the bearing interface in the FE and AA directions (**Error! Reference source not found.**). There was no measurement in the IER direction because implementing a torque measuring system for the on-axis rotation was considered complex, out of scope and budget for this design iteration.

A universal joint was positioned above the acetabular cup holder such that the two rotations possible at the pivot were in the FE and AA directions only. The design intent of the subsystem was such that the cup holder rotated about the universal

joint in response to any friction at the head and liner articulating interface, applying load to the subsystem load cells. A similar setup had been reported in literature in the original pendulum-type simulators where floating hydrostatic bearings ensured transfer of frictional torques in the THR bearings directly to the piezoelectric transducer (Dowson *et al.*, 2003). The load cells were attached to a mounting frame via the use low friction linear bearings, and via rigid attachments to the acetabular cup holder and mounting frame (**Error! Reference source not found.**). Additional linear bearings were used to allow overall subsystem superior-inferior and medial-lateral translation to accommodate axial force application and medial-lateral displacement during testing. Post-assembly modifications of the subsystem introduced a 20N/mm spring as a counterweight mechanism to rectify posterior leaning of the subsystem in the FE direction only (See Appendix 8.1).

Due to space constraints, the AA motion on the modified SSHS was limited to a range of the +25 to -10°.

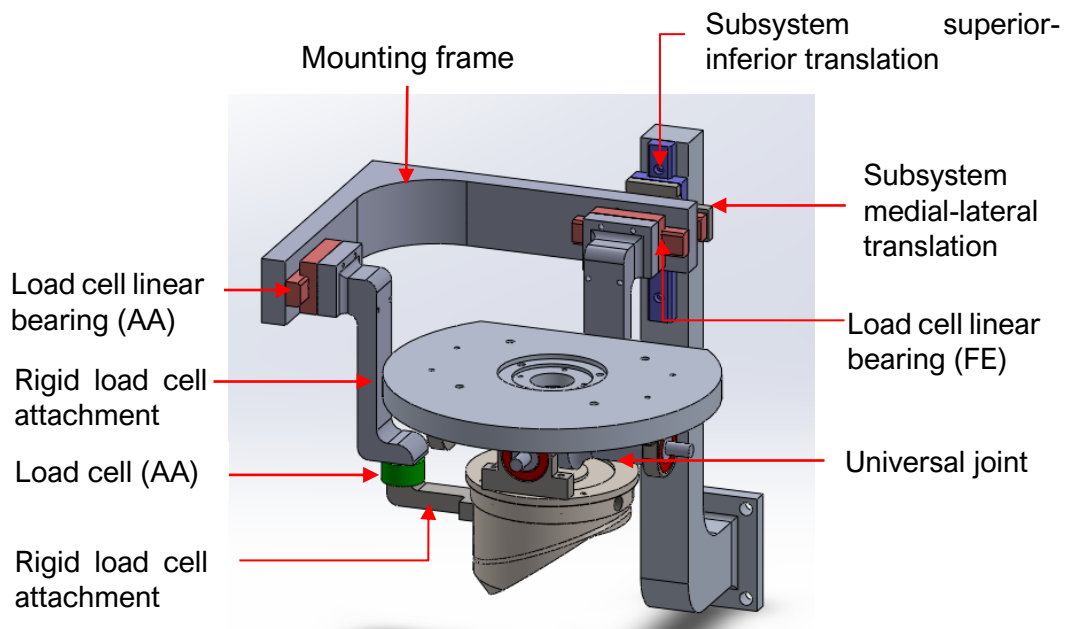


Figure 3.2 – CAD assembly of subsystem, showing positioning of the tension-compression load cells (AA direction only shown) and universal joint, including all supporting structures.

3.2.3 Comparison of capabilities of both systems

The table in this section (Table 3.1) provides a summary of the main functionalities on both systems.

Table 3.1 – Comparison of SSHS and modified SSHS capabilities

	SSHS	Modified SSHS with subsystem
Component orientation	Physiological	Physiological
Actuator	Electro-mechanic	Electro-mechanic
Transducer	Six-axis load cell	2 x uniaxial load cell
Axial load	0-5kN	0-5kN
Flexion-extension (FE)	±60°	±60°
Internal-external rotation (IER)	±25°	±25°
Abduction-adduction	±25°	+25 to -10°
Medial-lateral load	±1kN	±1kN
Medial-lateral displacement	±5mm	±5mm
Anterior-posterior displacement	±10mm (passive)	±10mm (passive)
Measure FE torque?	Yes	Yes
Measure AA torque?	Yes	Yes
Measure IER torque?	Yes	No

3.3 Calibration Methods

3.3.1 SSHS calibration

Using custom designed fixtures and an externally calibrated precision device (reference load cell) of capacity 0-5kN (Omegadyne, Connecticut- USA), force, torque and displacement functions of the SSHS were calibrated using standard procedures developed by the manufacturer ProSim, UK.

Calibration of the SSHS system was performed by replacing THR bearings with a calibrated precision device fitted with a convex tip applied to a pressure plate with a shallow concave depression. The six-axis load cell was calibrated for loads (eg 100, 750, 1500, 2250, 3000N) within its range using an externally calibrated reference load cell. Using the least-squares method, deviations and offsets were minimised and used to generate calibration coefficients in all degrees of freedom for analogue to digital signal conditioning to produce output forces and moments (Figure 3.3).

Custom calibration fixtures were manufactured to ensure repeatable positioning of the reference load cell for each axis that was calibrated. Angular position was calibrated using a digital protractor (Mitutoyo, Japan) and displacement was calibrated using calibrated slip gauges.

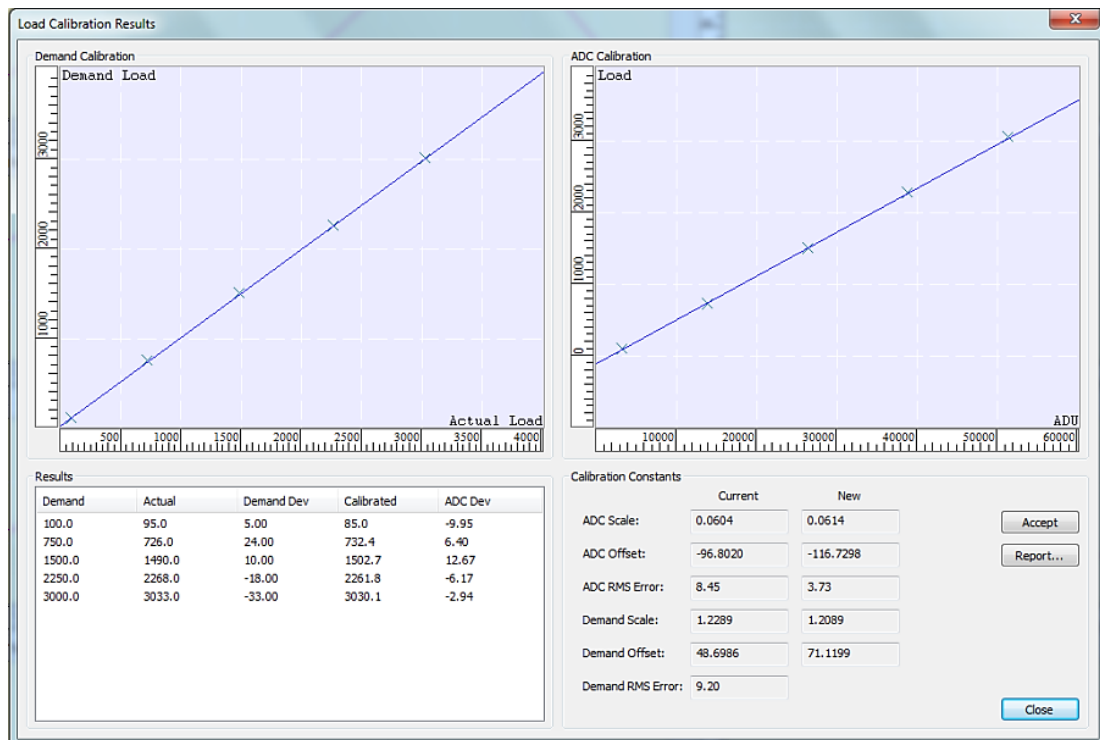


Figure 3.3 – Example screenshot of GUI screen generated during SSHS axial force calibration

3.3.1.1 Further static verification of six-axis load cell torque measurement

Calibrated masses of 0.1, 0.2, 0.4, 0.6, 0.8 and 1kg were positioned at arbitrary pre-determined distances (95mm and 105mm) via a temporary lever arm fastened to the top flange (at the location of the load cell) as an independent method to verify the level of error of the six-axis load cell torque measurement following SSHS calibration.

Verification of the torque measurements by the six-axis load cell was conducted in both positive and negative directions of the two horizontal axes (FE and AA). For each given mass and distance, instantaneous measurements from the six-axis load cell were taken. These tests were repeated three times.

Linear regression between the expected torque (based on applied mass and distance) and the measured torque by the six-axis load cell resulted in $R^2 = 0.99$ for all positive and negative directions of FE and AA measurements, in agreement with the outputs of the SSHS calibration.

3.3.2 Modified SSHS with friction measuring subsystem calibration

In addition to the calibration steps described in section 3.3.1 for the SSHS, the uniaxial load cells of the subsystem were also calibrated for repeatable data collection.

Both uniaxial load cells of the subsystem were calibrated using a universal testing machine (Instron® 3366, 500N load cell, Instron® UK). Using the universal testing machine, static loads of 10, 20, 50, 100, 200 and 400N were independently applied to each rigidly mounted load cell. This was repeated at the following sampling rates; 10, 20, 50, 100, 500 and 1000Hz. Linear regression between the applied static loads and measured raw voltage outputs resulted in $R^2 = 0.9995$ at 1000Hz for both load cells. The R^2 values were lower at lower sampling rates due to the collection of fewer data points for the given sample time. 1000Hz was therefore identified as the optimum sampling rate as per the calibration procedure.

3.4 Data Collection

All tests conducted on both multi-axis systems were run for 125 cycles, with a motion frequency of 1Hz (average walking speed as defined in ISO 14242-1:2014). Applied loading during all testing was ramped up gradually for the first 10 cycles. System-specific data collection characteristics are provided in the following sections.

3.4.1 Single Station Hip Simulator

Data collected by the six-axis load cell was logged and recorded via the HipSim software at a sampling rate of 255Hz. The outputs of the SSHS were:

- i. Axial force (F_Y)
- ii. Angular motion (FE, AA and IE)
- iii. Torques in FE direction (M_X)
- iv. Torques in AA direction (M_Z)
- v. Torques in IE direction (M_Y)
- vi. Lateral force in AP direction (F_Z)
- vii. Lateral force in ML direction (F_X)

3.4.2 Modified SSHS with friction measuring subsystem

The data collected following modification of the SSHS to include the friction measuring subsystem included both (i) data outputs from the SSHS six-axis load cell and (ii) data outputs from the uniaxial subsystem loads cells.

Data outputs from the SSHS were identical to those listed in Section 3.4.1. Data collected by the uniaxial subsystem load cells was logged and recorded via a data acquisition device (Model type USB 6351 supplied by National Instruments, UK) at a sampling rate of 1000Hz. An additional connection (independent of the SSHS normal data acquisition) was made from the axial force motor drive to the subsystem data acquisition device. This was done to ensure that the data collected from the subsystem load cells were appropriately synchronised with other functions of the SSHS. A graphical user interface (GUI) was developed in LabVIEW™ and was required to handle and process the data acquired from the subsystem load cells.

The outputs of the modified SSHS with a friction measuring subsystem were:

Subsystem load cells

- i. Axial force (F_Y)
- ii. Force measured by FE subsystem load cell (F_{Y_FEcell})
- iii. Force measured by AA subsystem load cell (F_{Y_AAcell})

SSHS six-axis load cell

- iv. Axial force (F_Y)
- v. Angular motion (FE, AA and IE)
- vi. Torques in FE direction (M_X)
- vii. Torques in AA direction (M_Z)
- viii. Torques in IE direction (M_Y)
- ix. Lateral force in AP direction (F_Z)
- x. Lateral force in ML direction (F_X)

3.5 Frictional torque analysis

3.5.1 THR frictional torque determined using the six-axis load cell measurement on the SSHS

Given the relatively low speeds, it was assumed that moments of inertia would be negligible, and the system was in static equilibrium. It was also assumed that deformations were small, and therefore the setup behaved as a rigid body. The frictional torques of THRs in the two horizontal axes (FE and AA) were therefore determined by developing equations for the vertical and horizontal force, and moment equilibria, using free body diagrams (FBD).

Considering the acetabular cup holder as a free body, the following forces and moments are acting up on it:

At the load cell: The axial force F_Y applied by the simulator and the resistive moment (M_x and M_z) generated as the load cell is prevented in rotating about the x-axis and z-axis respectively.

At the point of contact with the femoral head in the polar region of the cup: The friction force F_R of the rotating femoral head which occurs tangential to the surface and the normal reaction force F_N .

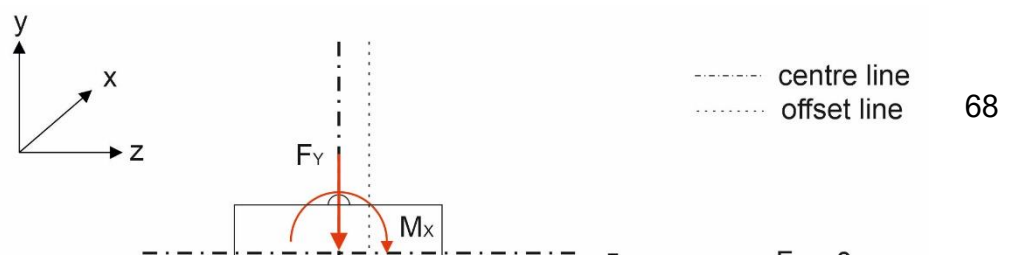
In an ideal setup, the presence of frictionless lateral bearings (in both AP and ML directions) would decouple the lateral forces at the joint from the load cell and mean no lateral force could be measured by the six-axis load cell i.e., lateral force in AP direction (F_z) = 0 and lateral force in ML direction (F_x) = 0.

Rotations about each axis will be considered in the following sections, in turn, to derive the equations for the frictional torque in that axis.

Sagittal plane under FE motion (ideal conditions)

Considering only FE motion of the bearing, the free body diagram for the sagittal plane is shown in **Error! Reference source not found..** As the femoral head rotates, it rolls over the surface of the acetabular cup with increasing contact angle θ and the friction force increases until the static friction (F_R) is exceeded, causing the joint to slide.

A lateral offset (d) of the axial contact force (F_Y) from the centre of the load cell generates the measured moments M_x . The relationship between the lateral offset, the femoral head radius (r) and the contact angle was used to define the lateral offset.



In the sagittal plane under FE motion,

Sum of moments about point A = 0

$$M_x = F_y \cdot d \quad (3.1)$$

Sum of forces in the y-axis = 0

$$F_y = F_{NFE} \cos \theta + F_{RFE} \sin \theta \quad (3.2)$$

Sum of forces in the z-axis = 0

$$0 = F_{NFE} \sin \theta - F_{RFE} \cos \theta \quad (3.3)$$

From equation (3.3), $F_{NFE} \sin \theta = F_{RFE} \cos \theta$

$$\frac{F_{RFE}}{F_{NFE}} = \frac{\sin \theta}{\cos \theta} = \tan \theta$$

$$\text{However, by definition } \frac{F_{RFE}}{F_{NFE}} = \mu_{FE} \quad (3.4)$$

$\mu_{FE} = \tan \theta$; for small angles such as θ , $\tan \theta \approx \theta$

$$\text{Therefore, } \mu_{FE} = \theta \quad (3.5)$$

Where μ_{FE} is the coefficient of friction in the FE direction.

Determining offset (d)

$$d = r \sin \theta$$

For small angles such as θ , $\sin \theta \approx \theta$

$$\text{Then } d = r \theta$$

but from (3.5), $\mu_{FE} = \theta$

$$\text{so } d = r \mu_{FE} \quad (3.6)$$

substituting (3.6) into (3.1),

$$M_x = F_y \cdot r \mu_{FE}$$

$$\text{Therefore } \mu_{FE} = \frac{M_x}{F_y \cdot r}$$

where M_x and F_y are measured by the six-axis load cell and r is known based on the diameter of the THR bearing.

Coronal plane under AA motion (ideal conditions)

Considering only AA motion of the bearing, the free body diagram for the sagittal plane is shown in **Error! Reference source not found..**

A lateral offset (e) of the axial contact force (F_Y) from the centre of the load cell generates the measured moments M_Z . The relationship between the lateral offset, the femoral head radius (r) and the contact angle was used to define the lateral offset.

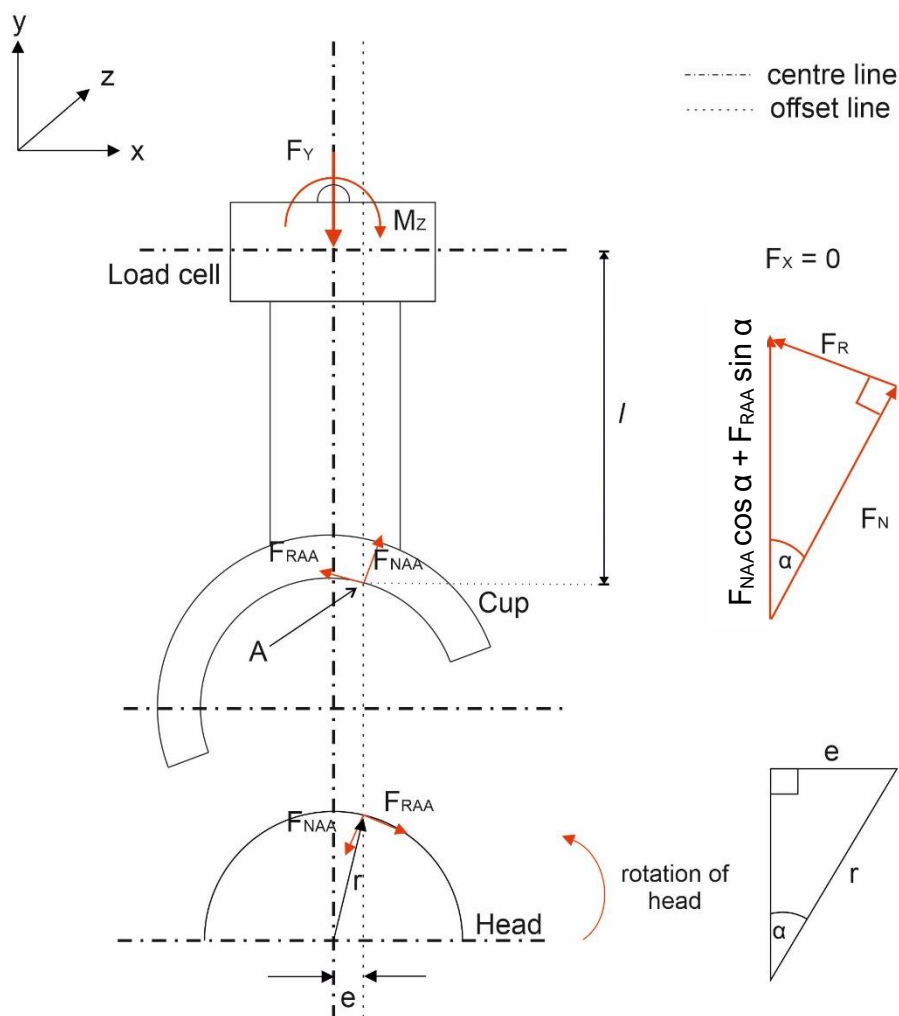


Figure 3.4 - Free body diagram of an ideal setup of the THR and SSS in the coronal plane, showing forces and moments on the system. This FBD considers AA motion such that the femoral head contacts the acetabular cup at point A, producing a normal force F_{NAA} and tangential friction force F_{RAA} .

In the coronal plane under AA motion,

Sum of moments about the z-axis = 0

$$M_Z = F_Y \cdot e \quad (3.7)$$

Sum of forces in the y-axis = 0

$$F_Y = F_{NAA} \cos \alpha + F_{RAA} \sin \alpha \quad (3.8)$$

Sum of forces in the z-axis = 0

$$0 = F_{NAA} \sin \alpha - F_{RAA} \cos \alpha \quad (3.9)$$

From equation (3.9), $F_{NAA} \sin \alpha = F_{RAA} \cos \alpha$

$$\frac{F_{RAA}}{F_{NAA}} = \frac{\sin \alpha}{\cos \alpha} = \tan \alpha$$

$$\text{However, by definition } \frac{F_{RAA}}{F_{NAA}} = \mu_{AA} \quad (3.10)$$

$\mu_{AA} = \tan \alpha$; for small angles such as α , $\tan \alpha \approx \alpha$

$$\text{Therefore, } \mu_{AA} = \alpha \quad (3.11)$$

Where μ_{AA} is the coefficient of friction in the AA direction.

Determining offset (e)

$$e = r \sin \alpha$$

For small angles such as α , $\sin \alpha \approx \alpha$

$$\text{Then } e = r \alpha$$

but from (3.5), $\mu_{AA} = \alpha$

$$\text{so } e = r \mu_{AA} \quad (3.12)$$

substituting (3.7) into (3.1),

$$M_Z = F_Y \cdot r \mu_{AA}$$

$$\text{Therefore } \mu_{AA} = \frac{M_Z}{F_Y \cdot r}$$

where M_Z and F_Y are measured by the six-axis load cell and r is known based on the diameter of the THR bearing.

3.5.1.1 Inclusion of lateral forces in the derivation of frictional torques

However, in reality, it is not possible to achieve completely frictionless bearings and therefore, lateral forces may arise due to friction in the lateral bearings and will impact the derived frictional torques as shown in the following sections:

Sagittal plane under FE motion

Considering only FE motion of the bearing, the free body diagram in the sagittal plane taking into account the presence of a lateral force is shown in Figure 3.6.

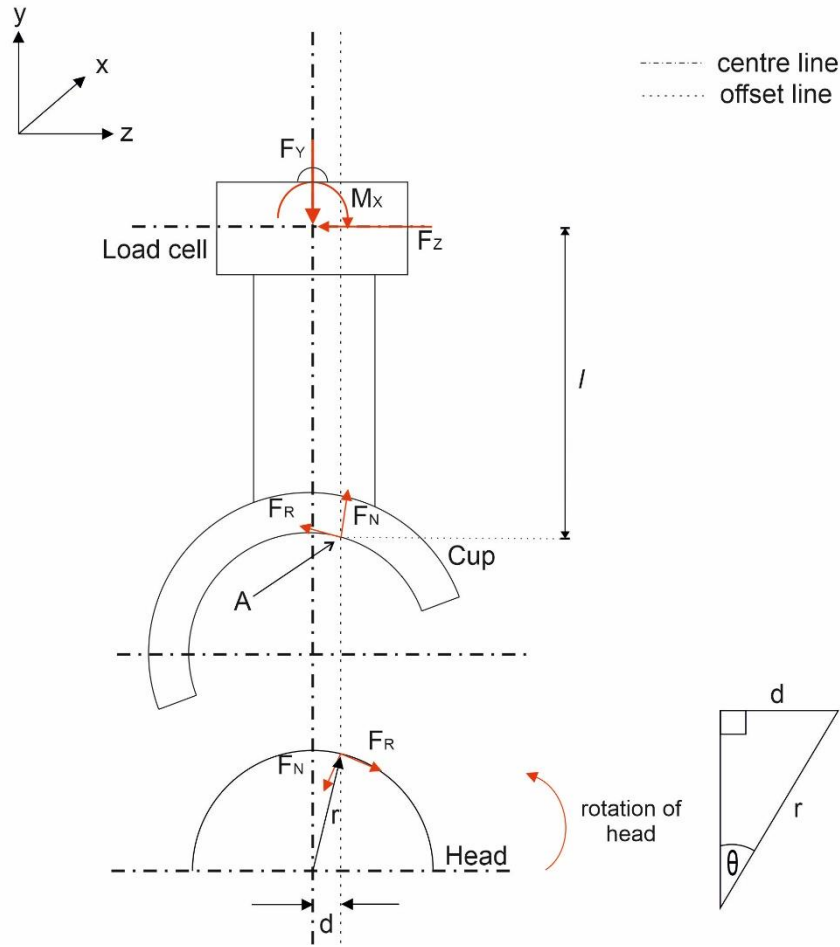


Figure 3.5 - Free body diagram of the representative THR and SSBS setup in the sagittal plane, showing forces and moments on the system. This FBD considers FE motion such that the femoral head contacts the acetabular cup at point A, producing a normal force F_{NFE} and tangential friction force F_{RFE} , and the presence of lateral force F_z

In the sagittal plane under FE motion,

$$\text{Sum of moments about A} = 0$$

$$M_x = F_y \cdot d - F_z \cdot l \quad (3.13)$$

$$\text{Sum of forces in the y-axis} = 0$$

$$F_y = F_{NFE} \cos \theta + F_{RFE} \sin \theta \quad (3.14)$$

$$\text{Sum of forces in the z-axis} = 0$$

$$F_z = F_{RFE} \cos \theta + F_{NFE} \sin \theta \quad (3.15)$$

Determining offset (d)

From equation (3.13), $M_X - F_Z \cdot l = F_Y \cdot d$

$$\text{Therefore, } d = \frac{M_X + F_Z \cdot l}{F_Y} \quad (3.16)$$

Where M_X , F_Z and F_Y are measured by the six-axis load cell, and l is the known distance from the centre of the load cell to the bearing interface.

Determining angle θ

$$\sin\theta = \frac{d}{r}; \theta = \sin^{-1} \frac{d}{r}$$

$$\text{for small angles, } \sin^{-1} \frac{d}{r} = \frac{d}{r},$$

$$\text{therefore } \theta = \frac{d}{r} \quad (3.17)$$

Where d is known from (3.16) and r is the known radius of the bearing.

Determining F_{NFE} and F_{RFE}

Resolving the vector forces at point A,

$$F_{RFE} = F_Z \cos \theta + F_Y \sin \theta \quad (3.18)$$

$$F_{NFE} = F_Y \cos \theta - F_Z \sin \theta \quad (3.19)$$

Determining the frictional torque in the FE direction (τ_{FE})

$$\text{By definition, } \tau_{FE} = F_{RFE} \cdot r \quad (3.20)$$

From Pythagoras theorem, $r^2 = (r \cos \theta)^2 + d^2$;

$$\cos \theta = \frac{\sqrt{r^2 - d^2}}{r} \quad (3.21)$$

Substituting equations (3.18) into (3.20)

$$\tau_{FE} = (F_Z \cos \theta + F_Y \sin \theta) \cdot r \quad (3.22)$$

Substituting (3.17) and (3.21) into (3.22)

$$\tau_{FE} = F_Z \left(\frac{\sqrt{r^2 - d^2}}{r} \right) \cdot r + F_Y \cdot \frac{d}{r} \cdot r$$

$$\tau_{FE} = F_Z \cdot \sqrt{r^2 - d^2} + F_Y d$$

Assuming r is much greater than d , $\sqrt{r^2 - d^2} = \sqrt{r^2} = r$

$$\tau_{FE} = F_Z \cdot r + F_Y \cdot d$$

But from (3.16), $d = \frac{M_X + F_Z \cdot l}{F_Y}$

$$\tau_{FE} = F_Z \cdot r + F_Y \left(\frac{M_X + F_Z \cdot l}{F_Y} \right)$$

$$\therefore \tau_{FE} = F_Z \cdot r + M_X + F_Z \cdot l \quad (3.23)$$

Where M_X and F_Z are measured by the six-axis load cell, r is the known radius of the bearing and l is the known distance from the centre of the load cell to the bearing interface.

Coronal plane under AA motion

Considering only AA motion of the bearing, the free body diagram in the coronal plane taking into account the presence of a lateral force is shown in Figure 3.7.

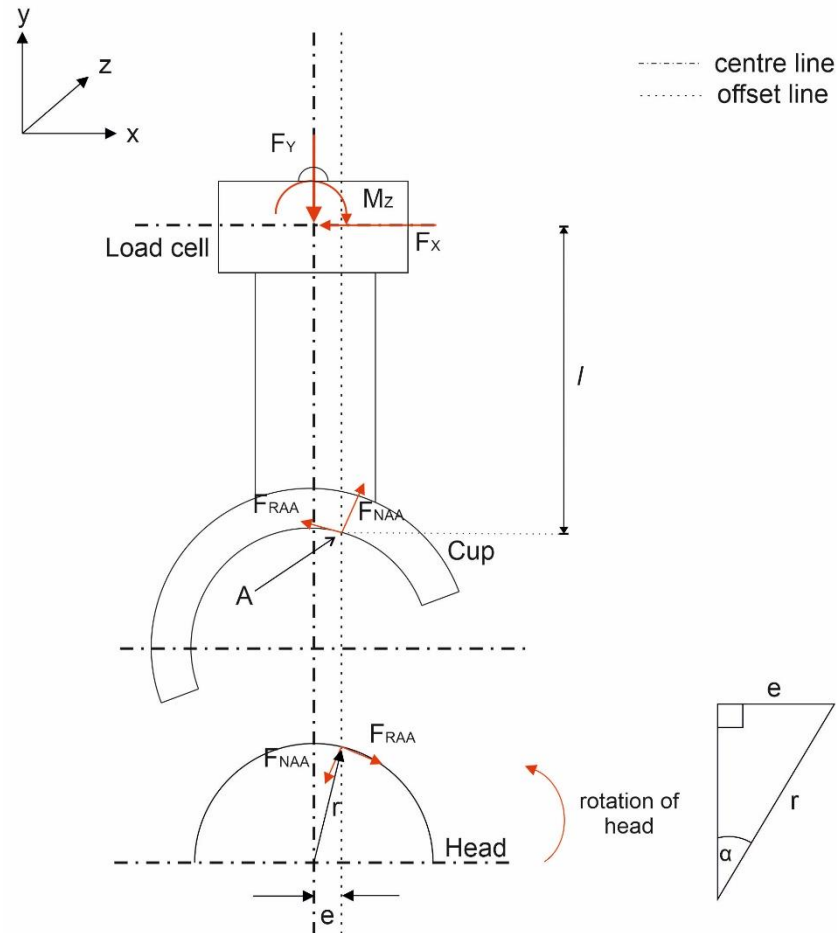


Figure 3.6 - Free body diagram of the representative THR and SSHS setup in the coronal plane, showing forces and moments on the system. This FBD considers AA motion such that the femoral head contacts the acetabular cup at point A, producing a normal force F_{NAA} and tangential friction force F_{RAA} , and the presence of lateral force F_x

In the coronal plane under AA motion,

Sum of moments about A = 0

$$M_Z = F_Y \cdot e - F_X \cdot l \quad (3.24)$$

Sum of forces in the y-axis = 0

$$F_Y = F_{NAA} \cos \alpha + F_{RAA} \sin \alpha \quad (3.25)$$

Sum of forces in the x-axis = 0

$$F_X = F_{RAA} \cos \alpha + F_{NAA} \sin \alpha \quad (3.26)$$

Determining offset (e)

From equation (3.24), $M_Z = F_Y \cdot e - F_X \cdot l$

$$\text{Therefore, } e = \frac{M_Z + F_X \cdot l}{F_Y} \quad (3.27)$$

Where M_z , F_x and F_y are measured by the six-axis load cell, and l is the known distance from the centre of the load cell to the bearing interface.

Determining angle α

$$\sin\alpha = \frac{e}{r}; \alpha = \sin^{-1}\frac{e}{r}$$

$$\text{but for small angles, } \sin^{-1}\frac{e}{r} = \frac{e}{r}$$

$$\text{therefore, } \alpha = \frac{e}{r} \quad (3.28)$$

Where e is known from (3.26) and r is the known radius of the bearing.

Determining F_{NAA} and F_{RAA}

Resolving the vector forces at point A,

$$F_{RAA} = F_x \cos \alpha + F_y \sin \alpha \quad (3.29)$$

$$F_{NAA} = F_y \cos \alpha - F_x \sin \alpha \quad (3.30)$$

Determining the frictional torque in the AA direction (τ_{AA})

$$\text{By definition, } \tau_{AA} = F_{RAA} \cdot r \quad (3.31)$$

Using Pythagoras theorem, $r^2 = (r \cos \alpha)^2 + e^2$;

$$\cos \alpha = \frac{\sqrt{r^2 - e^2}}{r} \quad (3.32)$$

Substituting equation (3.29) into (3.31)

$$\tau_{AA} = (F_x \cos \alpha + F_y \sin \alpha) \cdot r \quad (3.33)$$

Substituting (3.32) and (3.28) into (3.33)

$$\tau_{AA} = F_x \left(\frac{\sqrt{r^2 - e^2}}{r} \right) \cdot r + F_y \cdot \frac{e}{r} \cdot r$$

$$\tau_{AA} = F_x \cdot \sqrt{r^2 - e^2} + F_y \cdot e$$

Assuming r is much greater than e , $\sqrt{r^2 - e^2} = \sqrt{r^2} = r$

$$\tau_{AA} = F_x \cdot r + F_y \cdot e$$

But from (3.27), $e = \frac{M_z + F_x \cdot l}{F_y}$

$$\tau_{AA} = F_x \cdot r + F_y \left(\frac{M_z + F_x \cdot l}{F_y} \right)$$

$$\therefore \tau_{AA} = F_x \cdot r + M_z + F_x \cdot l \quad (3.34)$$

Where M_z and F_x are measured by the six-axis load cell, r is the known radius of the bearing and l is the known distance from the centre of the load cell to the bearing interface.

Transverse plane under IE rotation

Considering only IER of the bearing, the contact point would be in line with the axial load. However, since this contact involves a sphere (the femoral head) rotating on-axis at this point, a rigid free body method could not be used to derive the frictional torque. Under IE rotation only, there would also not be any lateral movement or forces expected, and therefore it can be assumed that;

$$\tau_{IER} = M_y \quad (3.35)$$

In conditions where there is motion in all three directions, it would still be expected that lateral offsets d and e , and lateral forces F_x and F_z would be very small, and their effects on τ_{IER} negligible. Equation (3.35) would still hold true.

The frictional torques in FE, AA and IER may be vector summed to produce an overall frictional torque acting on the acetabular cup component. This is provided in Equation 3.33.

$$\tau_{resultant} = (\tau_{FE}^2 + \tau_{AA}^2 + \tau_{IE}^2)^{1/2} \quad (3.36)$$

3.5.1.2 Conclusion

Although lateral forces were generated in the x - and z - axes of this setup, it was still possible to derive the coefficient of friction and the frictional torques at the

bearing interface of THRs tested using the SSHS. While the analysis in this section assumed that these lateral forces may have been generated due to friction in the lateral bearings of the SSHS, it is also possible that these may have been generated as a result of electronic crosstalk between the different channels. The effects of crosstalk and potential mitigations against its effects on the SSHS data output is further discussed in Section 3.6.1.

3.5.2 THR frictional torque determined using the two uniaxial load cell measurements of the subsystem

Based on the same assumptions as in Section 3.5.1, it was assumed that the system was in static equilibrium and that the parts behaved as rigid bodies. The frictional torques of THRs in two rotational axes (FE and AA) were determined by solving the three equilibrium equations in each plane. The forces and moments in the FE and AA directions were measured by the two uniaxial load cells of the subsystem.

The FBD for the acetabular cup, load cells and associated fixturing to the SSHS load cell is shown in Figure 3.9 and Figure 3.10. The forces acting on the free body diagram are as follows:

At pivot B: The axial force F_Y applied by the simulator and lateral forces (F_X and F_Z) caused by friction in the lateral bearings.

At the point of contact with the femoral head in the polar region of the cup: The friction force F_R of the rotating femoral head which occurs tangential to the surface and the normal reaction force F_N and reaction to the axial force $F_{Y_{CP}}$.

At FE subsystem load cell (Figure 3.9): The axial force on the uniaxial load cell ($F_{Y_{FEcell}}$), the off-axis lateral force $F_{Z_{FEcell}}$ and the moment on the loadcell (M_{FEcell}).

At AA subsystem load cell (Figure 3.10): The axial force on the uniaxial load cell (F_{Y_AAcell}), the off-axis lateral force F_{X_AAcell} and the moment on the loadcell (M_{AAcell}).

The axial force F_Y applied by the simulator to the acetabular cup component and the rotation of the femoral head results in a frictional reaction, tangential to the surface of the acetabular cup. The contact between the femoral head and acetabular cup occurs in the polar region of the assembly.

The presence of the universal joint decoupled the THR bearing and subsystem from the six-axis load cell positioned above.

Sagittal plane under FE motion

Considering only FE motion of the bearing, the free body diagram in the sagittal plane is shown in Figure 3.9.

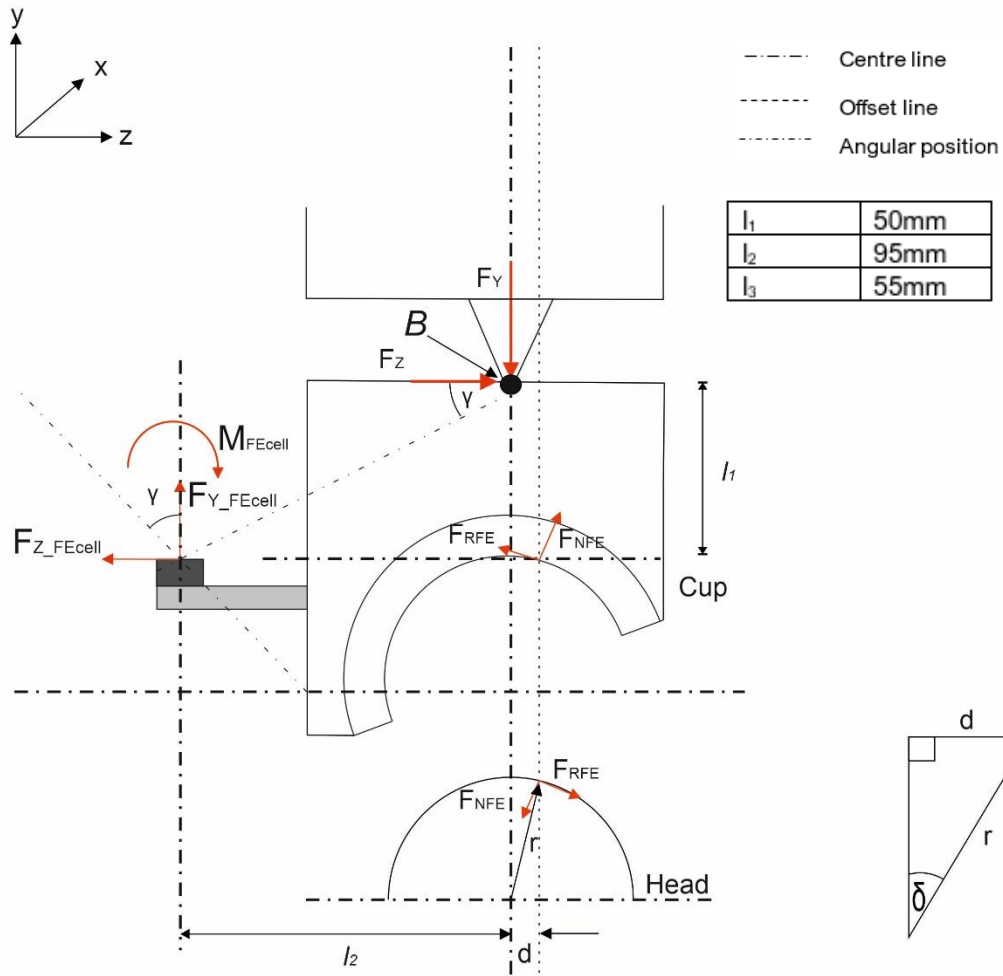


Figure 3.7 - Free body diagram of the subsystem on the SSHS, illustrating the position of the universal joint (pivot B), and the position of one uni-axial load cell in relation to the bearing (sagittal plane)

In the FE direction,

Sum of moments about B = 0

$$F_{Y_{CP}} \cdot d + F_{Z_{CP}} \cdot l_1 - F_{Y_{FEcell}} \cdot l_2 + F_{Z_{FEcell}} \cdot l_1 - M_{FEcell} = 0 \quad (3.37)$$

Where $F_{Y_{CP}} = F_{NFE} \cos \theta + F_{RFE} \sin \theta$ and $F_{Z_{CP}} = F_{NFE} \sin \theta - F_{RFE} \cos \theta$

Sum of forces in the y-axis = 0

$$F_Y = F_{NFE} \cos \delta + F_{RFE} \sin \delta + F_{Y_{FEcell}} \quad (3.38)$$

Sum of forces in the z-axis = 0

$$F_Z + F_{RFE} \cos \delta = F_{NFE} \sin \delta + F_{Z_{FEcell}} \quad (3.39)$$

Where F_Y is the axial force, d is the lateral offset, F_{Y_FEcell} is the vertical axial force on the subsystem load cell, M_{FEcell} is the moment at the subsystem load cell and F_{Z_FEcell} is the off-axis force on the subsystem load cell, F_{Y_CP} is the vertical component of forces F_{RFE} and F_{NFE} and F_{Z_CP} is the horizontal component of forces F_{RFE} and F_{NFE} .

$$\text{By definition, } \mu_{FE} = \frac{\tau_{FE}}{F_{NFE} \cdot r}; \text{ where } F_{RFE} = \mu_{FE} \cdot F_{NFE}$$

F_{RFE} is required to calculate frictional torque in the FE direction, τ_{FE} . Equations (3.37), (3.38) and (3.39) need to be solved in terms of the forces at the load cells to be able to obtain F_{RFE} . However, there are three equations and four unknown variables F_N , F_R , M_{FEcell} and F_{Z_FEcell} .

Coronal plane under AA motion

When considering only AA motion of the bearing, the free body diagram in the sagittal plane is shown in Figure 3.10. The same findings in the sagittal plane (FE direction) were true for this direction, where there were four unknown variables and three equations, and therefore the frictional torque in the AA direction (τ_{AA}) could not be determined.

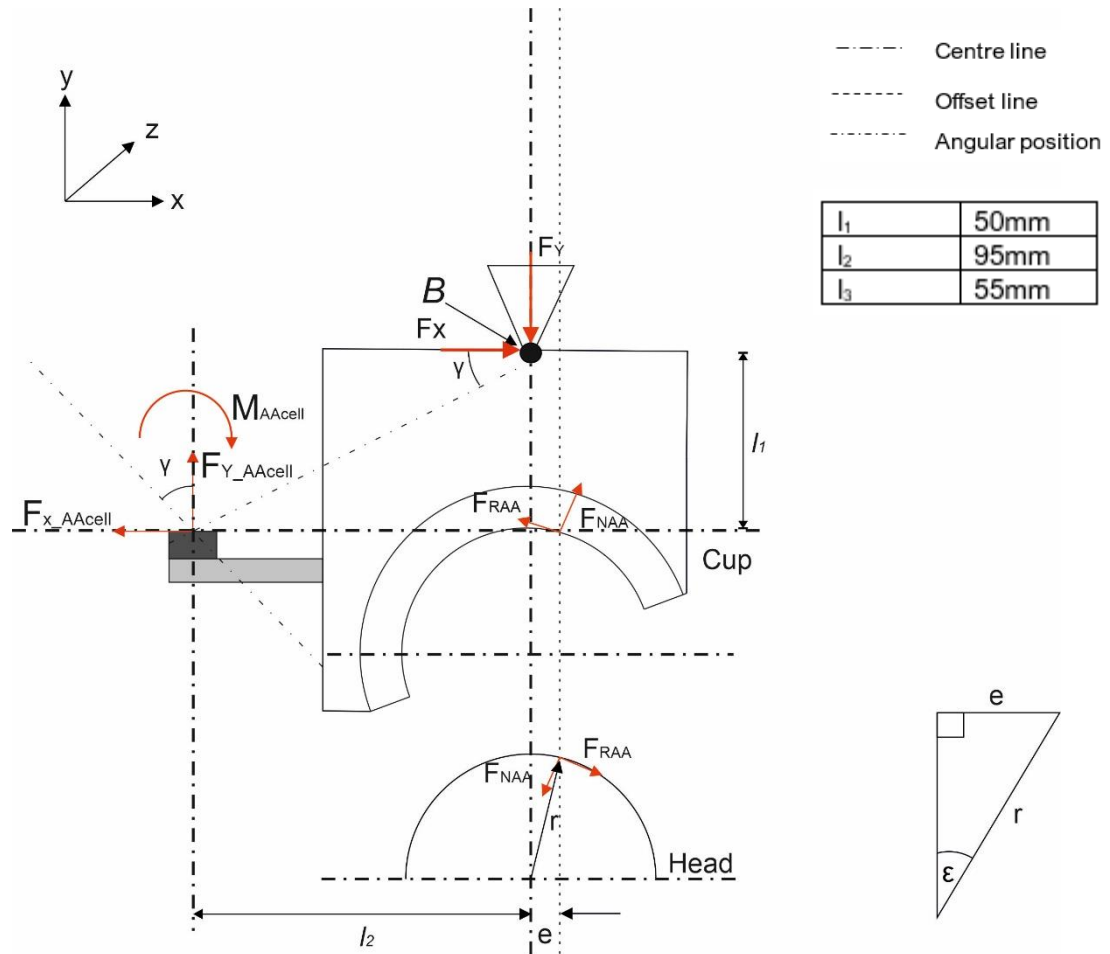


Figure 3.8 - Free body diagram of the subsystem on the SSHS, illustrating the position of the universal joint (pivot B), and the position of one uni-axial load cell in relation to the bearing (coronal plane).

3.6 Discussion

This chapter compared the frictional torque measuring capabilities of two electromechanical multi-axis systems to determine the best approach for further frictional torque testing. The two systems were (i) an electromechanical single station hip simulator equipped with a six-axis load cell for the measurement of force and torque in the three orthogonal axes and (ii) a custom-built electromechanical friction measuring system designed to work as a subsystem for a single station hip simulator.

3.6.1 Calibration

Calibration of the two systems shared a common method where the SSHS itself was concerned (Section 3.3.1). Static calibration methods like those described for the SSHS are widely used in calibrating multi-axis sensors and can achieve high precision. They are however not always robust for dynamic applications such as hip simulation where load, motion and displacement may be applied dynamically. In these dynamic applications, deviations from static calibration coefficients may begin to occur when measurements approach the resonance frequency of the sensor (Schleichert and Fröhlich, 2015). Dynamic calibration methods can be used to compensate for these deviations by identifying the frequency-related response of the sensor.

The static calibration method in Section 3.3.1 can be improved by developing a method that allows a range of oscillating frequencies to be applied during calibration to determine the SSHS six-axis load cell's frequency-dependent response, and therefore ensuring that this can be compensated for during testing (Bishop, Waldow and Morlock, 2008).

In addition, although the R^2 values from the static calibration in Section 3.3.1.1 showed good correlation between the input and outputs, it was difficult to determine reliability of the results. This was because measured THR torques in the SSHS were orders of magnitude lower than the maximum load capacity of the six-axis load cell. In this range, the measurements may be affected by crosstalk from coupling of the different axes, noise or vibrations from accelerations in the system or even friction present in the lateral bearings.

Six-axis sensors like the SSHS load cell are designed to have six measurement channels for the detection forces and torques: force channels F_x , F_y , F_z and torque (moment) channels M_x , M_y , M_z . In theory, signals in any of these channels are not intended to produce outputs in any other channel. In practice however, this is rarely the case as unwanted outputs are measured across other channels for a

given load due to limitations in manufacturing processes and coupling of the axes, known as crosstalk (Hong, Li and Jeong, 2012). Crosstalk is repeatable and therefore can be compensated for if/when known.

An improvement to the SSHS calibration method in further study could look to increasing the applied masses (to the limit of the load cell) and to develop a method for determining and compensating for the crosstalk in the system to increase confidence in measured outputs from testing. A compensation matrix may be developed for post-processing the measured outputs.

3.6.2 Frictional torque measurement

Using free-body diagrams, methods for determining the frictional torques of THRs tested on these two multi-axis systems was assessed. In Section 3.5.1, equations for determining the frictional torques of THRs tested on the SSHS were derived. Despite the presence of linear bearings, the six-axis load cell was capable of detecting resistance present in the x- and z-axes. These lateral forces measured in the x- and z-axes were likely a combination of ‘real’ force due friction/ resistance in the lateral bearings (as they were not completely frictionless) and some crosstalk from the high axial loads applied in the y-axis. Although it was possible to derive the frictional torques at the bearing interface of THRs tested using the SSHS, it did not include compensation for potential crosstalk. This can however be done when known as suggested in Section 3.6.1.

In Section 3.5.2 however, it was not possible to determine the frictional torques of THRs measured by the modified SSHS with a subsystem due to the presence of unknown forces leading to an inability to resolve the equations. This section discusses why and how this was not possible to do.

Overall, the subsystem was unstable due to the universal joint, and multiple uncontrolled linear bearings introducing significant motion and elasticity to the system. While the supporting brackets and frames were essential support features

to hold the remaining components of the subsystem, the unbalanced weight of these parts resulted in impinged components and could have also introduced forces that would skew the measured outputs even with the addition of counterweight measures such as the passive spring.

The load cells used in this sub-system were uniaxial load cells. The concept of positioning the load cells outside the acetabular cup holder to detect forces was adapted from the pendulum friction hip simulator, where the cup holder mounted on frictionless hydrostatic bearings would be driven into a load cell as a result of friction at the bearing interface. However, uni-axial load cells are not designed to be loaded off-axis, and therefore the incorrect vertical positioning of the subsystem load cells coupled with their rigid attachment to the cup holder and other support features of the subsystem would have left them prone to off-axis loading leading to bending and shear (F_{Z_FEcell} and F_{X_AAcell}). These off-axis lateral forces were unknown as they could not be measured due to the uni-axial operation of the load cell. Equations 3.16 and 3.19 also show that these forces were essential for determining the frictional torques in both FE and AA directions.

Due to the location and operation of the universal joint decoupling the acetabular cup holder from the lateral linear bearing above, it was also unlikely that the effect of any lateral forces generated in the linear bearing would have been isolated and adequately transmitted to any measurement devices. In this setup having two centres of rotation (pivot A and the joint centre), as well as the addition of multiple linear bearings increased the degrees of freedom of the system and resulted in the presence of uncontrolled motion and off-axis loading. The axes of rotation of the universal joint would need to pass through the joint centre to eliminate the additional pivot and ensure that any lateral forces were detected as part of deriving the frictional torques in the bearing. These issues with the design of system and the inability to derive a suitable equation for determining the frictional torques of

THRs meant the system was not fit for purpose and data collected from the subsystem load cells could not be used for further testing.

3.7 Conclusion

The critical analysis of the two electromechanical multi-axis systems for the purposes of measuring frictional torque in total hip replacements revealed that the SSHS was the better system of the two. A better calibration process to include dynamic assessment and crosstalk compensation would improve the reliability of measured data in future testing.

CHAPTER FOUR

Assessment of a multi-axis hip simulator for the measurement of frictional torques in total hip replacements

4.1 Introduction

A multi-axis single station hip simulator (ProSim, UK) with a six-axis load cell was identified as the more appropriate of two systems assessed for measuring the frictional torques of total hip replacements in Section 3.6. A range of tests were conducted to verify the measurement capabilities of the simulator, similar in part to the approach used by Sonntag *et al.*, (2017) when assessing the Minibionix 852 (MTS Systems, USA) hip simulator for the measurement of friction in total hip replacements during wear simulation. As a new system that had not previously been used assessing the different axes and functionalities available on the multi-axis single station hip simulator (SSHS) would allow for better understanding of their effects, prior to the assessment of representative clinical load conditions. An incremental parametric approach was employed to systematically couple the

different motions and loads available on the SSHS and assess their effects on the measured frictional torque. Following parametric verification of the individual functionalities, clinically relevant dynamic load and motion conditions were introduced as would be expected in the human gait cycle (ISO 14242-1) to determine their influence on the frictional torques measured.

Verification of the SSHS measurements was performed by:

1. Assessing the friction measuring capacity of the SSHS in the AA direction
2. Assessing the effects of restricting anterior-posterior and medial-lateral translation on the measured frictional torques.
3. Comparing the friction measurements taken by the SSHS in the flexion extension axis only with friction measured by a pendulum friction hip simulator under static and dynamic load.
4. Assessing the effects of applied motions on the measured frictional torque by the SSHS

4.2 Multi-Axis Single Station Hip Simulator (SSHS)

The SSHS, described in detail in Section 3.2.1, was a single station electromechanical anatomical hip wear and friction simulator (ProSim, UK) with an on-board six-axis load cell for the measurement of forces and moments in the three orthogonal axes.

The simulator applied simultaneous multi-axis motion and loading: dynamic axial load, flexion-extension and abduction-adduction motion, internal-external rotation as well as medial-lateral (ML) load and displacement. The axial load as well as the ML load and displacement was applied via the acetabular cup whereas the angular rotations FE, AA and IER were applied via the femoral head component.

The SSHS was calibrated as described in Section 3.3.

4.3 Materials

Three 36mm diameter total hip replacement components were supplied by DePuy Synthes® (Leeds, UK). These components included Articul/eze® metal and BioloX® Delta ceramic femoral head components, as well as Marathon™ and BioloX® Delta ceramic acetabular liners and Porocoat® acetabular shells from the PINNACLE® cup system. Further details including constituent materials and product reference numbers have previously been provided in Table 2.1 (Chapter 2). Bovine calf serum 25% (v/v) was used as a lubricant (Section 2.2.1, Chapter 2). Sample sizes varied for the different preliminary studies conducted and will be provided along with the details of the study.

Bovine calf serum 25% (v/v) was used as a lubricant for all tests in this chapter.

4.3.1 *Component Preparation and Pre-Test Procedures*

Pre-test procedures including placement of alignment marks, geometric measurements and surface analyses were carried out as described in Section 2.3. MOP and COC bearing components used in this study were re-used after tests described in Section 2.7 following surface analyses tests described in Section 2.3 indicated minimal change in the surface roughness (Ra). For MOP bearings, the average change in Ra was less than 3nm for the femoral heads and less than 200nm in the acetabular cups. For COC bearings, the average change in Ra was less than 2nm for both the femoral heads and acetabular cups. Components were cleaned as described in Section 2.3.

Component set up

The centre of rotation (COR) of the femoral head and acetabular assembly were aligned with the COR of the SSHS to eliminate offset loads and experimental errors.

4.3.2

Using a height gauge and custom-made stainless-steel fixtures, the femoral head was impacted onto a spigot and the COR fixed at a distance of 95mm from the base of the fixture, corresponding with the COR position of the SSHS (Figure 4.1).

Using a 2:1 ratio of non-sterile poly-methyl methacrylate bone cement cold cure powder to liquid monomer (WHW Plastics, Hull-UK), Porocoat® acetabular shells were secured into acetabular cup fixtures. These were positioned such that the COR of inserted acetabular liners were coincident with the COR of the SSHS, this was 109.82mm from the bottom of the mounting surface (Figure 4.2).

Femoral head and acetabular cup fixtures containing THR components were assembled outside the simulator and placed within a gaiter containing 500mL 25% (v/v) new-born bovine calf serum. Jubilee clips were placed around the gaiter ends to create an air-tight seal to hold the serum and prevent leaking. The assembled test cell containing the components and lubricant was then mounted in the simulator.

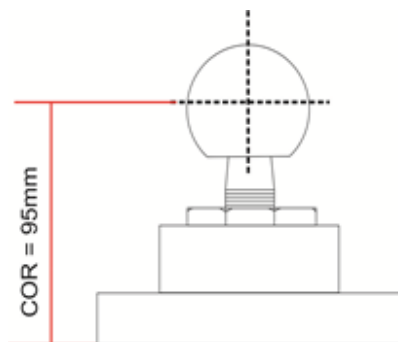


Figure 4.1 - Femoral head fixture for SSHS, showing COR position

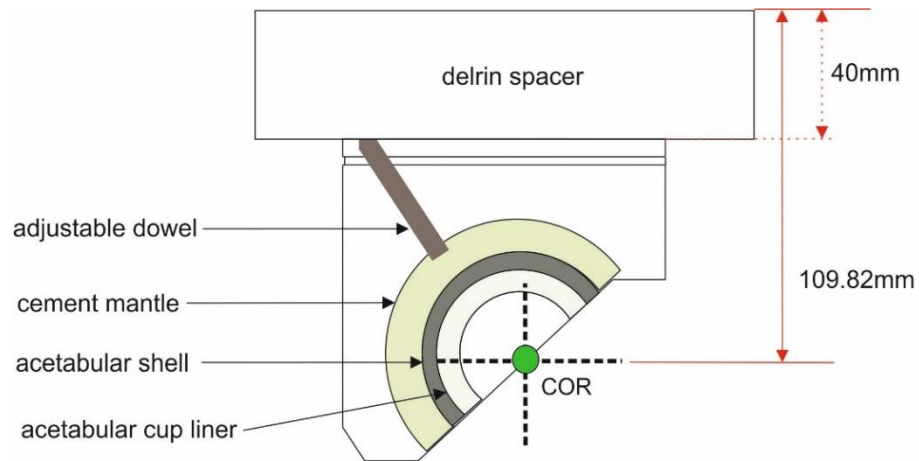


Figure 4.2 - Acetabular cup fixture for SSHS, showing COR position. Acetabular shell cemented with dental grade poly-methyl methacrylate bone cement

4.4 Testing and Data Collection

All tests were conducted for 125 cycles at a frequency of 1Hz. This is the average walking speed defined in ISO 14242-1:2014. Loading during testing was ramped up gradually for the first 10 cycles. Beginning at cycle number 30, five cycles at 30 cycle intervals were recorded (30-34, 60-64...). Data collected by the six-axis load cell was logged and recorded via the HipSim software at a sampling rate of 255 data points per second. The outputs of the SSHS were:

- i. Axial force (F_Y)
- ii. Angular motion (FE, AA and IE)
- iii. Torques in FE direction (M_X)
- iv. Torques in AA direction (M_Z)
- v. Torques in IE direction (M_Y)
- vi. Lateral force in AP direction (F_Z)
- vii. Lateral force in ML direction (F_X)

Torques and forces measured by the SSHS in the peak ML translation, peak velocity region were used to derive the frictional torques in the tested THRs using the equations discussed in Section 3.5.1. These were:

Frictional torques in the FE direction; $\tau_{FE} = M_X + F_Z \cdot l + F_Z \cdot r$ (Equation 3.23)

Frictional torques in the AA direction; $\tau_{AA} = M_Z + F_X \cdot l + F_X \cdot r$ (Equation 3.34)

Frictional torques in the IE direction; $\tau_{IE} = M_Y$ (Equation 3.35)

Resultant frictional torque: $\tau_{resultant} = (\tau_{FE}^2 + \tau_{AA}^2 + \tau_{IE}^2)^{1/2}$ (Equation 3.36)

Data processing

Data processing varied for the different preliminary tests conducted on the SSHS

4.4.1 and will be provided on a study-by-study basis.

4.5 Assessments of SSHS for measuring THR frictional torque

The research objectives stated in section 1 were investigated to assess the ability of the SSHS to measure frictional torques at the bearing interface of THRs. This section addresses each objective independently as a sub-study and discusses the sub-study's findings as well as its influence on subsequent studies, if any.

4.5.1

Assessing the friction measuring capacity of the SSHS in the AA direction

4.5.1.1 *Introduction*

Unlike previously used uniaxial hip simulators, the SSHS was equipped with additional axes of motion, in addition to FE motion i.e., AA and IER. Torque measurements in the two horizontal axes, FE and AA, were expected to be similar. This study therefore compared torques measured in the FE and AA directions to assess the capacity of the SSHS to accurately measure frictional torque in the AA direction.

4.5.1.2 *Materials and methods*

Tests were carried out on 36mm ceramic-on-polymer (COP) THR bearings (n =3).

Torques were measured under constant load and FE only motion. These tests were also repeated under constant load and AA only motion. However, during the AA only motion testing, the acetabular cup holder was rotated 90° (with respect to the initial FE only motion orientation) so that the applied AA motion was in effect FE motion relative to the bearing orientation (Figure 4.3).

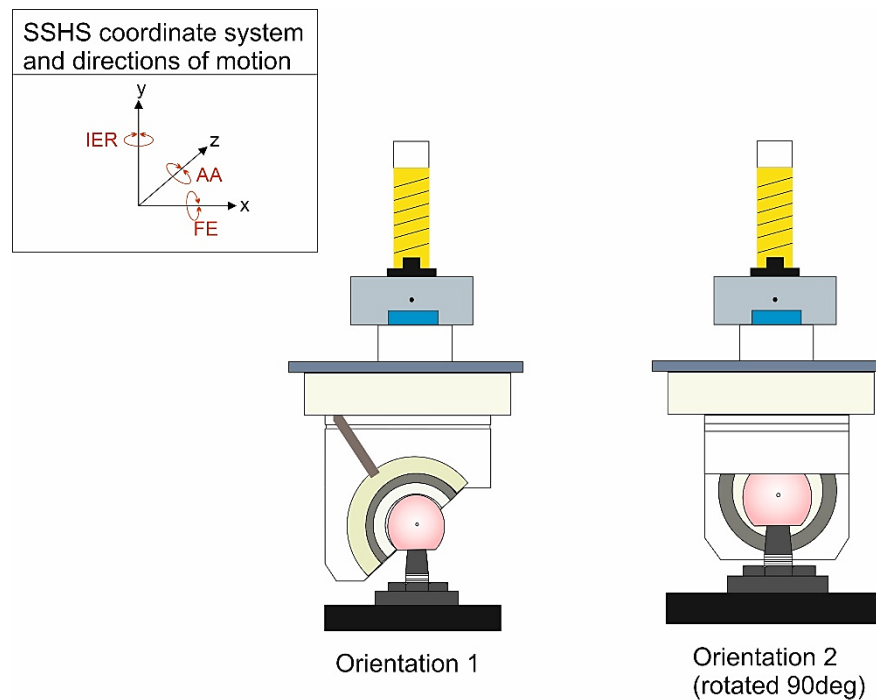


Figure 4.3 – Front view of mounted components in the SSHS during the measurements in the AA axis assessment, illustrating the two orientations used. Orientation 1: FE direction of components coincided with FE direction of SSHS. Orientation 2: FE direction of components coincided with AA direction of SSHS.

Axial loading and motion

A constant axial load of 1kN was applied using the SSHS HipSim software. Constant load was used to reduce the potential variables introduced by dynamic loading, thereby isolating the effects of applied motion.

Symmetric sinusoidal motion in the range of $\pm 10^\circ$ FE and $\pm 10^\circ$ AA motion was applied independently under 1kN constant load to components mounted as described in orientation 1 and 2 respectively (Table 4.1).

Table 4.1 - Summary of conducted tests for the assessment of directional sensitivity of torque measured (orientations described in Figure 4.3)

Load	Motion	Test time (s) & Frequency (Hz)
Orientation 1 (n=3, COP)		
1kN	$\pm 10^\circ$ FE	125 seconds at 1Hz
Orientation 2 (n=3, COP)		
1kN	$\pm 10^\circ$ AA	125 seconds at 1Hz

Data processing and statistics

Data output was recorded as described in section 4.4. For this study, the data output of interest was frictional torques in the FE direction ($\tau_{FE(i)}$) for all tests conducted in orientation 1 and frictional torques in the AA direction ($\tau_{FE(ii)}$) for all tests conducted in orientation 2.

Mean $\tau_{FE(i)}$ and $\tau_{FE(ii)}$ of five data points in the high velocity region of the applied motion was calculated for each recorded cycle. A mean of $\tau_{FE(i)}$ and $\tau_{FE(ii)}$ for all recorded cycles per test was calculated, and repeated for all three samples. An overall mean $\tau_{FE(i)}$ for COP bearings (n=3) in orientation 1, and an overall mean $\tau_{FE(ii)}$ for COP bearings (n=3) in orientation 2 were obtained.

A paired student t-test was used to assess the difference between the two means. The null hypothesis (H_0) for this analysis assumed no significant difference between the mean $\tau_{FE(i)}$ and $\tau_{FE(ii)}$.

4.5.1.3 Results

The mean $T_{FE(i)}$, representing torques in the FE direction for orientation 1, was $2.11 \pm 1.4\text{Nm}$. The mean $T_{FE(ii)}$, representing torques in the FE direction for orientation 2, was $1.88 \pm 0.3\text{Nm}$. There was no statistical difference found between the torques measured in orientation 1 and orientation 2 ($p=0.49$).

4.5.1.4 Discussion

This study was conducted to assess SSHS measurements of frictional torque in the AA axis when compared to the FE axis. This study found that measurements in the AA axis were able to replicate measurements in the FE axis, as it was not possible to reject the null hypothesis indicating there was no statistical difference between $T_{FE(i)}$ and $T_{FE(ii)}$.

When compared to literature, the average $T_{FE(i)}$ and $T_{FE(ii)}$ were 2.11Nm and 1.88Nm respectively for 36mm COP bearings were lower than the average frictional torque measured of 3.3Nm by Scholl *et al.* (2016). Although the same bearing size and materials combinations were used, the applied constant loads were dissimilar. Scholl *et al.* (2016) used a higher load of 2450N in their study when compared to the 1000N constant load applied in this study. A higher applied load will generate a larger moment or torque for a given distance (bearing radius of 18mm for both studies) assuming all other conditions are same.

4.5.2

Assessing the effects of anterior-posterior and medial-lateral translation restriction on the measured frictional torques.

4.5.2.1 Introduction

The AP translation via a quasi-frictionless lateral bearing on the SSHS was passive and designed to allow restoration of joint centre for mounted components should there have been an offset during standard condition testing. Standard conditions for *in-vitro* hip simulator tests were defined as conditions where the mounted femoral and acetabular components were fully concentric such that the loading axis intersected with the joint centre of rotation (COR). Standard conditions also assumed that these factors were maintained throughout the testing regime.

ML translation however was actuated and could be controlled on the SSHS via the HipSim software. When disengaged from its motor however, it could also be left passive for the restoration of joint centres.

The design of the SSHS was such that, for both AP and ML translations, a shoulder screw could be used to 'hold' the linear bearings at their midpoint thereby centring the mounted components with respect to the SSHS COR and restricting any additional translation (Figure 4.4 and Figure 4.5).

The effects of restricting these two translations were unknown although it was hypothesised that restricting these translations, independently or simultaneously, would create varying degrees of stiffness in the system and subsequently affect the measured torques.

It was also important to understand the ML translation functionality as this was to be responsible for simulating variations in surgical translational positioning (discussed further in Chapter 5).

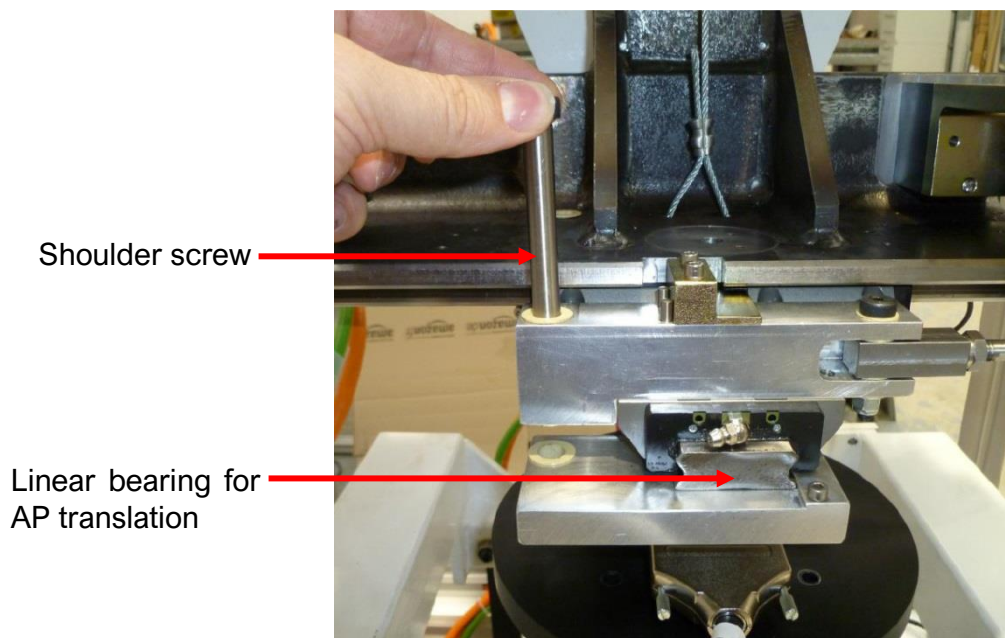


Figure 4.4 – Position of AP translation linear bearing and positioning of shoulder screw to lock AP translation on the SSHS

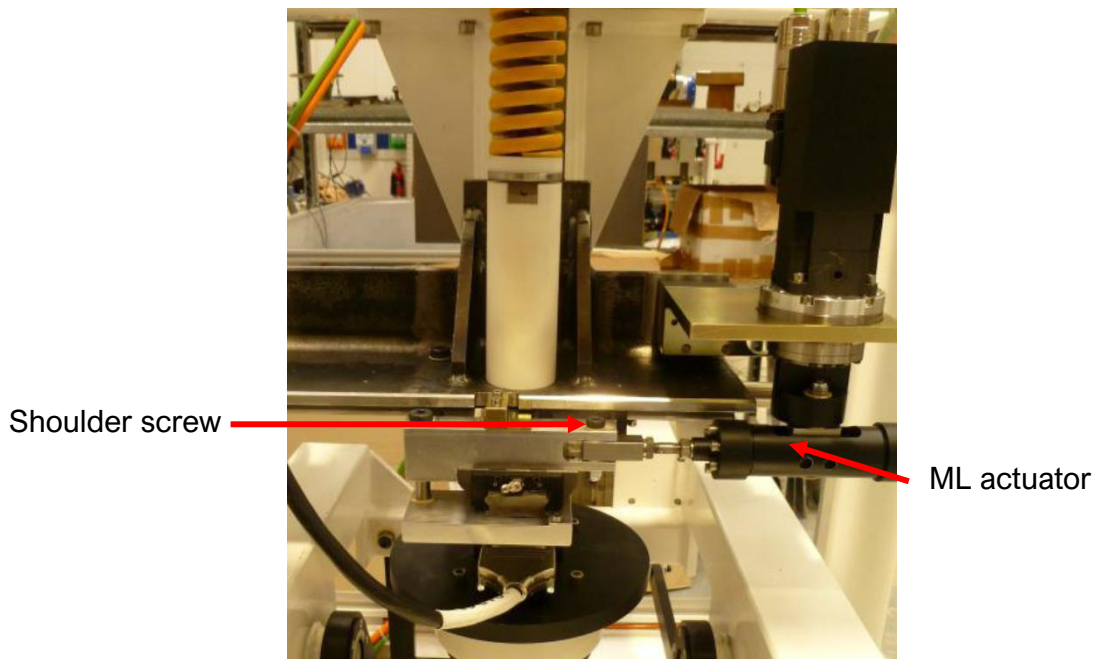


Figure 4.5 - Position of ML actuator and positioning of shoulder screw to lock ML translation on the SSHS

4.5.2.2 Materials and methods

Tests were carried out on 36mm ceramic-on-polymer (COP) THR bearings (n =3).

Axial loading, motion and combinations of AP and ML restrictions

A constant axial load of 1kN was applied using the SSHS HipSim software.

Symmetric sinusoidal motion in the range of $\pm 10^\circ$ FE, $\pm 10^\circ$ AA and $\pm 10^\circ$ IE motion was applied under 1kN constant load to mounted components.

The effects of independently and/or concurrently restricting AP and ML translations on the torques in FE, AA and IE directions were assessed. A summary of the test input parameters and the combinations of translations investigated are provided in Table 4.2. Tests were conducted at 1Hz for 125 seconds.

Table 4.2 - Summary of conducted tests for assessing the effects of AP and ML translation restriction on the output torque

Sample	Load	Motion	AP translation	ML translation
36mm COP (n=3)	1kN	±10° FE	Free	Free
			Free	Held
			Held	Free
			Held	Held
		±10° AA	Free	Free
			Free	Held
			Held	Free
			Held	Held
		±10° IE	Free	Free
			Free	Held
			Held	Free
			Held	Held

Data processing and statistics

Data output was recorded as described in section 4.4. For this study, the data output of interest were torques in the FE direction (M_x), torques in the AA direction (M_z) and torques in the IE direction (M_y).

Mean M_x , M_y and M_z of five data points in the high velocity region of the applied motion were calculated for each recorded cycle. A mean of M_x , M_y and M_z for all recorded cycles per test was calculated and repeated for all three samples. Overall means for M_x , M_y and M_z for sample size of three for all investigated test conditions were calculated and presented.

Graphical representation shows 95% confidence limits (using standard deviation and sample size) for illustration of variability in the data.

4.5.2.3 Results

Tests were carried out on 36mm COP (n=3) bearings under 1kN constant load and $\pm 10^\circ$ FE, AA or IE motion whilst varying combinations of restricted (held) or unrestricted (free) AP and ML translations.

Overall, restricting the AP translation showed an increase in torques in the FE direction whereas restricting the ML translation showed increases in torques in the AA and IE direction. The highest change in measured torque across all conditions was seen in the FE direction (Figure 4.6).

For both conditions when AP translation was unrestricted and FE only motion was applied, measured torques in the FE direction were 2.12 ± 1.46 Nm and 2.03 ± 1.20 Nm. Torques in the FE direction however increased to 10.68 ± 13.79 Nm after AP translation was restricted (with unrestricted ML translation) and to 14.46 ± 11.41 Nm when AP and ML translation were both restricted.

For both conditions when ML translation was unrestricted and AA only motion was applied, measured torque in the AA direction was 1.88 ± 0.27 Nm and 1.88 ± 0.33 Nm. Torques in the AA direction however increased to 3.52 ± 1.14 Nm after ML translation was restricted (with unrestricted AP translation) and to 3.65 ± 1.01 Nm when AP and ML translation were both restricted.

For both conditions when ML translation was unrestricted and IE only motion was applied, measured torques in the IE direction was 0.17 ± 0.12 Nm and 0.29 ± 0.24 Nm. Torques in the IE direction however increased to 4.96 ± 2.33 Nm after ML translation was restricted (with unrestricted AP translation) and to 4.89 ± 2.22 Nm when AP and ML translation were both restricted.

On average, the measured lateral force (F_x , AP force) increased from approximately 10N (when both AP and ML translations were free) to 20N (Free AP, locked ML) to 80N (both translations locked). The measured lateral force (F_z , ML force) however increased from approximately 10N (when both AP and ML

translations were free) to 20N (Free AP, locked ML) to 30N (both translations locked).

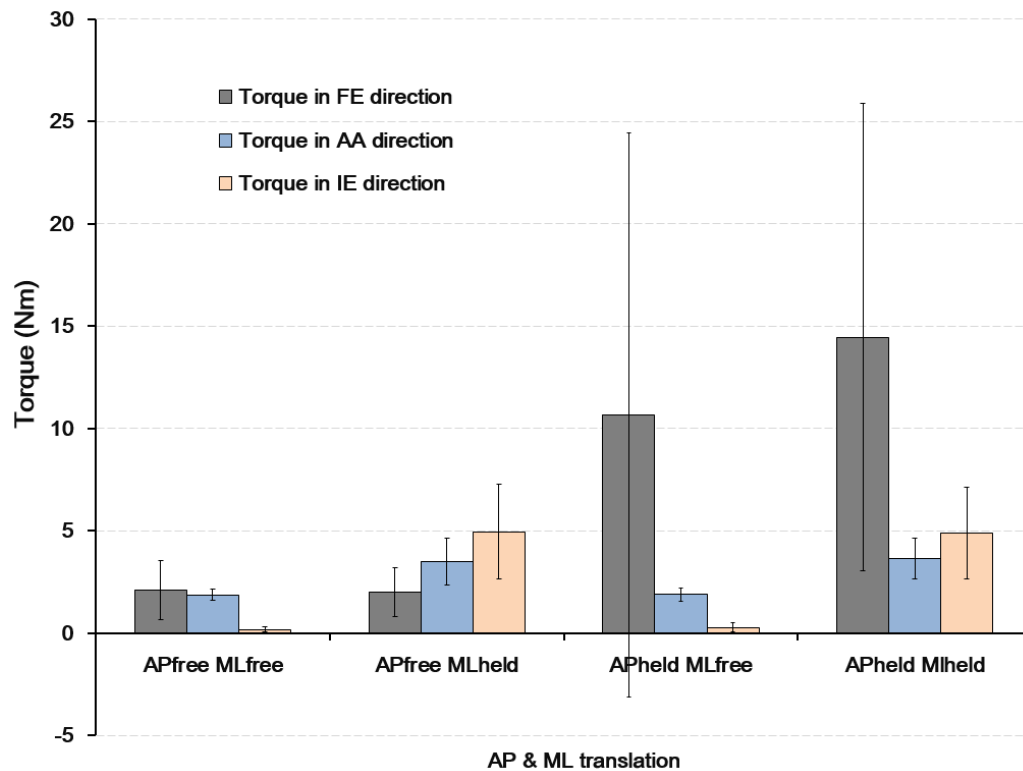


Figure 4.6 – Mean torques in the FE, AA and IE directions of a 36mm COP bearing measured using a SSHS whilst applying four different combinations of AP and ML translation. Graphs illustrate mean \pm 95% confidence limits (n=3)

4.5.2.4 Discussion

The tests in this study were conducted to determine the effects of AP and ML translation on the torques of THRs to inform the method development for assessing THR frictional torques using the multi-axis SSHS. The findings of the study determined whether AP and ML were to be left restricted or unrestricted during testing of THRs under standard conditions.

Unsurprisingly, restricting AP and ML translation resulted in increases in the measured torques in the FE and AA directions respectively. Torques in the FE direction measured by the SSHS showed a five-fold increase when AP only was restricted compared to a seven-fold increase when both AP and ML were restricted. The variation in the data for a sample size of three was however very

high for these two conditions and therefore were not found to be statistically significantly different from each other.

The free body diagram in Figure 4.7 shows the interaction between the femoral head and acetabular cup in the sagittal plane, and considering rotation about the x-axis only (FE direction). This was first introduced as part of the frictional torque analysis conducted for the SSHS in Section 3.5.1., and the same assumptions for static equilibrium hold true. In this free body diagram, the lateral force F_z measured by the six-axis load cell was as a result of some friction in the linear bearings and is only true in the present study for the unlocked AP translation state. In the locked state however, the linear motion in the AP direction is restricted by inserting a pin. This lock couples the part of the setup above the six-axis load cell to the THR below such that the combined rigid body experiences a resistive force (F_{zp}) exerted by the lock at the six-axis load cell (Figure 4.8).

The free-floating or unlocked state of the linear bearing is important in ensuring the COR of the bearing is coincident throughout testing. Locking this translation is likely therefore to result in elevated forces during testing for even the smallest of offsets introduced during the component set up process. The measured elevated moments observed in this study demonstrated that achieving a setup where the COR of the bearing is perfectly aligned with the COR of the SSHS is challenging and realistically unlikely.

The same interaction and behaviour was true when considering rotation about the z-axis (AA motion) in the coronal plane where locking the translation in the ML direction observed elevated moments.

The findings of this study indicated the importance of unrestricted AP and ML translation during testing under standard conditions. These findings also indicate the possibility of elevating measured AA moments and lateral forces during future tests assessing the effects of translational positioning by connecting the ML actuator, although not as high as observed in the FE direction.

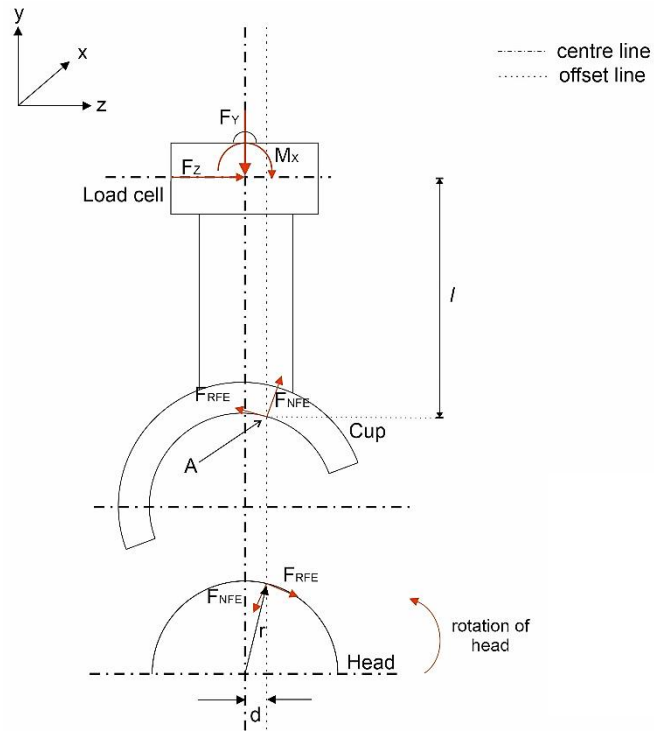


Figure 4.7 - Free body diagram of the representative THR and SSHS setup in the sagittal plane, showing the linear roller bearing and the presence of lateral force (F_z) as a result of some friction in the bearing

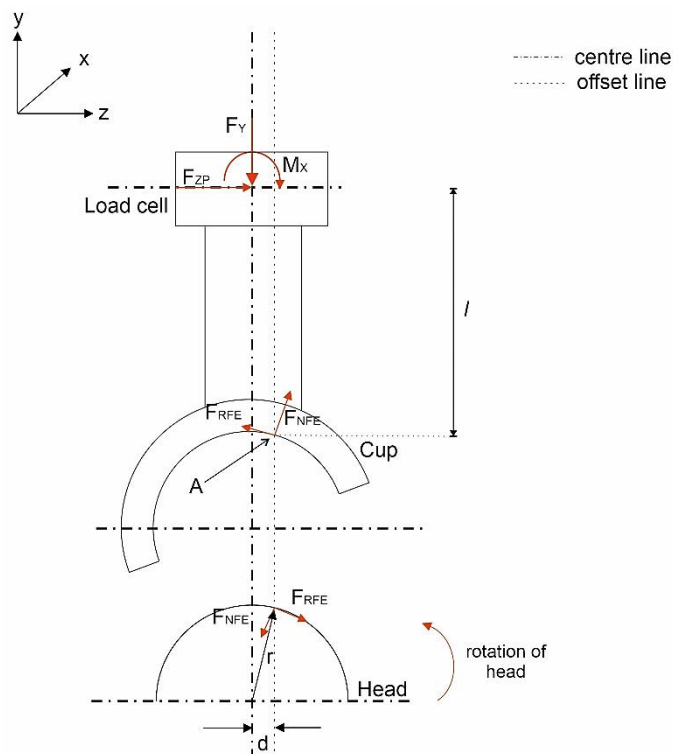


Figure 4.8 - Free body diagram of the THR and SSHS setup in the sagittal plane, showing the removal of the lateral translation and the introduction of resistive force (F_{zP})

Comparison of outputs between pendulum friction hip simulator and SSHS

4.5.3.1 Introduction

4.5.3 This study compared tests conducted on the SSHS with similar tests previously conducted on a pendulum friction hip simulator (Chapter 2). With the pendulum friction hip simulator being a previously validated system, the aim of the study was to compare the frictional torques measured using the new SSHS under different test conditions with the data collected from Chapter 2.

It was not expected for the SSHS to replicate the outputs of the pendulum friction hip simulator. However, the output of the pendulum friction hip simulator was found to be able to detect frictional torque changes as a result of varying loading conditions and the ability of the SSHS to do similar was also investigated to ensure its capacity to detect other types of variations in loading conditions in future tests.

The objectives of this sub study were:

- To examine the effects of constant load on the THR frictional torques
- To examine the effects of increasing range of flexion-extension motion on the THR frictional torques
- To examine the effects of different bearing materials on the THR frictional torques

4.5.3.2 Differences between pendulum friction simulator and SSHS

The pendulum friction hip simulator was a servo-hydraulic system with a 0-3kN range for the applied axial load, whereas the SSHS was an electromechanical system with a 0-5kN range for the applied axial load. Both simulators applied constant and dynamic axial loading. However, as the SSHS was an electromechanical system this had a higher potential accuracy and reliability than the hydraulic system in the application of dynamic loading profiles. The pendulum friction simulator had a piezoelectric transducer located in the front of the mobile

carriage for the detection of friction in the bearing (as described in Chapter 2), whereas the SSHS had a strain gauge based six-axis load cell located above the components for the detection of forces and moments in the three orthogonal axes.

The orientation of mounted components on the pendulum friction hip simulator was inverted when compared to the anatomical orientation. In the SSHS, components were positioned in an anatomical orientation with the acetabular cup above the femoral head. The SSHS applied motion in the FE, AA and IER direction to the head component, whereas the pendulum simulator applied FE motion only to the head.

Some studies assessing variations in translational positioning were able to replicate a limited range of ML displacement on the pendulum simulator via the use of a passive spring (Al-Hajjar *et al.*, 2015). Using an electromechanical actuator, it was possible to better apply and control the required medial-lateral displacement during simulation.

A summary of the differences between the two systems is provided in Table 3.3.

Table 3.3 – Differences between the Pendulum Friction Hip Simulator and the Single Station Hip Simulator (*Italicised text indicate component that motion or displacement is applied to*)

	Single Station Hip Simulator	Pendulum Friction Hip Simulator
Component orientation	Physiological	Inverted
Actuator	Electro-mechanic	Servo-hydraulic
Transducer	Six-axis load cell	Piezoelectric
Axial load	0-5kN <i>Constant and dynamic</i>	0-3kN <i>Constant and dynamic</i>
Flexion-extension	$\pm 60^\circ$ <i>Applied to femoral head</i>	$\pm 25^\circ$ <i>Applied to femoral head</i>
Internal-external rotation	$\pm 25^\circ$ <i>Applied to femoral head</i>	-
Abduction-adduction	$\pm 25^\circ$ <i>Applied to femoral head</i>	-
Medial-lateral load	$\pm 1\text{kN}$	-
Medial-lateral displacement	$\pm 5\text{mm}$ <i>Applied to acetabular cup</i>	1mm <i>Achieved via passive spring to acetabular cup</i>
Anterior-posterior displacement	$\pm 10\text{mm}$ <i>Passive, acetabular cup</i>	-

4.5.3.3 Materials and methods

Tests were carried out on 36mm metal-on-polymer (MOP) THR bearings (n =6) and 36mm ceramic-on-ceramic (COC) THR bearings (n=6). All tested MOP and COC components on the SSHS were prepared and set up as detailed in Section 4.3. Based on the findings of Section 4.5.2, both AP and ML translations on the SSHS were left unrestricted for the tests described in this study.

Input Parameters

The load and motion profiles used in Section 2.5 on the pendulum friction hip simulator were repeated on the SSHS (Figure 4.9). All tests were conducted at a

frequency of 1Hz for 125seconds, and all input parameters tested were specified using the SSSS HipSim software.

The test conditions investigated are summarised in

Table 4.4.

Table 4.4 - Summary table of comparative study input parameters for six MOP and six COC components on both pendulum friction and single station hip simulators

Load			Flexion-extension angle	
1kN constant	2kN constant	2kN peak, 100N swing phase load	±10°	±25°
✓				✓
	✓		✓	
	✓			✓
		✓	✓	
		✓		✓

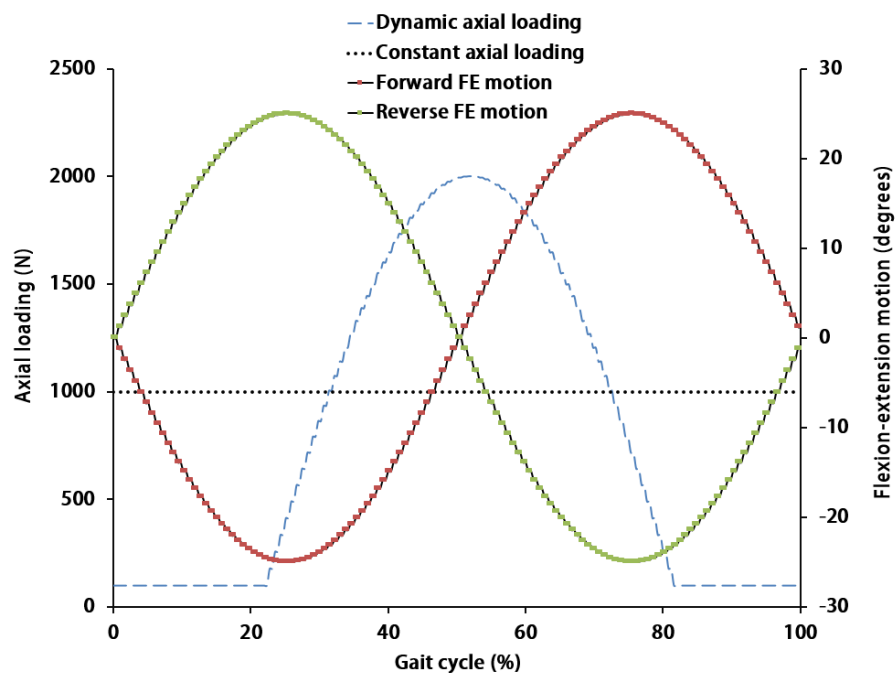


Figure 4.9 - Example graphical representation input profile for a forward test showing the relationship between the axial loads (constant and dynamic) and flexion-extension motion for the comparative study on the pendulum friction hip simulator and SSSS

Data processing and statistics

Data output was recorded as described in section 4.4. For this study, the frictional torques in FE only (τ_{FE}) were calculated using equation 3.23 and were compared with results from the pendulum friction hip simulator presented in section 2.7.

Mean M_x and F_z obtained from five data points in the high velocity region of the applied motion were used. An overall mean τ_{FE} for a sample size of six for all investigated test conditions was calculated and presented.

Graphical representation shows 95% confidence limits (using standard deviation and sample size) for illustration of variability and reliability in the data.

The statistical differences between the tested groups on the SSHS was determined by conducting a one-way ANOVA with a post-hoc analysis Tukey range test (significance level of 0.05). The null hypotheses assumed for the tests are below:

Objective 1: To examine the effects of constant load on the THR frictional torques

H_0 = No difference between frictional torques measured under 1kN and 2kN constant loads for both MOP and COC bearings

Objective 2: To examine the effects of increasing range of flexion-extension motion on the THR frictional torques

H_0 = No difference between frictional torques measured under $\pm 10^\circ$ and $\pm 25^\circ$ under both 2kN constant and dynamic loading for MOP and COC bearings

Objective 3: To examine the effects of different bearing materials on the THR frictional torques

H_0 = No difference between frictional torques measured in MOP and COC bearings.

4.5.3.4 Results

For the tests where the applied load was increased from 1kN to 2kN while applying a $\pm 25^\circ$ FE motion in 25% (v/v) bovine calf serum, the frictional torques increased for both MOP and COC bearings. The mean frictional torque measured increased from 2.34 ± 0.34 Nm to 3.48 ± 0.58 Nm in 36mm MOP bearings, and 1.32 ± 0.36 Nm to 1.99 ± 0.25 Nm in 36mm COC bearings (Figure 4.11).

For both 2kN constant load and 2kN dynamic load with a 100N swing phase load, the statistical comparison of measured frictional torques could not reject the null hypothesis and no statistical differences were observed when the range of FE motion was increased from $\pm 10^\circ$ to $\pm 25^\circ$.

When tested under 2kN dynamic load with a 100N swing phase load and $\pm 25^\circ$ motion only, the measured friction torques were statistically significantly different in the 36mm MOP bearing group when compared to the 36mm COC bearing group. The mean frictional torque measured under dynamic loading was 2.29 ± 0.38 Nm in the 36mm MOP bearings and 1.10 ± 0.23 Nm in 36mm COC bearings (Figure 4.10).

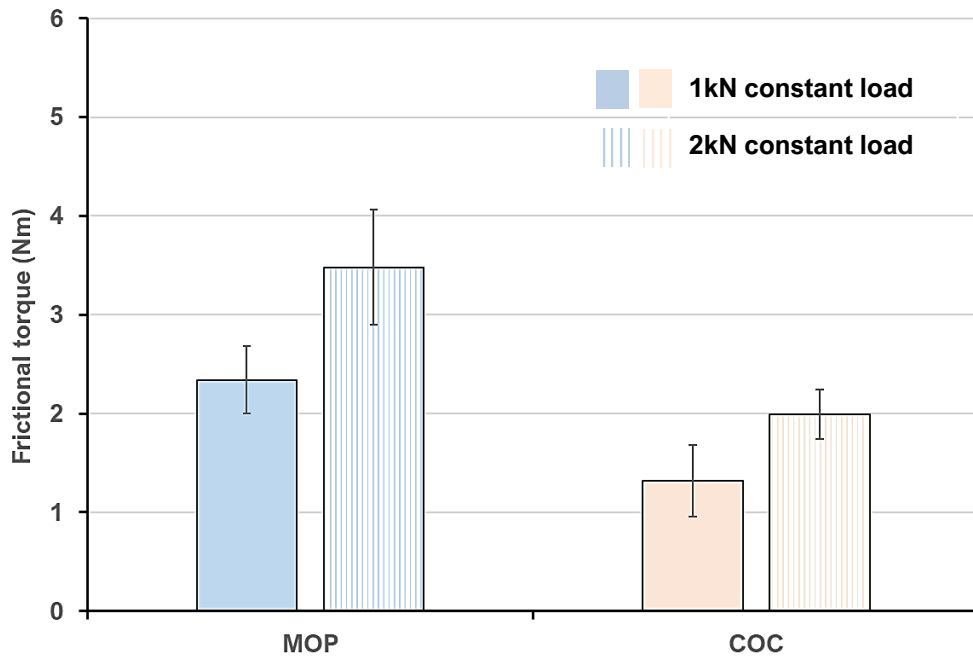


Figure 4.11 - Mean frictional torque measured in 36mm MOP and 36mm COC bearings tested under 1kN and 2kN constant load and $\pm 25^\circ$ FE motion tested on the SSHS (mean $\pm 95\%$ confidence, n=6)

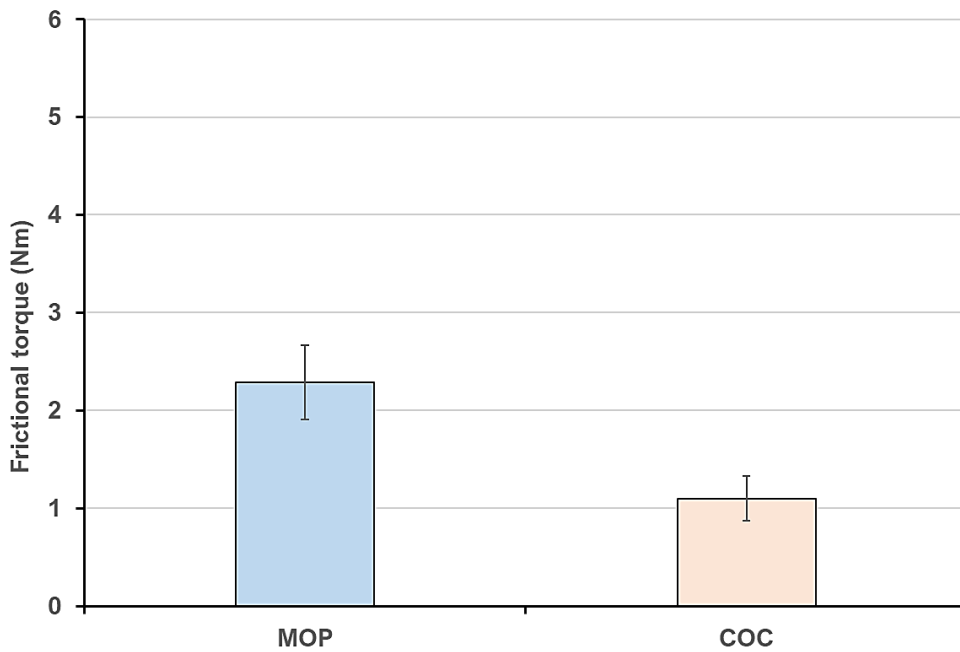


Figure 4.10 - Mean frictional torque measured in 36mm MOP and 36mm COC bearings tested under 2kN peak load with 100N swing phase load and $\pm 25^\circ$ FE motion on the SSHS (mean $\pm 95\%$ confidence, n=6)

4.5.3.5 Discussion

Comparison between the data collected from the SSHS and the pendulum friction hip simulator indicates the capability of the multi-axis SSHS to measure frictional torques. Although the frictional torques measured by the SSHS were significantly different to those measured by the pendulum friction hip simulator, they exhibited the same trends as previously observed in the validated pendulum friction hip simulator.

The differences observed in the measured frictional torques by the SSHS compared to the pendulum may be attributed to differences in measuring approaches (piezoelectric transducer vs six-axis load cell). While the tests conducted on the SSHS were compared to the data output from the pendulum friction hip simulator, it was not expected for the outputs to be identical. Rather, the expectation was to understand the ability of the SSHS to replicate relationships between the test conditions as seen on the pendulum friction hip simulator and generate appropriate frictional torque values.

Equation 3.23 shows that the frictional torques of THRs measured on the SSHS is dependent on the measured moment (M_x), the measured lateral force (F_z), the radius and the distance of the six-axis load cell from the bearing centre of rotation. The measured lateral force (F_z) for the conditions tested were however orders of magnitude smaller than the peak applied load and the maximum load capacity of the six-axis load cell, in the range of approximately 10-30N for all tests conducted. Similar to the discussion of findings in Section 3.6.1, reliability of data outputs that includes measurements at this level is challenging due to the potential effects of crosstalk, noise or vibrations due to accelerations in the system.

It is therefore important to note that while the results in this section demonstrated the ability of the SSHS to detect changes in measured frictional torques at the bearing interface of THRs in response to different test conditions, further work is needed to determine what proportion of the measured signal is artefact.

Assessing the effects of applied motions on the measured torques by the SSHS

All the preceding conducted tests in this chapter has assessed the torques or frictional torques with uniaxial applied motion. However, the multiaxial capability **4.5.4** of the SSHS had not yet been studied and was important for the method development and interpretation of outputs for future testing conducted under multiaxial motion and loading.

This study was therefore conducted to assess the effects of FE, AA and IER motion on the torques of THRs measured using the multi-axis SSHS. To do this, FE, AA and IER were decoupled and their individual effects on the measured torques investigated. These were then systematically recoupled to understand their combined effects on the torque of THRs. In addition to determining the torques measured in the axis coincident with the axis of applied motion, this study also gave insight into the potential crosstalk measured in the other torque channels.

4.5.4.1 Materials and methods

Tests were carried out on 36mm metal-on-polymer (MOP) THR bearings (n = 6). All tested components on the SSHS were prepared and set up as detailed in Section 4.3. Bovine calf serum 25% (v/v) was used a lubricant for all tests conducted. The SSHS is described in Section 4.2.

Input Parameters

All tests were conducted at a frequency of 1Hz for 125seconds, and all input parameters tested specified using the SSHS HipSim software.

Motion

The ISO standard also provides simplified gait motion profiles for FE, AA and IE motions based on physiological motion. The range of applied motion was 25° to -18° for FE motion, 7° to -4° for AA motion and 2° to -10° for IE motion (ISO 14242-

1:2014). To better understand the effects of these motions on the torque, the following combinations were assessed:

FE only, AA only, IE only, FE and AA, FE and IE, AA and IE, and all three motions combined.

Axial loading

Paul (1966) defined the forces at the hip joint as having a characteristic double peak load during stance phase and a low load during swing phase of the gait cycle. This study used a simplified gait cycle with twin peak loads of 3kN in the stance phase, representing an average 75kg person (ISO 14242-1:2014). This gait cycle also featured a constant 300N load for the swing phase, spanning the 60-100% region of the gait cycle.

Data processing and statistics

Data output was recorded as described in section 4.4.

Mean torque of five data points in the high velocity region of the applied motion was calculated for each recorded cycle. For all recorded cycles per test, the mean torque was calculated. An overall mean for a sample size of six for all investigated test conditions was calculated and presented.

Graphical representation shows 95% confidence limits (using standard deviation and sample size) for illustration of variability and reliability in the data.

4.5.4.2 Results and Discussion

Overall, as expected, the dominant torques measured were in the axes coincident with applied motion(s) (Figure 4.12). Torques in the IER direction (M_y) were however relatively constant averaging approximately $1.7 \pm 0.18 \text{ Nm}$ irrespective of applied motion.

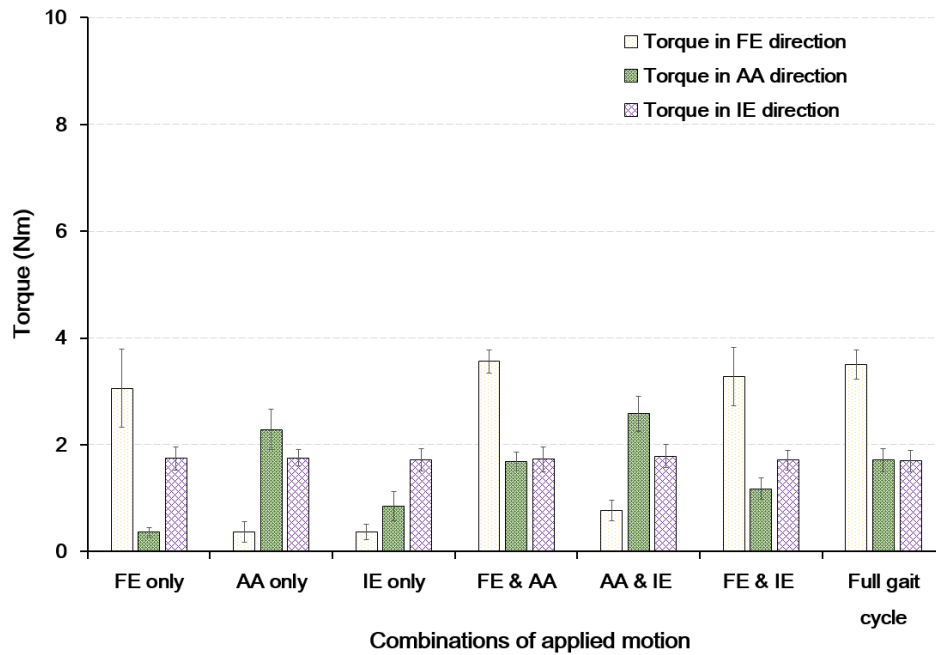


Figure 4.12 – Effects of different combinations of FE, AA and IE motion on the torques of 36mm THRs when tested on a multi-axis single station hip simulator under 3kN twin peak and 300N swing phase load. Graphs illustrate mean \pm 95% confidence limits

Torque in the FE direction (M_x) exhibited the highest torques, with the highest being $3.56 \pm 0.2\text{Nm}$ from combined FE and AA motion (Figure 4.12). This value was however not statistically different from M_x measured for all other conditions where FE motion was applied.

Similar to the observations in Section 4.5.2 and 4.5.3, although the lateral AP force and ML forces appeared to be affected by the applied motion, they were very low ($<30\text{N}$), most likely due to the fact that the bearings in AP and ML directions were left free-floating to ensure the centring of the COR during testing.

When FE only motion was applied, approximately 10% of the measured FE torque (M_x) signal was detected in the AA torque (M_z) channel. Similarly, when AA motion only was applied, approximately 10% of the measured AA torque (M_z) was detected in the FE torque (M_x) channel. When IER only was applied, approximately 20% of the measured IE torque was detected in the FE torque channel and approximately 50% of the measured IE torque was detected in the AA channel. However, with the constant and unchanging nature of the IER torque measured,

the large proportion of FE and AA torque detected when IER was applied was not considered reliable. The behaviour of the IER torque measurement should be subject to a root cause analysis in further study to provide better insight.

While determining the proportion of signal detected in other channels did not constitute a formal crosstalk assessment and compensation, it provided insight into this system behaviour that would be beneficial in future testing.

One of the limitations of this study was the application of dynamic axial loading rather than a constant loading regime. In a study such as this, it would have been more appropriate to limit the variables in the first instance and systematically reintroduce, to observe the effects of the tested variables.

4.6 Conclusion

A range of studies were conducted using 36mm MOP and COC bearings to determine the capacity of the newly acquired multi-axis SSHS for the assessment of frictional torques in THRs. These assessments provided useful insight for further study on the SSHS and deemed it capable of measuring the frictional torques. However due to the low range of torques and lateral forces measured, it was identified that the data collected and reported in these studies may be impacted by the lack of crosstalk compensation and dynamic calibration. Overall, due to the small sample sizes used in the different sub-studies presented, the statistical power was low and therefore there is a high risk of Type II errors (failing to reject a null hypothesis when it is false). Further testing will be required to gather more data with an increased sample size, to increase the statistical power and reduce the chance of these Type II errors.

In addition to demonstrating the capabilities of the new simulator, the findings of this chapter have also documented the response of the different measurement channels of the six-axis load cell to different loading and motion conditions. This forms a baseline for further study in Chapter 5 that may use similar loading and motion conditions.

CHAPTER FIVE

Assessing the effects of variations in translational positioning on the frictional torques in total hip replacements

5.1 Introduction

Variations in rotational and translational positioning of hip replacements have been reported to cause edge loading of liners. This has have been implicated in both early and late modes of implant failure including mechanical loosening, wear, osteolysis and aseptic loosening (Nevelos *et al.*, 1999, 2000; Dennis *et al.*, 2001; Al-Hajjar *et al.*, 2010; Al-Hajjar *et al.*, 2013; Ali *et al.*, 2017; Leng *et al.*, 2017). Edge loading occurs when the femoral head is loaded on or near the rim of the acetabular cup.

Variations in positioning of the acetabular cup component can lead to edge loading, and this can be caused by both the orientation and position of the cup. The orientation of the acetabular cup component is defined in terms of its inclination (rotational position in the coronal plane) and version (rotational position in the transverse plane) angle (Figure 5.1). The translational position of the

acetabular cup refers to medial-lateral or superior translation of the acetabular cup centre with respect to the femoral head centre, and subsequent failure to restore joint centre (Figure 5.2).

While the effect of translational positioning on wear of THR has been investigated, the effects on other modes of failure such as those indicated to be associated with excessive frictional torques have not yet been experimentally assessed. Sariali *et al.* (2010) assessed the effect of edge loading on the friction of 32mm COC bearings by applying flexion-extension (FE) motion only and simulating one level of high cup inclination angle (75°) reported an increase in friction co-efficient with the incidence of edge loading. A computational assessment by Liu *et al.*, (2013) assessing the effects of translation between head and cup centres of rotation in the range of 0-5mm also reported an increase in torques at the articulating interface of MOP, MOM and COC bearings. To date an experimental study under clinically relevant conditions that includes variations in translational positioning and subsequent effects on the measured torques of THRs has not been undertaken.

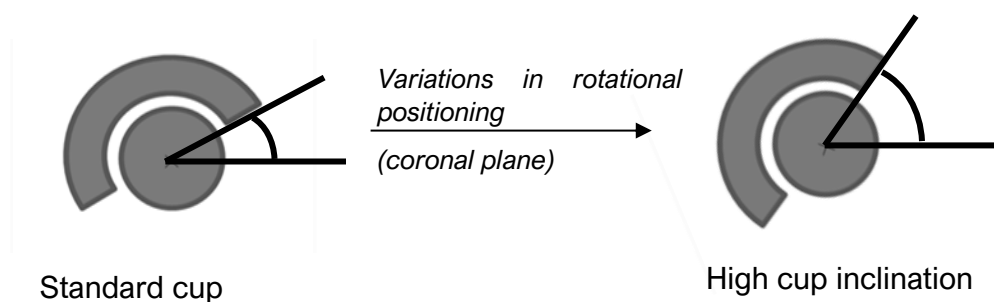


Figure 5.1 - Schematic of possible variation in rotational positioning of THR components

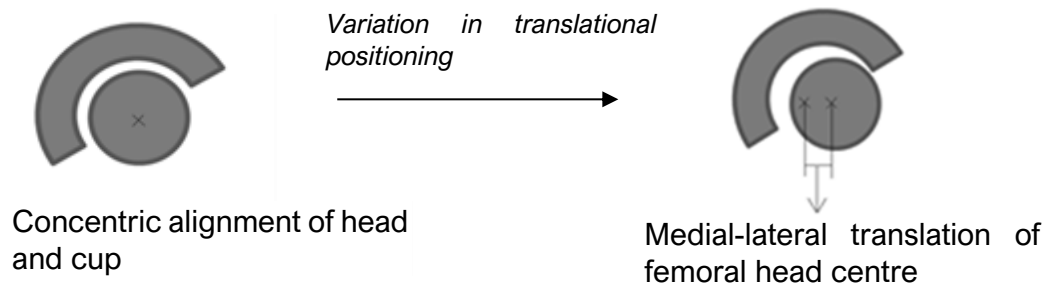


Figure 5.2 - Schematic of possible variation in translational positioning of THR components

The aim of this study was to determine the effects of medial lateral translation of the acetabular cup with respect to the femoral head on the frictional torque at the bearing interface of THRs. This study was conducted on the modified SSHS with a custom friction measuring subsystem. However, as discussed in Section 3.5 and 3.6, due to the presence of unknown variables, the frictional torques of THRs could not be accurately derived from the outputs of the subsystem, as initially proposed. Despite this, the design of the subsystem and its integration into the SSHS was such that the six-axis load cell of the SSHS simultaneously collected data during testing. This was used for the purposes of this study, from the data collected on the SSHS, it was possible to calculate the frictional torques at the bearing interface under different test conditions and determine the relative effect of translational positioning. The effects of translational positioning assessed were relative (rather than absolute) in reference to the presence of the subsystem on the SSHS. It was recognised that although frictional torques could be calculated based on SSHS output, this data included an artefact due to interference and/or interaction with the subsystem components. This artefact was however expected to be consistent across all tests, although not quantifiable. The results of this chapter provide an indication of the effects of varying medial-lateral translation on the frictional torques at the bearing interface of THRs under different loading conditions.

The objectives were to:

- Assess the effects of varying medial-lateral translation on the frictional torques of THRs under constant axial load
- Assess the effects of increasing constant axial loading on the frictional torques of THRs measured under variations in medial-lateral translation
- Compare the effects of varying medial-lateral translation on the frictional torques of THR under constant and dynamic loading

5.2 Materials

Three 36mm diameter total hip replacement components were supplied by DePuy Synthes® (Leeds, UK). These components included Articul/eze® metal femoral head components, Marathon™ acetabular liners and Porocoat® 56mm acetabular shells from the PINNACLE® cup system. Further details including constituent materials and product reference numbers have previously been provided in Table 2.1 (Chapter 2). Bovine calf serum 25% (v/v) was used as a lubricant (Section 2.2.1, Chapter 2).

5.2.1 Component Preparation and Pre-Test Procedures

Pre-test procedures including placement of alignment marks, geometric measurements and surface analyses were carried out as described in Section 2.3. Components used in this study were re-used after tests described in Section 4.5 following surface analyses tests described in Section 2.3 that indicated minimal change in the surface roughness (Ra), with an Ra of less than 8nm for the femoral heads and less than 300nm in the acetabular cups. Components were cleaned as described in Section 2.3.

5.3 Multi-Axis Single Station Hip Simulator

The electromechanical single station hip simulator (SSHS) with a six-axis load cell, described in Section 3.2.1, was used to measure the frictional torques of total hip replacements for tests conducted in this study.

The original intent of the tests conducted in this study was to assess the frictional torques at the bearing interface of THRs using a custom biaxial friction measuring subsystem mounted on the SSHS, presented in Section 3.2.2. It was however identified in Section 3.5.2 that this subsystem was not capable of accurately determining the frictional torques at the bearing interfaces of tested THRs. This was because some critical variables required to derive the frictional torques were unknown. The subsystem was, however, designed to be supplementary to the SSHS, and therefore the SSHS could still apply motion, load and displacement, and the six-axis load cell recorded outputs. The data presented in the current Chapter was acquired directly from the SSHS six-axis load cell and not the subsystem.

The SSHS was calibrated as described in Section 3.5.

5.4 Input parameters

The input parameters used to assess the relative effects of variations in medial-lateral translation on the output frictional torque of 36mm MOP bearings (n=3) using the SSHS and six-axis load cell are discussed in this section. All input parameters were specified for testing using the inbuilt SSHS HipSim software.

5.4.1 Axial Loading

As a pilot study investigating the effects of medial lateral translation on the frictional torque of THRs, arbitrary constant loads of 500 and 1000N were chosen.

A dynamic loading profile featuring a single peak load of 1kN spanning the first 60% of a 1Hz cycle and a 200N swing phase load spanning the remaining 40% was also used to represent a simplified gait cycle.

5.4.2 Motion

FE and AA motion were either decoupled and applied independently or applied to simultaneously. This allowed the combined effects of applied motion and medial-lateral translation to be assessed. No IER was applied due to the tests originally being conducted with the intention of collecting data from the biaxial friction measuring system on the modified SSHS.

A sinusoidal FE motion with a range of $\pm 10^\circ$ was applied at a frequency of 1Hz. The frictional torques measured under $\pm 10^\circ$ FE motion had previously not been found to be significantly different from that measured under $\pm 25^\circ$ (Section 2.7.2).

A sinusoidal AA motion with a range of $\pm 7^\circ$, applied at a frequency of 1Hz was used. This range is within the range of acceptable AA motion capable on the modified SSHS and represented a similar range of motion as exhibited in the human gait cycle and defined by 1SO14242-1:2012. A sample input profile for simultaneously applied FE and AA motions for this study is provided in Figure 5.3.

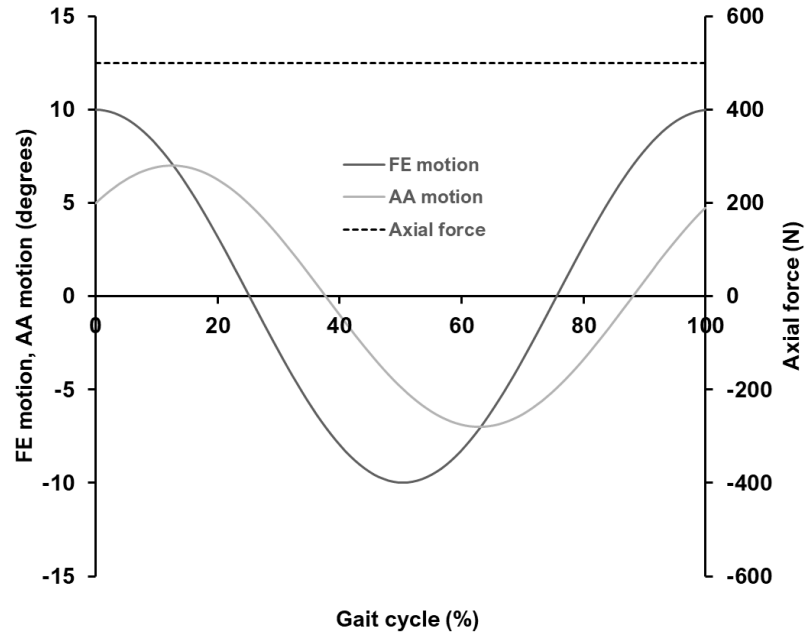


Figure 5.3 – Sample input profile showing relationship between FE and AA, ranges of $\pm 10^\circ$ and $\pm 7^\circ$ respectively

5.4.3 Medial-lateral translation

Clinically, variations in translational positioning are difficult to assess statically, though the resultant separation of the joint that occurs has been observed in fluoroscopy studies (Komistek *et al.*, 2002). In-vivo translational positioning between the centres of rotation of the femoral head and acetabular cup may vary for a range of reasons. These include offset deficiency where there is inadequate soft tissue tension around the joint to retain the femoral head within the acetabular cup, acetabular cup or femoral stem migration, or poor surgical positioning such as excessive acetabular cup reaming (cup medialisation) or insufficient neck length (head lateralisation).

Experimental and computational studies investigating the effects of varied translational positioning between the centres of rotation of the femoral head and acetabular cup (on the wear of THRs) have used a method where the femoral head centre was displaced laterally with respect to the acetabular cup centre. A spring

element was used to apply a force to the femoral head in the medial direction (Sariali *et al.*, 2010; Al-Hajjar *et al.*, 2013; Leng *et al.*, 2017).

Previous studies have investigated a range between 0 and 5mm of fixed displacement between the head and cup centres of rotation (at 1mm intervals), that resulted in a range of dynamic separations. In this pilot study, lower increments of 0.5mm fixed translation were investigated for the arbitrary range of 1.5mm to -1.5mm, primarily selected to prevent potentially causing damage to the simulator, with intention to extend the range to clinically relevant ranges with further testing.

Variations in translational positioning between the centres of rotation of the femoral head and acetabular components were replicated by applying medial-lateral (ML) translation to the acetabular cup component between 65 and 95% of each cycle (Figure 5.4). ML translation was applied in this region for two reasons:

(a) Previous *in-vivo* studies have identified hip joint separation as occurring in the swing phase of the gait cycle (Lombardi *et al.*, 2000; Dowson, Dalmaz and Lubrecht, 2003), which is represented in the latter 40% a full gait cycle with a frequency of 1Hz (Paul, 1966).

(b) This region coincides with the high velocity regions of applied FE and AA motions, thereby excluding any noise generated by changing directions of the motion arm.

The ML translation actuator remained engaged (but with no applied translation) for 0mm ML translation conditions. This was useful for assessing the ML force and translation baseline prior to the application of ML translation.

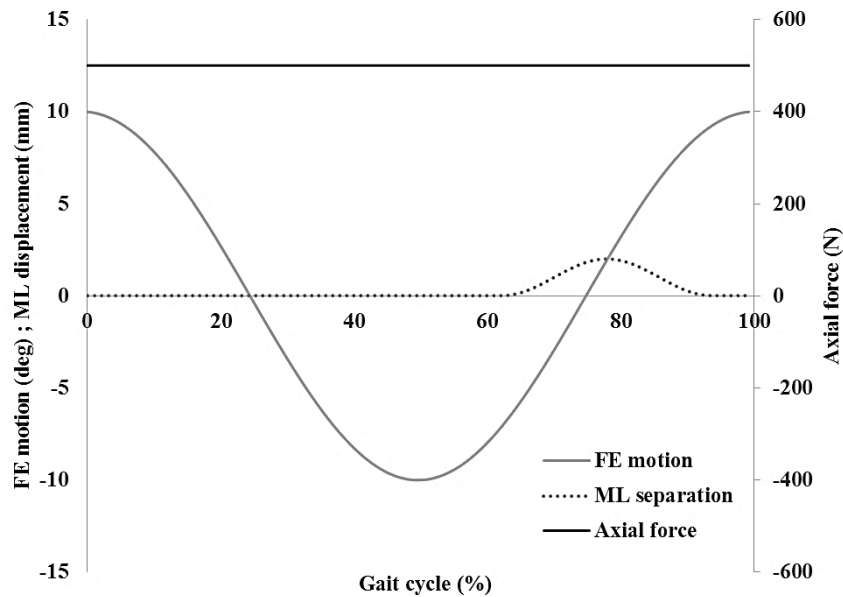


Figure 5.4 - Sample input profile showing position of applied ML translation during the gait cycle, with a constant load of 500N and $\pm 10^\circ$ of FE motion

5.4.4 Summary of conducted tests

Tests were carried out on 36mm metal-on-polymer (MOP) THR bearings ($n = 3$) for each conducted test. Acetabular cup components were inclined at 30° for all tests. Tests where no translation was applied were conducted in the first instance to produce a baseline reference for comparison. This baseline was compared to subsequently conducted tests where ML translation was applied.

The summary of tests conducted are as follows:

Objective 1: Assessing the frictional torque under constant load, to determine the effects of ML translation on the frictional torques of THRs under FE, AA and combined FE AA motion. To do this, bearings were tested under 500N and FE and/or AA motion initially with no ML translation applied. ML translation in the $\pm 1.5\text{mm}$ range was then applied to the bearings under the same conditions.

Objective 2: Assessing whether increasing the applied constant load alters the effects of ML translation on the frictional torques of THRs under FE, AA and

combined FF AA motion. To do this, bearings were tested under 1kN and FE and/or AA motion initially with no ML translation applied. ML translation in the $\pm 1.5\text{mm}$ range was then applied to the bearings under the same conditions. The outputs of this were then compared to the outputs from objective 1 to determine the effects of increasing the constant load from 500N to 1kN.

Objective 3: Assessing whether dynamic loading alters the effects of ML translation under FE, AA and combined FF AA motion on the frictional torque. To do this, bearings were tested under a dynamic loading and FE and/or AA motion initially with no ML translation applied. ML translation in the $\pm 1.5\text{mm}$ range was then applied to the bearings under the same conditions. The outputs of this were then compared to the outputs from objective 2.

5.5 Data output

All tests were conducted for 125 cycles at a frequency of 1Hz. Loading during testing was ramped up gradually for the first 10 cycles. Beginning at cycle number 30, five cycles at 30 cycle intervals were recorded (30-34, 60-64...). Data collected by the six-axis load cell was logged and recorded via the HipSim software at a sampling rate of 255 data points per second. The variables recorded by SSHA were:

- i. Axial force (F_Y)
- ii. Angular motion (FE, AA and IE)
- iii. Torques in FE direction (M_X)
- iv. Torques in AA direction (M_Z)
- v. Torques in IE direction (M_Y)
- vi. Lateral force in AP direction (F_Z)
- vii. Lateral force in ML direction (F_X)

Torques and forces measured by the SSHS in the peak ML translation, peak velocity region were used to derive the frictional torques in the tested THRs using the equations discussed in Section 3.5.1. These were:

$$\text{Frictional torques in the FE direction; } \tau_{FE} = M_x + F_z \cdot l + F_z \cdot r \quad (\text{Equation 3.23})$$

$$\text{Frictional torques in the AA direction; } \tau_{AA} = M_z + F_x \cdot l + F_x \cdot r \quad (\text{Equation 3.34})$$

$$\text{Frictional torques in the IE direction; } \tau_{IE} = M_y \quad (\text{Equation 3.35})$$

5.6 Data processing

The main objective of this chapter was to assess the effects of varying medial-lateral translation THRs on the measured frictional torques using the SSHS. The presence of the subsystem on the modified SSHS was likely to affect the measured frictional torque of the SSHS. This was however hypothesised to be a constant artefact of the data collected.

The effects of variations in ML translation on the measured frictional torques, assessed by deducting the baseline frictional torques from tests where ML translation was applied, was referred to as the frictional torque difference. For each level of ML translation applied ($n=3$), a mean frictional torque difference was calculated.

Statistical testing to determine the effects of the different levels of medial-lateral translation on the measured frictional torques and the mean frictional torque difference was conducted. With the data meeting the assumptions of normality and equal variance, a one-way ANOVA with a post-hoc analysis Tukey range test was conducted at significance level of 0.05 to assess the following hypotheses:

Objective 1: H_0 = No difference between mean frictional torque difference measured for the levels of applied medial-lateral translation under constant load.

Objective 2: H_0 = No difference between mean frictional torque difference measured under variations in medial-lateral translation and 500N constant load vs 1kN constant load.

Objective 3: H_0 = No difference between mean frictional torque difference measured under variations in medial-lateral translation and 1kN constant load vs dynamic load.

5.7 Results

5.7.1 Frictional torque of 36mm MOP THRs using a modified SSHS (baseline)

This section presents the baseline FE and AA frictional torques of 36mm THRs measured under 500N and 1kN constant loads dependent on whether bearings were tested under FE only, AA only or combined FE AA motion. The mean frictional torques measured under 500N constant load were very low due to low applied load (Figure 5.5). While also relatively low, the mean FE frictional torques measured under 1kN constant load were 2.56 ± 0.51 Nm when FE motion only was applied and 1.25 ± 0.63 Nm when FE and AA motions were applied (Figure 5.6a). The mean FE frictional torque when combined FE and AA was applied was lower than the frictional torques when FE only was applied independently.

The mean AA frictional torques measured under 1kN constant load were 2.57 ± 0.60 Nm when AA motion only was applied and 3.48 ± 0.58 Nm when FE and AA motions were applied (Figure 5.6). The mean AA frictional torque when combined FE and AA was applied was higher than the frictional torques when AA only was applied independently.

The shaded bars in Figure 5.5 and Figure 5.6 show parallel measurements detected in the other channels when data was collected. These non-zero values

are likely due to a combination of crosstalk in the system and artefacts generated by the presence of the subsystem.

Without further assessment to determine exactly how these non-zero values could be compensated in the different measurement channels, the baseline frictional torques presented here were therefore to be compared against frictional torques obtained from subsequent testing, to isolate the effects of applied ML translation in the 60-95% region of the test cycle. This was presented as the mean torque difference.

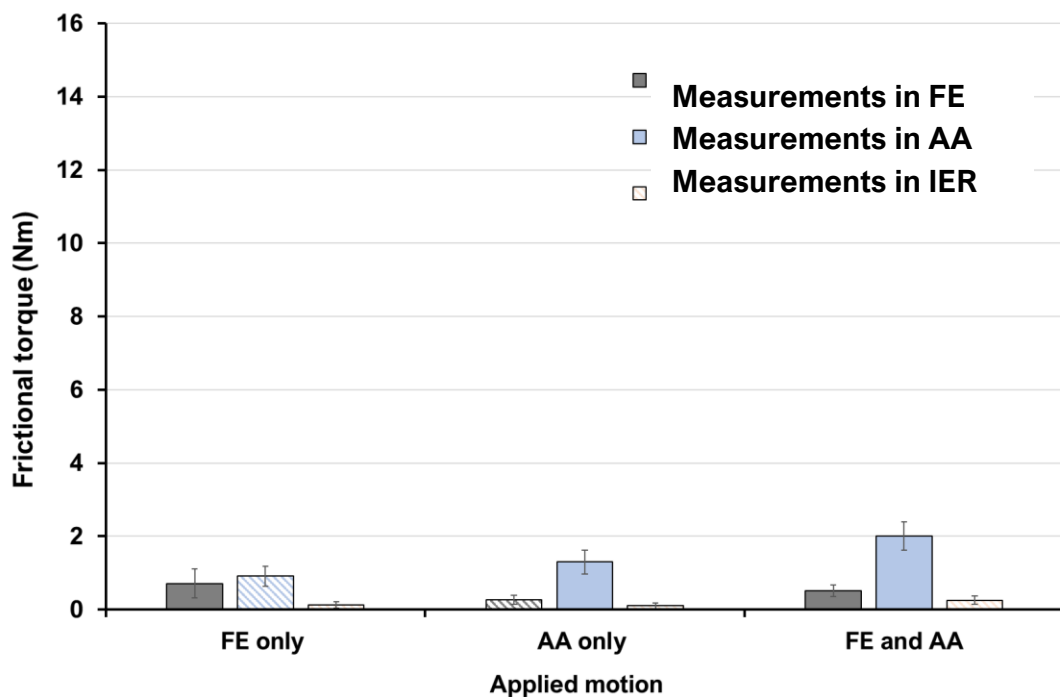


Figure 5.5 - Mean frictional torques in FE and AA directions measured under 500N constant load and indicating FE, AA, or IE measurements (shaded regions) detected in directions not coincident with the direction of applied motion, n= 3 (Mean \pm 95% confidence level)

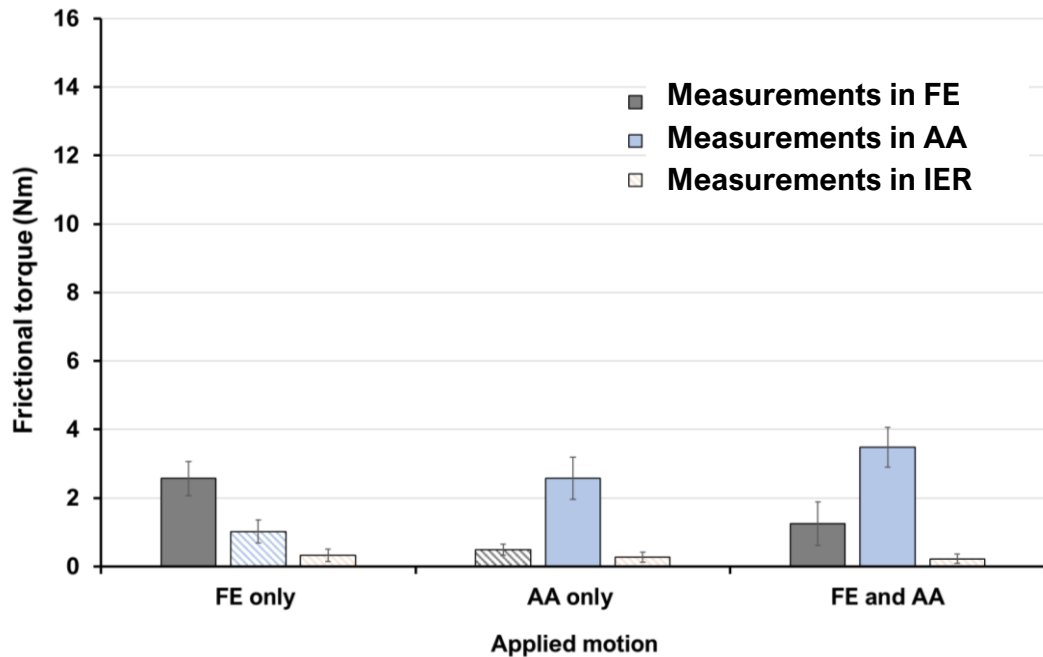


Figure 5.6 - Mean frictional torques in FE and AA directions measured under 1kN constant load and indicating FE, AA, or IE measurements (shared regions) detected in directions not coincident with the direction of applied motion, n= 3 (Mean \pm 95% confidence level)

5.7.2 Assessing the relative effects of varying medial-lateral translation on the torques of THRs measured under constant axial load

Overall, the mean force (both medial and lateral) increased with applied ML translation when tested under 500N and 1kN constant load. The ML force measured when no translation was applied was in the range of 30-50N, with the highest measured ML force measuring $111.4 \pm 14.02\text{N}$ for the 1kN tests (Figure 5.7). However, while the measured ML forces in response to applied ML translation were all significantly higher than the no translation condition, there did not appear to be consistently significant increases as the level of translation increased.

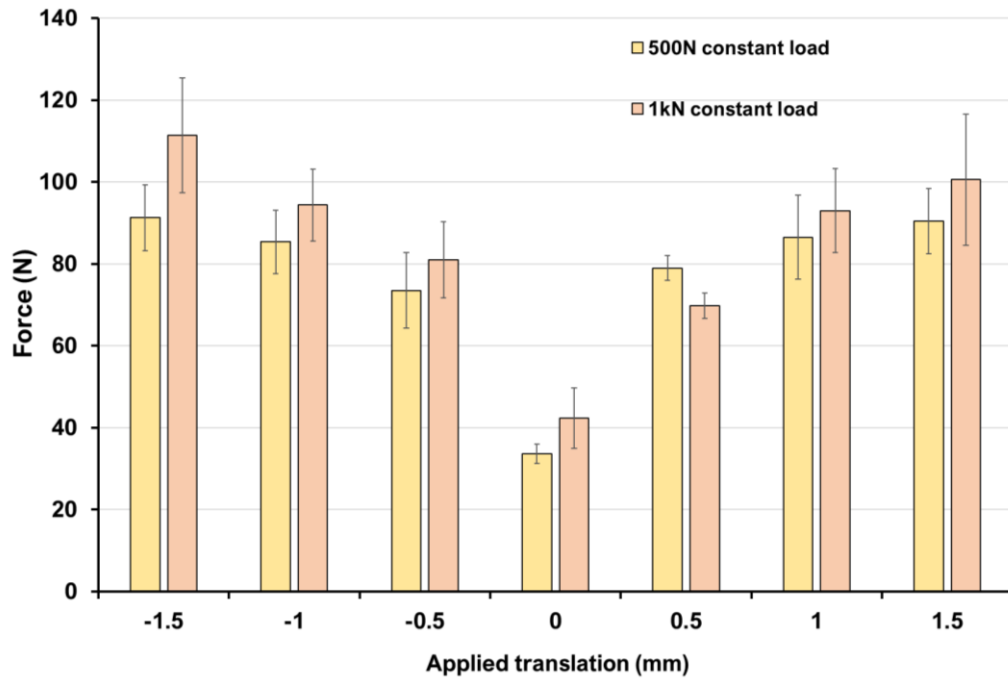


Figure 5.7 – Mean ML forces in response to varying levels of ML translation under 500N and 1kN constant load for 36mm MOP bearings, n= 3 (Mean ± 95% confidence level)

The mean frictional torque difference measured in the FE direction was approximately 1Nm in all test conditions assessed under 1kN constant load where FE motion was applied (Figure 5.8). The mean frictional torque difference measured in the AA direction for test conditions under 1kN where AA motion was applied however, increased with applied ML translation, with a peak mean torque difference of 12.78 ± 1.27 Nm when 1.5mm lateral translation was applied (Figure 5.9). However, while the mean torque differences under AA motion in response to applied ML translation were all significantly higher than the no translation condition, there did not appear to be consistently significant increases as the level of translation increased.

Similarly, under 500N constant load, the mean frictional torque difference in the FE direction for tests including FE motion did not exhibit significant differences with varying levels of ML translation. Again, similar to the 1kN constant condition,

the mean frictional torque difference increased in the AA direction for 500N condition, with increasing applied ML translation. The results under 1kN constant load were higher than the 500N constant load condition.

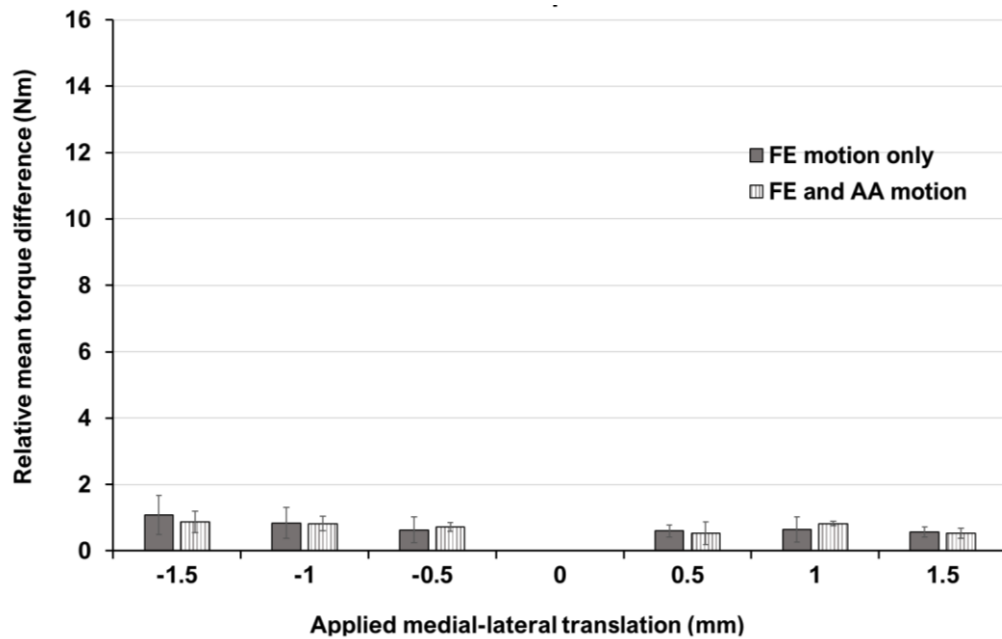


Figure 5.8 – Mean FE torque difference in response to increasing levels of medial lateral translation measured in 36mm MOP bearings (n=3) under 1kN constant load and FE or FEAA motion (Mean \pm 95% confidence level)

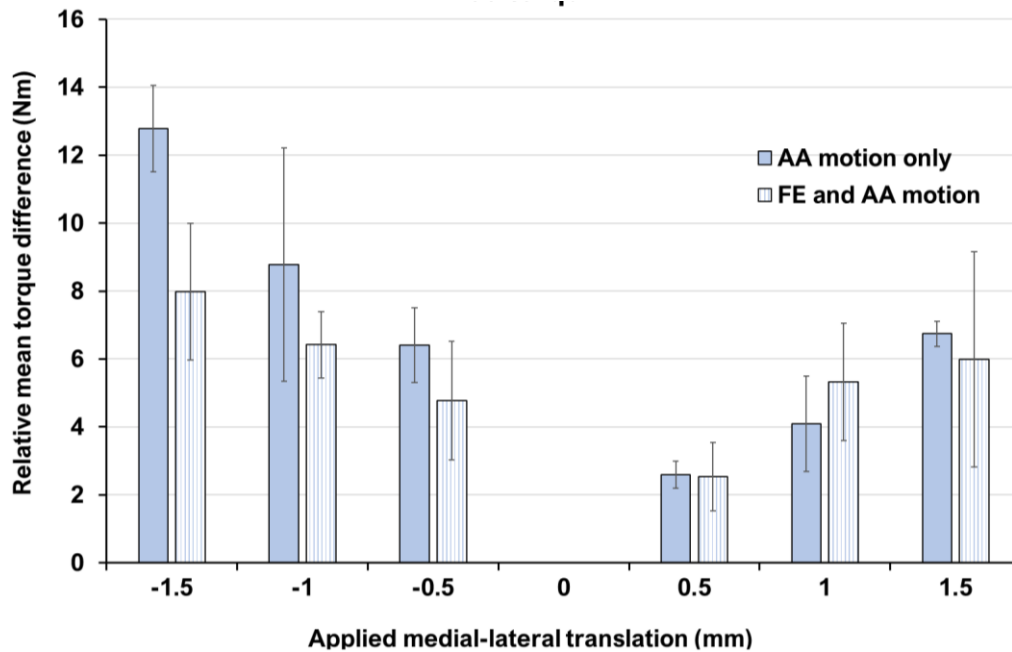


Figure 5.9 - Mean AA frictional torque difference in response to increasing levels of medial lateral translation measured in 36mm MOP bearings (n=3) under 1kN constant load and AA or FEAA motion (Mean \pm 95% confidence level)

5.7.3 Comparison of the relative effects of varying medial-lateral translation on the THR frictional torques measured under constant and dynamic loading

Similar to the constant load conditions, the measured ML forces increased with applied ML translation when compared to the no translation condition (Figure 5.10). The mean ML force measured when no translation was applied was $35.31 \pm 9.89\text{N}$, with the highest measured ML force measuring $106.86 \pm 10.41\text{N}$. However, while the measured ML forces in response to applied ML translation were all significantly higher than the no translation condition, there did not appear to be consistently significant increases as the level of translation increased.

The mean frictional torque difference measured in the FE direction was approximately 0.5Nm or lower for all levels of ML translation applied (Figure 5.11). The mean frictional torque difference measured in the AA direction for test

conditions where AA motion was applied however, increased with applied ML translation, with a peak mean torque difference of 9.93 ± 1.79 Nm when 1.5mm lateral translation was applied (Figure 5.12). When compared to the 1kN constant load condition, there did not appear to be consistent significant differences between the measured mean torque differences under the different levels of ML translation.

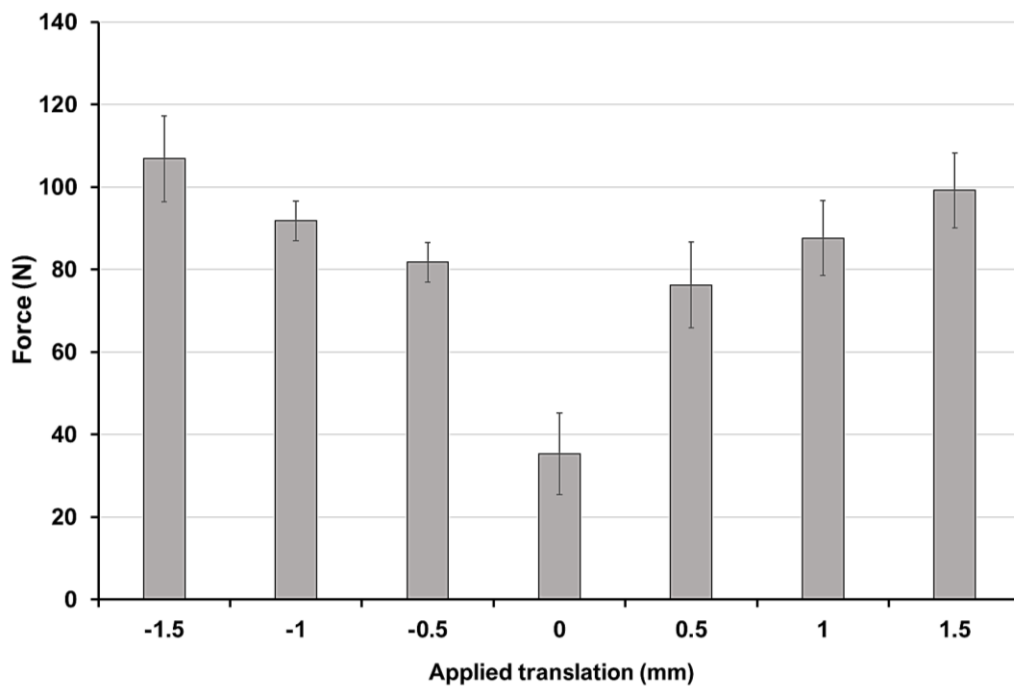


Figure 5.10 - Mean ML forces in response to increasing levels of ML translation under dynamic loading for 36mm MOP bearings, n= 3 (Mean \pm 95% confidence level)

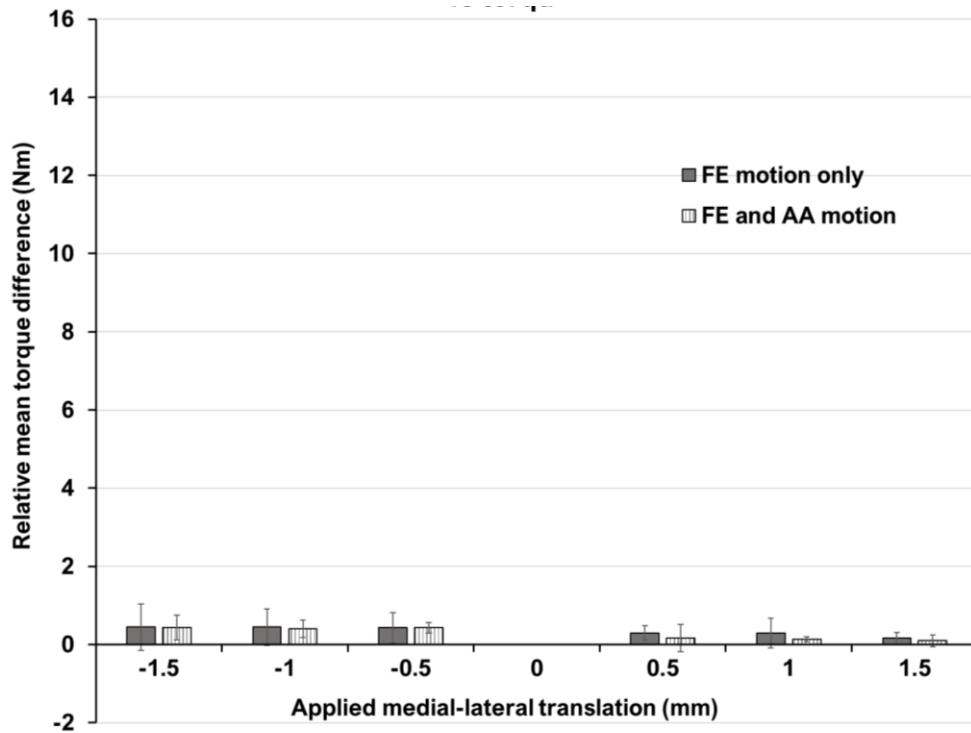


Figure 5.11 - Mean FE torque difference in response to increasing levels of medial lateral translation measured in 36mm MOP bearings (n=3) under dynamic loading and FE or FEA motion (Mean \pm 95% confidence level)

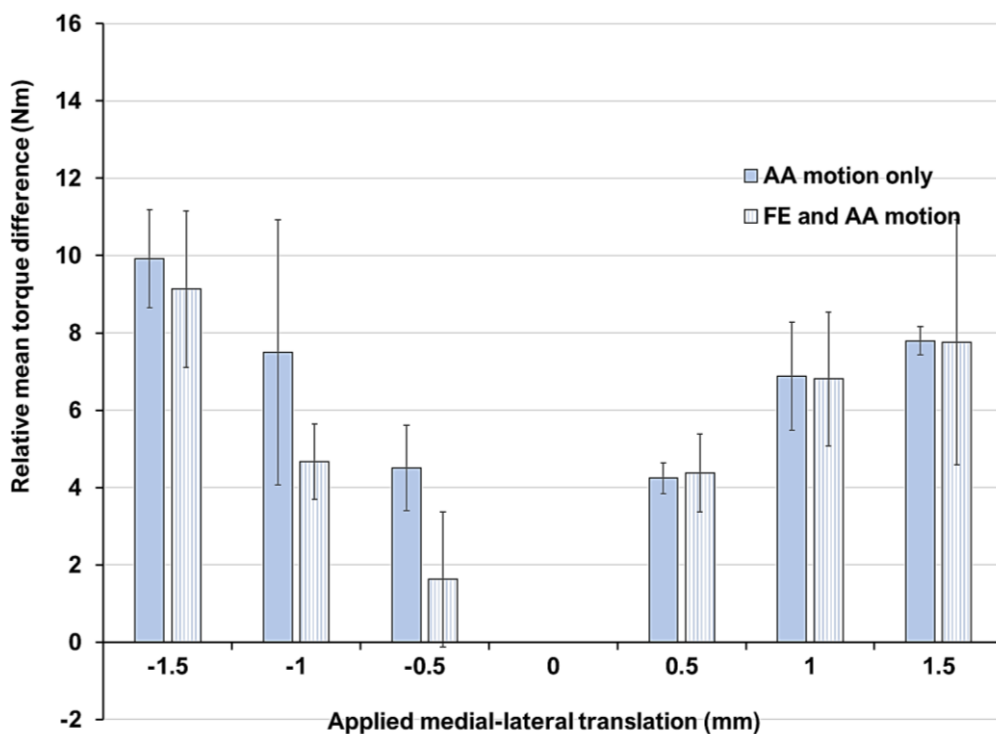


Figure 5.12 - Mean AA torque difference in response to increasing levels of medial lateral translation measured in 36mm MOP bearings (n=3) under dynamic loading and AA or FEA motion (Mean \pm 95% confidence level)

5.8 Discussion

This study assessed the relative effects of varying translational position of 36mm MOP bearings (n=3) on the measured frictional torque using the SSHS modified with a supplementary subsystem, tested in 25% bovine calf serum. Frictional torque measurements were calculated from outputs of the SSHS six-axis load cell and not the subsystem. Although some experimental assessment of the effects of high acetabular cup inclination in hard-on-hard has been conducted and found to significantly increase the measured torques (Sariali *et al.*, 2010; Bishop *et al.*, 2013), there has only been one experimental study assessing the effects of varying medial-lateral translation on the torques assessed using a uni-axis pendulum friction hip simulator with a passive spring element to replicate the translation (Al-Hajjar *et al.*, 2015). To date, there is not a study assessing the effects of medial lateral translation on the measured torques in THRs in a multi-axis system with actuated control of medial lateral translation.

Baseline frictional torque was obtained from tests where no translation was applied to understand the effects of the applied translations to the frictional torques and to allow comparison with previous studies on the SSHS. Comparison with previous studies helped understand the effects of the supplementary system on the six-axis load cell measurements. The mean FE frictional torque obtained from the SSHS in early preliminary testing (Section 4.5) for 36mm MOP bearings tested in 25% bovine calf serum when tested under 1kN constant load and $\pm 10^\circ$ FE motion only was $3.10 \pm 0.81\text{Nm}$. In the present study, under comparable conditions but testing on the modified SSHS, the mean FE frictional torque measured was $2.56 \pm 0.51\text{Nm}$. Even with the presence of the subsystem, there was no significant differences in the measured frictional torques in the FE direction. In addition, AP lateral forces measured in the no translation condition of the present study was in a similar range to those found in Section 4.5.3 ($\sim 10\text{-}20\text{N}$ vs $\sim 10\text{-}30\text{N}$). The similarities in the AP lateral forces would indicate that this was likely due to

crosstalk in the measurement channels. Lateral forces in the ML direction were however a little higher in the present study than previously observed in the SSHS assessment tests (Section 4.5.4). This could have been due in part to the engagement of the ML actuator for the ML translation study but also potentially due to the presence of the subsystem providing additional resistance in the ML direction. The free body diagram presented in Section 4.5.2 suggested that locking the ML 'frictionless' lateral bearing would result in a stiff system that results in elevated forces due to resistance. This coupled with the potential additional resistance presented by the subsystem could explain this increase in ML force.

In determining the capacity of the six-axis load cell on the modified SSHS in detecting changes in the measured frictional torque in response to medial-lateral translation, it was important to determine the effects of artefacts presented by the subsystem and/or crosstalk. It was hypothesised that if these erroneous components were constant, their effects would not mask the effects of applied medial-lateral translation. The crosstalk was however likely to be proportional to the largest input signal. However, for each given sub-study, only the medial-lateral translations were changed, and all other parameters remained constant. Therefore, the effects of the applied medial-lateral translation could be determined when compared to the no translation test of that sub-study.

An assessment was carried out with the subsystem present to determine the ability of the system to detect theoretically expected changes such as an increase in measured frictional torques in response to increased applied load, and found the six-axis load cell on the modified system able to detect an increase in measured frictional torques (Section 5.7.1). It was therefore assumed that while crosstalk and/or the presence of the subsystem affected the data output of the six-axis load cell, it did not mask relative changes and therefore the system was capable of detecting the relative effects of medial lateral translation on the in frictional torque.

Overall, introducing ML translation increased the mean frictional torque difference when compared to conditions where no translation was applied, particularly in the AA direction where the mean torque differences measured were significantly higher (up to 12.78Nm) than those measured in the FE and IE directions. This was anticipated and could be attributed to the fact that the calculation of frictional torques in the AA direction was dependent on the lateral force in the x-direction (F_x , ML force) which was elevated due to the applied ML translation (equation 3.34). Again, the relatively low mean frictional torque difference in the FE direction was anticipated because equation 3.23 shows that these are dependent on the lateral force in the z-direction (F_z , AP force). F_z in this setup and test would have arisen due to friction in the lateral bearings and therefore low. Mean frictional torque difference measured in the IE direction were also expected to be zero since there was no applied motion in that direction. Analysis of the IE torque measurements observed non-zero values which was attributed to measurement errors, noise and crosstalk in the system.

Al-Hajjar *et al.*, 2015 reported an increase in measured THR torque in response to applying a 0.5mm translation in 36mm MOP, COC and COP bearings when tested under dynamic loading and FE only motion only in a pendulum friction hip simulator. The pendulum friction hip simulator in this study measured frictional torques in the FE direction, the study applied translation in the same (FE) axis ensuring that the transducer detected effects of the translation.

Applying a dynamic load profile of 1kN peak and 200N swing phase load in the present study to 36mm MOP bearings while assessing the effects of medial-lateral translation presented similar behaviour to testing conducted under constant loading. The frictional torques in FE and IE were significantly lower than the frictional torques measured in the AA direction. This may have been because the data collection was from the constant load (swing phase) region of the test, and therefore not influenced by the peak load of the dynamic load profile. Comparing

the mean frictional torque differences measured, there was no significant increase in response to increasing the constant load from 200N (from the dynamic loading profile) to 500N or 1kN.

Even with the applied axial loads being relatively low and no crosstalk compensation on the SSHS output, it was possible to estimate that the crosstalk signals particularly in the AP and ML channels were in the 10-30N range. This was an estimate based on analysis and observation of unexpected signals across the different tests but did not form part of a formal crosstalk identification and compensation activity. For this reason, the estimated crosstalk value was not subtracted from any of the measured outputs until further assessment and verification of the magnitude of crosstalk could be carried out in future work.

While further study is required without the subsystem on the SSHS and following the implementation of a crosstalk compensation protocol, the results presented in this study have provided insight into the behaviour of THRs when tested under adverse conditions such as varied medial-lateral translation assessed in a multi-axis system with actuated control of the applied translation. The results presented have shown that the frictional torques of THRs increase when medial and lateral translation between the acetabular cup and femoral head increase during testing of 36mm MOP bearings, and can be as high as $15.35 \pm 1.93\text{Nm}$. The potential impact of these high frictional torques, if transferred to the fixation interface, was of interest and formed the basis of the next chapter investigating the torque levels needed to displace an uncemented acetabular cup.

5.8.1 Limitations and further study

The main limitation of this study is the presence of the subsystem and its effects on measured frictional torque. The subsystem was incapable of reliably measuring frictional torques in THRs (discussed in Section 3.5) and should not have been

used. However, only data collected by the SSHS assessing the effects of varying medial lateral translation while the subsystem was present was available. Further study would look to remove the subsystem and repeat these tests to better understand the effects of medial lateral translation on the frictional torques measured in THR. Although 500N is above the 1% non-repeatable error range of the six-axis load cell, it is a relatively low load for a 5kN load cell and was chosen in this pilot study to ensure early assessment did not overload or damage the system. The generated frictional torques were low and below the non-repeatable error range of the systems torque measurement of $\pm 1\text{Nm}$. Further study would also look to increase the constant loads applied as well as assess more representative load and motion conditions, such as recommended by ISO 14242-1:2012. This would assess all gait cycle motion (including IE rotation) and at the recommended range of motion. As mentioned previously in section 3.6, further study to identify and compensate for the crosstalk would also be significant in providing confidence in the collected data. As seen from the equations for τ_{FE} and τ_{AA} , in the two horizontal axes, the frictional torques are dependent on the lateral forces F_z and F_x measured by the six-axis load cell. However, the studies conducted in Section 4.5 and in the current chapter have demonstrated the possibility that all or the majority of the measured forces in these two channels are potentially crosstalk, particularly when testing in the no translation conditions. Theoretically, outputs were expected to be low in the lateral force channels since the type of linear bearings on the SSHS were designed to be as close as possible to frictionless, thereby providing minimal resistance. With the measured forces in non-excited channels continuously in a predictable range for tests conducted on the SSHS and the modified SSHS, it was assumed that the crosstalk and subsystem artefacts remained constant, and therefore the mean frictional torque difference would still be able to identify any characteristic frictional torque behaviour in response to applied medial lateral translation. Further work would therefore be needed to either accurately map out

the crosstalk in all channels for post-process compensation or to improve the load cell and electrical wiring so that crosstalk effects are reduced.

In addition, because the medial or lateral translations were applied in the swing phase region, further study could assess the combined effects of varying the swing phase load and the medial lateral translation on the measured frictional torques such as was conducted by Williams *et al.*, 2006 in the study of wear, friction and lubrication of MOM bearings. Varied rotational positioning (acetabular cup version and inclination) could be assessed independently or combined with translational positioning to assess effects on the frictional torques of THRs. Increasing the sample size from three would also increase reliability of the collected data, by increasing the statistical power. The statistical power for the current presented data was low and therefore there is a higher risk of Type II errors (failing to reject a null hypothesis when it is false). Further testing will be required to gather more data with an increased sample size and reduce the risk and likelihood of these Type II errors.

5.9 Conclusion

The results from this chapter have shown that there is an increase in measured frictional torques at the bearing interface of THRs in response to increasing medial lateral translation, as might occur in a patient when there is lateral misalignment between the centres of the femoral head and acetabular cup, and can be as high as 15Nm.

CHAPTER SIX

Methodology to assess the torque required to displace uncemented acetabular cups in total hip replacements

6.1 Introduction

Approximately 60% of implanted primary total hip replacements reported in the National Joint Registry for England, Wales and Northern Ireland (NJR, 2021) included an uncemented acetabular shell. Uncemented components rely on a stable bone-prosthesis interface that minimises micromotion and promotes osseointegration of bone into the component (Cameron et al., 1973; Soballe et al., 1992). The initial stability of the bone-prosthesis interface immediately after implantation is also known as the ‘primary stability’ of the acetabular components. Primary stability can be attained by two fixation methods; line-to-line fixation or press-fit fixation (Callaghan et al., 2007). Line-to-line fixation describes the technique where the final ream diameter of the acetabulum cavity is equal to the artificial component to be inserted whereas press-fit fixation describes the use of a ream diameter less than that of the artificial component to be inserted (Callaghan et al., 2007).

While total hip replacement surgery remains the most successful orthopaedic intervention; aseptic loosening, dislocation (due to impingement) and subluxation of the prosthetic components are the leading causes of failure in primary hip replacements and can lead to acetabular cup loosening (Brown et al., 2008; NJR 2021). The presence of impingement and subluxation might result in increased forces exerted on one side of the acetabular cup liner causing eccentric loading that can be detrimental to the fixation interface. The increased use of larger diameter bearings in THRs may also result in higher torques generated at the articulating interface that can be translated to the fixation at the backside of the acetabular cup (Bishop et al., 2013). In addition, suboptimal primary fixation either from poor bone quality at the fixation site or from suboptimal reaming techniques are likely to result in lower force and/or torque required to loosen the fixation. The stability of implanted acetabular shells can be assessed either in load-to-failure tests or via micromotion and migration tests. While micromotion and migration tests assess the dynamic loading conditions that affect the primary stability of implanted acetabular shells, load-to-failure *in-vitro* studies have been conducted to assess the extreme loading conditions that can result in primary instability and subsequent displacement of the acetabular cup using both synthetic and cadaveric bone (Lachiewicz *et al.*, 1989; Stiehl *et al.*, 1991).

Previous studies to assess primary cup fixation have used various test methods that include lever-out tests (Adler *et al.*, 1992; Macdonald *et al.*, 1999), pull-out tests (Macdonald *et al.*, 1999), push-out (Crosnier *et al.*, 2014), twist out or torque tests (Kody *et al.*, 1990; Clarke *et al.*, 1991; Curtis *et al.*, 1992) and edge (or rim) loading tests (Saleh *et al.*, 2008; Huber and Noble, 2014). Current rim load-to-failure tests replicate edge loading as may be observed clinically during translational malpositioning between the femoral head and the acetabular cup, impingement or in dislocation when the femoral head, stem or bone comes into contact with the rim of the liner (Small *et al.*, 2013; Huber and Noble, 2014).

The findings presented in Section 5.7 indicated an increase in the measured torques in response to variations in medial-lateral translation (sub-optimal positioning), even under constant loading. Regardless of whether these sub-optimal positions cause edge loading in the bearing, the torques appear likely to increase in these conditions. While load-to-failure tests study worst-care scenarios, the aim of this chapter was therefore to investigate the torques required to displace a well-seated acetabular implant experiencing axial loading, thus providing an indication of whether the frictional torques identified at the bearing interface in Section 5.7 may be problematic when transferred to the backside of the cup in terms of fixation. This well-seated acetabular implant was characterised as a 1mm interference press-fitted acetabular shell in a hemispherically reamed Sawbone block with adequate initial stability, conformal bearing contact with the femoral head leading to evenly dispersed contact stress and contact forces acting through the joint centre.

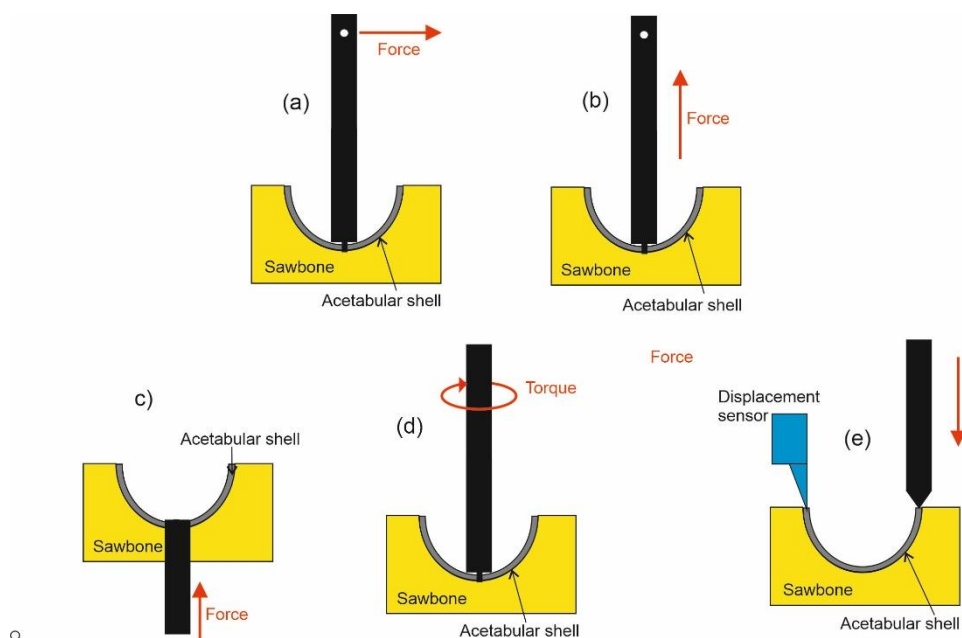


Figure 6.1 - Illustration of load-to-failure tests previously used in literature (a) push out test (b) edge loading tests (c) twist out or torque test (d) pull out test and (e) lever out test

6.2 Study Objectives

The aim of this study was to develop a test method for assessing the torque required to cause displacement of an acetabular shell that was press-fitted into two densities of saw bone (10pcf and 20pcf) under different axial loading conditions. The different axial loading conditions were used to provide information about how the torque required to displace an acetabular cup may change through the gait cycle. The method did not attempt to replicate a clinical scenario per se, rather provide information on the effect of axial load at its minimum and maximum in a gait cycle on the torque required for displacement of the shell. A comparative study using the lever-out method was also developed to allow comparison with existing literature.

The objectives of this study were to:

- i) Determine the torques required to displace uncemented acetabular shells using an established lever-out load-to-failure method in two densities of Sawbone
- ii) Develop test method and associated custom test rigs for assessing uncemented acetabular shell displacement by applying a torque-to-failure while simultaneously applying axial loading in two densities of Sawbone
- iii) Determine the torques required to displace uncemented acetabular shells by applying a torque-to-failure while simultaneously applying no load, 300N or 3kN axial load in two densities of Sawbone

6.3 Materials

6.3.1 Total hip replacement components

THR femoral and acetabular components from the PINNCALE® range were supplied by DePuy Synthes® (Leeds, UK). Details of all components used in this study are provided in Table 6.1. The sizes chosen for this study were the same as used in all hip friction simulation testing reported in Chapters 2, 3 and 5 of this thesis to allow for comparison of outcomes.

Table 6.1 - Details of THR components tested in study (ID: inner diameter, OD: outer diameter)

Commercial name	Material specification	Product reference
Femoral components, 36mm OD		
<i>Articul/eze® metal</i>	Cobalt-Chromium-Molybdenum (CoCrMo)	1365-52-000
Acetabular components (liners & acetabular shell), 36mm ID & 56mm OD		
<i>Marathon™ polyethylene acetabular liner</i>	Ultra-high molecular weight cross-linked polyethylene (UHMWPE)	1219-36-056
<i>Porocoat® acetabular shell</i>	Titanium with a sintered titanium bead surface	1217-01-056

6.3.2 Synthetic bone

Rigid polyurethane foam (Sawbone) blocks of dimensions 13cm x 18cm x 4cm were purchased from Sawbones® Europe (Malmö, Sweden) for use as a synthetic

bone substrate. Although Sawbone does not directly replicate bone structure, it can be supplied in a range of densities mimicking most human cancellous bone densities – ranging from 0.1 to 1gcm⁻³. According to ASTM F-1839-08, the uniformity and consistent properties of Sawbone make it an ideal material for the comparative testing of medical devices.

Two densities, 0.16gcm⁻³ (10pcf) and 0.48gcm⁻³ (20pcf) were chosen to simulate two types of bone quality. These are within the reported range of human cancellous bone density and allowed the simulation of healthy cancellous bone (20pcf) and also slightly lesser bone quality (10pcf) (Cowin, 2001; Helgason et al., 2008).

6.3.2.1 Synthetic bone preparation and reaming

Previous studies such as that conducted by Crosnier *et al.*, 2014 used computer numerical control (CNC) machines to ream the Sawbone to reduce variability. This present study however used a clinical reamer, the QUICKSET® grater, recommended by the manufacturer to create horizontal grooves in the cutting region which increase surface contact and engagement (Figure 6.2) (Rajesh, 2012). For practical reasons, reaming of the Sawbone blocks was conducted in a two-step process where the cavities were pre-reamed using a CNC milling machine to a depth of 47mm before completing the reaming to 55mm using progressively increasing sizes of the QUICKSET® grater heads (diameter sizes, 48 – 55mm). An acetabular cup QUICKSET® grater system was supplied by DePuy Synthes® (Leeds, UK) for the reaming of Sawbone blocks prior to insertion and fixation of acetabular shells. These were power-driven by the hand power tool Hall Power PRO-MAX System (ConMed, USA). Pre-reamed Sawbone blocks were fastened to a work bench with the use of G-clamps to prevent motion during the reaming procedure with the QUICKSET® grater.

Reaming was performed by a clinical product specialist from DePuy Synthes® with extensive experience teaching and training surgeons on the intended use of the QUICKET® grater. This was done to ensure close replication of clinical reaming techniques. This form of manual reaming introduces inter-sample variability in final depth. This was accounted for in the test methodology development (see section 6.3.3.2).

The outer diameter of acetabular shells used was 56mm. However, Sawbone blocks were under-reamed to 55mm to create a 1mm interference press-fit with acetabular shells. Under-reaming by 1mm is used in clinical conditions and has been replicated in previous experimental studies in literature (Antoniades et al., 2013; Crosnier et al., 2014). Under-reaming by more than 2mm may generate acetabular stresses in excess of bone yield stress and would therefore not be relevant (Zivkovic et al., 2010).

Once reaming was complete, a 5mm diameter hole was drilled into the base of the reamed cavity to aid extraction of acetabular components after testing.

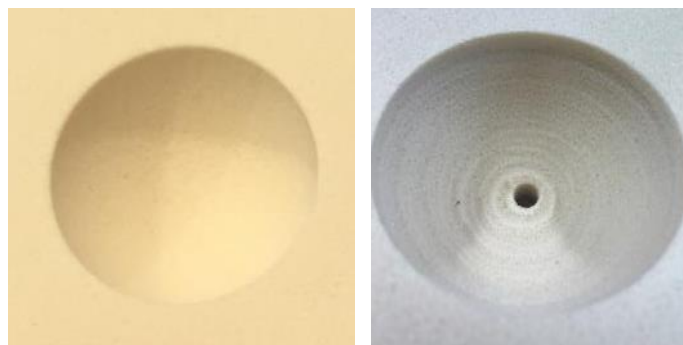


Figure 6.2 – (a) Smooth 47mm diameter cavity in a Sawbone block obtained from CNC reaming (b) Reamed 55mm diameter cavity in a Sawbone block showing horizontal grooves created by clinical reamer

6.3.3 Acetabular shell insertion

Impaction with a mallet, such as is recommended by manufacturers and is used in surgery has been commonly used in studies using saw bones reported in the

literature (Stiehl et al., 1991; Macdonald et al., 1999; Jin et al., 2006; Zivkovic et al., 2010). This method of insertion is however subjective to users and therefore creates variability in impaction forces and the number of impactions to reach a satisfactory seating. Universal testing machines have also been used to insert acetabular shells, for more repeatable insertion methodologies, by pre-defining a maximum load and rate of application, although these are also variable between studies (Adler et al., 1992; Small et al., 2013; Huber and Noble, 2014).

For this study, acetabular shells were inserted using an Instron® 3366 universal testing machine similar to the methodology used by Antoniadou *et al.* (2013). Acetabular shells were considered to be fully inserted when;

- a) The displacement of the acetabular shell (connected to the Instron® 3366 via a custom insertion rod, section 6.5.2) was equivalent to the depth of the reamed cavity
- b) The entire Porocoat® surface of the acetabular shell was seated within the Sawbone, leaving only the inner lip visible.

Insertion fixture

The insertion fixture was a 20mm diameter rod that connected to the screw thread at the apex of the acetabular shell on one end and to the Instron® 3366 load cell on the other end. The insertion of the attached acetabular shell into the reamed cavity of a Sawbone block was controlled by the Instron® 3366 (Figure 6.3).

6.3.3.1 Acetabular shell insertion protocol

The final depth of Sawbone cavity after reaming was measured using Vernier callipers and recorded. The acetabular shell insertion rod was screwed into the hole at the apex of the acetabular shell to be inserted and attached to the Instron® 3366 load cell.

The Sawbone cavity was centred below the Instron® 3366 load cell, and the block fastened to ensure it was immobile during insertion. A uniform 2mm thick aluminium bar was placed across the cavity and the Instron® 3366 crosshead manually lowered to apply a load of 1N (compressive load), bringing the acetabular shell apex in contact with the aluminium bar. This was to ensure a verifiable starting position. This load was low enough to ensure contact was achieved without significantly loading the Sawbone prior to testing.

The displacement sensor of the Instron® 3366 was reset to zero, and the aluminium bar removed. The crosshead was then lowered 2mm (compensating for the thickness of the aluminium bar) and the displacement sensor reset again. This position was then determined as zero, the position where the apex of the acetabular shell was level with the top of the Sawbone block. The load cell was also reset.

A compressive load applied at a rate of 20mm/min was used to insert the acetabular shell. The load was no longer applied when a displacement equal to the cavity depth was reached. Preliminary assessments conducted showed that maximum load required to insert cups into the higher density 20pcf Sawbone blocks was approximately 9kN. To ensure no damage was caused to the Instron® load cell and to the Sawbone blocks, “soft stop” of 9.5kN was specified in the programme on the universal testing machine.

Once acetabular shells had been successfully inserted into the Sawbone blocks, the Sawbone fasteners were released and the insertion rod disconnected from the materials tester and unscrewed from the acetabular shell. Successful insertion was based on the criteria described in section 6.3.2.1 and a fully inserted acetabular shell is shown in Figure 6.4.

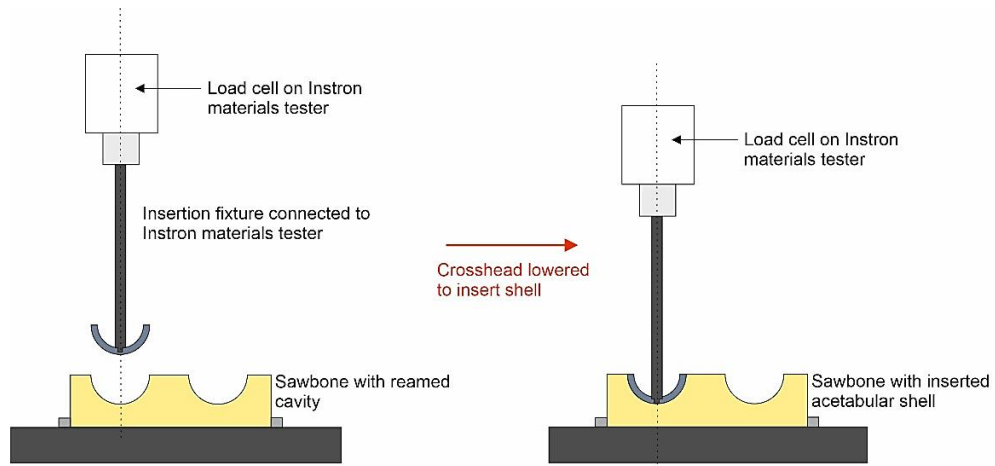


Figure 6.3 – Illustration of the custom rig in the acetabular shell insertion configuration

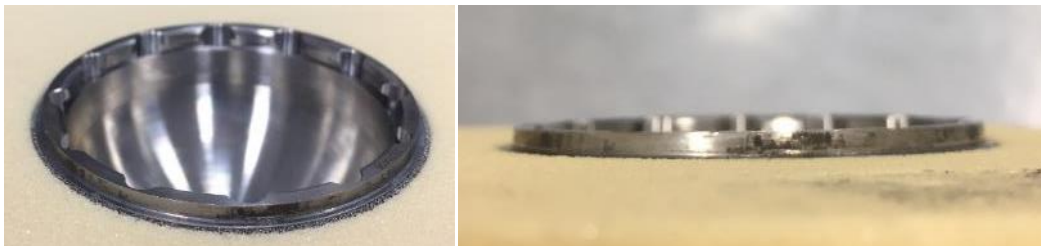


Figure 6.4 - Acetabular shell fully inserted into the saw bone block, showing coverage of Porocoat® coating only leaving the shell inner lip visible

6.3.3.2 Fixation mechanics and shell-Sawbone engagement

Due to the replication of clinical reaming techniques, there was some variation in the final depth of reamed cavities prior to insertion of acetabular shells. Preliminary assessments were conducted to assess the fixation and engagement of acetabular shells within Sawbone blocks. Adler, Stuchin and Kummer (1992) concluded that mechanical stability of acetabular shells was determined by the shells' engagement around their outer periphery.

A preliminary study was therefore conducted to investigate the engagement of acetabular shells for four mean reamed cavity depths (28, 29, 30 and 31mm). These depths were obtained from measuring the final depths of cavities after

reaming with the QUICKSET® grater. Acetabular shells were inserted and extracted using an Instron® 3366 at a rate of 20mm/min. Images were taken of the outer Porocoat® surface showing the residue of Sawbone, indicative of the region of contact and engagement (Figure 6.5). ImageJ public domain software (National Institute of Health) was used to quantify the engagement region. Five height measurements were taken across each region and a mean calculated (Table 6.2). The results indicated peripheral contact and engagement for all depths investigated, confirming initial mechanical stability was achieved prior to testing regardless of depth.

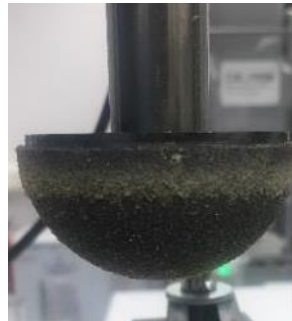


Figure 6.5 - Porocoat® acetabular shell showing region of engagement following insertion to a depth of 30mm in a Sawbone block (10pcf)

Table 6.2 - Mean height of Sawbone-acetabular shell engagement region for acetabular shells inserted at different depths

Depth of reamed cavity (mm)	Mean height of engagement region (mm)
28	5.37
29	5.32
30	5.18
31	5.52

6.3.4 Instron® universal testing machine

An Instron® 3366 universal testing machine (Instron®, UK) with maximum load capacity of 10kN and a resolution of 0.0001kN (externally calibrated in tension and

compression by Denison Mayes Group to UKAS calibration standards, 2017) was used to apply loads to the rim of the acetabular shell. The load cell of the Instron® 3366 was connected to a mobile crosshead that moved downwards to apply a compressive force and upwards to apply a tensile force. It was controlled via a personal computer running the Bluehill®2 software for the input of test parameters such as rate of load application, displacement and number of applied cycles etc.

6.4 Assessing the torque required to displace uncemented acetabular cups (Lever-out method)

Load-to-failure tests have been used to assess the primary stability uncemented acetabular shells as a result of impingement or articulation forces (Adler et al., 1992; Macdonald et al., 1999; Meneghini et al., 2010).

This section describes the lever out load-to-failure test conducted to assess the torque required to displace 1mm interference press-fitted acetabular shells from 10pcf and 20pcf Sawbone blocks. The methodology used was modified from the studies conducted by Meneghini et al., 2010.

6.4.1 Method

Acetabular shells were press-fit into Sawbone blocks with a 1mm interference fit (section 6.3.2.1).

The press-fit acetabular shell was connected to a lever arm and the Sawbone block securely fastened in the universal testing machine such that the loading axis of the machine was perpendicular to the lever arm, at a distance of 15mm from the centre of the acetabular shell (Figure 6.6). A preload of 2N was manually applied to the lever arm using the materials tester to ensure there was contact prior to the start of the test. The materials tester was then used to apply load at a

rate of 1mm/min. The maximum displacement permissible was 5mm and was specified as a software limit, ensuring the test automatically stopped at this point. A maximum load capacity of 9kN was also specified. To prevent possible damage to the Instron® 3366 load cell, a sudden increase or decrease of applied load by 40% caused a trip of the load cell and stopped the test.

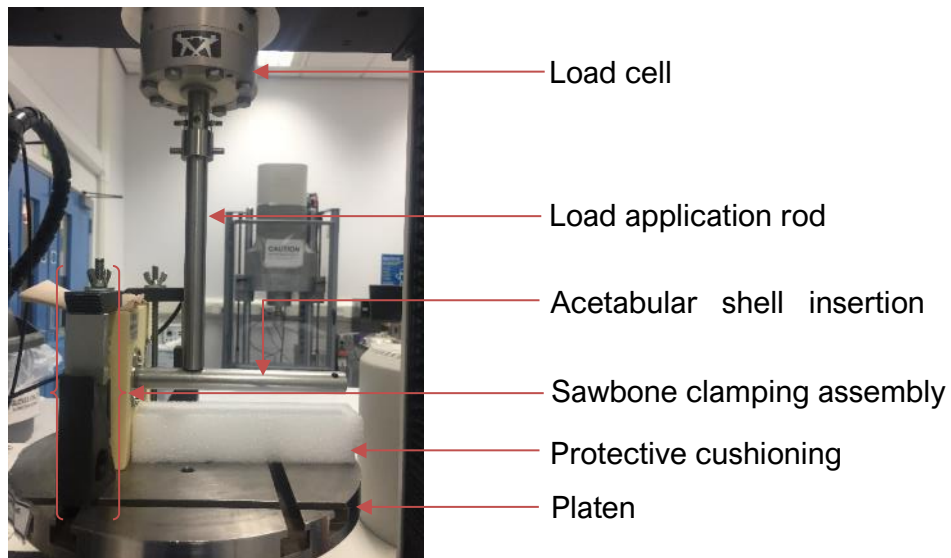


Figure 6.6 - Lever out study set up on an Instron® 3366 universal testing machine

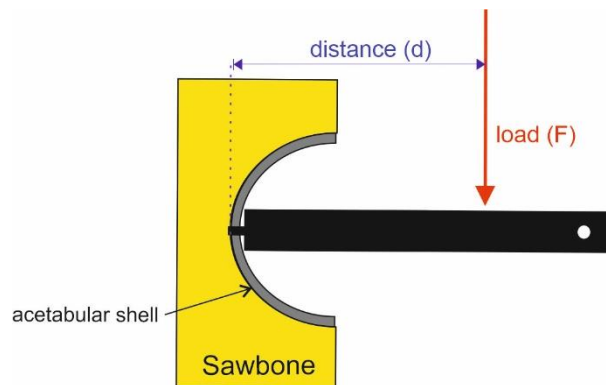


Figure 6.7 - Illustration showing the position of the applied load and the distance from the pivot

$$\text{Lever-out torque} = F \times d$$

Equation 6.1

Where F is the maximum applied load required to loosen the fixation and d is the distance between the load and the shell attachment point.

Equation 6.1 was used to calculate the lever out torque using the maximum load required to cause an acetabular shell displacement greater than or equal to 2mm and the distance between the position of the applied load and the pivot (Figure 6.7).

The average lever-out torque was obtained for both 10pcf and 20pcf Sawbone, sample size of three for each group. The variability of data about the mean was assessed using 95% confidence limits.

6.4.2 Results and Discussion

This lever-out study was conducted on both 10 and 20pcf Sawbone blocks (n=3) to assess the torque needed to displace acetabular shells during the early time period following implantation where primary stability is important. In this study, primary stability was achieved with a 1mm interference press-fit of acetabular shell into Sawbone. The lever-out torques measured in this study were $13.9 \pm 1.5\text{Nm}$ for the 10pcf and $33.7 \pm 8.8\text{Nm}$ for the 20pcf Sawbone (Figure 6.8). Macdonald et al., 1999 reported 23.15Nm as their lever-out torque for displacing acetabular cups in one undisclosed density of Sawbone block tested. Meneghini et al., 2010 also reported a lever-out torque of $32.0 \pm 17.8\text{ Nm}$, also for acetabular cups in an undisclosed density of Sawbone.

Due to several differences between this study and some of the existing literature, no direct comparisons were possible. Some of the differences include the use of a pulley system for levering out the acetabular shell in the study by Macdonald et al., 1999 and Adler et al., 1992 or the additional screw fixation used in the study by Meneghini et al., 2010.

This load-to-failure method of assessing the torques needed for displacing acetabular shells however did not account for loading conditions such as is experienced by the bearing during the gait cycle i.e. the transfer of torques at the

articulating surface to the backside of the cup. A new methodology was therefore developed that would allow simultaneous axial loading during a load-to-failure study assessment.

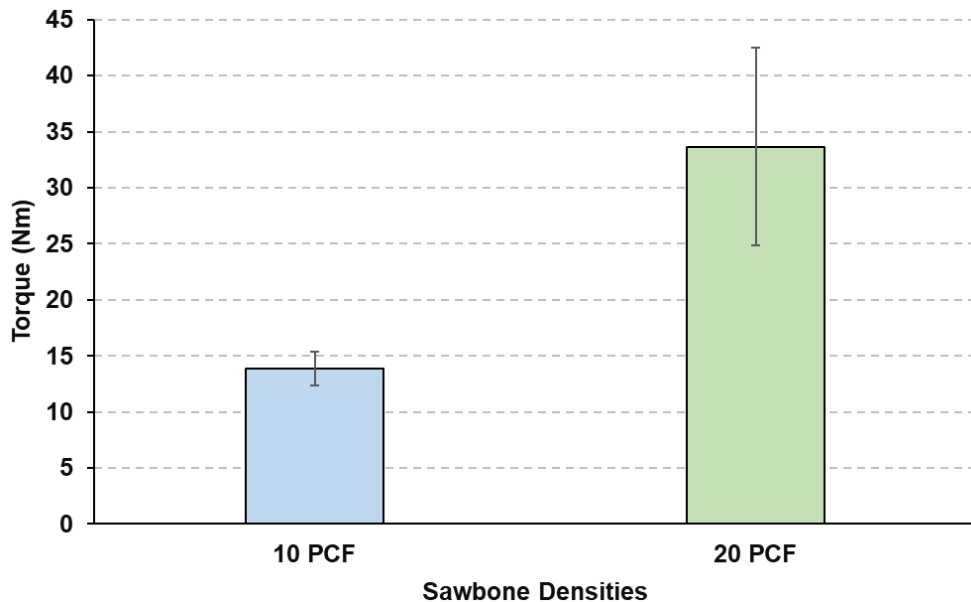


Figure 6.8 – Graph showing the mean torque required to displace uncemented acetabular shells in 10 and 20pcf Sawbone using the lever-out load to failure method (n=3, error bars represent 95% confidence)

6.5 Experimental Method Development for assessment of acetabular shell displacement under load

This section describes the development out of a methodology to assess uncemented acetabular cup displacement in a rim loading load-to-failure study under simultaneous axial loading. The two load-to-failure test methods identified that were compatible with a simultaneous axial load were the push out and rim loading methods. The rim loading was however identified as the more clinically representative type of load-to-failure study for developing this methodology.

The activities carried out are summarised below;

- Custom rig and fixtures design for acetabular shell insertion and all load-to-failure studies conducted

- Methodology development for rim-loading load-to-failure under axial loading study

6.5.1 Design requirements for custom rig and accompanying fixtures

Requirements were identified for the design of the custom rig and all accompanying fixtures. These are shown below:

- To allow the mounting of total hip replacements, such that the femoral head is positioned superior and concentric to the acetabular cup press-fitted into hemispherical cavity in Sawbone
- To allow application of a rim load to the edge of acetabular shell
- To allow simultaneous application and measurement of axial loading through a femoral head during rim-loading
- To be robust enough to undergo a maximum load of 10kN applied by the Instron® 3366 without bending
- To not be wider than 400mm or higher than 600mm to fit within the test space of the Instron® 3366
- To allow secure fastening to an existing platen on the Instron® 3366 to prevent rig motion during testing
- To ensure accurate positioning of Sawbone blocks for on-axis loading during shell insertion and testing
- All associated fixtures to be robust to withstand bending under load
- All load-application fixtures for the rig to be compatible with fixation features on the Instron 3366 load cell
- Rim loading fixture to be able to apply localised point loads to the rim of acetabular shells and could not lose contact with the rim of the shell during testing.

6.5.2 Design description of custom rig and accompanying fixtures

The designed rig and its fixtures were multi-functional and could be used:

- For acetabular shell insertion into Sawbone blocks (Figure 6.3)
- For conducting rim-loading load-to-failure tests (Figure 6.9) with or without axial loading

Unless otherwise specified, components of this custom rig were manufactured from the alloy grade 303 stainless steel. Appendix 8.2 provides detailed drawings of all individual parts of this custom rig and associated fixtures.

The following sections describe the capabilities of the rig and fixtures in detail.

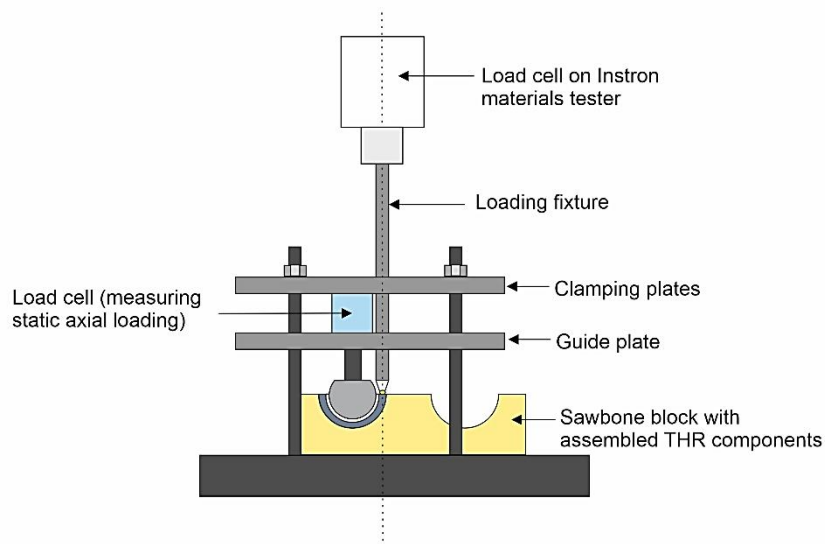


Figure 6.9 – Schematic of the custom rig in the rim-loading with axial loading test configuration

6.5.2.1 Generating static axial loading

One of the requirements of the rig was to allow the application of a simultaneous axial load during rim-loading load-to-failure testing. It was not possible to have two controlled loading axes however due to the functional design of the Instron® 3366 materials tester. The rig was therefore designed to generate static axial loading

through the femoral head to the acetabular component, and the Universal testing machine used to control the rim load.

This static axial loading was achieved via a clamping mechanism that comprised of a load cell (Omegadyne, Connecticut- USA) positioned between a top clamping plate and a lower guide plate and supported by four rods (Figure 6.10). The static load generated and transferred to the femoral head by tightening or loosening the hex nuts above the clamping mechanism could then be measured by the load cell. Polymer bushings were used in the guide holes to reduce the friction generated from contact.

The load cell was constrained by two centralising fixtures to prevent off-axis loading of the femoral head. The lower guide plate included slots that allowed for fine adjustment of the femoral head. This in conjunction with the adjustment capable on the base plate for the Sawbone block allowed for optimal positioning.

The dimensions of the clamping plates were optimised during the method development. The initial design featured clamping and guide plates that were the same width and length as the base plate measuring 320 x 200 x 30mm. A computational assessment of this design using SolidWorks® indicated that this would increase the weight of the rig and thereby making handling difficult during testing such as anticipated difficulty sliding the plates up and down the clamping rods. This initial design is provided in Appendix 8.2.

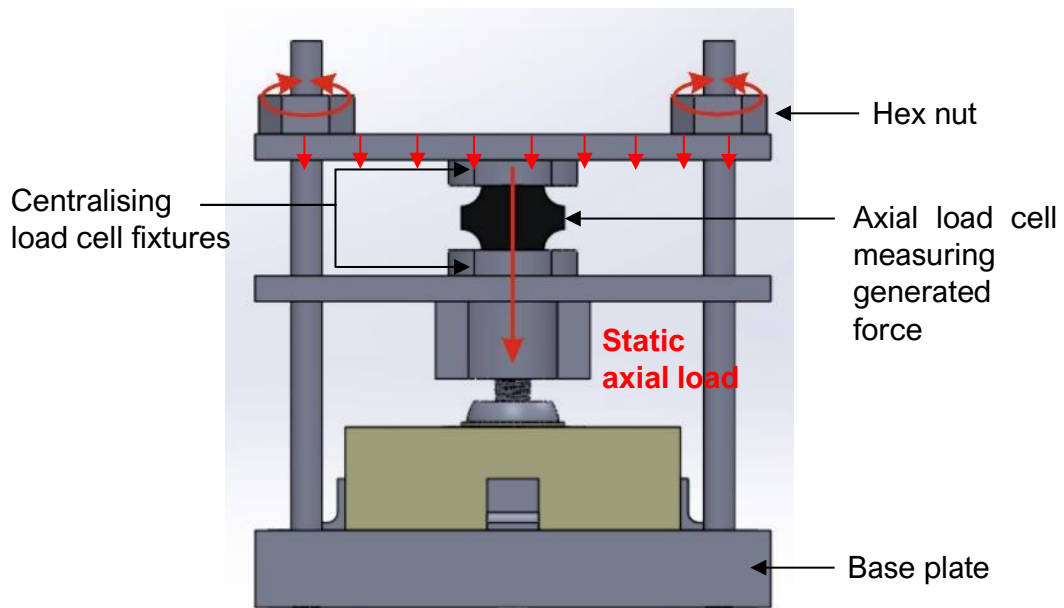


Figure 6.10 – CAD illustration of clamping mechanism; showing tightening nuts and direction of static axial femoral head load

6.5.2.2 Rim load application fixture

The fixture (a 20mm diameter rod) was designed to be attached directly to the load cell of the Instron® 3366 for the application of rim loads to the acetabular shell. The connector available on the Instron® 3366 to which both fixtures were attached was an 18mm outer diameter (OD), 12mm inner diameter (ID) hollow cylinder with four perpendicular 6mm diameter holes for the use of fastening dowels (Figure 6.11).

This fixture featured a curved-end rod that was attached for load application during the rim-loading study (Figure 6.12). This part had a 1.5mm radial curved end to ensure contact was maintained throughout testing regardless of acetabular shell motion (Figure 6.13). To prevent direct contact with the clamping and guide plates, and to ensure the trajectory of the assembled rim loading fixture was maintained, a plain polymer bushing used (RS Components, UK. Part number JFM-1517-09).



Figure 6.11 - Attachment mechanism for Instron® 3366 universal testing machine; also showing cross section of connector

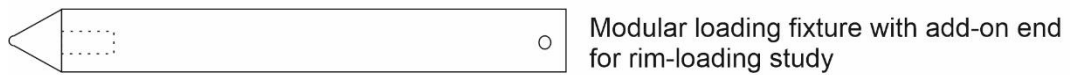


Figure 6.12 – Schematic of load application fixtures

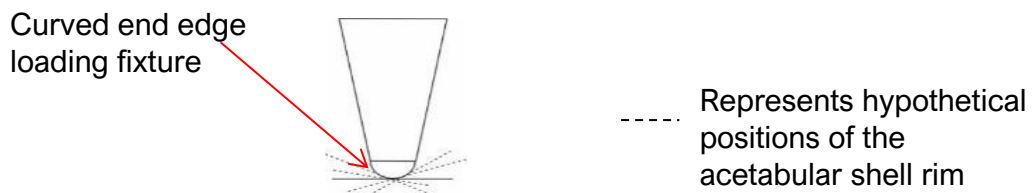


Figure 6.13 – Schematic of curved-end add-on for the modular loading fixture illustrating how contact with rim was maintained regardless of acetabular shell displacement (cross-sectional view)

6.5.3 Rim-loading load-to-failure study with axial femoral head loading

A test method was developed for assessing the torques required to displace uncemented acetabular shells whilst experiencing different static axial loading.

Porocoat® acetabular shells were inserted into Sawbone blocks as described in section 6.3.2.1. Marathon™ acetabular liners were then placed into acetabular

shells. The lower guide plate was positioned above the Sawbone block, such that the attached *Articul/eze*® femoral head component was concentric within the acetabular liner (Figure 6.14). An axial load cell (Omegadyne, Connecticut- USA) with accompanying centralising fixtures was then positioned between the clamping and guide plates. The nuts were tightened to generate the required static femoral head load of 300N or 3kN, such as is seen at the minimum and maximum points in the human gait cycle. This was then measured by the axial load cell and recorded. This static load was transferred from the clamping mechanism through the femoral head to the acetabular components and fixation.

The assembled rim-loading fixture was attached to the Instron® 3366 and manually lowered through the polymer bushings in the clamping plates using the Instron® 3366 controls. With the aid of the T-slots in the base plate and the slotted counterbores on the lower guide plate, the Sawbone block and femoral head component positions were adjusted to ensure the rim loading fixture was positioned to contact the rim of the shell. The anti-translation tabs were then fastened to secure the Sawbone from moving.

A compressive preload of 2N was manually applied using the Instron® 3366 controls to ensure contact between the edge loading fixture and the acetabular shell rim prior to testing.

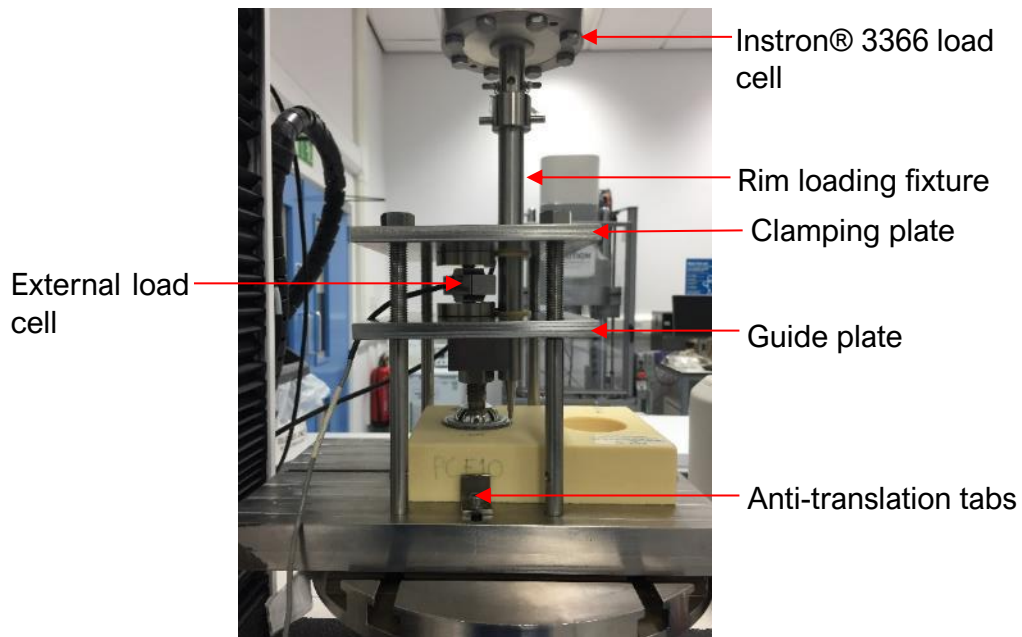


Figure 6.14 – Load-to-failure study with axial femoral head loading set up on an Instron® 3366 universal testing machine

6.5.4 Rim-loading load-to-failure study without axial femoral head loading

A control test to understand the effects of the different applied axial loads was conducted by modifying the developed method to allow rim-loading with no axial loading (Figure 6.15).

This was achieved by removing the femoral head and clamping mechanism but retaining Sawbone alignment and support features.

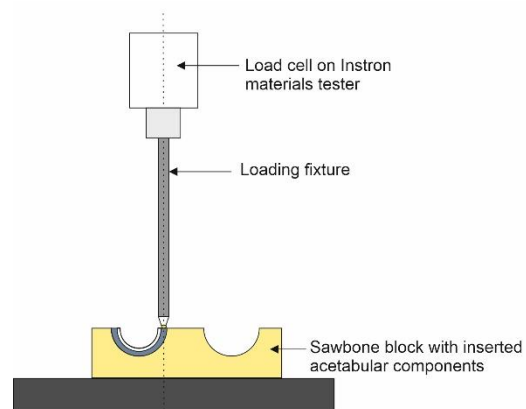


Figure 6.15 – Schematic of the custom rig in the rim-loading without axial loading test configuration

6.6 Method

Sawbone blocks of pcf 10 and 20 were used to conduct lever-out and rim-loading load-to-failure tests as described in Table 6.3. A sample size of three was used for each condition. A sample refers to a 54mm Porocoat® acetabular shell and a corresponding 36mm metal femoral head-on-polymer acetabular cup bearing combination.

Table 6.3 – Sample sizes used for each study conducted in this chapter

Study	Sample size	
	10pcf Sawbone	20pcf Sawbone
Rim-loading study with no axial load	3	3
Rim-loading study with 300N axial load	3	3
Rim-loading study with 3kN axial load	3	3

6.6.1 Data output, processing and statistics

Raw data of the applied load, and the subsequent displacement of the acetabular shell denoting motion at the fixation interface was collected.

The torque required for displacement of the acetabular shell greater than or equal to 2mm was calculated using the maximum recorded load and the distance between the position of the applied load and the centre of rotation of the bearing (Figure 6.16).

The average torque required to displace the acetabular shell while under axial loading was obtained for both 10pcf and 20pcf Sawbone, sample size of three for each group. The level of significance for the average torques obtained for all test groups was $p < 0.05$, and the variability of data about the mean was assessed using 95% confidence limits.

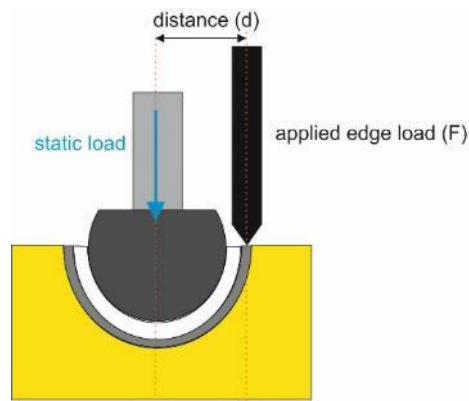


Figure 6.16 - Illustration showing the position of the applied edge load and the distance from the centre of rotation of the bearing

Statistics

A one-way ANOVA was used to determine the statistical differences between the torques measured during lever-out and rim-loading tests for both 10 and 20 pcf Sawbone. The null hypothesis assumed no significant difference between the torques generated in the 10pcf and 20pcf groups for all tests conducted.

6.7 Results

A rim loading load-to-failure methodology was used to test 54mm Porocoat® acetabular shells inserted with a 1mm interference press-fit into 10pcf and 20pcf Sawbone, and assembled with 36mm MOP bearings (n=3) whilst applying a axial loads of either 300N or 3kN simultaneously. A rim loading study with no axial loading was conducted to understand the effects of simultaneous axial loading, and a lever-out load-to-failure study was also conducted as a comparison of the new methodology with existing tests in the literature (n=3).

With no axial load, the average torque measured using the rim-loading method was 19.4 ± 7.8 Nm for 10pcf Sawbone and 38 ± 6.3 Nm for 20pcf Sawbone. Under an initial axial load of 300N, the average torque measured was 55.6 ± 11.2 Nm and 92 ± 1.5 Nm for 10pcf and 20pcf Sawbones, respectively (Figure 6.17). Under 3kN

initial axial load, the average torque measured was $80.1 \pm 9.6 \text{ Nm}$ and $133 \pm 6.5 \text{ Nm}$ for 10pcf and 20pcf, respectively. During testing, the initial axial loads of 300N and 3kN decreased to approximately 28N and 737N respectively.

Overall, the torques required to displace acetabular shells in 20pcf Sawbone were higher than the torques required to displace acetabular shells in 10pcf Sawbone ($p < 0.05$). In both 10pcf and 20pcf Sawbone also, higher torques were required to displace acetabular shells during the rim loading with simultaneous axial loading test than in the lever-out or rim loading with no axial loading tests ($p < 0.05$). The torques required to displace acetabular shells under 3kN axial load were also found to be higher than under the 300N axial load, for both 10pcf and 20pcf Sawbone ($p < 0.05$).

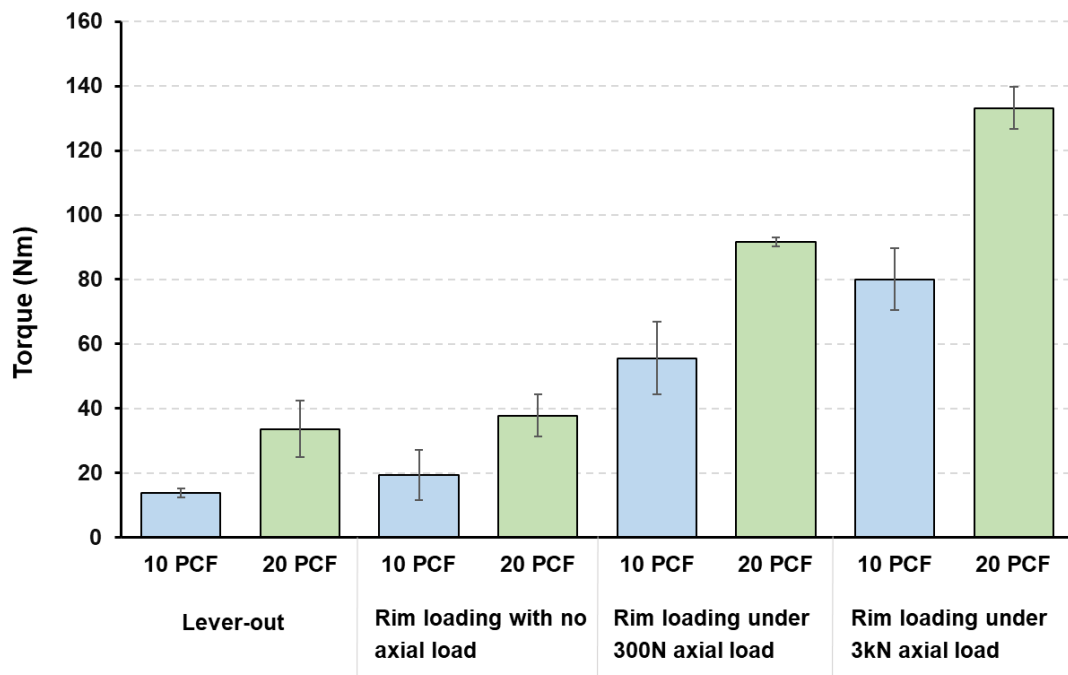


Figure 6.17 – Mean torques required to displace uncemented acetabular shells measured in a lever-out load-to-failure test, and rim-loading tests with and without axial loading using 10 and 20pcf Sawbone density (n=3, error bars represent 95% confidence limits)

6.8 Discussion

Given that it had been shown in Section 5.7 that sub-optimal positioning of the bearing as a result of variations medial-lateral translation increased the frictional torque at the bearing interface during the loading cycle, a methodology was developed in this chapter to determine whether these frictional torques were significant enough to result in acetabular cup displacement. The method developed in this chapter involved loading the acetabular shell rim while simultaneously applying an axial load through the femoral head to the acetabular components.

The use of cementless implants in primary hip replacement surgery has doubled and the use of hybrid implants tripled since 2006, according to the National Joint Registry for England, Wales and Northern Ireland (NJR, 2021). Research is continuously being conducted into ways of improving cementless total hip replacement survival and long term outcomes (Apostu et al., 2018). These include preoperative approaches such as implant design and material selection to encourage better osseointegration (Taniguchi et al., 2016; Xue et al., 2020), intraoperative approaches such as optimising component placement (Miyakawa et al., 2004), and postoperative approaches such as bone metabolism enhancing medication and avoidance of high impact activities (Cherian et al., 2015; Apostu et al., 2017).

The study was interested in understanding the forces that would be required to create primary instability by displacing the acetabular shell and subsequently resulting in loosening at the implant-bone interface. Unsurprisingly, it was found that with an increase in the axial femoral load, the torque required to cause displacement at the fixation increased in both Sawbone types. The presence of a concentrically positioned femoral head with good contact with the acetabular cup stabilises the joint and minimises offset torques that can propagate to the fixation interface (Liu et al., 2013).

The rim loading without axial loading test group in this study recorded $755.8 \pm 123\text{N}$ for the 10pcf group which was similar to results presented by Huber and Noble, 2014 who reported loads of $837.3 \pm 18.3\text{N}$ for a similar diameter uncemented acetabular shell press-fit into 10pcf Sawbone with 1mm interference fit.

While no direct comparisons can be made due to the differences in test procedure, it is unlikely that applying the torques measured in the simulator studies generated under variations in translational positioning (Section 5.7) will reach the torque requirement for displacing acetabular cups in the load-to-failure tests with axial loading conducted in this chapter. To be able to explore the worst possible case comparison, the highest frictional torque measured during testing on the modified SSHS was used, where for a 36mm MOP bearing the measured resultant frictional torque was $15.35 \pm 1.93 \text{ Nm}$, measured when a 1.5mm lateral translation was applied under 1kN load (Section 5.7). This torque if transferred from the articulating surface of the THR bearing to the acetabular cup fixation to bone however, has the potential to overload the fixation and displace acetabular cups in 10PCF Sawbone for both lever-out and rim test with no axial loading studies.

The consequences of elevated frictional torques at the bearing interface under implant malpositioning conditions (with or without edge loading) result in shear stresses that may be transferred to the fixation interface of the acetabular cup and result in displacement or loosening. Without the additional stabilisation introduced by the femoral head, it was unsurprising that the test conditions without axial loading were likely to be the most susceptible to the effects of these elevated frictional torques. Using telemetry in instrumented hip replacements, Bergmann et al., 2001 observed that overall, lateral forces were lower than axial force. However, axial force was found to decrease significantly to approximately same level as lateral forces during the swing phase. This may indicate that in instances, such as during the swing phase, when the applied axial force is at its lowest, lateral

forces can result in femoral head translation towards the acetabular cup rim and subsequently edge loading leading to failure.

However, overall, the torque requirements for displacing acetabular cups measured in the present study were greater than the elevated frictional torques measured under variations in translational positioning. This could be due to a number of factors that include the static nature of the applied rim load in comparison to the cyclical loading of the acetabular component associated with simulated activity as well as the likely joint separation that occurs in translational malpositioning resulting in a temporary lack of applied femoral head load. In addition, the elevated torques measured under variations in translational position (Section 5.7) were generated under the relatively low 1kN axial load and a reduced range of motion. Results from testing in this thesis (Section 4.5 and Section 5.7) indicate that increasing the applied axial load increases the measured frictional torque. McGrory *et al.* (1995) found that with a larger femoral offset from the centre of the acetabular cup, there was larger lateral motion needed and subsequently higher force exerted in the AA direction. These higher AA forces which are likely to applied away from the joint axis may result in shear forces and increased frictional torques transferred to the fixation interface. However, it is more likely that these elevated forces and torques will contribute to progressive loading and failure of the bone-implant interface over time, rather than immediate or instantaneous failure. Further study is therefore required to determine the effects of translational positioning on the measured frictional torques under more clinically representative load and motion conditions, for further comparison with the data generated in this chapter.

The results of this study showing a significantly higher torque requirement to displace acetabular cups in 20PCF Sawbone in all tested conditions, also indicate that poor bone quality at time of implantation may result in the creation of

suboptimal primary stability for uncemented implants and increase susceptibility to the effects of translational malpositioning.

The results presented in this chapter have shown that including femoral head load during static load-to-failure testing significantly changes the torque requirement to cause uncemented acetabular cup displacement. This indicates a need to better represent clinical loading conditions (and not just worst-case conditions) to allow for better understanding of fixation mechanics using these simplified load-to-failure tests.

6.8.1 Limitations and future recommendations for the study

A limitation of the study was the use of synthetic bone to simulate the behaviour and properties of natural bone, however this was deemed appropriate for the development of this new methodology without the need to acquire biological tissue.

In future, an improvement to the methodology would be to employ the use of a controlled system for the application of axial femoral head load. As was discussed in the chapter, it was observed that due to the static nature of the axial load (with no feedback loop to ensure the load was kept constant) and the viscoelastic nature of the sawbone, the initial axial load applied via clamping drastically reduced during the test. An ability to control that applied axial load will give a better representation of the torques required under the given axial load.

The design of the current study was limited to instantaneous load conditions rather than a cyclical load to fatigue and damage the fixation over time. Future iterations of this study can assess the cyclical forces required to result in fixation failure. This will allow better comparison with data obtained from simulator studies conducted.

CHAPTER SEVEN

Discussion and Conclusion

7.1 Introduction/ Clinical Need

An increasing number of younger and active patients are receiving total hip replacements (NJR, 2021). This means patients now expect more from their total hip replacements, not only by undergoing more strenuous high-load activities but also requiring the implants to last longer. Failure of total hip replacements results in pain for the patient, loss of function, impaired lifestyle and revision surgery. Revision surgeries in addition to being more complex and costly than primary total hip replacement procedures, have lower functional outcomes and patient satisfaction (Crowe *et al.*, 2003; Saleh *et al.*, 2003).

There is therefore an increased need for more robust pre-clinical testing procedures to ensure better assessment of implants to meet the increased demands, and also to understand the performance of THRs in different functional environments. In addition to excessive wear being a detrimental to THR longevity, concerns have increased around high friction in total hip replacements and its potential role in mechanical loosening of fixation or fretting and corrosion at the femoral head-neck taper junction (Bishop, *et al.*, 2013; Damm, *et al.*, 2015; Scholl, *et al.*, 2016; Sonntag, *et al.*, 2017). Robust pre-clinical testing of friction behaviour of total hip replacements should include simulation of physiological loading and

motion as well as impingement and variations in surgical implant positioning, factors that have been identified to contribute to THR failure modes. Similar to ISO 14242 -1, -2, -3 and -4 that defines standardised *in-vitro* hip simulator testing methods for the wear of total hip replacements or ASTM F3143 – 20 that defines a standardised test method for determining the frictional torque and friction factor of THRs using a uni-axial friction simulator, a robust and standardised methodology for assessing frictional torques of total hip replacements using a multi-axis physiological simulator is needed. The development of such methodology requires research to underpin understanding of critical factors relating to the *in-vitro* hip simulator testing of frictional torques at the bearing interface of THRs.

Clinical studies studying the surgical rotational positioning of the acetabular cup have defined a 'safe zone' for acetabular cup version and inclination, outside of which dislocation and impingement may occur (Lewinnek *et al.*, 1978; McCollum and Gray, 1990; Barrack *et al.*, 2001). The effects of rotational surgical implant positioning outside of these safe zones and of translational positioning have also been studied in regard to the wear performance of total hip replacements in both experimental and computational studies (Al-Hajjar *et al.*, 2010; Al-Hajjar *et al.*, 2014; Hua *et al.*, 2014; Ali *et al.*, 2016; Leng *et al.*, 2017; O'Dwyer Lancaster-Jones *et al.*, 2017). In general, these studies all found the wear rates to increase significantly with rotational and/or translational mal-positioning.

Preoperative planning prior to total hip replacement surgery includes templating on radiograph which includes predictions of the required component sizing, neck length and resection, as well as femoral offset. It can be difficult to accurately assess, particularly because this process requires the femur to be rotated 15-20° in the AP plane and errors can lead to suboptimal restoration of femoral head centre, limb length and neck-shaft angle (Armfield and Towers, 2007; Barrack *et al.*, 2007). In addition, following surgery it is important to determine the position of

the components to determine optimal positioning and to observe any changes during follow up. While there are multiple ways of imaging or examining these, one plane radiographs cannot fully or accurately give the position of all implanted components. In addition, static imaging is not able to detect dynamic conditions such as edge loading that occurs from joint separation, steep acetabular cup inclination or excessive acetabular cup version (Kwon et al., 2012). Using fluoroscopy for dynamic assessment, it has been found that separation between the femoral head and acetabular cup centres occur during the gait cycle (Lombardi et al., 2000; Dennis et al., 2001). The occurrence of separation resulting in edge loading *in-vivo* has also been observed during retrieval analyses on ceramic-on-ceramic bearings where stripe wear was found on the femoral heads due to contact with the acetabular cup rim (Nevelos et al., 1999, 2000).

However, the effects of implant positioning on the frictional behaviour of total hip replacements have only been subject to limited assessment and there is a gap in understanding how implant positioning and the restoration of natural biomechanics can impact the behaviour and performance of total hip replacements. To date, using uni-axial hip simulators, only Sariali *et al.*, (2010), Bishop *et al.*, (2013) and Al-Hajjar *et al.*, (2015) have assessed the effects of edge loading and/or steep cup inclination angles on the friction at the bearing interface of total hip replacement and found significant increases in the measured friction.

Similar to these studies, the majority of existing *in-vitro* studies investigating the effects of different factors on the friction and frictional torques of total hip replacements have been conducted using uni-axial friction hip simulators. These have included studying the effects of bearing size, lubrication, materials combinations, contact mechanics, loading and motion (Scholes and Unsworth, 2000; Scholes *et al.*, 2000; Williams *et al.*, 2006, 2008; Brockett *et al.*, 2007, 2008; Bishop *et al.*, 2008; 2013).

While these uniaxial hip simulators have been reported in literature for the pre-clinical testing of friction behaviour of total hip replacements, they are limited in their ability to test under clinically relevant conditions such as the application of simultaneous multi-axial motion and loading. Studies conducted by Weisenburger *et al.* (2013), Haider *et al.*, (2016) and Sonntag *et al.*, (2017) have employed the use of multi-axis hip simulators to assess the frictional torques at the bearing interface of total hip replacements under physiological conditions. None of these studies however investigated the effects of non-optimum implant positioning on the frictional torques.

The aim of this project was therefore to develop a pre-clinical testing method using a newly acquired multi-axis hip simulator to assess the frictional torques present at the bearing interface of total hip replacements under both standard and sub-optimal implant positions, with a particular focus on variations in translational implant position. To understand the potential detrimental effects of the measured frictional torques in sub-optimal implant position conditions, this project also developed an *in-vitro* load-to-failure study to investigate the torques required to cause acetabular cup displacement at the fixation interface.

7.2 Multi-axis measurement of frictional torque in total hip replacements

As part of developing the method for assessing the frictional torques at the bearing interface of total hip replacements, two multi-axis friction measuring systems were compared in Chapter 3. The two systems were (i) an electromechanical single station hip simulator equipped with a six-axis load cell for the measurement of force and torque in the three orthogonal axes and (ii) a custom-built electromechanical friction measuring system designed to work as a subsystem for a single station hip simulator.

Frictional torque analyses of the two systems were conducted by developing equations in the three orthogonal directions for each system using free body diagrams. These analyses demonstrated that the six-axis load cell of the single station hip simulator (SSHS) was the better of the two systems and that the custom-built friction measuring subsystem was not capable of accurately determining the frictional torques of total hip replacements. This was a result of poor design that resulted in variables necessary for the frictional torque calculations being unknown.

Although there are some differences in system setup and configuration, similar frictional torque analyses for multi-axis hip simulators were conducted by Haider *et al.*, (2016) and Sonntag *et al.*, (2017), who also found that the frictional torques of total hip replacements tested were dependent on measured moments and some lateral forces detected by a multi-axis transducer. Measured moments and lateral forces in these systems are generally expected to be orders of magnitude lower than the peak applied axial load, and crosstalk compensation in the present study would have provided better confidence in the data collected. The simulators used in the studies conducted by both Haider *et al.*, (2016) and Sonntag *et al.*, (2017) had crosstalk compensation functionalities as part of their calibration process. While the present study did not apply a post-process compensation matrix to the data collected, efforts were made to identify the crosstalk signals detected particularly in the lateral force channels, as these were very low but were critical in determining the frictional torque of total hip replacements throughout this thesis (Sections 4.5 and 5.7). This lack of crosstalk compensation was one of the main limitations with the use of the SSHS and should be addressed in future study either by incorporating this into the SSHS calibration process or by applying a compensation matrix as a post-process. As discussed in Section 3.6.1, the current static calibration process could also be improved by developing a dynamic

calibration process that allows for the compensation of any frequency-dependent effects.

7.3 Assessment of the effects of medial-lateral translation on the frictional torques of total hip replacements

Using the modified SSHS (with the subsystem) but taking all data from the SSHS six-axis load cell only, the effects of medial-lateral translation on the frictional torques at the bearing interface of total hip replacements were assessed. Utilising the frictional torque equations and method developed in Chapters 3 and 4, this study showed for the first time that frictional torques of total hip replacements did significantly increase with increasing variation in electromechanically applied medial-lateral translation as might occur in a patient when there is lateral misalignment between the centres of the femoral head and acetabular cup in both uni- and bi-axial motion conditions. The overall highest frictional torque was observed when 1.5mm lateral translation was applied (under 1kN constant load and AA motion only) and was 15.35Nm.

Al-Hajjar *et al.*, (2015) measured frictional torques of approximately 2.7Nm when 0.5mm medial-lateral translation was applied using a spring element with comparable acetabular cup inclination, under 2kN dynamic load and FE only motion. Using the uni-axial condition of AA only applied motion for comparison, in the current study (under an axial load of 1kN), the frictional torque was 8.98Nm when 0.5mm lateral translation was applied and 5.17Nm when 0.5mm medial translation was applied. The frictional torques measured in the current study are significantly higher than was observed by Al-Hajjar *et al.*, (2015). As was observed in the pendulum simulator/SSHS comparison study, data generated on these two differing systems are unlikely to agree (Chapter 2 and 4). However, what is consistent between the two studies is the significant increase in frictional torque

generated in response to variations in the medial-lateral translation and indicates that clinical factors such as head offset deficiency, joint laxity and medialised acetabular cup components which all result in medial-lateral translational mismatch between the femoral head and acetabular cup centres warrants even further pre-clinical assessment.

The main limitations with this study were the presence of the subsystem on the SSHS during testing and the potential effects of crosstalk on the collected data. In addition to the subsystem's inability to generate all the relevant data needed to calculate the frictional torque; a review of its function in Section 3.6, identified instability due to the presence of a universal joint and multiple uncontrolled linear bearings. The effects of these on the data generated were a concern. However, baseline data (testing under 1kN constant load and no ML translation) generated with the modified subsystem were not significantly different when compared with data generated in Section 4.5 under similar test conditions. Also, when considering the crosstalk, it was expected that crosstalk would be proportional to the largest applied signal (typically the applied load). However, in this study, the applied load and motions between the baseline and ML translation cases did not change, and therefore the crosstalk was assumed to be constant. It was hypothesised that the artefacts generated by the subsystem and crosstalk would be constant and therefore the best way to isolate the effects of the ML translation would be to subtract from the baseline state (Section 5.7).

Further study would need to repeat these tests without the subsystem present to better determine the effects of medial-lateral translations on the measured frictional torques at the bearing interface of total hip replacements. Following this, tests should therefore be designed to assess more clinically relevant conditions such as applying all gait cycle motion and dynamic axial loading such as recommended by ISO 14242-1:2012. Further study could also investigate the individual effects of rotational implant positioning by varying the acetabular cup

inclination and version angles (Nevelos, et al., 2001; Al-Hajjar, et al., 2010; Williams, et al., 2013). The effects of these should be combined with varying medial-lateral translations to assess their compound effect on the measured frictional torque. Additional effects of swing phase load and different bearing materials combinations could also be considered in further study.

All tests conducted in this thesis used 25% (v/v) new-born bovine calf serum (BCS) as a lubricant, which serves as a substitute for human synovial fluid due to similarities in rheology and protein content. While this represents an idealised lubrication regime, it is possible that *in-vivo* lubrication following surgical implantation of a THR may not behave in the same manner. This could be as a result of compromised joint function following hip disease or even trauma to the synovial capsule during surgical implantation that may cause disruption to the lubricant. While assessing the effects of adverse conditions such as surgical implant positioning, it would be beneficial to assess worst case lubrication conditions as a clinically relevant measure. Studies by Bishop, *et al.*, 2008; Bishop *et al.*, 2013 have demonstrated using hard-on-hard bearings that measured friction increases significantly when assessed in compromised lubrication such as dry conditions or low concentration BCS (17%).

Retrieval analysis of failed THRs have shown high wear and significant changes to the bearing surfaces (Nevelos *et al.*, 1999; Korim *et al.*, 2014; Scholes *et al.*, 2017). Studies by Korim *et al.*, 2014 and Haider *et al.*, 2016 have shown that surface roughness found in explants or induced artificially on the bearing surface significantly increases the measured friction of THRs. Surface roughness for THR bearings used in this project were measured before and after conducted studies to determine any changes to the bearing surfaces. On average, the changes in surface roughness were minimal on both bearing surfaces of MOP and COC implants assessed, and were far lower than have been seen in retrieval studies. These minimal changes were expected, particularly due to the short run tests

conducted. This was important to determine to ensure that the frictional behaviour observed during testing was not affected or skewed by increasing surface roughness and was representative of the assessment conditions. However, in addition to studying the effects of compromised lubrication, assessment of the effects of worn bearing surfaces would also allow representation of clinically relevant conditions.

7.4 Assessment of the torques required to displace uncemented acetabular components in total hip replacements

The results discussed in Chapter 5 investigating the effects of variations in medial-lateral translation on the frictional torque showed significant increases in the measured frictional torque. The clinical implications when these increased frictional torques are transferred from the bearing interface to the fixation interface was unknown. A methodology was therefore designed to determine whether the increased frictional torques measured in Chapter 5 as a consequence of varying medial-lateral translations when transferred to the acetabular fixation may result in acetabular cup displacement, and subsequent loosening.

The highest measured frictional torque of 15.35Nm is likely to have been able to displace acetabular cups in 10 PCF Sawbone for both the lever-out and rim test with no axial loading studies. Beyond these, the torques measured in this current study, particularly when axial loading was applied, when compared to the frictional torques measured in the hip simulation study under variations in medial-lateral translation (chapter 5), were greater. However, applied load and motion conditions in Chapter 5 were lower than is generally expected in the average human gait cycle and may therefore not fully represent the frictional torque generated at the bearing interface. Section 4.5.3 demonstrated that increasing the applied load increases the measured frictional torque. Therefore, following further study

incorporating a full gait cycle as discussed in Section 7.3, a re-assessment of the effects of the generated simulator frictional torque should be conducted to determine if the potentially increased frictional torques generated will be capable of displacing uncemented acetabular cups experiencing axial loading.

As discussed in Section 6.8.1, the main limitations of this study were the use of synthetic bone to simulate natural bone behaviour and the use of static loading to replicate axial loading. In addition, acetabular cups were mounted flat in Sawbone (i.e., 0° cup inclination) and not at a clinically representative angle.

Future work would therefore look to employ the use of a controlled axial load application system where a feedback mechanism would ensure that the applied load did not decrease as the Sawbone bone relaxed over time. This actuated control system would be capable of both constant and dynamic/cyclical loading to also allow the study of time-dependent effects. Acetabular cups should also be mounted at clinically representative angles and may form the basis of assessing rotational surgical implant positioning within this load-to-failure test method. In addition, a more accurate method of characterising the cup displacement would be to use a linear displacement transducer.

A stretch target for future work would be to integrate cementless fixation into simulator testing where the acetabular shell is press-fit in to a synthetic or natural bone model within the cup holder. This may allow direct assessment of the impact of the frictional torques generated under different conditions on the fixation.

7.5 Summary of Future Work

Following the studies conducted during this project, the main areas to be considered in future work are: -

- Improved calibration to include dynamic calibration methods and implementation of crosstalk compensation process.

- Root cause analysis of internal-external rotation frictional torque measurement discrepancies and incorporation of internal-external rotation into testing.
- Re-assessment of the effects of medial lateral translation on the frictional torques of total hip replacements on the SSHS without the subsystem present.
- Assessment of the combined effects of rotational and translational implant positioning on the measured frictional torques in different types of total hip replacements under clinically relevant loading and motion conditions.
- Use of a controlled loading system for the application of constant and dynamic axial loading during the developed load-to-failure study.

7.6 Clinical and Research Impact

Despite limitations, the methodologies developed through this project have provided insight into the *in-vitro* frictional response of total hip replacements to clinical conditions such as the medial-lateral translation between the femoral head and the acetabular cup, and the potential impact of these on bone-prosthesis fixation interface.

Clinical and Industry applications: These findings and the methodologies used could therefore be developed further to be used as a pre-clinical testing method in the future design of implants and surgical process (in terms of defining the critical limits such as safe zones for surgical implant positioning). These solutions can lead to improved implant performance and potentially reduce mechanical fixation loosening, wear or corrosion at the taper junctions, or even aggravated bearing surface wear. Overall, improved implant performance and longevity results in reduced incidence of revision and a better patient experience.

Research: The findings and methodologies used can inform the development of a standardised pre-clinical test protocol for the assessment of frictional torques using multi-axis hip simulator systems under both standard and adverse conditions. The findings of this project have demonstrated that assessment and testing of frictional response of total hip replacements can be challenging.

Therefore, the methodologies, findings, challenges faced, and the errors made can also serve as guide for future research.

7.7 Conclusion

From the studies conducted in this project, the following conclusions were made:-

- The developed method using a multi-axis hip simulator found that increasing the medial-lateral translation increased the frictional torques measured at the bearing interface of 36mm MOP bearings under constant load.
- The effects of medial-lateral translation on the frictional torques at the bearing interface of 36mm MOP bearings did not appear to be different under constant and dynamic loading.
- The developed method allowing the load-to-failure testing of uncemented acetabular cups under simultaneous axial loading found that the addition of axial loading increased the torque required to displace uncemented cups in 10 and 20PCF density Sawbone. It also found that increasing the applied axial load from 300N to 3kN further increased the torque required to displace the acetabular cup in both Sawbone densities.
- The elevated frictional torques generated under variations in medial-lateral translation was found to be capable of displacing uncemented acetabular cups in 10PCF Sawbone under lever-out and rim test with no axial load test conditions only. However, it is likely that increasing the axial loading applied during testing of medial-lateral translation in the simulator study will elevate the frictional torques significantly enough to cause displacement in some rim test with axial loading applied, particularly in the lower density 10PCF Sawbone.

Overall, this project demonstrated that surgical implant malpositioning can result in elevated frictional torques at the bearing interface of THRs. However, the impact of these elevated frictional torques on cup fixation is undetermined, as further work is necessary to examine surgical implant malpositioning in THRs under more representative loading and motion conditions.

REFERENCES

- Adler, E., Stuchin, S.A. and Kummer, F.J. 1992. Stability of press-fit acetabular cups. *J Arthroplasty*. 7(3), pp.295–301.
- Affatato, S. 2012. *Wear of orthopaedic implants and artificial joints*. Elsevier.
- Al-Hajjar, M. et al. (2010) 'Effect of cup inclination angle during microseparation and rim loading on the wear of BIOLOX® delta ceramic-on-ceramic total hip replacement', *Journal of Biomedical Materials Research Part B: Applied Biomaterials*, 95(2), pp. 263–268.
- Al-Hajjar, M. et al. (2013) 'Edge Loading in Total Hip Replacements Due to Translational Surgical Mal-Positioning: In Vitro Techniques', *Bone & Joint Journal Orthopaedic Proceedings Supplement*, 95-B(SUPP 34), p. 2. Available at: http://www.bjjprocs.boneandjoint.org.uk/content/95-B/SUPP_34/2.abstract.
- Al-Hajjar, M. et al. (2014) 'Wear of Large Diameter Ceramic-on-Ceramic Bearings in Total Hip Replacements under Edge Loading Conditions', in *ORS Annual Meeting 2014*. New Orleans.
- Al-Hajjar, M. et al. (2015) 'Increased Torque in Hip Replacement Bearings due to Translational Surgical Mal-Positioning; ORS Poster No. 1759', in.
- Al-Hajjar, M., Clarkson, P., Williams, S., Jennings, L., Thompson, J. and Fisher, J. 2013. Edge Loading in Total Hip Replacements Due to Translational Surgical Mal-Positioning: In Vitro Techniques. *Bone & Joint Journal Orthopaedic Proceedings Supplement*. 95-B(SUPP 34), p.2.
- Al-Hajjar, M., Fisher, J., Hardaker, C., Kuring, G., Thompson, J. and Williams, S. 2014. Wear of Large Diameter Ceramic-on-Ceramic Bearings in Total Hip Replacements under Edge Loading Conditions In: *ORS Annual Meeting 2014*. New Orleans.
- Al-Hajjar, M., Leslie, I.J., Tipper, J., Williams, S., Fisher, J. and Jennings, L.M. 2010. Effect of cup inclination angle during microseparation and rim loading on the wear of BIOLOX® delta ceramic-on-ceramic total hip replacement. *Journal of Biomedical Materials Research Part B: Applied Biomaterials*. 95(2), pp.263–268.

- Ali, M. et al. (2016) 'Wear and Deformation of Metal-on-Polyethylene Hip Replacements under Variations in Surgical Positioning', in.
- Ali, M. et al. (2017) 'Variations in Component Positioning Leading to Dynamic Separation and Edge Loading Influences the Deformation and Wear of Metal-on-Polyethylene Hip Replacement Bearings', ORS 2017 Annual Meeting, 4(5). Available at: <http://www.ors.org/Transactions/63/1032.pdf> (Accessed: 14 September 2017).
- Antoniades, G., Smith, E.J., Deakin, A.H., Wearing, S.C. and Sarungi, M. 2013. Primary stability of two uncemented acetabular components of different geometry: hemispherical or peripherally enhanced? *Bone & joint research*. 2(12), pp.264–9.
- Apostu, D., Lucaciu, O., Berce, C., Lucaciu, D. and Cosma, D. 2018. Current methods of preventing aseptic loosening and improving osseointegration of titanium implants in cementless total hip arthroplasty: a review. *Journal of International Medical Research*. 46(6), pp.2104–2119.
- Apostu, D., Lucaciu, O., Lucaciu, G.D.O., Crisan, B., Crisan, L., Baciut, M., Onisor, F., Baciut, G., Câmpian, R.S. and Bran, S. 2017. Systemic drugs that influence titanium implant osseointegration. *Drug Metabolism Reviews*. 49(1), pp.92–104.
- Auger, D. D. et al. (1993) 'Friction and lubrication in cushion form bearings for artificial hip joints', ARCHIVE: Proceedings of the Institution of Mechanical Engineers, Part H: Journal of Engineering in Medicine 1989-1996 (vols 203-210), 207(18), pp. 25–33. doi: 10.1243/PIME_PROC_1993_207_265_02.
- Barrack, R. L. et al. (2001) 'Virtual reality computer animation of the effect of component position and design on stability after total hip arthroplasty', *Orthopedic Clinics of North America*, 32(4), pp. 569–577. doi: [https://doi.org/10.1016/S0030-5898\(05\)70227-3](https://doi.org/10.1016/S0030-5898(05)70227-3).
- Bergmann, G. et al. (2012) 'High-Tech Hip Implant for Wireless Temperature Measurements In Vivo', *PLoS ONE*. Edited by H. A. Awad, 7(8), p. e43489. doi: 10.1371/journal.pone.0043489.
- Berry, D.J. and Lieberman, J. 2012. *Surgery of the Hip*. Elsevier Health Sciences.

- Bishop, N. E., Hothan, A. and Morlock, M. M. (2013) 'High friction moments in large hard-on-hard hip replacement bearings in conditions of poor lubrication', *J Orthop Res.* 2012/12/15, 31(5), pp. 807–813. doi: 10.1002/jor.22255.
- Bishop, N. E., Waldow, F. and Morlock, M. M. (2008) 'Friction moments of large metal-on-metal hip joint bearings and other modern designs', *Med Eng Phys*, 30(8), pp. 1057–1064. doi: DOI 10.1016/j.medengphy.2008.01.001.
- Bishop, N.E., Hothan, A. and Morlock, M.M. 2013. High friction moments in large hard-on-hard hip replacement bearings in conditions of poor lubrication. *J Orthop Res.* 31(5), pp.807–813.
- Bowsher, J. G. and Shelton, J. C. (2001) 'A hip simulator study of the influence of patient activity level on the wear of crosslinked polyethylene under smooth and roughened femoral conditions', *Wear*, 250(1–12), pp. 167–179. doi: [http://dx.doi.org/10.1016/S0043-1648\(01\)00619-6](http://dx.doi.org/10.1016/S0043-1648(01)00619-6).
- Bowsher, J.G., Hussain, A., Williams, P.A. and Shelton, J.C. 2005. Large head diameters have the potential to reduce ion release in metal-on metal hip wear simulations. *ORS Washington DC.*, p.1626.
- Brockett, C. L. et al. (2008) 'The influence of clearance on friction, lubrication and squeaking in large diameter metal-on-metal hip replacements', *Journal of Materials Science: Materials in Medicine*, 19(4), pp. 1575–1579.
- Brockett, C. L. et al. (2013) 'Squeaking hip arthroplasties: a tribological phenomenon', *J Arthroplasty.* 2012/04/07, 28(1), pp. 90–97. doi: 10.1016/j.arth.2012.01.023.
- Brockett, C., Williams, S., Jin, Z., Isaac, G. and Fisher, J. 2007. Friction of total hip replacements with different bearings and loading conditions. *J Biomed Mater Res B Appl Biomater.* 81(2), pp.508–515.
- Callaghan, J.J., Rosenberg, A.G. and Rubash, H.E. 2007. *The Adult Hip.* Lippincott Williams & Wilkins.
- Cameron, H.U., Pilliar, R.M. and MacNab, I. 1973. The effect of movement on the bonding of porous metal to bone. *J Biomed Mater Res.* 7(4), pp.301–311.
- CeramTec (2012) BIOLOX®delta. Available at: <https://www.ceramtec.com/ceramic-materials/biolox/delta/> (Accessed: 4 July 2017).

- Charnley, J. (1961) 'Arthroplasty of Hip - a New Operation', *Lancet*, 1(718), pp. 1129-
- Charnley, J., Mckee, G.K., Coltart, W.D. and Scales, J.T. 1961. Arthroplasty of the Hip by the Low-Friction Technique. *Journal of Bone and Joint Surgery-British* Volume. 43(3), p.601.
- Cherian, J.J., Jauregui, J.J., Banerjee, S., Pierce, T. and Mont, M.A. 2015. What Host Factors Affect Aseptic Loosening After THA and TKA? *Clinical Orthopaedics and Related Research*. 473(8), pp.2700–2709.
- Clarke, H.J., Jinnah, R.H., Warden, K.E., Cox, Q.G. and Curtis, M.J. 1991. Evaluation of acetabular stability in uncemented prostheses. *J Arthroplasty*. 6(4), pp.335–340.
- Cowin, S.C. (Stephen C. 2001. *Bone mechanics handbook*. CRC Press.
- Crosnier, E.A., Keogh, P.S. and Miles, A.W. 2014. A novel method to assess primary stability of press-fit acetabular cups. *Proceedings of the Institution of Mechanical Engineers, Part H: Journal of Engineering in Medicine*. 228(11), pp.1126–1134.
- Crowe, J. F., Sculco, T. P. and Kahn, B. (2003) 'Revision Total Hip Arthroplasty', *Clinical Orthopaedics and Related Research*, 413(413), pp. 175–182. doi: 10.1097/01.blo.0000072469.32680.b6.
- Curtis, M.J., Jinnah, R.H., Wilson, V.D. and Hungerford, D.S. 1992. The initial stability of uncemented acetabular components. *J Bone Joint Surg Br*. 74(3), pp.372–376.
- Damm, P. et al. (2013) 'Friction in total hip joint prosthesis measured in vivo during walking', *PLoS One*, 8(11), p. e78373. doi: 10.1371/journal.pone.0078373.
- Davim, J.P. 2013. *Biotribology*. Wiley.
- Dennis, D. A. et al. (2001) 'In vivo' determination of hip joint separation and the forces generated due to impact loading conditions.', *Journal of biomechanics*, 34(5), pp. 623–9. Available at: <http://www.ncbi.nlm.nih.gov/pubmed/11311703> (Accessed: 13 September 2017).

- Dowson, D. et al. (1985) 'Influence of Counterface Topography on the Wear of Ultra High Molecular Weight Polyethylene Under Wet or Dry Conditions', in, pp. 171–187. doi: 10.1021/bk-1985-0287.ch012.
- Dowson, D., Dalmaz, G. and Lubrecht, A. A. (2003) *Tribological Research and Design for Engineering Systems: Proceedings of the 29th Leeds-Lyon Symposium*. Elsevier Science.
- Dowson, D., Hardaker, C., Flett, M. and Isaac, G.H. 2004. A hip joint simulator study of the performance of metal-on-metal joints: Part II: design. *J Arthroplasty*. 19(8 Suppl 3), pp.124–130.
- Fisher, J. 2011. Bioengineering reasons for the failure of metal-on-metal hip prostheses: an engineer's perspective. *J Bone Joint Surg Br*. 93(8), pp.1001–1004.
- Fisher, J. and Dowson, D. 1991. Tribology of total artificial joints. *Proc Inst Mech Eng H*. 205(2), p.73.
- Gore, T. A., Higginson, G. R. and Kornberg, R. E. (1981) 'Some evidence of squeeze-film lubrication in hip prostheses'. Available at: http://journals.sagepub.com/doi/pdf/10.1243/EMED_JOUR_1981_010_026_02 (Accessed: 5 July 2017).
- Haider, H., Weisenburger, J. N. and Garvin, K. L. (2016) 'Simultaneous measurement of friction and wear in hip simulators', *Proc Inst Mech Eng H*, 230(5), pp. 373–388. doi: 10.1177/0954411916644476.
- Hall, R.M. and Unsworth, A. 1997. Friction in hip prostheses. *Biomaterials*. 18(15), pp.1017–1026.
- Harris, W.H. 2012. Edge Loading Has a Paradoxical Effect on Wear in Metal-on-Polyethylene Total Hip Arthroplasties. *Clinical Orthopaedics and Related Research*. 470(11), pp.3077–3082.
- Helgason, B., Perilli, E., Schileo, E., Taddei, F., Brynjó Lfsson, S. and Viceconti, M. 2008. Mathematical relationships between bone density and mechanical properties: A literature review.
- Hong, D., Li, C. and Jeong, J. (2012) 'A Crosstalk Compensation of a Multi-axis ForceTorque Sensor Based on the Least Squares Method Using LabVIEW', in

2012 Fourth International Conference on Computational and Information Sciences, pp. 1127–1130. doi: 10.1109/ICCIS.2012.12.

Hua, X. et al. (2014) 'Contact mechanics of modular metal-on-polyethylene total hip replacement under adverse edge loading conditions', *Journal of biomechanics*, 47(13), pp. 3303–3309.

Hua, X., Li, J., Wang, L., Jin, Z., Wilcox, R. and Fisher, J. 2014. Contact mechanics of modular metal-on-polyethylene total hip replacement under adverse edge loading conditions. *Journal of biomechanics*. 47(13), pp.3303–3309.

Huber, W.O. and Noble, P.C. 2014. Effect of design on the initial stability of press-fit cups in the presence of acetabular rim defects: experimental evaluation of the effect of adding circumferential fins. *International Orthopaedics*. 38(4), pp.725–731.

Jin, Z.M., Dowson, D. and Fisher, J. 1994. A parametric analysis of the contact stress in ultra-high molecular weight polyethylene acetabular cups. *Medical Engineering & Physics*. 16(5), pp.398–405.

Jin, Z.M., Meakins, S., Morlock, M.M., Parsons, P., Hardaker, C., Flett, M. and Isaac, G. 2006. Deformation of press-fitted metallic resurfacing cups. Part 1: Experimental simulation. *Proceedings of the Institution of Mechanical Engineers, Part H: Journal of Engineering in Medicine*. 220(2), pp.299–309.

Jin, Z.M., Stone, M., Ingham, E. and Fisher, J. 2006. (v) Biotribology. *Current Orthopaedics*. 20(1), pp.32–40.

Johnson, A. T. (Arthur T. (2011) *Biology for engineers*. CRC Press.

Kody, M.H., Kabo, J.M., Markolf, K.L., Dorey, F.J. and Amstutz, H.C. 1990. Strength of initial mechanical fixation of screw ring acetabular components. *Clin Orthop Relat Res*. (257), pp.146–153.

Lachiewicz, P.F., Suh, P.B. and Gilbert, J.A. 1989. In vitro initial fixation of porous-coated acetabular total hip components. *J Arthroplasty*. 4(3), pp.201–205.

Leng, J. et al. (2017) 'Dynamic virtual simulation of the occurrence and severity of edge loading in hip replacements associated with variation in the rotational and translational surgical position', *Proceedings of the Institution of Mechanical Engineers, Part H: Journal of Engineering in Medicine*, 231(4), pp. 299–306. doi: 10.1177/0954411917693261.

- Lewinnek, G. E. et al. (1978) 'Dislocations after total hip-replacement arthroplasties', *J Bone Joint Surg Am*, 60(2), pp. 217–220.
- Liao, Y.-S. et al. (2003) 'The effect of frictional heating and forced cooling on the serum lubricant and wear of UHMW polyethylene cups against cobalt–chromium and zirconia balls', *Biomaterials*, 24(18), pp. 3047–3059.
- Liu, F. et al. (2013) 'Effect of head contact on the rim of the cup on the offset loading and torque in hip joint replacement', *Proceedings of the Institution of Mechanical Engineers, Part H: Journal of Engineering in Medicine*, p. 0954411913496016.
- Livermore, J., Ilstrup, D. and Morrey, B. 1990. Effect of femoral head size on wear of the polyethylene acetabular component. *The Journal of Bone & Joint Surgery*. 72(4), pp.518–528.
- Lombardi, A. V. et al. (2000) 'An in vivo determination of total hip arthroplasty pistoning during activity', *The Journal of Arthroplasty*, 15(6), pp. 702–709. doi: 10.1054/arth.2000.6637.
- Longaray, J. et al. (2013) 'How Do Bearing Size and Bearing Material Affect Frictional Torque? a Hip Simulator Evaluation', *Bone & Joint Journal Orthopaedic Proceedings Supplement*, 95(SUPP 34), p. 121.
- Macdonald, W., Carlsson, L. V, Charnley, G.J. and Jacobsson, C.M. 1999. Press-fit acetabular cup fixation: principles and testing. *Proc Inst Mech Eng H*. 213(1), pp.33–39.
- Malik, S. S. (2015) *Orthopaedic biomechanics made easy*.
- McCollum, D. E. and Gray, W. J. (1990) 'Dislocation after total hip arthroplasty. Causes and prevention.', *Clinical orthopaedics and related research*, (261), pp. 159–170.
- McKellop, H. et al. (1981) 'Friction and wear properties of polymer, metal, and ceramic prosthetic joint materials evaluated on a multichannel screening device', *Journal of Biomedical Materials Research*, 15(5), pp. 619–653. doi: 10.1002/jbm.820150503.
- McMinn, D. J. W. (2009) *Modern Hip Resurfacing*. Springer.

- Meneghini, R.M., Meyer, C., Buckley, C.A., Hanssen, A.D. and Lewallen, D.G. 2010. Mechanical Stability of Novel Highly Porous Metal Acetabular Components in Revision Total Hip Arthroplasty. *J Arthroplasty*. 25(3), pp.337–341.
- Miller, M.D., Thompson, S.R. and Hart, J. 2012. *Review of Orthopaedics*. Elsevier Health Sciences.
- Miyakawa, S., Kawamura, H., Mishima, H. and Yasumoto, J. 2004. Grit-blasted and hydroxyapatite-coated total hip arthroplasty: An 11- to 14-year follow-up study. *Journal of Orthopaedic Science*. 9(5), pp.462–467.
- Morlock, M., Bishop, N. and Huber, G. (2011) 'Biomechanics of Hip Arthroplasty', in Knahr, K. (ed.) *Tribology in Total Hip Arthroplasty*. Springer Berlin Heidelberg, pp. 11–24. doi: 10.1007/978-3-642-19429-0_2.
- Nevelos, J. E. et al. (1999) 'Analysis of retrieved alumina ceramic components from Mittelmeier total hip prostheses', *Biomaterials*, 20(19), pp. 1833–1840. doi: 10.1016/S0142-9612(99)00081-2.
- Nevelos, J. E. et al. (2001) 'The influence of acetabular cup angle on the wear of "BIOLOX Forte" alumina ceramic bearing couples in a hip joint simulator', *Journal of Materials Science: Materials in Medicine*, 12(2), pp. 141–144.
- Nevelos, J., Ingham, E., Doyle, C., Streicher, R., Nevelos, A., Walter, W. and Fisher, J. 2000. Microseparation of the centers of alumina-alumina artificial hip joints during simulator testing produces clinically relevant wear rates and patterns. *J Arthroplasty*. 15(6), pp.793–795.
- NJR (2021) 'National Joint Registry for England, Wales and Northern Ireland'.
- O'Dwyer Lancaster-Jones, O. et al. (2017) 'An in vitro simulation model to assess the severity of edge loading and wear, due to variations in component positioning in hip joint replacements', *Journal of Biomedical Materials Research Part B: Applied Biomaterials*. doi: 10.1002/jbm.b.33991.
- Paul, J. (1966) 'Forces transmitted by joints in the human body', *Proceedings of the Institution of Mechanical Engineers*. Available at: http://journals.sagepub.com/doi/abs/10.1243/PIME_CONF_1966_181_201_02 (Accessed: 30 June 2017).
- Rajesh, M. 2012. *Mastering Orthopedic Techniques Total Hip Arthroplasty*. Jaypee Brothers Pvt. Ltd.

- Revell, P.A. 2008. Joint replacement technology Preface. Joint Replacement Technology.,
- Rieker, C.B., Schön, R., Konrad, R., Liebentritt, G., Gnepf, P., Shen, M., Roberts, P. and Grigoris, P. 2005. Influence of the clearance on in-vitro tribology of large diameter metal-on-metal articulations pertaining to resurfacing hip implants. *Orthopedic Clinics of North America*. 36(2), pp.135–142.
- Saikko, V. (1992) 'A simulator study of friction in total replacement hip joints', *Proc Inst Mech Eng H*. 1992/01/01, 206(4), pp. 201–211. Available at: <http://www.ncbi.nlm.nih.gov/pubmed/1300112>.
- Saikko, V. (1993) 'Wear and friction properties of prosthetic joint materials evaluated on a reciprocating pin-on-flat apparatus', *Wear*, 166(2), pp. 169–178. doi: 10.1016/0043-1648(93)90259-O.
- Saikko, V. 2009. Friction measurement in the biaxial rocking motion hip joint simulator. *Journal of tribology*. 131(1), p.11201.
- Saikko, V.O. 1996. A three-axis hip joint simulator for wear and friction studies on total hip prostheses. *Proceedings of the Institution of Mechanical Engineers, Part H: Journal of Engineering in Medicine*. 210(3), pp.175–185.
- Saleh, K. J. et al. (2003) 'Functional Outcome After Revision Hip Arthroplasty', *Clinical Orthopaedics and Related Research*, 416(416), pp. 254–264. doi: 10.1097/01.blo.0000093006.90435.43.
- Saleh, K.J., Bear, B., Bostrom, M., Wright, T. and Sculco, T.P. 2008. Initial stability of press-fit acetabular components: an in vitro biomechanical study. *Am J Orthop (Belle Mead NJ)*. 37(10), pp.519–522.
- Sariali, E. et al. (2010) 'In vitro investigation of friction under edge-loading conditions for ceramic-on-ceramic total hip prosthesis', *Journal of Orthopaedic Research*, 28(8), pp. 979–985.
- Schleichert, J. and Fröhlich, T. (2015) 'A1.4 - Dynamic Calibration of a Multi-Component Force-/Torque Transducer', in, pp. 46–49. doi: 10.5162/sensor2015/A1.4.
- Scholes, S. C. and Unsworth, A. (2000) 'Comparison of friction and lubrication of different hip prostheses', *Proceedings of the Institution of Mechanical Engineers, Part H: Journal of Engineering in Medicine*, 214(1), pp. 49–57.

- Scholes, S. C. and Unsworth, A. (2006) 'The effects of proteins on the friction and lubrication of artificial joints', *Proceedings of the Institution of Mechanical Engineers Part H-Journal of Engineering in Medicine*, 220(H6), pp. 687–693. doi: Doi 10.1243/09544119jeim21.
- Scholes, S. C. et al. (2000) 'The effects of material combination and lubricant on the friction of total hip prostheses', *Wear*, 241(2), pp. 209–213. doi: Doi 10.1016/S0043-1648(00)00377-X.
- Scholes, S. C., Unsworth, A. and Goldsmith, A. A. (2000) 'A frictional study of total hip joint replacements', *Phys Med Biol*, 45(12), pp. 3721–3735. Available at: <http://www.ncbi.nlm.nih.gov/pubmed/11131195>.
- Scholl, L. et al. (2016) 'Friction in modern total hip arthroplasty bearings: Effect of material, design, and test methodology', *Proceedings of the Institution of Mechanical Engineers, Part H: Journal of Engineering in Medicine*, 230(1), pp. 50–57. doi: 10.1177/0954411915619452.
- Small, Scott R, Berend Md, M.E., Howard Bs, L.A., Rogge Phd, R.D., Buckley Phd, C.A. and Ritter, M.A. 2013. High Initial Stability in Porous Titanium Acetabular Cups: A Biomechanical Study. *Journal of Arthroplasty*. 28, pp.510–516.
- Smith, A.J., Dieppe, P., Vernon, K., Porter, M., Blom, A.W., National Joint Registry of, E. and Wales 2012. Failure rates of stemmed metal-on-metal hip replacements: analysis of data from the National Joint Registry of England and Wales. *Lancet*. 379(9822), pp.1199–1204.
- Smith, S.L., Dowson, D. and Goldsmith, A.A.J. 2001. The effect of femoral head diameter upon lubrication and wear of metal-on-metal total hip replacements. *Proceedings of the Institution of Mechanical Engineers, Part H: Journal of Engineering in Medicine*. 215(2), pp.161–170.
- Soballe, K., Hansen, E.S., H, B.R., Jorgensen, P.H. and Bunger, C. 1992. Tissue ingrowth into titanium and hydroxyapatite-coated implants during stable and unstable mechanical conditions. *J Orthop Res*. 10(2), pp.285–299.
- Sonntag, R., Braun, S., Al-Salehi, L., Reinders, J., Mueller, U. and Kretzer, J.P. 2017. Three-dimensional friction measurement during hip simulation J. L. Williams, ed. *PLOS ONE*. 12(9), p.e0184043.

- Sonntag, R., Reinders, J., Rieger, J.S., Heitzmann, D.W.W. and Kretzer, J.P. 2013. Hard-on-Hard Lubrication in the Artificial Hip under Dynamic Loading Conditions. *PLoS One*. 8(8), p.e71622.
- Stiehl, J.B., MacMillan, E. and Skrade, D.A. 1991. Mechanical stability of porous-coated acetabular components in total hip arthroplasty. *J Arthroplasty*. 6(4), pp.295–300.
- Taniguchi, N., Fujibayashi, S., Takemoto, M., Sasaki, K., Otsuki, B., Nakamura, T., Matsushita, T., Kokubo, T. and Matsuda, S. 2016. Effect of pore size on bone ingrowth into porous titanium implants fabricated by additive manufacturing: An in vivo experiment. *Materials Science and Engineering C*. 59, pp.690–701.
- Totten, G.E. 2006. *Handbook of Lubrication and Tribology: Volume I Application and Maintenance*, Second Edition. Taylor & Francis.
- Unsworth, A. (1978) 'The effects of lubrication in hip prostheses', *Physics in Medicine and Biology*, 23(2), p. 004. doi: 10.1088/0031-9155/23/2/004.
- Unsworth, A. and Percy, M. J. (1988) 'Frictional properties of artificial hip joints'. Available at: http://journals.sagepub.com/doi/pdf/10.1243/EMED_JOUR_1988_017_029_02 (Accessed: 5 July 2017).
- Wang, A., Essner, A. and Klein, R. 2001. Effect of contact stress on friction and wear of ultra-high molecular weight polyethylene in total hip replacement. *Proceedings of the Institution of Mechanical Engineers, Part H: Journal of Engineering in Medicine*. 215(2), pp.133–139.
- Weisenburger, J., Garvin, K. and Haider, H. (2013) 'Friction Factors of Various Metal on Plastic Hip Replacement Designs With Scratched Femoral Heads Captured During Testing on a Multi-Station Hip Simulator', *Bone & Joint Journal Orthopaedic Proceedings Supplement*, 95(SUPP 34), p. 584.
- Weisenburger, J.N., Naylor, M.G., Schroeder, D.W., White, B.F., Unsworth, A., Garvin, K.L. and Haider, H. 2011. A884. Correlation of friction measurements with wear characteristics during multi-station hip simulator wear tests. *Journal of Bone & Joint Surgery, British Volume*. 93(SUPP IV), p.448.
- Williams, S. et al. (2006) 'Effect of swing phase load on metal-on-metal hip lubrication, friction and wear', *Journal of biomechanics*, 39(12), pp. 2274–2281.

- Williams, S. et al. (2008) 'Friction of ceramic-on-ceramic and metal-on-metal total hip replacements tested under different lubrication regimes', *Journal of Bone & Joint Surgery, British Volume*, 90(SUPP I), p. 189.
- Williams, S., Butterfield, M., Stewart, T., Ingham, E., Stone, M. and Fisher, J. 2003. Wear and deformation of ceramic-on-polyethylene total hip replacements with joint laxity and swing phase microseparation. *Proceedings of the Institution of Mechanical Engineers, Part H: Journal of Engineering in Medicine*. 217(2), pp.147–153.
- Wimmer, M. A. et al. (2001) 'Friction and wear properties of metal/metal hip joints - Application of a novel testing and analysis method', *Materialwissenschaft Und Werkstofftechnik*, 32(12), pp. 891–896. doi: Doi 10.1002/1521-4052(200112)32:12<891::Aid-Mawe891>3.0.Co;2-Y.
- Xue, T., Attarilar, S., Liu, S., Liu, J., Song, X., Li, L., Zhao, B. and Tang, Y. 2020. Surface modification techniques of titanium and its alloys to functionally optimize their biomedical properties: Thematic review. *Frontiers in Bioengineering and Biotechnology*. 8, p.1261.
- Yan, Y. et al. (2009) 'The influence of swing phase load on the electrochemical response, friction, and ion release of metal-on-metal hip prostheses in a friction simulator'. doi: 10.1243/13506501JET568.
- Zivkovic, I., Gonzalez, M. and Amirouche, F. 2010. The Effect of Under-Reaming on the Cup/Bone Interface of a Press Fit Hip Replacement. *Journal of Biomechanical Engineering*. 132(4), p.041008.

APPENDICES

APPENDIX 8.1

8.1 Design and development of a subsystem for a multi-axis hip simulator for the measurement of frictional torque in total hip replacements

This appendix provides information about the design of the subsystem presented in Chapter 3 as part of the modified SSHS.

8.1.1 Design Objectives and Requirements

This section discusses the design and develop an electromechanical subsystem for use with a multi-axis single station hip simulator, capable of measuring the frictional torques present at the head-cup interface of THRs, under a range of pre-clinical test conditions.

8.1.2 Requirements of the sub-system

Mode of operation

1. Must be a sub-system of the Single Station Hip Simulator.
2. Must measure frictional torques generated at the bearing interface.
3. Must not resist or restrict normal function of SSHS

Load, motion and displacement

4. Must operate without failure under a maximum of 5kN axial loading applied by the SSHS
5. Must withstand $\pm 60^\circ$ flexion/extension, $\pm 25^\circ$ abduction/adduction and $\pm 25^\circ$ internal/external rotation without impingement or damage to components or the SSHS
6. Must allow translation of components in range of $\pm 5\text{mm}$ in the medial-lateral directions to replicate variations in translational positioning

Component positioning and sizes

7. Must allow the placement in acetabular cup version in the range of -20° to 40°

8. Must allow acetabular cup inclinations of 35° (standard conditions) and 45° - 65° to the horizontal (adverse conditions)
9. Must be compatible with THR components of different diameters

General

10. All mobile components must have coefficient of friction ≤ 0.001 under a 3kN axial load (to be lower than the friction being measured)
11. Sub-system function must be compatible for use with components mounted in ~500ml of lubrication in a gaiter
12. The function of the sub-system must be safe for operators and bystander
13. Materials used must be non-corrosive and non-reactive
14. Cost of manufacture must not exceed £8000

8.1.3 Design Solution: SSHS with integrated subsystem

An overview of the design sub system is provided: it consisted of a near frictionless universal joint that acted as a pivot above the acetabular cup holder, and two vertically positioned uni-axial load cells mounted at the level of the femoral head – acetabular cup interface (Figure 8.1 - Final design concept for the SSHS subsystem including universal joint for biaxial rotation and two uni-axial load cells positioned at bearing interface level in FE and AA directions (blue indicates existing parts of SSHS, not part of subsystem))

). The subsystem also comprised of a range of support structures for mounting the different components to the SSHS.

The SSHS applied all loads, motion and displacement as normal, however friction measurements were to be collected from the subsystem load cells.

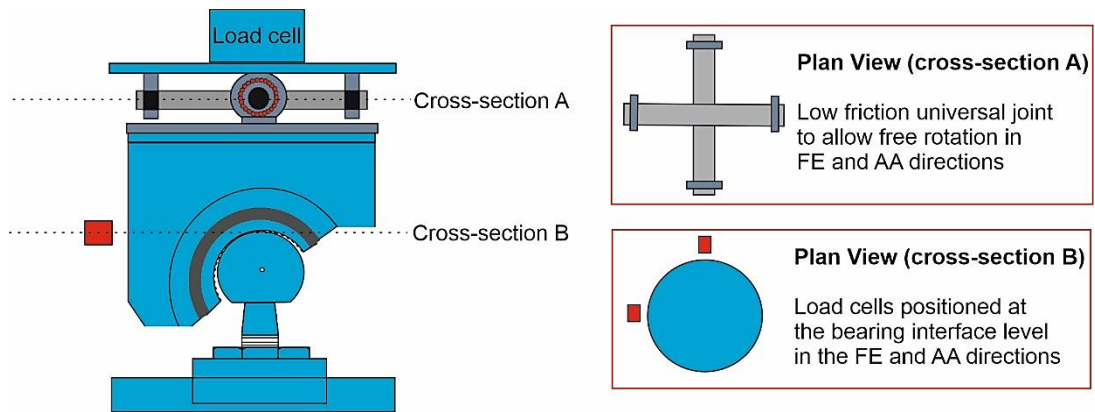


Figure 8.1 - Final design concept for the SSHS subsystem including universal joint for biaxial rotation and two uni-axial load cells positioned at bearing interface level in FE and AA directions (blue indicates existing parts of SSHS, not part of subsystem)

8.1.4 Measurement of frictional torques in the FE and AA directions

The measurement of THR friction by the subsystem was facilitated by two tension-compression load cells positioned at the level of the bearing interface in the FE and AA directions. As the first iteration of the design, measurement in the IER direction was not included because implementing a torque measuring system for the on-axis rotation was considered complex and out of budget but was planned for future iterations.

These load cells were positioned at the level of the bearing interface to minimise the distance between the bearing and the measuring load cell, as earlier work by the author had incorrectly concluded that the distance between the six-axis load cell and the bearing was a factor in the inability of the SSHS to measure THR frictional torque.

8.1.5 A quasi-frictionless universal joint for biaxial rotation of the acetabular cup holder

The universal joint was positioned above the acetabular cup holder such that the two rotations possible at the pivot coincided with the FE and AA directions. The design of the subsystem was such that the cup holder rotated about the universal joint in response to any friction at the head and liner articulating interface, applying load to the subsystem load cells.

A similar setup has been reported in literature in the original pendulum-type simulators where floating hydrostatic bearings ensured transfer of frictional torques in the THR bearings directly to the piezoelectric transducer (Dowson *et al.*, 2003).

An important feature of the original pendulum-type simulator setup was the very low frictionless hydrostatic bearings ($\mu=0.00001$), which meant all measured friction in the system could be attributed to the friction in the THR bearings (Unsworth *et al.*, 1975). Similarly, to ensure the frictional torque being transferred to the sensors of the new subsystem were solely due to the friction at the head and liner articulating interface, and not attenuated or countered by friction present in the bearings of the universal joint, the universal joint was expected to have very low friction ($\mu \leq 0.001$). The specification of friction coefficient for the new subsystem was not as low as was seen in the previous devices, however this was due to practical limitations on resources and budget. The design specification of friction coefficient less than or equal to 0.001 lower than that previously reported in low friction COC THR bearings, ensuring confidence that the measured frictional torques would be representative of that at the bearing interface (Jin *et al.*, 2006).

An illustration of the final design concept for the SSHS setup with the integrated subsystem is shown in Figures 8.2 and 8.3. With the integrated subsystem, the combined function could be described as a multi-axis hip simulator with bi-axial

frictional torque measurement capabilities. Section 8.1.8 provides 2D drawings of the subsystem.

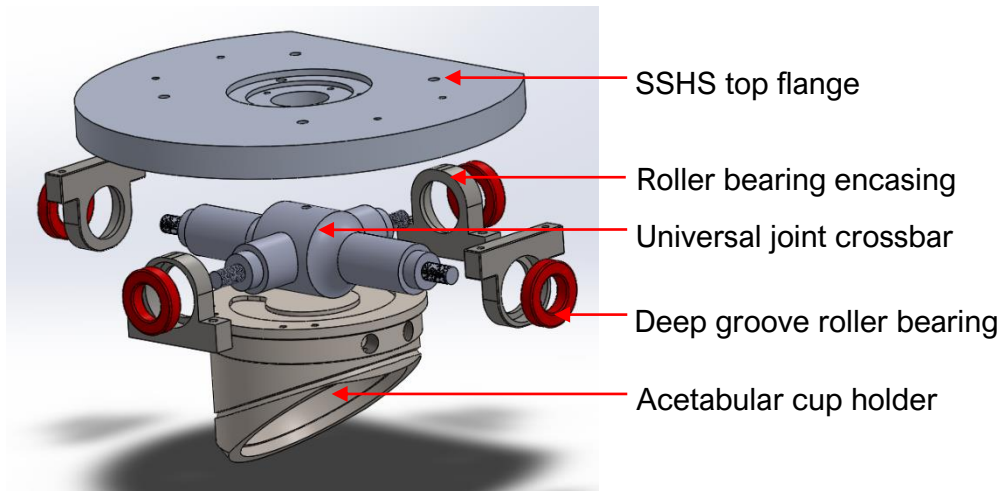


Figure 8.3 – Exploded CAD model of the individual components of the universal joint illustrating its position between the cup holder and the SSHS top flange

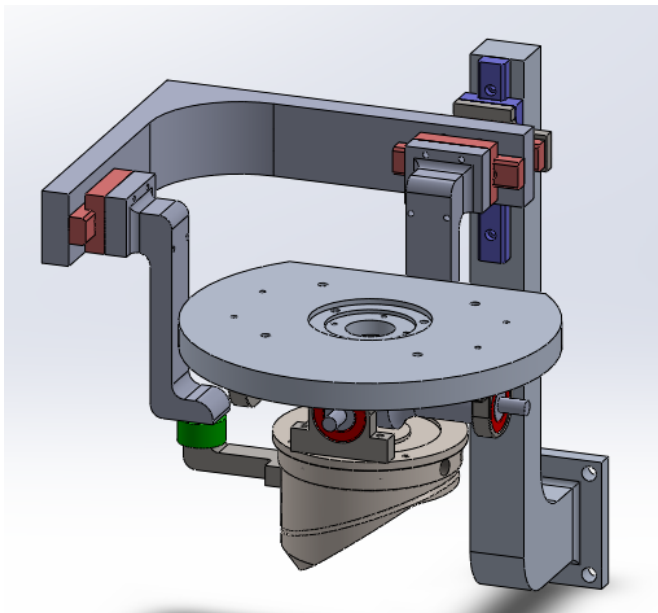


Figure 8.4 – Full CAD assembly of subsystem

8.1.6 Post-assembly assessment and modifications of subsystem

Once the subsystem was manufactured, it was assembled within the SSHS. This assembly however used dummy load cells manufactured of AISI 303 stainless steel to ensure any arising issues in the initial subsystem integration testing did not result in damage to the actual subsystem load cells.

Following initial assembly onto the SSHS, some areas of improvement were identified and modified.

8.1.7 Main support bracket modification

A lack of clearance between the main support bracket and the moving cradle of the SSHS resulted in impingement during motion. The impingement was relieved by removing material from the posterior side of the main support bracket (Figure 8.4 – Illustration of impingement between main support bracket and moving cradle and the material removal solution implemented

). The material removal solution implemented was not to have a detrimental effect on the mechanical robustness of the bracket.

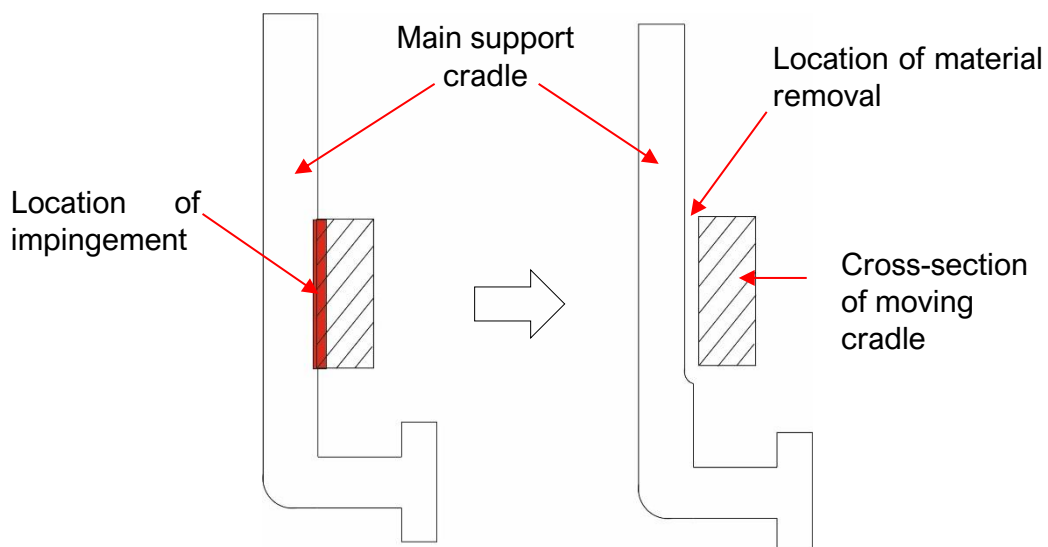


Figure 8.6 – Illustration of impingement between main support bracket and moving cradle and the material removal solution implemented

Initial assessments also observed that the design of the subsystem restricted anterior-posterior (AP) translation of the mounted components. Anterior-posterior translation was an important function that allowed re-centring of components during testing and had to be restored. This restriction was rectified by the bifurcation of the main support bracket and integrating a linear guide (Figure 8.5 –

Modification of support bracket to include bifurcation of bend and the addition of a linear bearing

).

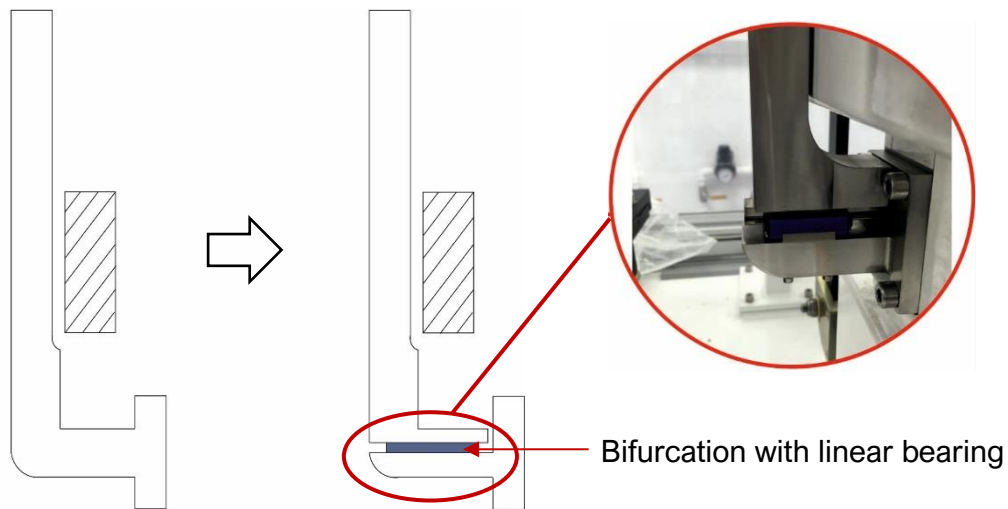


Figure 8.7 – Modification of support bracket to include bifurcation of bend and the addition of a linear bearing

Impingement between the main support bracket and the moving cradle re-occurred however following the restoration of AP translation. This impingement resulted in overloading and subsequent failure to the AA motor. This was identified to be a result of posterior leaning of subsystem components, particularly from the weight of the mounting frame and fluidity of the subsystem facilitated by the linear guides.

To rectify this issue, a counterweight or a mechanism resulting in an anterior force opposing to the leaning weight was required. The counterweight solution was discounted due to its potential to overload the on-board motors. A spring mechanism was chosen to restore and maintain the clearance between the support bracket and the moving cradle. When fully compressed, the length of the spring (spring constant 20N/mm) was to be equal to a minimum clearance of 3mm plus the distance to the spring support (Figure 8.6 – Illustration of spring mechanism used to maintain 4mm clearance throughout testing between main support bracket of subsystem and moving cradle on SSHS

). A previous *in-vitro* hip simulator wear study by O'Dwyer Lancaster-Jones *et al.*, (2017) had shown that springs with a stiffness of 100N/mm could apply significant medial-lateral forces and simulate offset in surgical positioning. It was therefore

expected that the effect of the chosen spring would have a negligible effect on the anterior-posterior force and translation in the subsystem.

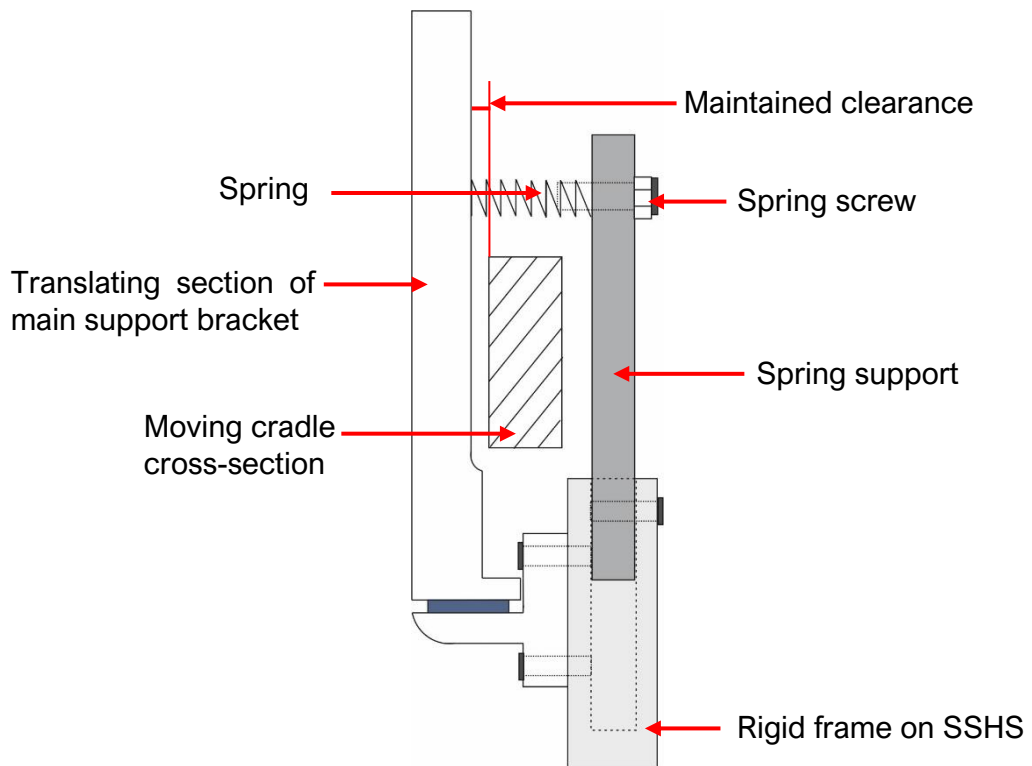


Figure 8.9 – Illustration of spring mechanism used to maintain 4mm clearance throughout testing between main support bracket of subsystem and moving cradle on SSHS

8.1.8 This section provides 2D drawings of components of the subsystem.

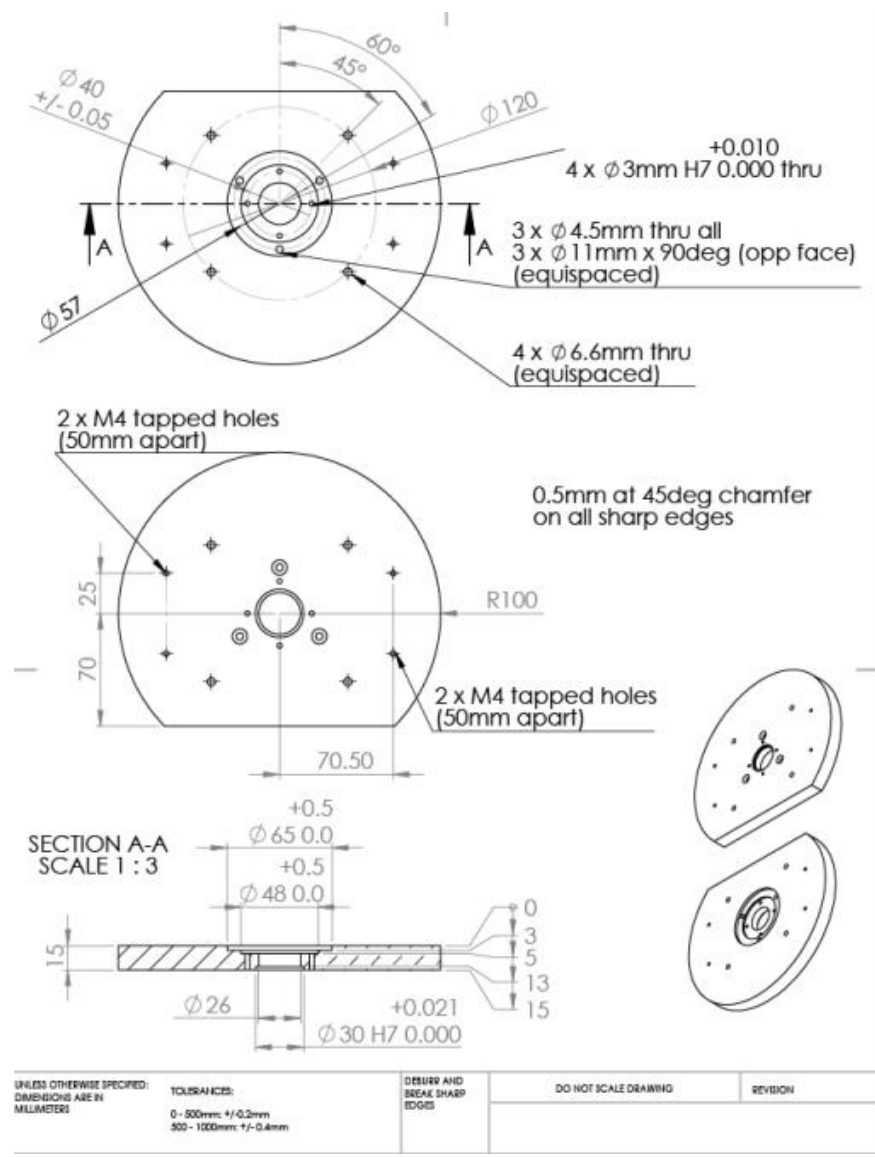


Figure 8.10 - Modification to SSWS top flange

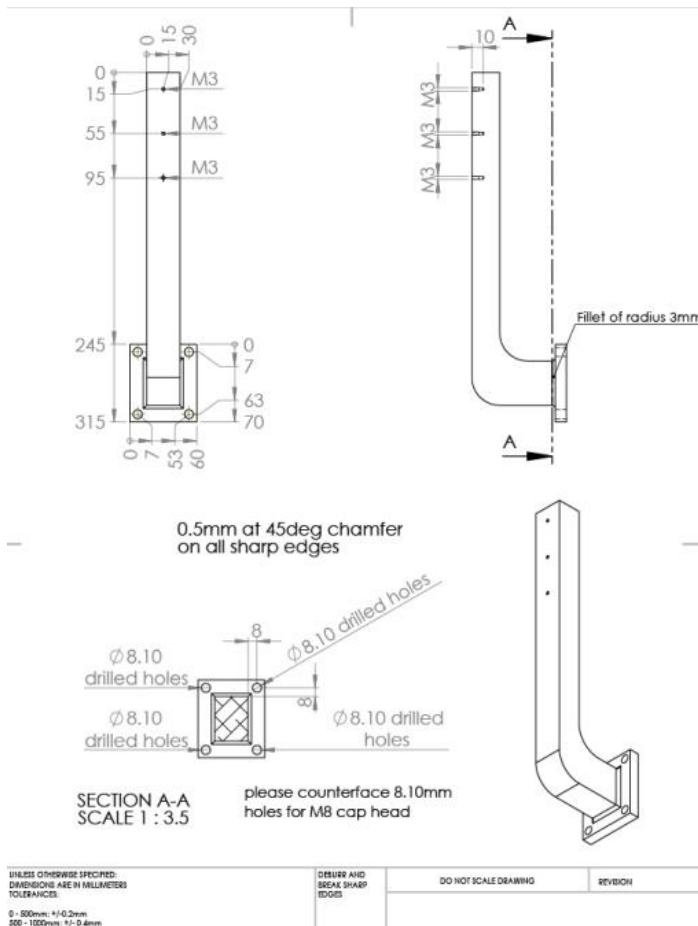


Figure 8.11 - Main support bracket

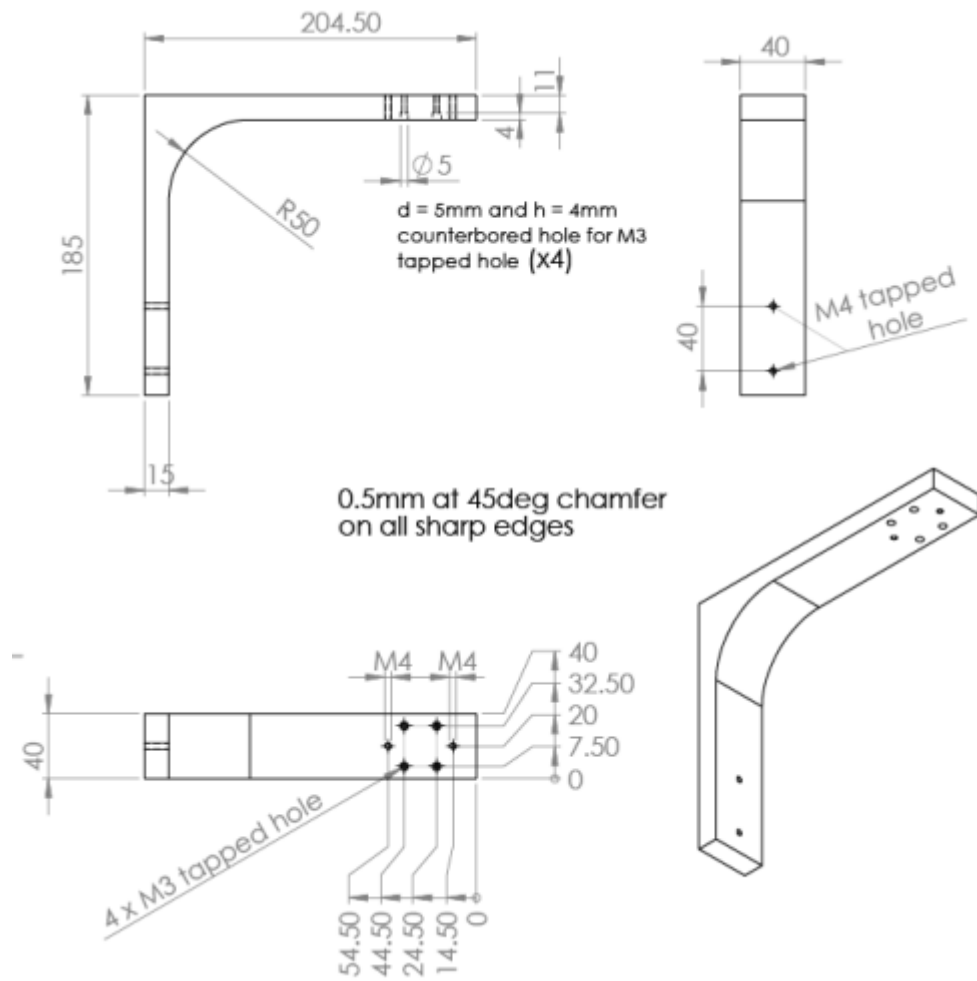


Figure 8.12 – L-shaped mounting frame

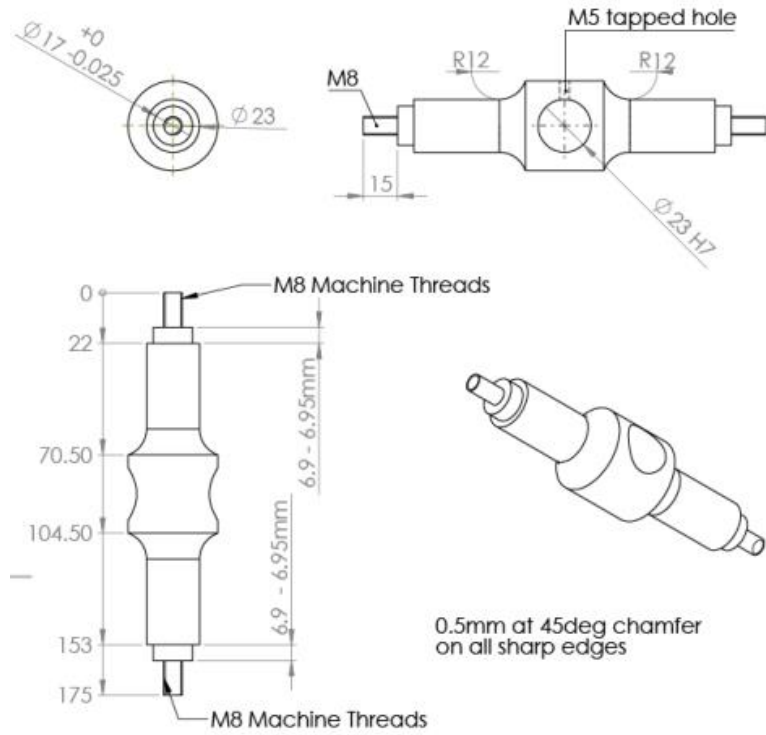


Figure 8.13 - Universal joint crossbar - female

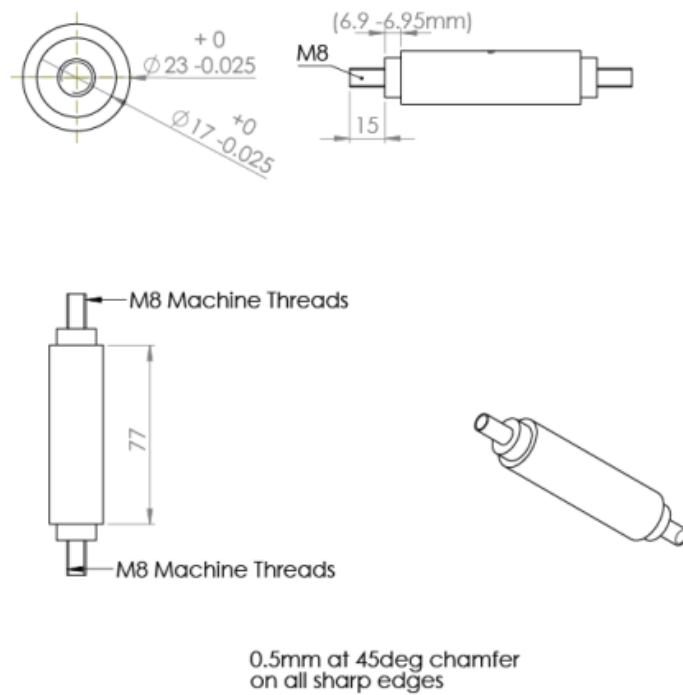


Figure 8.14 - Universal joint crossbar (male)

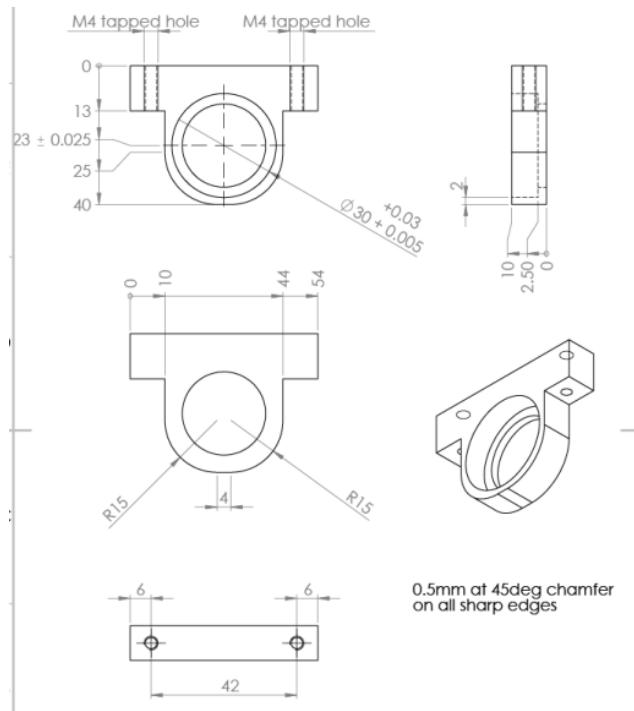


Figure 8.15 - Roller bearing encasing

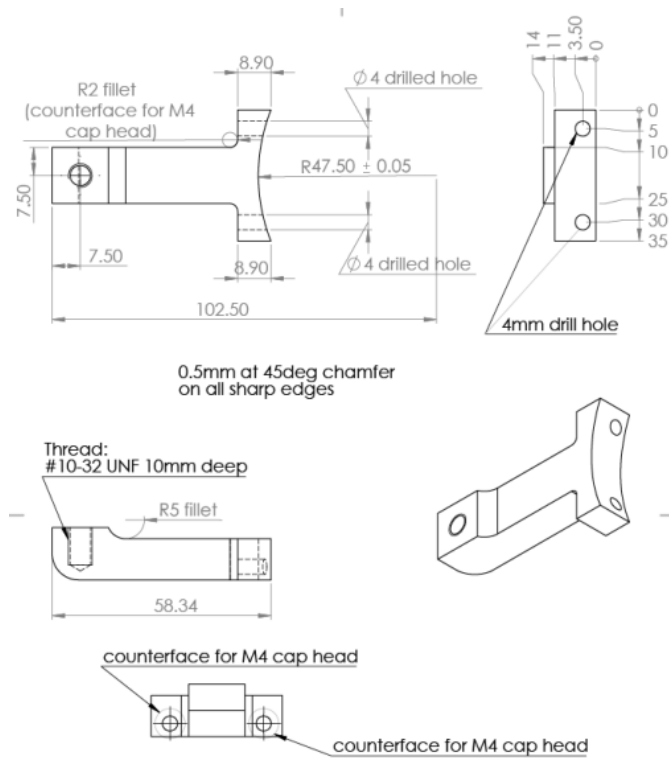


Figure 8.16 – Load cell support fixture (AA direction)

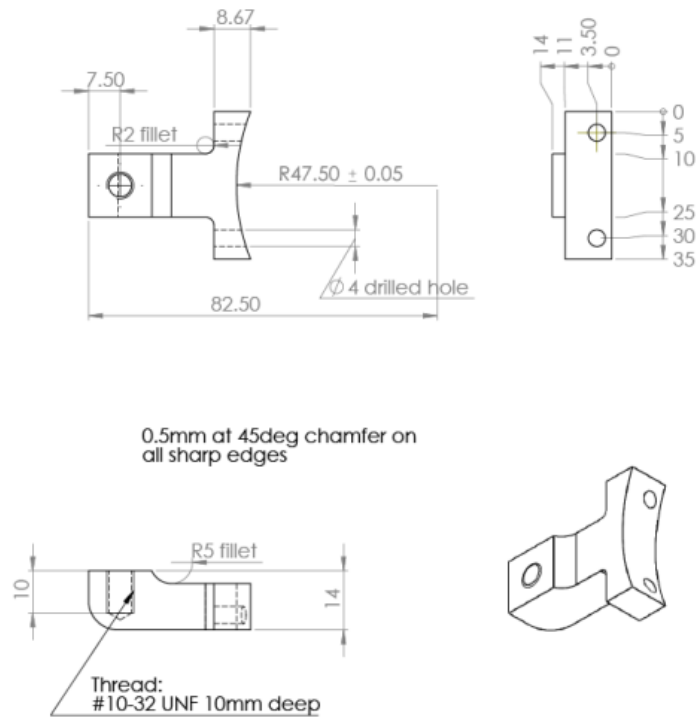


Figure 8.17 - Load cell support fixture (FE direction)

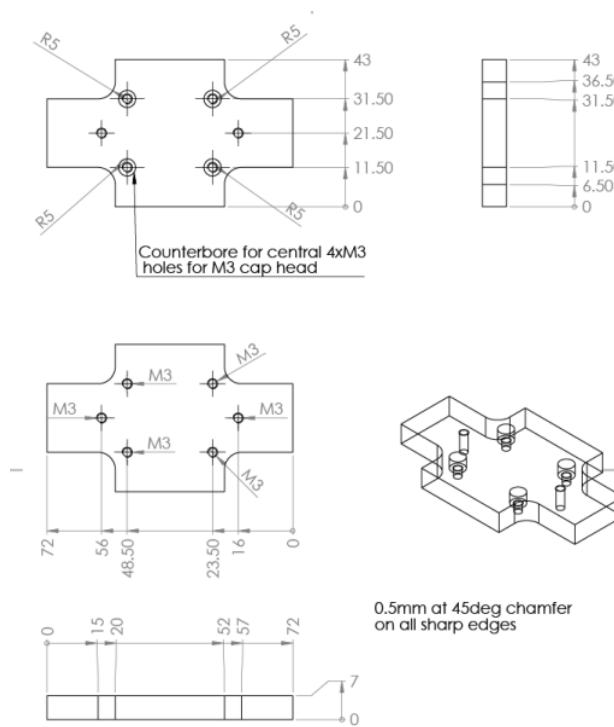


Figure 8.18 – Mounting frame bearing to main support bracket bearing fixture

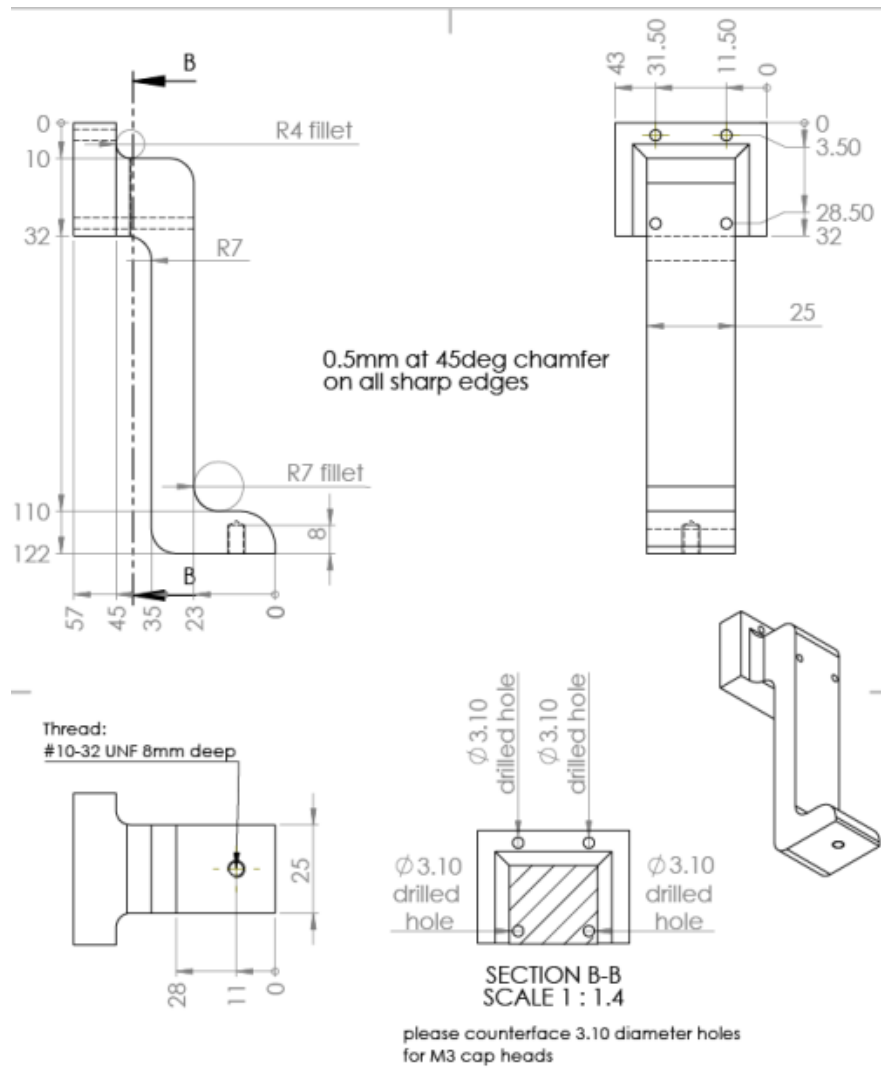


Figure 8.19 – Load cell-to-linear bearing fixture

APPENDIX 8.2

8.2 Chapter Six: Development of a methodology to assess the torque required to loosen uncemented acetabular fixation in total hip replacements

Early concept for custom rig featuring clamping plates measuring 320 x 200 x 30mm - same width and length as the base plate (Figure 8.17).

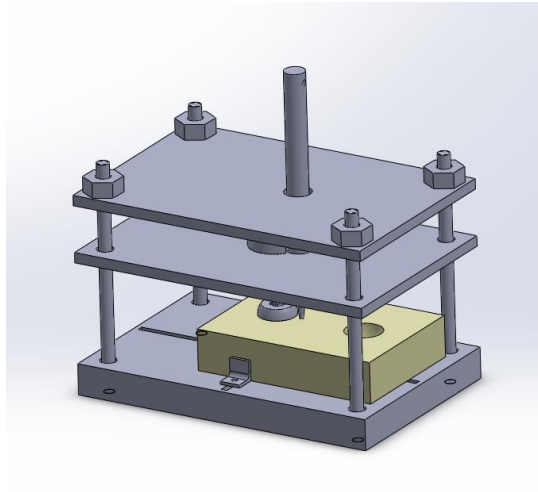


Figure 8.20 – Early rig concept for the assessment of torque required to loosen uncemented acetabular fixation

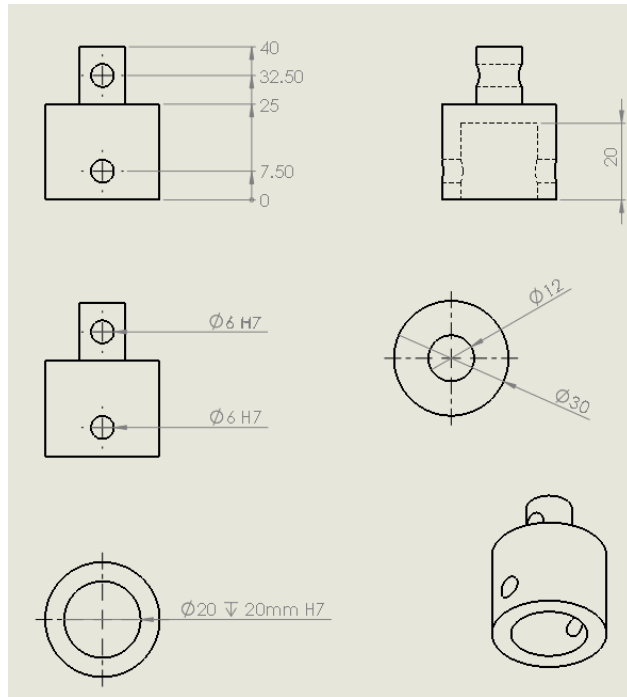


Figure 8.21 - Adaptor for Instron® 3366 connector

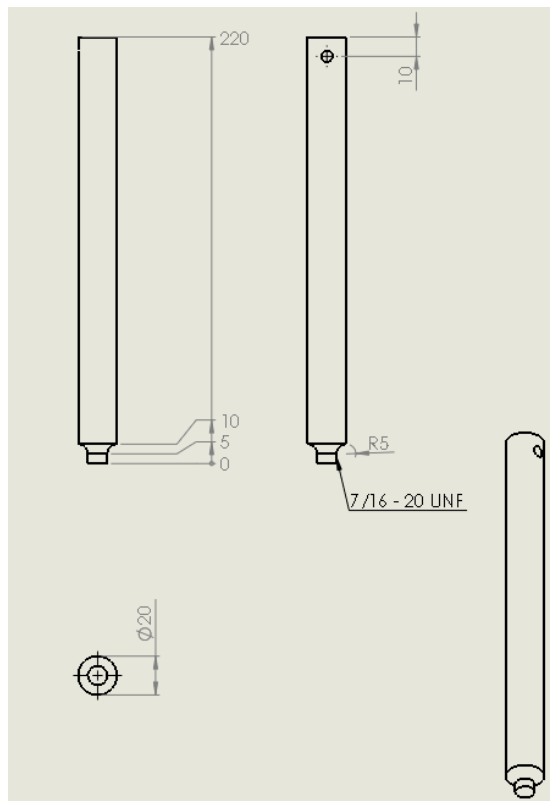


Figure 8.22 - Fixture for insertion of acetabular shells into sawbone blocks

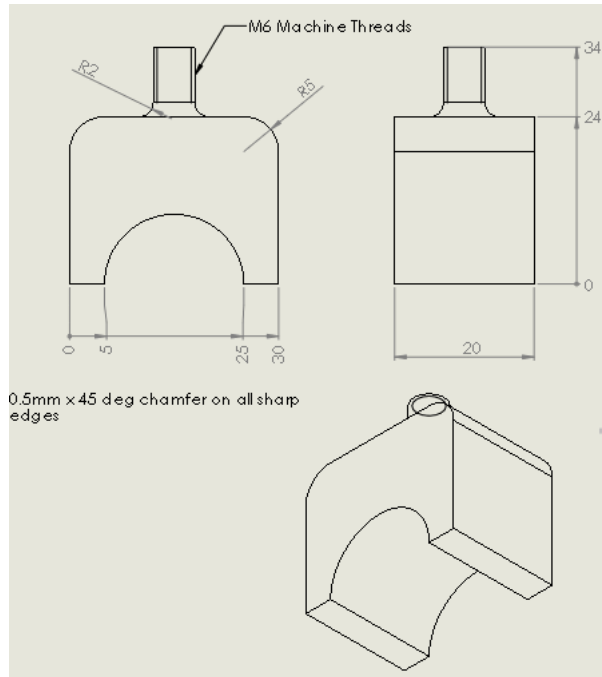


Figure 8.23 - Original concept for the lever-out study male attachment

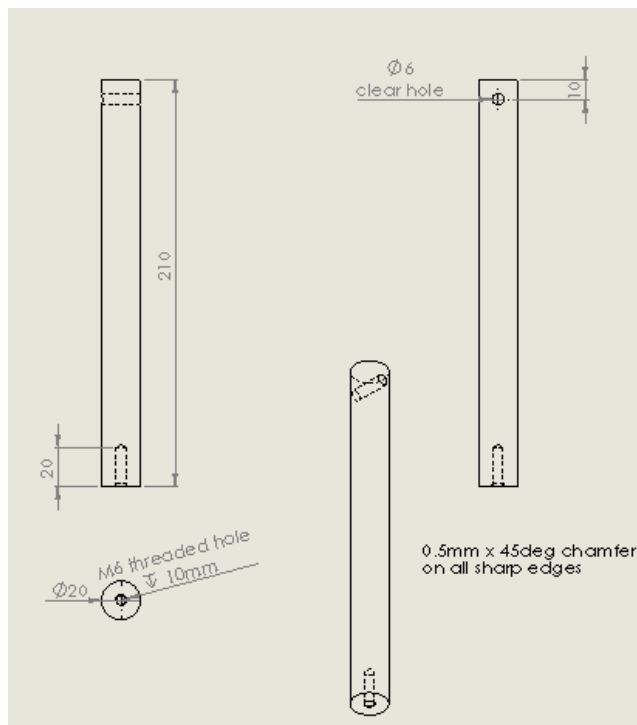


Figure 8.24 - A female modular loading fixture

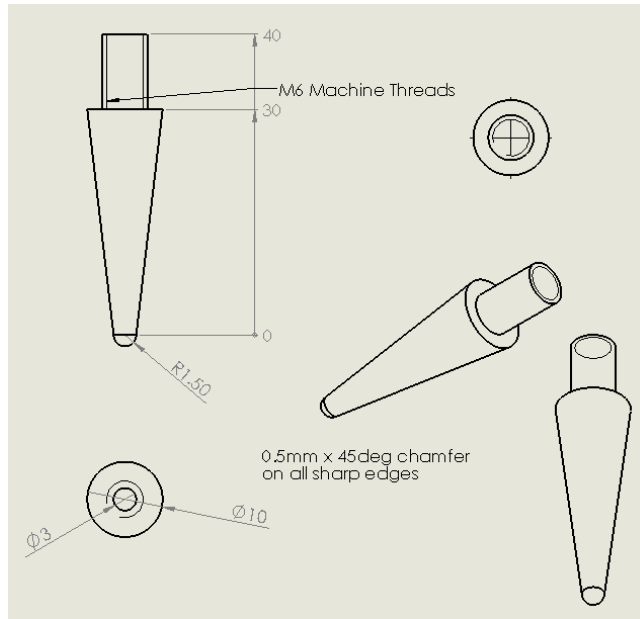


Figure 8.25 - Curved-end edge loading fixture

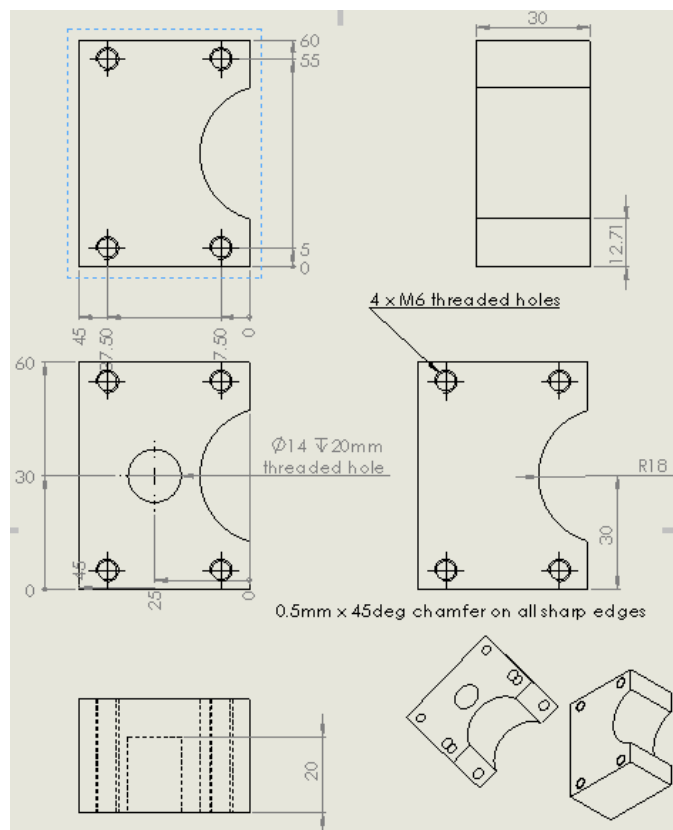


Figure 8.26 - Femoral head spigot insert

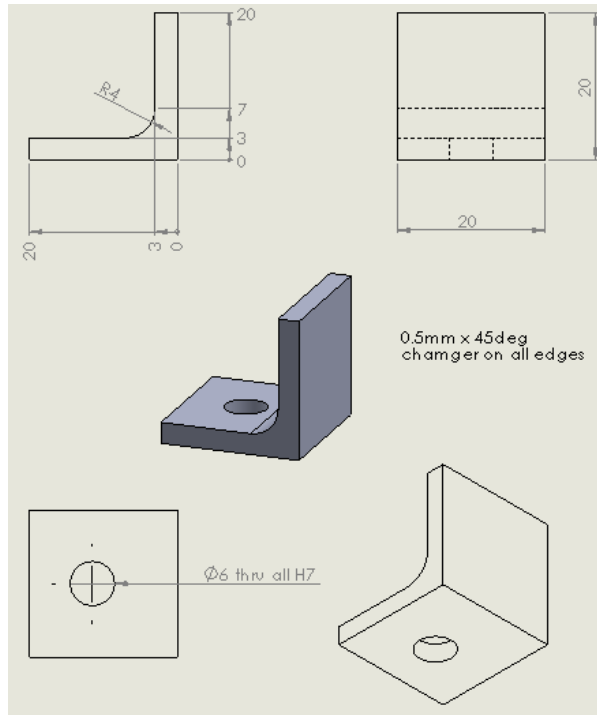


Figure 8.27 – Anti-translation tab

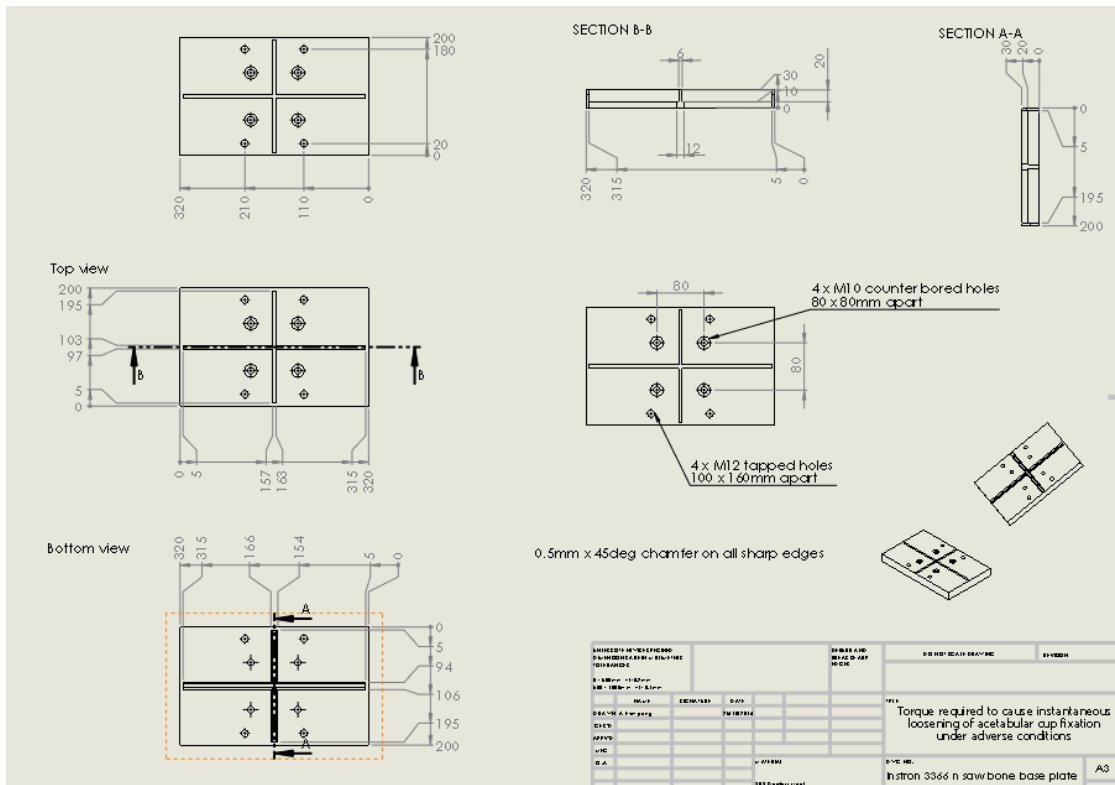


Figure 8.28 - Base plate

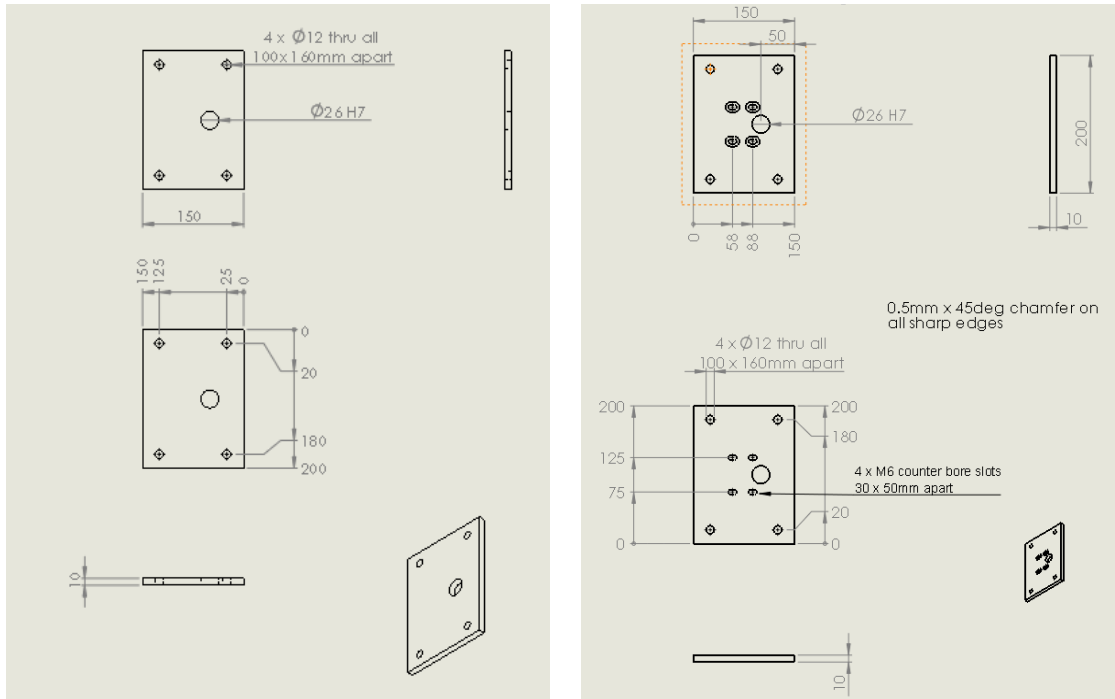


Figure 8.29 – Clamping plates

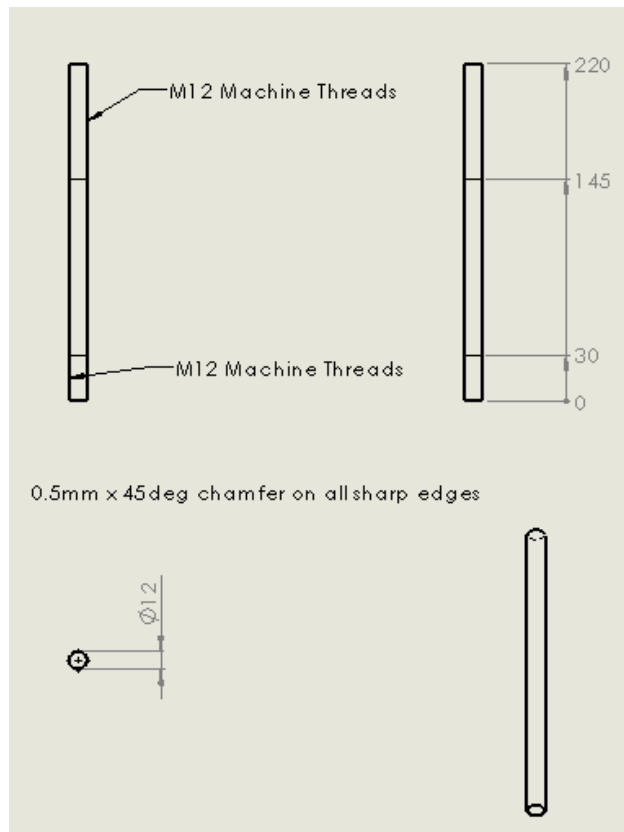


Figure 8.30 – Clamp rods

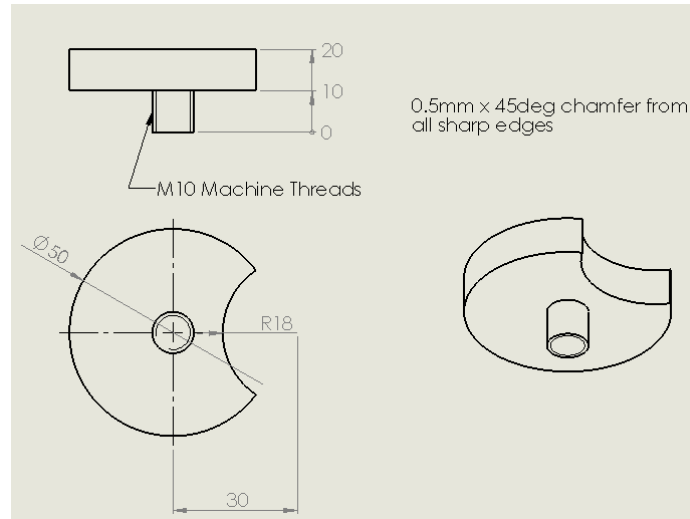


Figure 8.31 - Centralising load cell fixture